DOC.20041028.0008

QA: QA

ANL-EBS-MD-000005 REV 02

October 2004

NOTICE OF OPEN CHANGE DOCUMENTS - THIS DOCUMENT IS IMPACTED BY THE LISTED CHANGE DOCUMENT AND CANNOT BE USED WITHOUT IT.

---

1) ACN-001, DATED 06/17/2005

Stress Corrosion Cracking of the Drip Shield, the Waste Package Outer Barrier, and the Stainless Steel Structural Material

Prepared for:
U.S. Department of Energy
Office of Civilian Radioactive Waste Management
Office of Repository Development
1551 Hillshire Drive
Las Vegas, Nevada 89134-6321

Prepared by:
Bechtel SAIC Company, LLC
1180 Town Center Drive
Las Vegas, Nevada 89144

Under Contract Number
DE-AC28-01RW12101

DISCLAIMER

This report was prepared as an account of work sponsored by an agency of the United States Government. Neither the United States Government nor any agency thereof, nor any of their employees, nor any of their contractors, subcontractors or their employees, makes any warranty, express or implied, or assumes any legal liability or responsibility for the accuracy, completeness, or any third party's use or the results of such use of any information, apparatus, product, or process disclosed, or represents that its use would not infringe privately owned rights. Reference herein to any specific commercial product, process, or service by trade name, trademark, manufacturer, or otherwise, does not necessarily constitute or imply its endorsement, recommendation, or favoring by the United States Government or any agency thereof or its contractors or subcontractors. The views and opinions of authors expressed herein do not necessarily state or reflect those of the United States Government or any agency thereof.

Stress Corrosion Cracking of the Drip Shield, the Waste Package Outer Barrier, and the Stainless Steel Structural Material

ANL-EBS-MD-000005 REV 02

October 2004

INTENTIONALLY LEFT BLANK

OCRWM	MODEL SIGNATURE PAGE/CHANGE HISTORY	Page iii 1. Total Pages: 178

2. Type of Mathematical Model

☒ Process Model ☐ Abstraction Model ☐ System Model

Describe Intended Use of Model

To be used as input to License Application activities, such as the development of the Integrated Waste Package Degradation Analysis (ANL-EBS-PA-000001), to provide technical bases for assessing waste package and drip shield degradation due to stress corrosion cracking under exposure conditions anticipated in the repository.

3. Title

Stress Corrosion Cracking of the Drip Shield, the Waste Package Outer Barrier, and the Stainless Steel Structural Material

4. DI (including Rev. No., if applicable):

ANL-EBS-MD-000005 REV 02

5. Total Appendices	6. No. of Pages in Each Appendix
Two (2)	A-2, B-30

	Printed Name	Signature	Date
7. Originator	Gerald Gordon	Gerald Gordon	10/13/04
8. Independent Technical Reviewer	David Stahl	David Stahl	10/13/04
9. Checker	Gopal De	Gopal De	10/14/2004
10. QER	Charlie Warren	JC Dishaw 10/28/04 for Neil R. Brown	10/14/04
11. Responsible Manager/Lead	Dennis Thomas		10/13/04
12. Responsible Manager	Neil Brown	Neil R. Brown	10/14/04

13. Remarks

see CR 4028

Change History

14. Revision No.	15. Description of Change
00	Initial Issue
00/01	This model report has been changed to include "no backfill" design and more data in support of analysis in the Waste Package Degradation PMR ICN 01 (WP PMR) and SR-CR. Vertical bars in the right margin of the text indicate the changes made in this ICN.
01	Final Copy of REV 01 ICN 00. The entire document has been revised. Changes are too extensive to be identified by vertical bars at the right margin of each page.

3. Title
Stress Corrosion Cracking of the Drip Shield, the Waste Package Outer Barrier, and the Stainless Steel Structural Material
4. DI (including Rev. No., if applicable):
ANL-EBS-MD-000005 REV 02

Change History	
14. Revision No.	15. Description of Change
01/01	Final copy of REV 01 ICN 01. Changes are results of corrective actions required to close out Condition Reports, CR 773, CR 787, CR 792, CR 1150, CR 1138, CR 1173, and CR 1177, related to REV 01 ICN 00. Changes from REV 01 ICN 00 are too extensive to be identified by vertical bars at the right margin of each page.
02	This revision incorporates changes from the regulatory integration review and also includes a Seismic Crack Density Model. The entire model documentation has been revised since REV 01 ICN 01; changes were too extensive to use change bars. This revision also corrects the following DTNs: from L021105312215.023 to LL021105312251.023 (identified in CR 664C and TER-03-0043); and from LL03041252251.57 to LL030412512251.057 (also identified in CR 664C). Input DIRS 118611, TIC 247505 (Development and Use of Predictive Model of Crack Propagation in 304/316L, A533B/A508 and Inconel 600/182 Alloys in 288C Water) was revised from Technical Information to Direct Input, qualified (identified in CR 79B).

CONTENTS

Page

1. PURPOSE 1-1
1.1 PURPOSE AND BACKGROUND 1-1
1.2 MODEL OVERVIEW 1-2

2. QUALITY ASSURANCE 2-1

3. USE OF SOFTWARE 3-1

4. INPUTS 4-1
4.1 DIRECT INPUT 4-1
4.2 CRITERIA 4-7
4.3 CODES AND STANDARDS 4-7

5. ASSUMPTIONS 5-1

6. MODEL DISCUSSION 6-1
6.1 INTRODUCTION 6-1
6.2 CRACK INITIATION AND MANUFACTURING FLAWS 6-2
6.2.1 Threshold Stress for Initiation of Stress Corrosion Cracking 6-2
6.2.2 Manufacturing Flaws 6-9
6.3 THE BASE-CASE SLIP DISSOLUTION–FILM RUPTURE MODEL 6-15
6.3.1 Introduction 6-15
6.3.2 Slip Dissolution–Film Rupture Mechanism 6-16
6.3.3 Model Quantification 6-20
6.3.4 Adaptation of Slip Dissolution Model To Alloy 22 6-23
6.3.5 Threshold Stress Intensity Factor 6-29
6.3.6 Alternative Model: The Coupled Environment Fracture (CEF) Model 6-31
6.3.7 Stress Corrosion Cracking for the Drip Shield Titanium Grade 7 Material 6-33
6.4 EVALUATION OF STRESS INTENSITY FACTOR 6-35
6.4.1 Introduction 6-35
6.4.2 Calculations of Stress Intensity Factors for Waste Package Closure Welds 6-36
6.4.3 Impact of Corrosion 6-50
6.4.4 Mitigation of Weld Residual Stress 6-55
6.4.5 Uncertainty and Variability of Residual Stress and Stress Intensity Factor in Waste Package 6-61
6.5 ESTIMATE OF LENGTH AND INTERCRACK SPACING OF RADIAL THROUGH-WALL CRACKING AND CRACK OPENING 6-70
6.5.1 Estimated Length and Intercrack Spacing of Radial Through-Wall Cracking 6-70
6.5.2 Estimate of Crack Opening 6-71
6.6 FEATURES, EVENTS AND PROCESSES 6-72

7. MODEL VALIDATION 7-1
7.1. INTENDED PURPOSE OF THE MODEL 7-1

CONTENTS (Continued)

Page

7.1.1 Confidence-Building During Model Development to Establish Scientific Basis and Accuracy for Intended Use 7-1
7.1.2 Confidence-Building After Model Development To Support The Scientific Basis Of The Model 7-3
7.2. DETERMINATION OF THE LEVEL OF CONFIDENCE REQUIRED 7-3
7.3. VALIDATION ACTIVITIES AND ASSOCIATED CRITERION USED TO DETERMINE THAT THE REQUIRED LEVEL OF CONFIDENCE HAS BEEN OBTAINED 7-5
7.4 COMPARISON OF ACTIVITIES PERFORMED TO GENERATE CONFIDENCE IN THE MODEL WITH MODEL VALIDATION CRITERION 7-6
7.4.1 Activities Performed for Validating the SDFR Model Using Peer Reviewed Literature 7-7
7.4.2 Activity Performed for Validating the SDFR Model Applicable to Alloy 22 using Independently Obtained Experimental Data 7-8
7.4.3 Corroboration of SDFR Model with Available Alternative Conceptual Models 7-14
7.4.4 Activities Performed to Demonstrate the Technical Basis for the Selection of the Threshold Stress Intensity Factor and the Threshold Stress Parameter for SCC Initiation 7-15

8. CONCLUSIONS 8-1
8.1 CONCLUSION 8-1
8.2 COMPLIANCE WITH YMP ACCEPTANCE CRITERIA 8-2
8.2.1 System Description and Demonstration of Multiple Barriers 8-2
8.2.2 Degradation of Engineered Barriers 8-4
8.3 SUMMARY OF OUTPUT 8-10

9. INPUTS AND REFERENCES 9-1
9.1 DOCUMENTS CITED 9-1
9.2 CODES, STANDARDS, REGULATIONS, AND PROCEDURES 9-7
9.3 SOURCE DATA, LISTED BY DATA TRACKING NUMBER 9-8
9.4 OUTPUT DATA, LISTED BY DATA TRACKING NUMBER 9-9

APPENDIX A DATA QUALIFICATION PLAN A-1

APPENDIX B SEISMIC CRACK DENSITY MODEL B-1

FIGURES

Page

1-1. Flow Diagram of Stress Corrosion Cracking Modeling Approach 1-2

4-1. Applied Stress to Yield Strength Ratio versus Time-to-Failure 4-1

6-1. Ratio of the Stress Intensity Factor ($K(\theta)$) of a Crack Making an Angle (θ) with the Stress Direction to the Factor ($K(90°)$) of a Crack Oriented Perpendicular to the Stress Direction as a Function of the Angle (θ), for a Crack with an Arbitrary Stress and Crack Length 6-14
6-2. Schematic Oxidation Charge Density versus Time for a Strained Crack Tip and Unstrained Crack Sides in the Slip Dissolution Mechanism 6-18
6-3. Schematic of Oxidation Current Density versus Time Following Repeated Oxide Rupture Events 6-19
6-4. Crack Growth Rate (Presented by Observed Data Points and Predicted Curve) versus Crack Tip Strain Rate for Sensitized Stainless Steel Type 304 in Oxygenated 288°C Water 6-22
6-5. Temperature-Dependence of Sensitized Stainless Steel Type 304 and Alloy 600 6-24
6-6. Crack Growth Rate versus Stress Intensity Factor for Alloy 22 Based on the SDFR Model 6-29
6-7. Comparison of Predicted Crack Growth Rates for Stainless Steel Type 304 6-33
6-8. Sketch of Initially Recommended LA Design for Waste Package Final Closure Weld Region 6-38
6-9. Schematic and Dimensions for the CRM–21-PWR Waste Package Design 6-39
6-10. Finite Element Model for the CRM–21-PWR Waste Package Design 6-40
6-11. Selected Cross-Sections for CRM–21-PWR Waste Package Design 6-41
6-12. Selected Cross-Sections for the Modified CRM–21-PWR Waste Package Design 6-42
6-13. Flaw Orientation for Lid Welds 6-44
6-14. Hoop Stresses in Outer Lid of CRM–21-PWR Design 6-46
6-15. Outer Lid Circumferential Flaw Geometric Correction Factor 6-46
6-16. Finite Element Model Used for Study of Corrosion 6-51
6-17. Effect of Corrosion on Radial Stress in Outer Lid 6-52
6-18. Effect of Corrosion on Hoop Stress in Outer Lid 6-52
6-19. Stress Intensity Factor for Full-Circumference Flaw in Outer Lid 6-53
6-20. Stress Intensity Factor for Radial Elliptical Crack in Outer Lid 6-54
6-21. Mitigation of Weld Stress in Alloy 22 with Laser Peening 6-57
6-22. Stress in Outer Lid with and without Laser Peening 6-59
6-23. Stress Intensity Factors due to (a) Radial Stress and (b) Hoop Stress with and without Laser Peening 6-60
6-24. Variation of Hoop Stress Versus Depth for Waste Package Outer Closure Lid 6-65
6-25. Variation of Hoop Stress Versus Depth for Waste Package Middle Closure Lid 6-65
6-26. Variation of Stress Intensity Factor Versus Depth for Waste Package Outer Closure Lid. 6-66

FIGURES (Continued)

Page

6-27. Variation of Stress Intensity Factor Versus Depth for Waste Package Middle Closure Lid 6-66
6-28. Variation of Hoop Stress (θ = 0) Versus Depth for Waste Package Outer Closure Lid 6-67
6-29. Variation of Hoop Stress (θ = 0) Versus Depth for Waste Package Middle Closure Lid 6-67
6-30. Variation of Stress Intensity Factor (θ = 0) Versus Depth for Waste Package Outer Closure Lid 6-68
6-31. Variation of Stress Intensity Factor (θ = 0) Versus Depth for Waste Package Middle Closure Lid 6-68
6-32. Measured Stress (Using 1-Inch Ring Core Method) versus Depth for Alloy 22 Laser-Peened 1-Inch-Thick Gas Tungsten Arc Welding Welded Plate 6-69
6-33. Measured Stress (Using 1-Inch Ring-Core Method) versus Depth for Alloy 22 Controlled Plasticity Burnished 1-Inch-Thick Welded Plate 6-70

7-1. Frequency Distributions of the Ratio of the Calculated to Observed Crack Growth Rates for Stainless Steel Type 304 7-8
7-2. Comparison of the SDFR prediction model and measured data for Alloy 22 7-13

TABLES

Page

4-1. Input Data 4-2
4-2. Measured Crack Growth Rates for Alloy 22 Specimens 4-3
4-3. Coefficients of Stress Profiles for the Original and Modified CRM–21-PWR Design 4-3
4-4. Stress Intensity Factor (SIF) Profiles 4-4
4-5. Input Data for Yield Strength, and Modulus of Elasticity 4-6
4-6. 5-Year General Corrosion Rates 4-6

6-1. Chemical Composition of the Studied Alloy 22 Heats (wt %) 6-4
6-2. Slow Strain Rate Test Results for Annealed Alloy 22 (Strain Rate of 1.66×10^{-6} per second) 6-6
6-3. Measured Crack Growth Rates (mm/s) in 288°C, Oxygenated Water Due to Drop in Corrosion Potential 6-25
6-4. Summary of Source Data for Alloy 22 SDFR Model Quantification 6-28
6-5. Distribution of the Parameter ‘n’ 6-28
6-6. Distribution of the Threshold Stress Intensity Factor, K_{ISCC}, for Alloy 22 6-31
6-7. Stress Coefficients for the As-Welded Waste Package Outer Lid 6-47
6-8. Stress Coefficients for the As-Welded Waste Package Middle Lid 6-47
6-9. Stress Intensity Factor (SIF) Profiles for As-Welded Waste Package Outer Lid 6-48
6-10. Stresses and Stress Intensity Factors for the As-Welded Waste Package Middle Lid 6-49
6-11. Stress Coefficients for the Laser-Peened Waste Package Outer Lid 6-56
6-12. Stresses and Stress Intensity Factors for Laser-Peened Waste Package Outer Lid 6-57
6-13. Included FEPs 6-72

7-1. Supporting (Corroborating) Information Used to Validate the SDFR Model 7-3
7-2. Nominal Chemical Composition of Several Ni-Cr Base Alloys (wt %) 7-9
7-3. Summary of LLNL Crack Growth Rates in Compact Tension Specimens 7-13
7-4. Comparison of Predicted and Measured Crack Growth Rates for Alloy 22 7-14

8-1. Summary of Output 8-11
8-2. Stresses and Stress Intensity Factors for the As-Welded Waste Package Middle Lid 8-14
8-3. Stresses and Stress Intensity Factors for Laser-Peened Waste Package Outer Lid 8-15

INTENTIONALLY LEFT BLANK

ACRONYMS

ASME	American Society of Mechanical Engineers
BWR	boiling water reactor
CEF	coupled environment fracture
CLST	Container Life and Source Term
DCB	double cantilever beam
DOE	U.S. Department of Energy
DTN	Data Tracking Number
EBS	engineered barrier system
EDA	Enhanced Design Alternative
FEP	feature, event, or process
GEGRC	General Electric Global Research Center
HLW	high-level radioactive waste
IRSR	Issue Resolution Status Report
LA	License Application
LLNL	Lawrence Livermore National Laboratory
LTCTF	Long Term Corrosion Test Facility
LWR	light water reactor
NACE	National Association of Corrosion Engineers
NDE	nondestructive examination
NRC	U.S. Nuclear Regulatory Commission
OCRWM	Office of Civilian Radioactive Waste Management
PA	performance assessment
PWR	pessurized water reactor
QA	Quality Assurance
QAP	Quality Administrative Procedures
QARD	Quality Assurance Requirements and Description
QP	Quality Procedure

ACRONYMS (Continued)

SAW	simulated acidified water
SCW	simulated concentrated water
SC	Safety Category
SCC	stress corrosion cracking
SCDM	Seismic Crack Density Model
SCE	Saturated Calomel Electrode
SDFR	Slip Dissolution–Film Rupture
SECP	Single Edge Cracked Plate
SIA	Structural Integrity Associates
SIF	stress intensity factor
SNF	spent nuclear fuel
SSRT	Slow Strain Rate Test
TCP	Tetrahedrally Closed Pack
TSIF	Threshold Stress Intensity Factor
TSPA	Total System Performance Assessment
TSPA-LA	Total System Performance Assessment for License Application
WAPDEG	Waste Package Degradation Analysis
YMP	Yucca Mountain Project
YS	yield strength

1. PURPOSE

1.1 PURPOSE AND BACKGROUND

Stress corrosion cracking is one of the most common corrosion-related causes for premature breach of metal structural components. Stress corrosion cracking is the initiation and propagation of cracks in structural components due to three factors that must be present simultaneously: metallurgical susceptibility, critical environment, and static (or sustained) tensile stresses. This report was prepared according to *Technical Work Plan for: Regulatory Integration Modeling and Analysis of the Waste Form and Waste Package* (BSC 2004 [DIRS 171583]). The purpose of this report is to provide an evaluation of the potential for stress corrosion cracking of the engineered barrier system components (i.e., the drip shield, waste package outer barrier, and waste package stainless steel inner structural cylinder) under exposure conditions consistent with the repository during the regulatory period of 10,000 years after permanent closure. For the drip shield and waste package outer barrier, the critical environment is conservatively taken as any aqueous environment contacting the metal surfaces. Appendix B of this report describes the development of the SCC-relevant seismic crack density model (SCDM).

The consequence of a stress corrosion cracking breach of the drip shield, the waste package outer barrier, or the stainless steel inner structural cylinder material is the initiation and propagation of tight, sometimes branching, cracks that might be induced by the combination of an aggressive environment and various tensile stresses that can develop in the drip shields or the waste packages. The Stainless Steel Type 316 inner structural cylinder of the waste package is excluded from the stress corrosion cracking evaluation because the Total System Performance Assessment for License Application (TSPA-LA) does not take credit for the inner cylinder. This document provides a detailed description of the process-level models that can be applied to assess the performance of Alloy 22 (used for the waste package outer barrier) and Titanium Grade 7 (used for the drip shield) that are subjected to the effects of stress corrosion cracking. The use of laser peening or other residual stress mitigation techniques is considered as a means of mitigating stress corrosion cracking in the waste package final closure lid weld.

Upstream sources of inputs, DTNs, and cited references that support this report include: *Plugging of Stress Corrosion Cracks by Precipitates*, *Aging and Phase Stability of Waste Package Outer Barrier*, *Environment on the Surfaces of the Drip Shield and Waste Package Outer Barrier*, *Drip Shield Structural Response to Rock Fall*, *General Corrosion and Localized Corrosion of the Drip Shield*, *Structural Calculations of Waste Package Exposed to Vibratory Ground Motion*, *Commercial SNF Waste Package Design Report*, *21-PWR Waste Package Configuration,* and *Analysis of Mechanisms for Early Waste Package/Drip Shield Failure*.

This report also provides similar information to *General Corrosion and Localized Corrosion of the Drip Shield*, *Hydrogen Induced Cracking of Drip Shield*, *Screening Analysis of Criticality Features, Events, and Processes for License Application*, *WAPDEG Analysis of Waste Package and Drip Shield Degradation*, *FEPS Screening of Processes and Issues in Drip Shield and Waste Package Degradation*, and *Postclosure Modeling and Analyses Design Parameters*.

1.2 MODEL OVERVIEW

Stress corrosion cracking is the initiation and propagation of cracks in metal components due to three factors occurring simultaneously: material susceptibility, critical environment, and static (or sustained) tensile stress. Although Alloy 22, the material used for the waste package outer barrier, is highly corrosion resistant, its susceptibility to stress corrosion cracking is addressed for the repository environment and the coexisting stress conditions described in Section 6.4. Section 6.3.7 provides an analysis that forms the technical basis for screening out stress corrosion cracking in the drip shield. A lifetime-modeling approach was developed to assess the degradation of the waste package outer barrier due to stress corrosion cracking. Figure 1-1 shows how the approach considers crack initiation and preexisting manufacturing flaws (Section 6.2), stress conditions that drive crack initiation and propagation (Section 6.4), the stress threshold that defines crack initiation (Section 6.2.1), threshold stress intensity factor (Section 6.3.5) that defines propagation of both initiated incipient cracks and manufacturing flaws, and the crack growth model (based on the slip dissolution–film rupture theory) that determines the crack growth rate (Section 6.3). The stress corrosion cracking modeling approach provides the elements (Section 8) necessary to perform a lifetime prediction of the waste package outer barrier subjected to the effects of stress corrosion cracking.

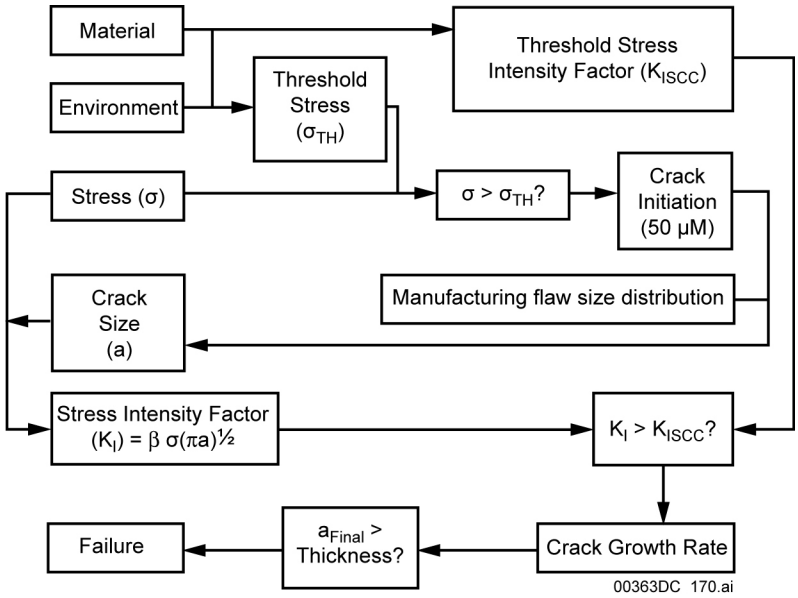

NOTE: When an indicated value of σ, K_I, or a_{Final} is less than the indicated parameter value, the corresponding crack initiation, crack growth, or breach does not occur.

Figure 1-1. Flow Diagram of Stress Corrosion Cracking Modeling Approach

2. QUALITY ASSURANCE

The Office of Civilian Radioactive Waste Management (OCRWM) Quality Assurance (QA) program applies to this report. All waste package configurations and drip shields have been determined to be important to waste isolation in accordance with AP-2.22Q, *Classification Analyses and Maintenance of the Q-List* and, therefore, are classified as Safety Category (SC) in *Q-List* (BSC 2004 [DIRS 168361], Appendix A; BSC 2004 [DIRS 170992], Section 6.4.2).

This report has been developed per AP-SIII.10Q, *Models*, as per *Technical Work Plan for: Regulatory Integration Modeling and Analysis of the Waste Form and Waste Package* (BSC 2004 [DIRS 171583]).

The inputs to this report are documented according to AP-3.15Q, *Managing Technical Product Inputs*. The methods used to control the electronic management of data as required by AP-SV.1Q, *Control of the Electronic Management of Information*, were accomplished in accordance with the technical work plan. The process for control of the electronic management of information on evaluation of work activities, processes, or process functions outlined in Section 5.0 of AP-SV.1Q, is followed to ensure accuracy, completeness, and security of information and data used in preparation of this report. Examples of process controls mentioned in AP-SV.1Q are: (a) access to the information contained on personal computer is password protected; (b) secured backup copies are appropriately labeled and stored before changes are made and kept until the changes are confirmed and correct; (c) physical electronic media (tape, diskette, CD-ROM, etc.) are appropriately labeled; and (d) for nonphysical electronic media, transport mechanisms can be e-mail, TCP/IP, NetBios, etc. and methods of receipt verification may include visual inspection, transmission verification settings, check sums, application information integrity check, etc.

Based on these controls, as well as those imposed by the relevant implementing procedures, the process-control evaluation performed in accordance with AP-SV.1Q, *Control of the Electronic Management of Information*, states that adequate controls are provided (Attachment I). Evaluation of activities in accordance with AP-2.27Q, *Planning for Science Activities*, reveals that each activity is subject to the requirements of *Quality Assurance Requirements and Description* (DOE 2004 [DIRS 171539]. Standard QA controls will apply to the development of analyses and models, as well as data qualification efforts.

Appendix B discusses quality assurance of the seismic crack density model.

INTENTIONALLY LEFT BLANK

3. USE OF SOFTWARE

No software or computer codes are used in developing this report or during model validation. The computer software-generated data on through-thickness residual stress and stress intensity factor profiles at the welds of the middle and outer lids of the waste package design were obtained by procurement from a qualified vendor. These data, presented in DTN: LL000316205924.142 [DIRS 148895], were developed using computer software internally qualified by the vendor (Structural Integrity Associates, Inc., San Jose, CA) in compliance with the Structural Integrity Associates Quality Assurance Program, which was approved by the YMP Office of Quality Assurance (OQA).

Microsoft Excel 97 was used to perform support calculations and graphics. Microsoft Excel 97 is a standardized commercial spreadsheet program designed to assist in routine calculations and graphics. The program provides built-in mathematical functions that can be used to automate the calculation process. It also includes a graphics package to assist in data presentation. Microsoft Excel 97 is a commercial off-the-shelf software program exempt from software qualification in accordance with Section 2.1 of LP-SI.11Q-BSC, *Software Management*. Furthermore, according to LP-SI.11Q-BSC, *Software Management,* Section 2.1, the graphical representation use of Excel are exempt, as are the calculations using built-in mathematical functions. When Excel is used for calculations (Section 6.3.4), information required for an independent person to reproduce the work (including the formula or algorithm used, and listing of inputs or outputs) is provided. The calculations using Microsoft Excel 97 can be independently performed on any platform capable of running this commercial software program, including Windows 95, 98, 2000, and NT.

MathCad 2001i is a commercial, off-the-shelf software program used in Section 6.4.5. The computations performed in this report using MathCad 2001i use only standard functions and produce results independent of the software program used. The program provides built-in mathematical functions that can be used to automate the calculation process. It also includes a graphics package to assist in data presentation. MathCad 2001i is a commercial off-the-shelf software program exempt from software qualification in accordance with Section 2.1 of LP-SI.11Q-BSC, *Software Management*. Furthermore, the graphical representation use of MathCad 2001i is exempt per Section 2.1 of LP-SI.11Q-BSC, as are calculations using built-in mathematical functions. When MathCad 2001i is used for calculations (Section 6.4.5), information required for an independent person to reproduce the work (including formula or algorithm used, and listing of inputs or outputs) is provided. The calculations using MathCad 2001i can be independently performed on any platform capable of running this commercial software program, including Windows 95, 98, 2000, and NT.

Appendix B discusses the use of software for the seismic crack density model.

INTENTIONALLY LEFT BLANK

4. INPUTS

Appendix B discusses seismic crack density model inputs.

4.1 DIRECT INPUT

The data providing input for the development of parameters or other databases, or both, used in the models or analyses documented in this report are identified in Table 4-1. While uncertainty in the input data is discussed in Section 6, Tables 4-1 through 4-6, and Figure 4-1 provide:

- A roadmap to what data are in the DTN, if applicable
- A description of how the data are used to develop model or analyses input parameters.

The input data are appropriate for use because they are either qualified acquired or developed data. Some of the developed data were obtained from established fact. No developed parameters or other input information are used in the model or analyses. To alleviate concerns about rounding errors, this report often uses exact rather than significant digits. Also, some inputs received in English units are left as is, although all output units in Section 8 are in metric units.

Data used to develop the SDFR model are not used subsequently to validate the model.

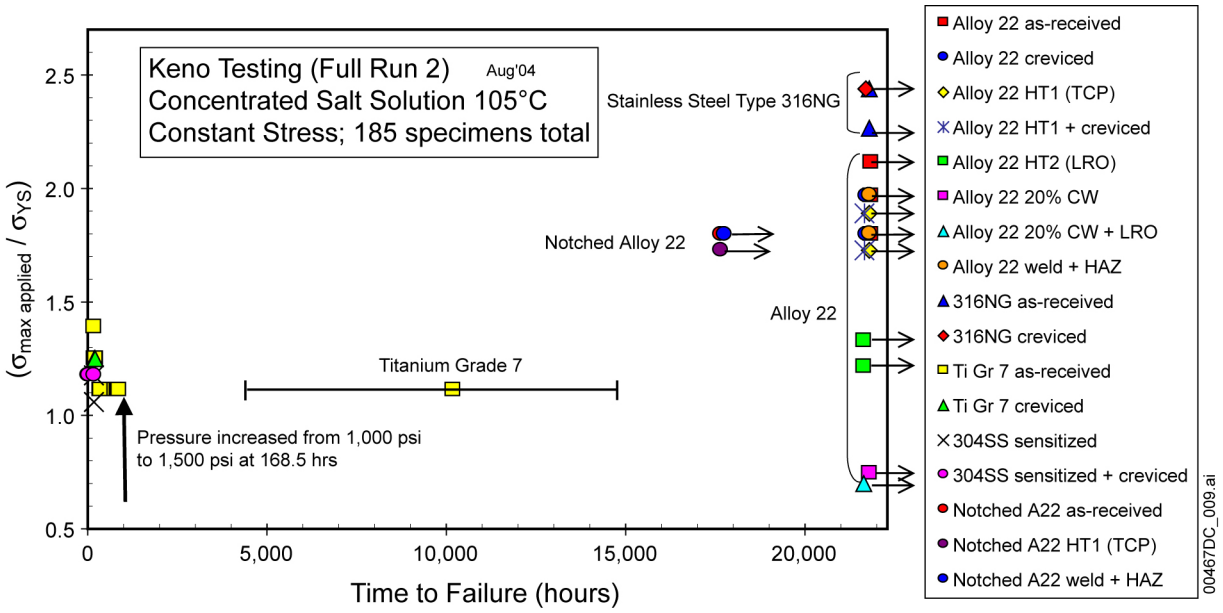

Source: DTN: MO0409GE835924.000 [DIRS 171564], p. 12.

NOTE: Target test solution composition: 0.27M Na_2CO_3, 0.35M KCl, 0.41M NaCl, 0.013M NaF, 0.43M $NaNO_3$, 0.03M Na_2SO_4, 0.04M $Na_2SiO_3.9H_2O$ (pH = 10.3 at 105°C), Table 2-1, DTN: LL021105312251.023 [DIRS 161253], p 99. This composition represents a concentrated, approximately 15% solution of Basic Saturated Water (BSW) whose target composition is given in DTN: LL021105312251.023 [DIRS 161253], p 3. σ_{YS} (for as-received condition) used in stress ratio for welded specimens.

Figure 4-1. Applied Stress to Yield Strength Ratio versus Time-to-Failure

Table 4-1. Input Data

Data Name	Data Source	DTN	Discussion
Measured crack growth rates in mm/s for Alloy 22 specimens c153, c144, and c152 tested for stress intensity factors of 30 and 45 MPa√m	Stress corrosion cracking initiation and growth measurements in environments relevant to high-level nuclear waste packages. Submittal date: 01/08/2003	LL021105312251.023 [DIRS 161253]	Input data (Table 4-2) are used in Section 6.3.4 for determining the repassivation slope 'n' of the slip dissolution–film rupture model.
Crack initiation measurements for Alloy 22 and Titanium Grade 7 specimens	Stress corrosion cracking initiation and growth measurements in environments relevant to high-level nuclear waste packages. Submittal date: 9/02/2004	MO0409GE835924.000 [DIRS 171564]	Input data (Figure 4-1) are used in Section 6.2.1 for determining the threshold stress for crack initiation for Alloy 22 and Titanium Grade 7.
Coefficients of stress profiles, A_0, A_1, A_2, and A_3	Stress corrosion cracking of the drip shield, the waste package outer barrier and the stainless steel structural material. Submittal date: 03/22/2000.	LL000316205924.142 [DIRS 148895]	Input data (Table 4-3) are used in Section 6.4.2 for stress profiles in as-welded and laser-peened Alloy 22 closure lids.
Stress intensity factor profiles	Stress corrosion cracking of the drip shield, the waste package outer barrier and the stainless steel structural material. Submittal date: 03/22/2000.	LL000316205924.142 [DIRS 148895]	Input data (Table 4-4) are used in Section 6.4.2.
YS (yield strength) for Alloy 22	Waste package material properties: corrosion-resistant materials.	MO0003RIB00071.000 [DIRS 148850]	Input data (Table 4-5) are used in Sections 6.2.1 and 6.4.5.
YS (yield strength) for Titanium Grade 7	Waste package material properties: corrosion-resistant materials.	MO0003RIB00073.000 [DIRS 152926]	Input data (Table 4-5) are used in Sections 6.2.1 and 6.3.7.
E (modulus of elasticity) for Titanium Grade 7	Waste package material properties: corrosion-resistant materials.	MO0003RIB00073.000 [DIRS 152926]	Input data (Table 4-5) are used in Section 6.3.7.
V_{gc}, general corrosion rates for Alloy 22	Corrosion rate calculations for Alloy C22 after 5+ years exposure.	LL030412512251.057 [DIRS 163712]	Input data (Table 4-6) are used in Section 6.3.5.
Initial size of incipient cracks	Ford and Andresen 1988 [DIRS 118611]	Qualified in Section 6.2.1 per AP-SIII.10Q, Section 5.2.1.k	Input data (0.05 mm incipient flaw size) used in Section 6.2.1
Circumferential variation in weld residual stress	Structural Integrity Associates Calculation Files 2004, Calculation TRW-06Q-304	MO0409GGSIACAL.000 [DIRS 171792]	Input data (5 ksi about the mean stress) used in Section 6.4.5

Table 4-2. Measured Crack Growth Rates for Alloy 22 Specimens

Specimen	Tested Stress Intensity Factor (MPa(√m))	Measured Crack Growth Rate (mm/s)[a]	Source
c153	30	2.5×10^{-10}	DTN: LL021105312251.023 [DIRS 161253], p. 11
c153	30	5.0×10^{-10}	DTN: LL021105312251.023 [DIRS 161253], p. 11
c144	30	[b]	DTN: LL021105312251.023 [DIRS 161253], p. 7
c152	45	[b]	DTN: LL021105312251.023 [DIRS 161253], p. 10
c152	45	4.0×10^{-10}	DTN: LL021105312251.023 [DIRS 161253], p. 10

NOTE: [a] Growth rates obtained at sustained constant load or at hold times of about 1 to 24 hours.
[b] Test results indicated that either cracking appeared to cease or growth rate seemed to arrest, indicating growth rates less than 10^{-11} mm/s, the growth rate detection threshold.

Table 4-3. Coefficients of Stress Profiles for the Original and Modified CRM–21-PWR Design

Stress Coefficient	A_0 (ksi)	A_1 (ksi/in)	A_2 (ksi/in^2)	A_3 (ksi/in^3)	Source in DTN
As-Welded 25-mm Lid, Radial Stress S_x	16.871	33.5486	-294.333	264.368	File Skvrbr1, Sheet UnAnneal, S_x, Cells C9 to C12
As-Welded 25-mm Lid, Hoop Stress S_z	55.4242	29.8255	-186.269	143.597	File Skvrbr1, Sheet UnAnneal, S_z, Cells C9 to C12
As-Welded 10-mm Lid, Sn on Section 1-1	26.34	-427.51	934.32	-596.71	File Thinlid11, Sheet UnAnneal,1-1,Sn, Cells C9 to C12
As-Welded 10-mm Lid, S_z on Section 2-2	31.90	101.42	-463.23	297.75	File Thinlid11, Sheet UnAnneal,2-2, S_z, Cells C9 to C12
Laser-Peened 25-mm Lid, Radial Stress S_x	-38.5684	383.082	-922.377	603.035	File Skvrbr1, Sheet Peening, S_x, Cells C9 to C12
Laser-Peened 25-mm lid, Hoop Stress S_z	-42.4391	656.764	-1,322.67	759.752	File Skvrbr1, Sheet Peening, S_z, Cells C9 to C12

Source: DTN: LL000316205924.142 [DIRS 148895].

Table 4-4. Stress Intensity Factor (SIF) Profiles

As-Welded Outer Lid, CRM–21-PWR Design			As-Welded 10-mm Lid, Modified CRM–21-PWR Design			Outer Lid with Laser Peening, CRM–21-PWR Design		
DTN File Skvrbr1			DTN File Thinlid11			DTN File Skvrbr1		
Sheet UnAnneal, S_x (Cells A87 to A136)	Sheet UnAnneal, S_x (Cells C87 to C136)	Sheet UnAnneal, S_z (Cells C87 to C136)	Sheet UnAnneal,1-1,Sn (Cells A89 to A138)	Sheet UnAnneal,1-1,Sn (Cells C89 to C138)	Sheet UnAnneal,2-2, S_z (Cells C89 to C138)	Sheet Peening, S_x (Cells A87 to A136)	Sheet Peening, S_x (Cells C87 to C136)	Sheet Peening, S_z (Cells C87 to C136)
Crack size, mm	SIF for S_x, MPa √m	SIF for S_z, MPa √m	Crack size, mm	SIF for Sn, MPa √m	SIF for S_z, MPa √m	Crack size, mm	SIF for S_x, MPa √m	SIF for S_z, MPa √m
0.3988	4.5146	9.1593	0.2438	4.9033	7.5754	0.3988	-9.1866	-5.6943
0.8001	6.5821	12.9737	0.4902	6.2685	10.9665	0.8001	-11.7979	-6.4965
1.1989	8.2395	15.9139	0.7341	6.8580	13.7144	1.1989	-13.0189	-6.1528
1.6002	9.6422	18.4031	0.9804	6.9761	16.1330	1.6002	-13.4298	-5.1372
1.9990	10.8381	20.6048	1.2243	6.7631	18.3358	1.9990	-13.2965	-3.6697
2.4003	11.8425	22.6028	1.4681	6.3044	20.3775	2.4003	-12.7780	-1.8824
2.7991	12.8589	24.4741	1.7145	5.8250	22.3816	2.7991	-12.2958	0.1212
3.2004	13.7858	26.2367	1.9583	5.2651	24.3197	3.2004	-11.7214	2.2821
3.5992	14.5688	27.9039	2.2047	4.6000	26.1726	3.5992	-11.0116	4.5533
3.9980	15.2083	29.4912	2.4486	3.8615	27.9459	3.9980	-10.2080	6.8939
4.3993	15.7061	31.0103	2.6924	3.0726	29.6433	4.3993	-9.3437	9.2702
4.7981	16.0778	32.4703	2.9388	2.2534	31.2668	4.7981	-8.4525	11.6543
5.1994	16.4072	33.9004	3.1826	1.4282	32.8922	5.1994	-7.6096	14.0165
5.5982	16.7029	35.3092	3.4290	0.5951	34.5292	5.5982	-6.8298	16.3364
5.9995	16.8783	36.6797	3.6728	-0.2400	36.1060	5.9995	-6.0675	18.6024
6.3983	16.9527	38.0157	3.9167	-1.0656	37.6220	6.3983	-5.3416	20.8003
6.7970	16.9314	39.3202	4.1631	-1.8707	39.0762	6.7970	-4.6612	22.9177
7.1984	16.8188	40.5961	4.4069	-2.6491	40.4676	7.1984	-4.0331	24.9441
7.5971	16.7108	41.8581	4.6533	-3.4047	41.8264	7.5971	-3.4507	26.9023
7.9985	16.7482	43.1357	4.8971	-4.1787	43.2168	7.9985	-2.8535	28.8612
8.3972	16.7231	44.3927	5.1410	-4.9390	44.5479	8.3972	-2.2745	30.7287
8.7986	16.6321	45.6302	5.3873	-5.6775	45.8181	8.7986	-1.7170	32.5008
9.1973	16.4938	46.8495	5.6312	-6.3965	47.0265	9.1973	-1.1860	34.1745
9.5987	16.3042	48.0515	5.8776	-7.0865	48.1718	9.5987	-0.6829	35.7479
9.9974	16.0808	49.2372	6.1214	-7.7528	49.2531	9.9974	-0.2101	37.2200
10.3962	16.0751	50.4839	6.3652	-8.2576	50.3451	10.3962	-0.3513	38.4530

Table 4-4. Stress Intensity Factor (SIF) Profiles (Continued)

As-Welded Outer Lid, CRM–21-PWR Design			As-Welded 10-mm Lid, Modified CRM–21-PWR Design			Outer Lid with Laser Peening, CRM–21-PWR Design		
DTN File Skvrbr1			DTN File Thinlid11			DTN File Skvrbr1		
Sheet UnAnneal, S_x (Cells A87 to A136)	Sheet UnAnneal, S_x (Cells C87 to C136)	Sheet UnAnneal, S_z (Cells C87 to C136)	Sheet UnAnneal,1-1,Sn (Cells A89 to A138)	Sheet UnAnneal,1-1,Sn (Cells C89 to C138)	Sheet UnAnneal,2-2, S_z (Cells C89 to C138)	Sheet Peening, S_x (Cells A87 to A136)	Sheet Peening, S_x (Cells C87 to C136)	Sheet Peening, S_z (Cells C87 to C136)
Crack size, mm	SIF for S_x, MPa √m	SIF for S_z, MPa √m	Crack size, mm	SIF for Sn, MPa √m	SIF for S_z, MPa √m	Crack size, mm	SIF for S_x, MPa √m	SIF for S_z, MPa √m
10.7975	15.9957	51.7195	6.6116	-8.7427	51.3729	10.7975	-0.5163	39.5674
11.1963	15.8601	52.9442	6.8555	-9.2143	52.3351	11.1963	-0.7070	40.5636
11.5976	15.6646	54.1589	7.1018	-9.6605	53.2313	11.5976	-0.9242	41.4432
11.9964	15.4259	55.3639	7.3457	-10.0894	54.0602	11.9964	-1.1690	42.2086
12.3977	15.1398	56.5598	7.5895	-10.4950	54.8214	12.3977	-1.4403	42.8627
12.7965	15.0982	57.8007	7.8359	-10.9446	55.4811	12.7965	-1.7949	43.4439
13.1978	15.0836	59.0538	8.0797	-11.4131	56.0586	13.1978	-2.1728	43.9342
13.5966	15.0159	60.3022	8.3261	-11.8636	56.5637	13.5966	-2.5554	44.3269
13.9954	14.8966	61.5462	8.5700	-12.3055	56.9965	13.9954	-2.9438	44.6272
14.3967	14.7274	62.7862	8.8138	-12.7309	57.3567	14.3967	-3.3378	44.8409
14.7955	14.5229	64.0228	9.0602	-13.1320	57.6444	14.7955	-3.7396	44.9743
15.1968	14.6570	65.2900	9.3040	-13.7114	57.7587	15.1968	-4.0160	45.0329
15.5956	15.1057	66.5871	9.5504	-14.4707	57.6946	15.5956	-4.1354	45.0208
15.9969	15.4787	67.8801	9.7942	-15.2333	57.5522	15.9969	-4.2182	44.9464
16.3957	15.7929	69.1690	10.0381	-15.9891	57.3322	16.3957	-4.2696	44.8182
16.7945	16.0516	70.4537	10.2845	-16.7277	57.0353	16.7945	-4.2904	44.6449
17.1958	16.2578	71.7343	10.5283	-17.4611	56.6626	17.1958	-4.2805	44.4361
17.5946	16.6700	73.0349	10.7747	-18.4707	56.1419	17.5946	-4.3087	44.2112
17.9959	17.6878	74.4062	11.0185	-20.3589	55.3276	17.9959	-4.5204	43.9968
18.3947	18.5558	75.7773	11.2624	-22.2128	54.4422	18.3947	-4.7313	43.7750
18.7960	19.2803	77.1483	11.5087	-24.0173	53.4878	18.7960	-4.9400	43.5578
19.1948	19.8861	78.5193	11.7526	-25.7872	54.6294	19.1948	-5.1487	43.3569
19.5961	20.3775	79.8904	11.9990	-27.4989	56.2191	19.5961	-5.3536	43.1853
19.9949	20.7777	81.2616	12.2428	-29.1709	57.7865	19.9949	-5.5551	43.0560

Source: DTN: LL000316205924.142 [DIRS 148895].

Table 4-5. Input Data for Yield Strength, and Modulus of Elasticity

Input Data Name (Input DTN or Reference)	Temperature K (°C)	Input Data Value	Input Data Unit
YS (yield strength) for Alloy 22 (DTN: MO0003RIB00071.000 [DIRS 148850])	Room Temperature	372	MPa
	366 (93)	338	MPa
	477 (204)	283	MPa
YS (yield strength) for Titanium Grade 7 (DTN: MO0003RIB00073.000 [DIRS 152926])	Room Temperature	275 to 450	MPa
	477 (204)	138 to 152	MPa
E (modulus of elasticity) for Titanium Grade 7 (DTN: MO0003RIB00073.000 [DIRS 152926])	294 (21)	106.87	GPa
	366 (93)	103.42	GPa
	422 (149)	100.66	GPa

Table 4-6. 5-Year General Corrosion Rates

Sample	Rate (nm/year)		Sample	Rate (nm/year)
DCA 019	9.40		DCA 175	0.82
DCA 020	8.22		DCA 176	0.81
DCA 021	8.63		DCA 177	46.67
DCA 022	6.36		DCA 178	8.40
DCA 023	9.75		DCA 179	5.24
DCA 024	22.52		DCA 180	5.28
DCA 049	12.04		DCB 019	10.24
DCA 050	17.29		DCB 020	6.94
DCA 051	15.75		DCB 022	5.84
DCA 052	5.76		DCB 023	6.89
DCA 053	8.30		DCB 049	16.07
DCA 054	6.40		DCB 050	14.51
DCA 079	3.06		DCB 052	4.29
DCA 080	3.10		DCB 053	5.92
DCA 081	4.19		DCB 079	2.00
DCA 082	9.52		DCB 080	7.88
DCA 083	7.23		DCB 082	19.58
DCA 084	14.71		DCB 083	13.61
DCA 109	5.81		DCB 109	4.32
DCA 110	11.60		DCB 110	2.01
DCA 111	5.77		DCB 112	9.05
DCA 112	3.11		DCB 113	10.86
DCA 113	10.56		DCB 139	0.00
DCA 114	10.91		DCB 140	2.85
DCA 139	4.71		DCB 142	2.03
DCA 140	3.54		DCB 143	5.69
DCA 141	2.74		DCB 175	0.41
DCA 142	6.27		DCB 176	2.08
DCA 143	5.89		DCB 178	1.25
DCA 144	8.27		DCB 179	0.41

Source: DTN: LL030412512251.057 [DIRS 163712].

4.2 CRITERIA

According to *Technical Work Plan for: Regulatory Integration Modeling and Analysis of the Waste Form and Waste Package* (BSC 2004 [DIRS 171583], Table 3-1) the following acceptance criteria are applicable to this report:

1. *System Description and Demonstration of Multiple Barriers* (NRC 2003 [DIRS 163274], Section 2.2.1.1.3; PRD-002/T-014, PRD-002/T-016):

   - AC1–Identification of Barriers is Adequate
   - AC2–Description of the Capability of Identified Barrier is Acceptable
   - AC3–Technical Basis for Barrier Capability is Adequately Presented.

2. *Degradation of Engineered Barriers* (NRC 2003 [DIRS 163274], Section 2.2.1.3.1.3; PRD-002/T-015):

   - AC1–System Description and Model Integration are Adequate
   - AC2–Data are Sufficient for Model Justification
   - AC3–Data Uncertainty is Characterized and Propagated Through the Model Abstraction
   - AC4–Model Uncertainty is Characterized and Propagated Through the Model Abstraction
   - AC5–Model Abstraction Output is Supported by Objective Comparisons.

The criteria as they relate to the waste package and drip shield barriers are addressed in Section 8.2, which discusses locations in the report that address individual acceptance criteria related to the two primary criteria.

4.3 CODES AND STANDARDS

The following codes or standards were used to generate this report:

- 10 CFR 63 [DIRS 156605]. Energy: Disposal of High-Level Radioactive Wastes in a Geologic Repository at Yucca Mountain, Nevada
- ASTM B 575-94 [DIRS 100497]. *Standard Specification for Low-Carbon Nickel-Molybdenum-Chromium and Low-Carbon Nickel-Chromium-Molybdenum Steel Alloy Plate, Sheet, and Strip*
- ASTM G 30-94 [DIRS 137688]. *Standard Practice for Making and Using U-Bend Stress-Corrosion Test Specimens*
- ASTM E 399-90 [DIRS 117480]. *Standard Test Method for Plane-Strain Fracture Toughness of Metallic Materials*
- ASTM G 129-00 [DIRS 171563]. *Standard Practice for Slow Strain Rate Testing to Evaluate the Susceptibility of Metallic Materials to Environmentally Assisted Cracking*
- ASTM G 49-85 [DIRS 171562]. *Standard Practice for Preparation and Use of Direct Tension Stress-Corrosion Test Specimens*.

INTENTIONALLY LEFT BLANK

5. ASSUMPTIONS

No assumptions were used to perform the model activity.

INTENTIONALLY LEFT BLANK

6. MODEL DISCUSSION

6.1 INTRODUCTION

One of the most common corrosion-related causes for premature fracture (breach) of metal structural components is stress corrosion cracking. Stress corrosion cracking is the initiation and propagation of cracks in structural components due to three factors that must be present simultaneously: metallurgical susceptibility, critical environment, and static (or sustained) tensile stresses.

This discussion of stress corrosion cracking is restricted to the waste package outer barrier and the drip shield, which are made of Alloy 22 and Titanium Grade 7, respectively. The stainless steel waste package inner structural cylinder is not modeled, since the TSPA-LA does not take corrosion credit for the stainless steel inner cylinder of the waste package.

Alloy 22, the material used for the waste package outer barrier, is highly corrosion-resistant, but its susceptibility to stress corrosion cracking cannot be ignored for the test conditions that simulate the Yucca Mountain environment (Sections 6.2 and 6.3) and the coexisting stress conditions induced by welding in the closure welds of the waste package final closure lids (Section 6.4). Section 6.3.7 provides an analysis that forms the technical basis for screening out stress corrosion cracking in the drip shield.

A lifetime-modeling approach is developed to assess the degradation of the waste package outer barrier due to stress corrosion cracking. As indicated by the flow diagram shown in Figure 1-1, the lifetime modeling considers both crack initiation and preexisting manufacturing flaws (Section 6.2), the stress conditions that drive the crack initiation and propagation (Section 6.4), the stress threshold that defines the crack initiation (Section 6.2.1), the threshold stress intensity factor that defines propagation of both initiated incipient cracks and manufacturing flaws (Section 6.3.5), and the crack growth model (based on the slip dissolution–film rupture theory) that determines the crack growth rate (Section 6.3). The stress corrosion cracking model provides all the elements (as summarized in Section 8) needed to assess the effects of stress corrosion cracking on waste package outer barrier performance.

Stress corrosion cracking has historically been separated into “initiation” and “propagation” phases (Jones and Ricker 1987 [DIRS 118672], p. 146). For the purpose of lifetime modeling, it is appropriate that initiation is associated with microscopic crack formation at localized corrosion or mechanical defect sites. Coalescence of these microscopically small cracks will lead to stress corrosion cracking initiation on an otherwise ‘smooth’ surface. Initial stress corrosion cracking can also initiate at surface breaking flaws (or defects) resulting from manufacturing processes (such as welding). Crack initiation (including the threshold stress for crack initiation) and manufacturing defects are discussed in Section 6.2.

To account for crack propagation, the slip dissolution–film rupture (SDFR) model is adopted as the base-case model to provide mathematical formulas for the prediction of crack growth rate. The SDFR model relates the advance (or propagation) of cracks, subsequent to crack initiation at the bare metal surface, to the metal oxidation that occurs when the protective film at the crack tip is ruptured. The SDFR stress corrosion cracking model is described in Section 6.3. A crack, however, may reach an “arrest” state after it enters the “propagation” phase. A threshold stress

intensity factor (SIF) exists that provides a criterion for determining if an initiated crack or preexisting flaw will reach the "arrest" state. The threshold SIF is based on the theory that below a threshold value (K_{ISCC}) for the stress intensity factor, K_I, no growth occurs for a given crack. K_{ISCC} is discussed in Section 6.3.5 and the determination of the weld-induced stress and K_I profiles through the waste package wall are described in Section 6.4. The threshold stress, threshold stress intensity factor, and parameters associated with the SDFR crack growth model are determined from experimental data developed for environments relevant to the waste package and drip shield materials used in the repository.

An alternative conceptual model, the coupled environmental fracture (CEF) model, was developed for the case where the internal and external environments are coupled by the need to conserve charge in the system. The CEF model represents an alternative approach to the base-case SDFR model for the prediction of the crack growth rate. It is considered only for the purpose of validation of the base-case model. The CEF model and the technical basis for screening out this model are discussed in Section 6.3.6.

The base-case SDFR and the alternative CEF models were initially developed to account for stress corrosion cracking of sensitized Stainless Steel Type 304 (i.e., stainless steel exposed to higher temperatures that make the grain boundaries more susceptible to corrosion). An evaluation of other stress corrosion cracking models for sensitized stainless steel indicates a weaker theoretical basis for these models (Macdonald and Urquidi-Macdonald 1991 [DIRS 162702]). Therefore, no additional alternative conceptual models for stress corrosion cracking are considered.

Output parameters associated with the base-case crack growth models developed are used as one input to the TSPA-LA. A summary of the various generated outputs is presented in Section 8.

6.2 CRACK INITIATION AND MANUFACTURING FLAWS

6.2.1 Threshold Stress for Initiation of Stress Corrosion Cracking

For a given alloy, metallurgical condition, set of environmental conditions, and in the absence of cyclic stresses, initiation of stress corrosion cracking will not occur on a "smooth surface" (without sharp defects such as weld defects that can generate a significant stress intensity factor) if the surface stress is below a threshold value defined as the threshold stress (ASM International 1987 [DIRS 103753], Vol. 13, p. 276). Stress corrosion cracking crack initiation measurements under constant load conditions reported in DTN: MO0409GE835924.000 [DIRS 171564] are summarized in Figure 4-1. These constant load tests were performed in general conformance with ASTM G 49-85 [DIRS 171562], but modified as indicated in DTN: LL021105312251.023 ([DIRS 161253]), Section 2.2). The crack initiation stress measurements are presented as applied stress ratio (the ratio of applied stress to yield strength) versus time-to-failure (or total exposure time without failure) for specimens subjected to over 21,000 hours of exposure in hot concentrated and aerated salt solution (pH=10.3 at 105°C), known as Basic Saturated Water (BSW), (DTN: LL021105312251.023 [DIRS 161253], Sections 2.2 and 2.5). As indicated in the note on Figure 4-1, the BSW was diluted to about 15% of full concentration to simulate the chemistry of concentrated Yucca Mountain ground water. The results shown in Figure 4-1 confirm and extend previously reported test results (DTN: LL021105312251.023 [DIRS 161253]) indicating that Alloy 22 exhibits excellent stress

corrosion cracking resistance since failure has not been observed for any of the 120 Alloy 22 specimens covering a variety of metallurgical conditions (including as-welded). The applied stress ratios were up to about 2.1 times the yield strength (YS) of the as-received material and up to 2.0 times the yield strength of the welded material. This stress ratio corresponds to an applied stress of about 89% to 96% of the measured ultimate tensile strength (DTN: LL021105312251.023 [DIRS 161253], Table 2-4).

These 120 constant load stress corrosion cracking initiation test specimens include both 'smooth surface' specimens and notched specimens with the notches located in either weld metal or in the weld heat affected zone (DTN: LL021105312251.023 [DIRS 161253], Figures 2-19 through 2-22 for notch details). They also encompass a range of different microstructures or metallurgical conditions, including the annealed condition (solution annealed at a high temperature and rapidly cooled); the as-welded condition, including weld metal and heat affected zone; the annealed plus thermally aged condition (i.e., heated in a temperature range where potentially deleterious precipitates can form) that produces extensive topologically (or tetrahedrally) close-packed (TCP) precipitation (700°C/175 h), the annealed plus thermally aged condition to produce long-range ordering (520°C/1,000 hr), and the cold-worked condition (20% coldwork) with and without thermal aging (700°C/175 hr). The various constant load test conditions evaluated were provided in Figure 4-1 and a more detailed description and a series of optical and SEM photomicrographs of the various microstructures are presented in DTN: LL021105312251.023 [DIRS 161253].

Findings summarized in *Aging and Phase Stability of Waste Package Outer Barrier* (BSC 2004 [DIRS 171924]) are consistent with the thermal aging conditions evaluated in these constant load tests being highly conservative. *Aging and Phase Stability of Waste Package Outer Barrier* (BSC 2004 [DIRS 171924], Section 8) concludes that the "…formation of TCP or ordered oP6 phases in Alloy 22 base metal and welds (which are deemed to be similar to base metal) will not be a concern for conditions of less than 300ºC for a period of 500 years followed by temperatures less than 200°C for a period of 9,500 years, conditions that bound the repository time-temperature profiles. To be conservative, the constant load test matrix included the two previously described thermal aging conditions to represent TCP and long-range ordering conditions. Based on *Aging and Phase Stability of Waste Package Outer Barrier* (BSC 2004 [DIRS 171924], Figure 91), the TCP heat treatment of 700°C/175 hr results in a grain boundary coverage fraction of about 100% and from Table 10 of the same reference (BSC 2004 [DIRS 171924]) a similar long-range ordering heat treatment at a somewhat higher temperature than the 520°C used for the test (i.e., 550°C/1,000 hr) results in an increase in Alloy 22 mircohardness from an as-received value of 217 Hv to an as-aged value of 329 Hv. This increase in hardness is consistent with the measured increase in yield strength (DTN: LL021105312251.023 [DIRS 161253], Table 2-4) noted for this Alloy 22 plate material (from 47 ksi (324 MPa) for the as-received Alloy 22 material to 70 ksi (483 MPa) for the long-range ordering heat-treated material).

The high degree of stress corrosion cracking initiation resistance for Alloy 22 determined with the constant load tests described above is corroborated by results of high magnification visual examination of a number of Alloy 22 U-bend specimens (fabricated and tested per ASTM G 30-94, [DIRS 137688]). The specimens were exposed at the Lawrence Livermore National Laboratory (LLNL) long-term corrosion test facility to a range of relevant aerated brine

environments at 60°C and 90°C (Fix et al. 2003 [DIRS 162700], p. 1). No evidence of stress corrosion cracking initiation has been observed in these U-bend specimens after five years of exposure. According to Fix et al. (2003 [DIRS 162700], p. 3):

> U-bend specimens chosen for laboratory testing contained residual stresses due to permanent deformation. The U-bend specimens were machined from sheet stock. The specimens were tested in the as-machined condition, which corresponded to a root mean square (RMS) roughness of 32 μ-inch. The specimens were degreased in acetone before testing. The U-bend specimens were prepared using ¾-inch (~19 mm) wide and 1/16-inch @1.6 mm) thick strips according to ASTM G 30. The resulting specimen had a constant nominal separation between both legs, or ends, of 0.5 inch (~13 mm) secured by a bolt, which was electrically insulated from the specimen through ceramic zirconia washers. The total plastic deformation in the external outer fiber of Alloy 22 was approximately 12%.

Single U-bends were produced using wrought sheets and welded sheets. In the welded specimens, the weld was across the apex of the bend. The weld process was gas metal arc welding (GMAW) using matching filler metal and the seam had full penetration. Table 6-1 lists the chemical composition of the sheet material and the filler metal used for the fabrication of the U-bend specimens.

Table 6-1. Chemical Composition of the Studied Alloy 22 Heats (wt %)

	SINGLE U-BEND	WELD FILLER METAL	SSRT
Element	**(Heat 2277-0-3264)**	**(Heat 2277-4-3263)**	**(Heat 2277-8-3126)**
C	0.004	0.002	0.004
Co	1.14	0.89	1.03
Cr	21.3	21.6	21.70
Fe	4.4	3.6	3.59
Mn	0.29	0.32	0.27
Mo	13.4	13.5	13.26
Ni	~56	~56	~5
P	0.01	0.009	0.006
S	<0.002	0.003	0.001
V	0.17	0.15	0.14
W	2.9	2.9	2.80

Source: Fix et al. 2003 [DIRS 162700], Table 2.

Additional corroboration of the very high threshold stress for stress corrosion cracking initiation is provided by a series of slow strain rate tensile tests (SSRT) performed in general conformance to ASTM G 129-00 [DIRS 171563] and over the range of potentially relevant and accelerated environments (Estill et al. 2002 [DIRS 167274]; King et al. 2004 [DIRS 170981]). These slow strain rate tests were performed on mill annealed Alloy 22 (alloy heat composition listed in Table 6-1) at 22°C to 120°C, and at a strain rate of 1.66×10^{-6} per second. Because the SSRT specimen is subjected to continuously increasing strain until failure, the test does not generally give a direct measure of the threshold stress for stress corrosion cracking initiation. Even though stress corrosion cracking may initiate during the test, it is usually not evident at that precise point

in the test. However, the absence of stress corrosion cracking in this test is consistent with the material being a stress corrosion cracking resistant material with a high threshold stress.

These Alloy 22 SSRT results for specimens tested at E_{corr} and above (i.e., anodically polarized) are summarized in Table 6-2. This table contains a consolidated compilation of results obtained from (Estill et al. 2002 [DIRS 167274], Table 6) and (King et al. 2004 [DIRS 170981], Table 2). The test data cover a broad range of relevant and potentially accelerated environments, with and without lead additions or anodically applied potential. Examination of the tabulated results confirm the expected high degree of stress corrosion cracking resistance at open-circuit potentials in environments evaluated, including approximately 8.5 M (saturated) $CaCl_2$-type brines (pH ~4) at 120°C, as well as 1% lead chloride solutions (pH ~4) at 95°C. The only two evaluated environments in which stress corrosion cracking initiation was or may have been observed were 1) simulated concentrated water (SCW) with an applied potential of 200 to 400 mV versus SSC, which is significantly above the corresponding open-circuit corrosion potential of between −76 and −241 mV versus SSC, and 2) 1M NaF at 90°C and polarized to +400 mV versus SSC versus an E_{corr} of –244 mV versus SSC. SCW is a concentrated (~1,000-fold) version of J-13 ground water with a pH of ~9-10 and pure 1M NaF with a pH = 7.6 is an accelerated and not directly relevant environment. Clearly, as described earlier, these results, in which the specimens are slowly pulled to the fracture stress, are consistent with the very low susceptibility of Alloy 22 to stress corrosion cracking. Even under these highly accelerated conditions (SCW at 90°C and at the high applied potential of 400 mV versus SSC), the stress at which the onset of stress corrosion cracking was first detected, using a sensitive acoustic emission monitoring technique, corresponded to an applied stress of 605 MPa, which is 156% of the room temperature yield strength for this Alloy 22 plate material (Fix et al. 2003 [DIRS 162700]). Although this acoustically determined, high stress corrosion cracking onset stress (and correspondingly high strain value) does not necessarily measure the initiation stress under the highly accelerated conditions, it is consistent with the threshold initiation stress being very high for this material.

With respect to the slow strain rate tests (SSRT), a given strain rate (actually, cross-head motion rate) is imposed on these specimens, and once stress corrosion cracking initiates, the crack growth rate is partially governed by the imposed strain rate that is much faster than the measured growth rates for Alloy 22 using valid compact tension specimens (loaded per ASTM E 399-90 [DIRS 117480]). Thus, these SSRT data were not used to generate crack growth rates in development of the stress corrosion cracking crack growth rate model (Section 6.3.4), as they are not representative. However, the SSRT results for the case where lead additions were evaluated are discussed in Section 6.3.4.

To further corroborate the high degree of resistance to stress corrosion cracking initiation indicated by the slow strain rate tests (SSRT), two Alloy 22 U-bend specimens (one annealed and one as-welded) were exposed for 28 days to 90°C SCW while polarized to +400 mV [SSC]. At this high potential, incipient stress corrosion cracking was observed under the severe, continuous straining condition in the SSRT case (Fix et al. 2003 [DIRS 162700]). Stereomicroscopic examination of these U-bend specimens following this exposure revealed no evidence of stress corrosion initiation consistent with the high degree of resistance of Alloy 22 to stress corrosion cracking.

Table 6-2. Slow Strain Rate Test Results for Annealed Alloy 22 (Strain Rate of 1.66×10^{-6} Per Second)

Specimen ID	Test Environment	Temperature (°C)	E_{corr} (mV versus SSC)	$E_{Applied}$ (mV versus SSC)	Time to Failure of the Specimen (hours)	Maximum Stress (MPa)	Reduction in Area (%)	Observation
012	Air	22	None	None	124	786	74	Ductile necking
040	Air	22	None	None	123	813	70	Ductile necking
098	1M NaCl at pH = 6.9	90	-104	+400	74 [b]	660	76	No SCC
123	4M NaCl at pH = 6.2	98	−323	+349	127	762	80	No SCC
091	1M NaF at pH = 9.2	85	133	E_{corr}	112	756	67	No SCC
130	1M NaF at pH = 7.6	90	-244	+400	112	727	67	Incipient SCC
004	8.5M $CaCl_2$ at pH ~ 6	120	−140 to −180	E_{corr}	127	752	71	No SCC
013	1% $PbCl_2$ at pH ~ 4 Aerated	95		E_{corr}	126	765	72	No SCC
015	SAW at pH ~ 3	63	−7 to +360	E_{corr}	118	758	79	No SCC
016	SAW at pH ~ 3 + 0.005% $Pb(NO_3)_2$	76	−6 to +370	E_{corr}	124	772	74	No SCC
017	SAW at pH ~ 3 + 0.005% $Pb(NO_3)_2$	76	0 to +350	E_{corr}	125	772	74	No SCC
003	SAW at pH ~ 3 + 0.005% $Pb(NO_3)_2$	95	−90 to +400	E_{corr}	118	752	85	No SCC
127	BSW at pH ~ 13 - $[NO_3 + SO_4]$ [a]	98	−240 to −220	E_{corr}	123	745	72	No SCC
124	BSW at pH ~ 13 - $[NO_3 + SO_4]$ [a]	105	−330	+100	120	745	78	No SCC
122	BSW at pH ~ 13 - $[NO_3 + SO_4]$ [a]	98	−245	+200	122	752	72	No SCC
120	BSW at pH ~ 13	105	−323	+400	99	745	74	No SCC
119	BSW at pH ~ 13	105	−301	+400	118	745	75	No SCC
115	BSW at pH ~ 13 - $[NO_3]$ [a]	105	−335	+400	115	752	77	No SCC
129	BSW at pH ~ 13 - $[SO_4=]$ [a]	105	−314	+400	119	731	82	No SCC
125	SSW at pH ~ 6	100	−154	+400	113	717	71	No SCC
020	SCW at pH ~ 9 to 10	22	−109	+400	116	800	85	No SCC
133	SCW at pH ~ 9 to 10	22	-128	+400	124	798	80	No SCC
032	SCW at pH ~ 9 to 10	50	-129	+400	110	757	75	Incipient SCC
134	SCW at pH ~ 9 to 10	65	-217	+400	97	684	59	SCC
112	SCW at pH ~ 9 to 10	73	−93	+400	91	697	71	SCC
021	SCW at pH ~ 9 to 10	73	−172	+400	90	665	64	SCC
033	SCW at pH ~ 9 to 10	86	-169	+400	76	642	44	SCC
113	SCW at pH ~ 9 to 10	75	-200	+317	116	765	63	Incipient SCC
030	SCW at pH ~ 9 to 10	85	-182	+300	98	725	65	SCC
020	SCW at pH ~ 9 to 10	22	-109	+291	116	800	85	No SCC
023	SCW at pH ~ 9 to 10	73	-224	+200	DNB	DNB	72	Incipient SCC
025	SCW at pH ~ 9 to 10	73	-172	+200	116	776	80	Incipient SCC
029	SCW at pH ~ 9 to 10	89	-144	+200	112	678	73	Incipient SCC
026	SCW at pH ~ 9 to 10	73	−241	+100	120	764	79	No SCC
037	SCW at pH ~ 9 to 10	22	-76	E_{corr}	DNB	DNB	32	No SCC
034	SCW at pH ~ 9 to 10	90	-143	E_{corr}	129	712	80	No SCC

Source: Estill et al. 2002 [DIRS 167274]; King et al. 2004 [DIRS 170981].

NOTE: DNB = did not break-equipment stoppage; SAW = simulated acidified water; BSW = basic saturated water; SCW = simulated concentrated water; SSW = simulated saturated water; SCC = stress corrosion cracking.
[a] BSW without the presence of nitrate or sulfate, or both;
[b] short time to failure due to crevice corrosion at coating interface

As indicated in Figure 4-1, Titanium Grade 7 was more susceptible to stress corrosion cracking initiation as indicated by specimen failures at applied stress ratios of about 1.1 to 1.4 times the yield strength in the constant load tests. Some specimens failed relatively early (≤168 hours) at applied stresses above 110% of yield strength but, at 110% of yield strength, there was a mixture of failure and nonfailure runout times from ~200 hours for first failure to at least several thousand hours without failure. This is consistent with a runout stress somewhat less than 110% of yield strength and is estimated to be at or slightly above the yield strength value. A threshold value near or slightly above the yield strength is also consistent with the observation that no stress corrosion cracking initiation was detected in a number of fixed deflection Titanium Grade 7 U-bend test specimens exposed for two years and Titanium Grade 16 (an analogous titanium–palladium alloy) specimens exposed for five years to a range of relevant environments at 60°C and 90°C (Fix et al. 2004 [DIRS 169321]). These U-bend specimens were bent ~180 degrees and then the legs were restrained to give an apex strain (cold-work level) of greater than about 10% that resulted in sustained stress levels near or somewhat above the yield strength (YS).

As the above stress corrosion cracking initiation test results are for exposures out to five years, an extrapolation scheme is necessary in order to derive a defensible threshold stress value associated with the lifetime of waste packages and drip shields from the available experimental results. The threshold stress may be derived from the minimum failure stress (or runout stress without failure) obtained from the constant load test results described in Figure 4-1 (i.e., 2.0 (YS) for Alloy 22 and 1.1 (YS) for Titanium Grade 7) by applying an appropriate safety factor with the resulting threshold stress limited to no greater than the yield strength. This approach results in threshold stress values of 0.9(YS) for Alloy 22 and 0.5(YS) for Titanium Grade 7 using a stress reduction factor (or safety factor) of 2.2. A safety factor of 2.0 has often been used in general engineering practice. For example, the American Society of Mechanical Engineers (ASME) (ASME 1969 [DIRS 162446], p. 20) uses a reduction factor of 2 on the runout stress (endurance limit) for defining fatigue lifetime cycles. The safety factor of 2.2 used for the threshold stress is consistent with and somewhat more conservative than the ASME practice. The YS values of Alloy 22 and Titanium Grade 7 are listed in Table 4-5. For conservative purposes the YS value at the maximum temperature is used. The estimated temperature is 200°C (with YS approximately 285 MPa) for the waste package (Section 6.3.4) and 140°C (with YS approximately 221 MPa) for the drip shield (Section 6.3.7).

As described above, the development of a threshold stress criterion is based primarily on uniaxial test data plus results obtained on U-bend specimens under a biaxial stress state. In contrast, design calculations that determine the integrity of components under expected loading conditions generally result in stress outputs described in terms of multiaxial stress components. The application of the multiaxial stress condition (e.g., using a result from a three-dimensional finite element model) to assess the potential for crack initiation and through-wall crack propagation in a component is consistent with the failure theory used by the ASME, which uses the Tresca criteria (maximum shear stress theory) as the failure basis and allows for comparison of multiaxial stresses with allowable stresses that were generated from uniaxial test results (Bernstein 1988 [DIRS 164860], p. 436).

For example, the prediction of stress-strain behavior in sophisticated elastic–plastic analyses (i.e., at high stress and strain values where permanent deformation occurs) typically uses the equivalent effective stress–strain approach and uniaxial material stress–strain data to assess

multiaxial stress conditions. In order to apply the uniaxial stress-strain information to multiaxial conditions, principal stresses are used. This approach considers that a combination of stresses can be equivalent to a uniaxial condition. Even in a uniaxial stress–strain test (where failure typically occurs along the 45-degree plane, in pure shear), the cross sections that are not perpendicular to the load line are in a multiaxial stress condition that is equivalent to the uniaxial condition. These multiaxial stress states can be observed using Mohr's circle (Timoshenko and Goodier 1951 [DIRS 122064], p. 14). Thus, the use of uniaxial stress-strain curves for multiaxial loading conditions is acceptable when used in combination with principal stresses determined from the stress analyses.

Stress corrosion cracking initiation can be treated as microscopic crack formation due to the repetitive process of passive film rupture at slip sites followed by a dissolution transient until passivation recurs (Section 6.3). According to Averbach (1968 [DIRS 164859], pp. 449 to 455), these microcrack formations are due to the plastic flow in the local state; yielding occurs by slip or twin formation; and these slip or twin formations occur in the plane that is subjected (and perpendicular) to the maximum stress.

By analogy to the theories and criteria used in structural type evaluations, initiation test data under the uniaxial test condition could be used to determine the initiation threshold under the triaxial stress state. The data can be used because the slip and twin formations occur perpendicularly to the maximum stress plane.

Threshold stress intensity factor is another established method of preventing crack propagation. In this case, crack propagation will not occur if the applied stress intensity factor remains below a threshold value (K_{ISCC}) (Section 6.3.5). The stress intensity factor is a direct function of the stress perpendicular to the crack plane. Thus, it is a function only of the stress perpendicular to a specific plane and similar to looking at uniaxial test data (for the same stress at the specific plane location).

In conclusion, the use of uniaxial test data to predict crack initiation and failure for a multiaxially loaded component is consistent with engineering practice.

Density of Incipient Cracks–In a commercial metal alloy, there is a relatively high density of potential incipient surface cracks associated with microscopic discontinuities (e.g., precipitates, grain boundaries, passive film rupture sites, etc.). The surface of the waste package is divided into many subdivisions, referred to as patches, in the performance assessment. Patch size in terms of width and length is determined by the size of the closure weld as well as the stress distribution in and near the weld as through-wall cracking can only occur in the closure weld region. In any given surface location where the principal tensile stress above the threshold value exists, multiple cracks may initiate and grow together, but only one becomes predominant. As discussed in Section 6.5.1, the minimum spacing between parallel through-wall radial cracks must be greater than the plate thickness for the stress (and resultant stress intensity factor) to be sufficient to drive a flaw through-wall.

Incipient Crack Size–Environmental cracking has historically been separated into "initiation" and "propagation" phases (Jones and Ricker 1987 [DIRS 118672], p. 146). Although the particular crack depth defining the separation of the two phases is arbitrary, when the stress exceeds the stress corrosion cracking threshold stress (for the purpose of lifetime modeling), the

initiation crack size (associated with microscopic crack formation at localized corrosion or mechanical defect sites) is taken as 0.05 mm as developed by Ford and Andresen (1988 [DIRS 118611], p. 798; Andresen 1991 [166965], Figures 39 to 41). Thereafter, the crack may either reach the arrest state or the "propagation" phase once the crack tip stress intensity factor exceeds the threshold K_{ISCC} value. Incipient crack size is one of the intrinsic properties of a material related to susceptibility to stress corrosion cracking. Demonstration that the initial size (0.05 mm or 50 microns) is suitable for intended use is based on the data evaluation criteria specified in the data qualification plan in Appendix A, which requires that one or more of the following factors (AP-SIII.10Q, Section 5.2.1.k) be used as is done here using all four factors:

- Reliability of data source—The initial size (0.05 mm) is based on expert observation documented in a technical paper (Ford and Andresen 1988 [DIRS 118611]) published in a refereed and peer-reviewed publication (i.e., Proceedings of the Third International Symposium published by the Metallurgical Society, Warrendale, Pennsylvania).

- Qualifications of personnel or organizations generating the data—General Electric Global Research Center researchers Ford and Andresen (1988 [DIRS 118611]), have more than 20 years experience in the field of stress corrosion cracking with international reputations.

- Prior use of the data—In addition to the data used by Ford and Andresen (1988 [DIRS 118611]), the initiation flaw size of 0.05 mm (or 50 microns) was also used as the upper range of the initiated crack size by Ford (1996 [DIRS 167203], p. 377), another technical paper published in a refereed and peer-reviewed publication (i.e., *Corrosion*, published by NACE International, Houston, Texas).

- Availability of corroborating data—Corroborating data is available in NRC NUREG/CR-5864 (Harris et al. 1992 [DIRS 168053], p. 3-8), where the size of initiating cracks was measured as 10^{-3} in. (~0.0254 mm or 25.4 microns). Compared to this value, the use of 0.05 mm (or 50 microns) as the crack size for incipient cracks is clearly conservative.

6.2.2 Manufacturing Flaws

6.2.2.1 Flaw Size and Flaw Density Distribution

Flaw size and flaw density distributions are addressed in *Analysis of Mechanisms for Early Waste Package/Drip Shield Failure* (BSC 2004 [DIRS 170024], Section 6.2.1).

The welding process for the waste package final closure weld is a gas tungsten arc welding process (CRWMS M&O 1996 [DIRS 124950], p. 5). Selection of this process is fully consistent with the recommendations resulting from an expert evaluation of a range of potential closure welding processes (Lundin 2002 [DIRS 161780]). This evaluation concluded that the cold wire feed gas tungsten arc welding process should be selected for the waste package final closure weld process to be implemented in a hot cell. This process was recommended primarily for its ability to provide high quality closure weld joints with optimum control of the welding variables. The process produces welds that can be readily inspected by automated and remote methods (Lundin 2002 [DIRS 161780]). According to Lundin (2002 [DIRS 161780]):

> The choice of the GTAW [gas tungsten arc welding] process also naturally limits and defines the size and other characteristics of the discontinuities that can be induced during welding. Further, the weld face is optimally contoured for ready inspection by remote visual methodologies. The discontinuities generated by GTAW are well defined and include lack of penetration, lack of fusion, porosity, and microfissuring. It is also possible to form defects such as tungsten inclusions, caused by the flaking of the tungsten electrode. The extent of any of the discontinuities noted above will be related to a single weld pass and do not have a tendency to propagate between passes during welding. Thus, they are of a nature, which naturally limits their size and orientation within the weld. Since the possible generation of discontinuities during welding is limited to the types indicated above, they are readily amenable to detection by remote and automated inspection using eddy current, ultrasonic and visual methods. With a prior knowledge of the type and orientation of any discontinuities, the non-destructive examination (NDE) processes most capable for detection and sizing of the discontinuities can be defined.

As the volumetric ultrasonic inspection method is employed as the primary flaw detection method for post-weld inspections, there should be no significant undiscovered subsurface defects for these welds. Additionally, eddy current or surface wave type ultrasonic inspections are planned for evaluating the surface of the weld to detect and repair any surface breaking defects. The lack of fusion defect is, by definition, oriented in the direction of the weld bead. The tungsten inclusion and porosity defects tend to be smaller rounded defects that have no effective directionality.

Consistent with the above discussion, the expected type, size and orientation of defects that can result from the gas tungsten arc welding process are supported by a recent weld defect evaluation study in which 16 full-diameter 21-PWR waste package Alloy 22 closure weld mockup ring specimens were fabricated using a prototypical gas tungsten arc welding process under conditions that simulated hot cell type access restrictions (Smith 2003 [DIRS 163114], Section 2.3). Weld defects present in these rings were examined by various NDE techniques, including liquid penetrant and eddy current surface examinations and volumetric radiographic and ultrasonic examinations (Smith 2003 [DIRS 163114], Section 3). These were followed by metallographic destructive examination (Smith 2003 [DIRS 163114], Section 4). Information gathered from these weld mockup experiments was used to develop a flaw density, orientation, and size distribution applicable to the closure welds of the waste package (BSC 2004 [DIRS 170024], Section 6.2.1). As stated in *Analysis of Mechanisms for Early Waste Package/Drip Shield Failure* (BSC 2004 [DIRS 170024]), the flaw detection and repair-size criterion is 1/16 inch or 1.6 mm as compared to the somewhat more sensitive 1-mm ultrasonic inspection defect detection threshold used for the weld mockup study. The 1-mm ultrasonic inspection defect detection threshold was confirmed by metallographic examinations, which verified the presence of eight defects (BSC 2004 [DIRS 170024], pp. 19 to 20) detected by ultrasonic and confirmed by metallography. The ultrasonic dimensions were consistent with or slightly overestimated, the metallographically measured dimensions (BSC 2004 [DIRS 170024], p. 12). Imperfections uncovered by metallographic examinations but not detected by ultrasonic inspections were gas bubbles, with the majority less than 0.003 inch (approximately 0.08 mm) in diameter (BSC 2004 [DIRS 170024], p. 20). Gas bubbles are spherical (BSC 2004 [DIRS

170024], p. 20) and are not sharp cracks that can propagate due to stress corrosion cracking (Andresen and Ford 1985 [DIRS 162528], p. 20). Crack initiation on the bubble surface due to stress concentration is ruled out, as weld-induced tensile stress at and near the waste package surface is mitigated. All flaws found in the mockup specimens were in the weld metal and root of the weld. The flaws were characterized as lack of fusion and were oriented parallel to the hoop-stress direction in each case (Smith 2003 [DIRS 163114], Sections 5.1 and 7). Based on the results of this 16-weld mockup ring study, the defect size and orientation distributions were determined and reported (BSC 2004 [DIRS 170024]).

The initial weld flaw size distribution is exponentially distributed with an upper-bound truncation due to the weld thickness. The size distribution parameter is uncertain and described by a gamma distribution (BSC 2004 [DIRS 170024], Section 6.2.1.1.1, Equation 2). Flaws are uniformly distributed spatially and their occurrence frequency represented by a Poisson distribution. The mean flaw density (Poisson distribution parameter) of the closure weld region is uncertain and described by a gamma distribution (BSC 2004 [DIRS 170024], Section 6.2.1.1.2, Equation 12). These densities were derived from analysis of the defects observed in 16 welded rings subjected to ultrasonic tests.

These weld flaw characteristics are representative of those to be expected in the noninspected weld. An ultrasonic inspection is performed in the shop for fabrication welds and in the site closure cell for waste package final closure lid welds to detect and repair the flaws that would affect the waste package performance. Consideration of this fact is modeled by use of a probability of nondetection curve to derive postinspection flaw size and density distributions (BSC 2004 [DIRS 170024], Equations 24 and 28).

6.2.2.2 Embedded Flaws

As general corrosion proceeds, embedded flaws can become surface breaking flaws. Consideration of preexisting surface breaking flaws only may not be conservative. As an alternative conservative approach, the fraction of flaws considered for propagation is increased by adding a fraction of the flaws embedded within the entire thickness region of the weld in the performance assessment. The fraction of surface breaking flaws is increased by adding the fraction of flaws embedded within the one-quarter-thickness region of the weld surface. This is conservative as, based on the mean general corrosion rate of 7.23 nm/yr (Section 6.3.5), it will take 864,400 years to remove the one-quarter thickness of the surface of the outer lid or 345,800 years to remove the one-quarter thickness of the surface of the middle lid.

6.2.2.3 Radial Crack versus Circumferential Crack in Waste Package Closure Welds

The defect description and orientation distribution obtained from the 16-ring study (BSC 2004 [DIRS 170024]) is consistent with Shcherbinskii and Myakishev (1970 [DIRS 149953]) who describe a statistical treatment of weld flaw orientations based on analysis of a significant data set of ultrasonic flaw orientation measurements and concludes that planar type weld defects detected ultrasonically tend to be predominately oriented in the direction of the weld center line. More than 98% of the defects fall within ±16 degrees of the weld center line in the case of steam pipe welds (e.g., the tails of the distributions fall to less than 2% probability as the azimuth approaches 90 degrees) (Shcherbinskii and Myakishev 1970 [DIRS 149953], Figure 1). A similar conclusion, drawn from the data for plate welds (Shcherbinskii and Myakishev 1970

[DIRS 149953], Figure 2), indicates that the statistical distribution of defects with respect to the orientation angle approximated by a centered normal distribution with a maximum standard deviation of 5 degrees yields a probability of 99% that the defects are located within about ±13 degrees. These data suggest that much less than 1% of these flaws have a potential to undergo stress corrosion cracking as radial cracks. There is an obvious typographical error in Shcherbinskii and Myakishev (1970 [DIRS 149953]) in Figures 1 and 2 of that reference. This reference is an English translation of a Russian publication. The frequencies given as 1.8 and 2.5 Hz in these figures should read 1.8 and 2.5 MHz, which is typical of those used in ultrasonic testing. However, this apparent mistranslation has no effect on the conclusion drawn from this paper.

As discussed above, manufacturing defects, especially those due to welding, would likely be oriented along the weld direction. When initiated, the propagation of cracks tends to follow the direction perpendicular to the maximum principal stresses, whether the cracks are propagating due to fatigue or stress corrosion. In structures where shear stress is not significant (i.e., thin wall pipes or plates), the maximum principal stresses are the same as the three directional component stresses. Thin wall pipes are usually defined by a radius-to-wall-thickness ratio greater than 10. For an axisymmetric structure or model, there is no shear stress in the in-plane direction. The hoop (circumferential) stress is usually the most dominant stress component and the stress in the through-wall direction (which would drive laminations) is usually the lowest among the three stress components. A typical example is a cylindrical shell subjected to internal pressure loading.

Due to the orthogonality effect of stresses, once an oblique-oriented crack (measured with respect to the direction of loading) turns into the direction perpendicular to the maximum stress, the stresses in the other directions have little effect in turning the crack from that direction. Thus, oblique-oriented flaws turning to become perpendicular to the maximum stress cannot be ruled out. However, once this occurs, the orientation will not change. Likewise, a radial flaw, which is already oriented perpendicular to the maximum (hoop) stress, will remain radially oriented.

In addition, cracks tend to propagate in the direction that offers the least resistance. If a crack initiates at the bottom of the weld, near or in the heat affected zone, it tends to propagate in the heat affected zone, parallel to the fusion line between the weld and base metal instead of turning into the base metal at an oblique angle. Therefore, any crack, initiated and oriented in any direction at its very early stage, would adjust its direction and tend to align and propagate in the hoop or circumferential orientation, whichever results in the largest stress intensity factor.

Based on the flaw orientation measurement data provided by Shcherbinskii and Myakshev (1970 [DIRS 149953]), there is a strong dependence of the flaw orientation on the direction of welding. This is consistent with the expected behavior that most defects are associated with the application of the weld metal and would tend to be oriented along the interface of deposited beads. Although it is unlikely that flaws are observed at significant oblique angles to the direction of the weld travel direction, this circumstance cannot be entirely ruled out. Depending on the quality of the welds and welding procedures, a more uniform distribution with regards to angular orientation may be obtained. However, very tightly controlled ASME/AWS and NDE processes will be in place when the waste package closure weld is produced. If flaws were

present that make a significant oblique angle with the direction of the weld placement, it would not be surprising to see the flaw direction turn towards the radial direction.

The potential for flaws turning or not turning towards the radial direction can be studied by determining the stress intensity factor for a crack in a plate with an angle, θ, to the direction of the load, subjected to a constant stress. As an example, for an arbitrary stress and crack length, the ratio of the stress intensity factor for a flaw at an angle, θ, with the direction of the load to the stress intensity factor oriented perpendicular to the stress direction (maximum stress intensity factor) can provide some insight to the expected behavior of flaws. Figure 6-1 shows the ratio ($\sin(2\theta)$) with respect to the angle that the flaw makes with the direction of the load. The analyses in the figure are based on the solutions presented in *The Stress Analysis of Cracks Handbook* (Tada et al. 2000 [DIRS 167756], p. 127). The results of this calculation demonstrate that for a circumferentially oriented flaw in the waste package closure welds subjected to hoop stress, the stress intensity factor would be very low. Thus, the ratio of the stress intensity factor for a circumferential flaw oriented at a small angle to the load direction subjected to hoop stress to that of a radial flaw oriented perpendicular to the load is very low. The ratio is 0.03 and 0.05 for flaws at 5 and 10 degrees to the load direction, respectively. This demonstrates a very low driving force for the crack to change orientation from circumferentially oriented to radially oriented. This same circumferential flaw would be oriented close to 90 degrees (perpendicular) to the radial stress. Figure 6-1 shows that the ratio of the stress intensity factors is at least 95% of a flaw perpendicular to the load direction ($\theta = 90°$). Thus, there is a significant driving force to keep the flaw in its circumferential direction. Combined with the presence of the heat-affected zone, it is unlikely that these flaws would become radial.

Combining the test results regarding flaw orientation from Shcherbinskii and Myakshev (1970 [DIRS 149953]) and the stress intensity factor ratio discussed above, it is concluded that the probability of an expected circumferentially oriented flaw becoming radial is very small. Only flaws that are oriented at angles greater than approximately 45 degrees with the load direction may turn in the radial direction and the probability that such flaws exist is very unlikely. Essentially all flaws are oriented towards the direction of the welding (circumferentially). An investigation of the stress intensity factor for flaws at oblique angles to the load direction supports the conclusion that flaws oriented to within approximately ±15 degrees of the loading direction will not be subjected to sufficient driving force to cause the flaw to turn radial. Supporting this conclusion also is the fact that the flaw would need to turn away from the path of least resistance, the heat affected zone, to grow into the base or weld metal. If a flaw were to occur and be oriented an angle greater than ±15 degrees from the load direction, the flaw orientation may change such that the flaw will become radially oriented. However, as noted earlier, the probability of such flaws occurring is small relative to flaws oriented within ±15 degrees of the welding direction.

In summary, radially oriented flaws are important to the stress corrosion cracking analysis for waste package lifetime calculations as the hoop stress, which drives the radially oriented cracks, is the dominant stress component. However, almost all of the flaws are more or less in the direction of the weld and only flaws that are oriented at angles greater than about 45 degrees with the weld direction may turn in the radial direction. As discussed earlier, about 98% to 99% of the flaws are within about ±13 to ±16 degrees of the weld centerline. Thus, it is conservative to recommend that radially oriented flaws (those with a 45-degree or greater angle from the

direction of the weld) comprise approximately 0.5% of the flaws. Note that a slightly more conservative value (0.8%) is recommended for this parameter in *Analysis of Mechanisms for Early Waste Package/Drip Shield Failure* (BSC 2004 [DIRS 170024], Table 12).

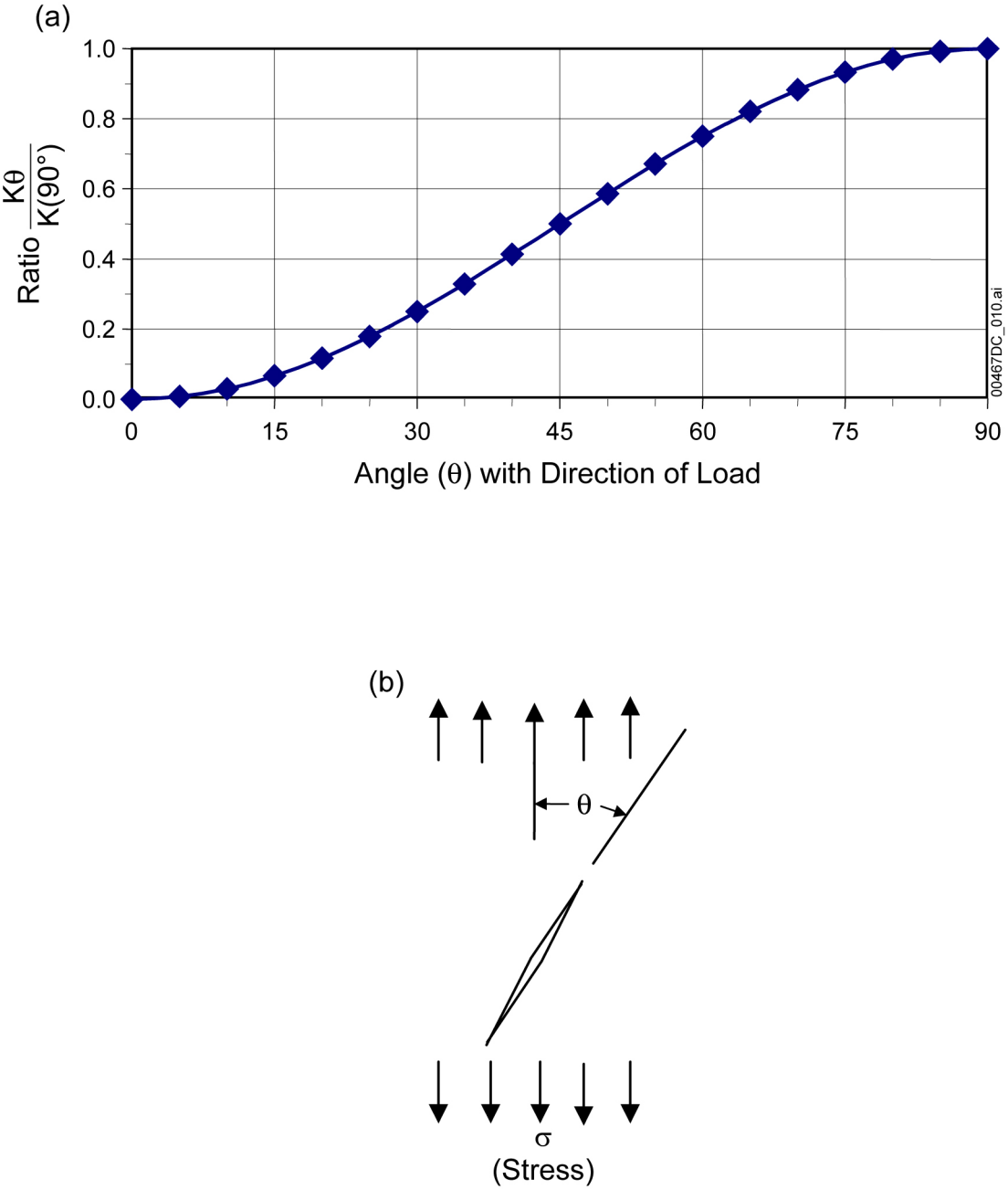

Source: Based on solutions presented by Tada et al. (2000 [DIRS 167756], p.127).

Figure 6-1. Ratio of the Stress Intensity Factor ($K(\theta)$) of a Crack Making an Angle (θ) with the Stress Direction to the Factor ($K(90°)$) of a Crack Oriented Perpendicular to the Stress Direction as a Function of the Angle (θ), for a Crack with an Arbitrary Stress and Crack Length

6.2.2.4 Crack Aspect Ratio

Crack aspect ratio relates crack length to depth and is an important input for determining crack opening area once a crack propagates through-wall. Determination of the crack length for either a manufacturing defect or an incipient crack is based on the following considerations:

Surface flaws are semielliptical with depth 'a' and length '2c.'

The aspect ratio (γ) is the ratio of one-half of crack length ('c') versus crack depth ('a') (i.e., $\gamma = c/a$). A semicircular flaw has an aspect ratio of 1 ($\gamma = 1$).

A crack maintains its aspect ratio during its growth until the depth reaches the wall thickness. Then, at this point, the shape instantaneously becomes rectangular.

The crack aspect ratio is 1 for radial cracks in the closure weld.

The crack aspect ratio is greater than 1 for circumferential cracks with an exponential distribution based on one of the formulations provided by Harris et al. (1981 [DIRS 118624], Equation 2-10, p. 29):

$$P\gamma(>\gamma) = e^{-(\gamma-1)/\lambda} \qquad \text{(Eq. 1)}$$

where λ is the standard deviation of γ and has the value of 0.7. From Equation 1, the mean and median values (γ_{mean} and γ_{50}) and the standard deviation (γ_{sd}) of γ can be obtained by the following formulas:

$$\gamma_{mean} = 1 + \lambda = 1.7$$

$$\gamma_{50} = 1 + \lambda \ln 2 = 1.485$$

$$\gamma_{sd} = \lambda = 0.7$$

A gamma or Weibull distribution with a shape factor of one is equivalent to an exponential distribution.

6.3 THE BASE-CASE SLIP DISSOLUTION–FILM RUPTURE MODEL

6.3.1 Introduction

A crack propagation rate prediction model can be achieved via a fundamental understanding of the cracking mechanism. The formulation of such a fundamentally based model of crack propagation requires the choice of a working hypothesis for the cracking mechanism and the evaluation of the parameters of importance in the mechanism. For the systems of interest, the slip dissolution–film rupture (SDFR) mechanism has been chosen. Slip is highly localized, microscopic strain that can lead to a surface offset or step where the slip plane intersects the surface and, thus, can rupture the passive film present at the surface. This cracking mechanism has been successfully applied to model stress corrosion cracking of stainless steel, low-alloy

steel, and nickel-based alloys in light water reactor environments (Ford and Andresen 1988 [DIRS 118611], pp. 789 to 800; Andresen and Ford 1994 [DIRS 118581], pp. 61 to 70).

6.3.2 Slip Dissolution–Film Rupture Mechanism

In accordance with the slip dissolution–film rupture theory, crack advance is faradaically related to the metal oxidation that occurs when the protective film at the crack tip is ruptured. Figure 6-2 (Ford and Andresen 1988 [DIRS 118611], Figure 2; Andresen and Ford 1994 [DIRS 118581], Figure 1) schematically shows the change in oxidation current and charge densities with time following the rupture of a protective film at the crack tip. In Figure 6-2, $\overline{V}_T$ is the average crack growth rate at the tip, V_S is the crack growth rate at the crack side, M and ρ are atomic weight and density of the crack tip metal, F is Faraday's constant, 'n' is the number of electrons involved in the oxidation of a metal atom, Q_f is the oxidation charge density per film rupture, $\dot{\varepsilon}_{ct}$ is the strain rate at the crack tip, and ε_f is the fracture strain of the film. The initial oxidation rate (and, hence, crack advance rate) is rapid, typically controlled by activation or diffusion kinetics as the exposed metal rapidly dissolves. Availability of the balancing cathodic reduction current is also necessary, but is generally not limiting in hot water environments. However, in most (if not all) hot water cracking systems, a protective oxide reforms at the bared surface, and the rate of total oxidation (and crack tip advance) slows with time. Thus, crack advance can only be maintained if the film rupture process is repetitive. Therefore, for a given crack tip environment, corrosion potential, and metallurgical condition, crack growth is controlled by the change in oxidation charge density with time and the frequency of film rupture at the strained crack tip. The latter parameter is determined by the fracture strain of the film, ε_f, and the strain rate at the crack tip, $\dot{\varepsilon}_{ct}$. By invoking Faraday's law, the average environmental crack growth rate, V_t, can be related to the strain rate at the crack tip, $\dot{\varepsilon}_{ct}$ ($\dot{\varepsilon}$ in Figure 6-2) by the following equation (Ford 1996 [DIRS 167203], Equation 1; Ford and Andresen 1988 [DIRS 118611], Figure 2, p. 790; Andresen and Ford 1994 [DIRS 118581], Figure 1, p. 62):

$$V_t = \frac{M}{z\rho F}\frac{Q_f}{\varepsilon_f}\dot{\varepsilon}_{ct} \qquad \text{(Eq. 2)}$$

where M, ρ = atomic weight and density of the crack tip metal
F = Faraday's constant
z = number of electrons involved in the oxidation of a metal atom ('n' in Figure 6-2)
Q_f = oxidation charge density per film rupture
ε_f = fracture strain of the film

The time, t_f, to reach the fracture strain, ε_f, is:

$$t_f = \varepsilon_f / \dot{\varepsilon}_{ct} \qquad \text{(Eq. 3)}$$

Figure 6-3 shows the schematic of oxidation current density versus time following repeated oxide rupture events. Repassivation current transients exhibit an initially high bare surface

dissolution current density, i_o, at an initial short time, t_o. Thereafter, oxide growth (or thickening) leads to a decay in the oxidation current density, which often follows a power law relationship:

$$i_t = i_o \left[\frac{t}{t_o} \right]^{-n} \quad \text{(Eq. 4)}$$

Because of this power law relationship, Equation 2 can be reformulated as follows (Andresen and Ford 1994 [DIRS 118581], Equation 1, p. 62):

$$V_t = A(\dot{\varepsilon}_{ct})^n \quad \text{(Eq. 5)}$$

where, for a given environment, 'A' and 'n' are material constants that can be measured from the repassivation response. The repassivation slope, 'n,' is the slope on a log-log plot of (i_t/i_o) versus (t/t_o) from Equation 4.

If a bare surface condition is maintained at the crack tip (i.e., $\varepsilon_f/\dot{\varepsilon}_{ct} < t_o$, or $t_f < t_o$, hence, $i_t = i_o$), a "maximum" crack growth rate should result. Integration of Equation 4 leads to:

$$Q_f = \int_0^{t_f} i_t dt = i_o(t_f) = i_o \left(\varepsilon_f \Big/ \dot{\varepsilon}_{ct} \right) \quad \text{(Eq. 6)}$$

Substitution of Equation 6 into Equation 2 yields the predicted maximum environmental crack growth rate:

$$V_{max} = \frac{M}{z\rho F} i_o \quad \text{(Eq. 7)}$$

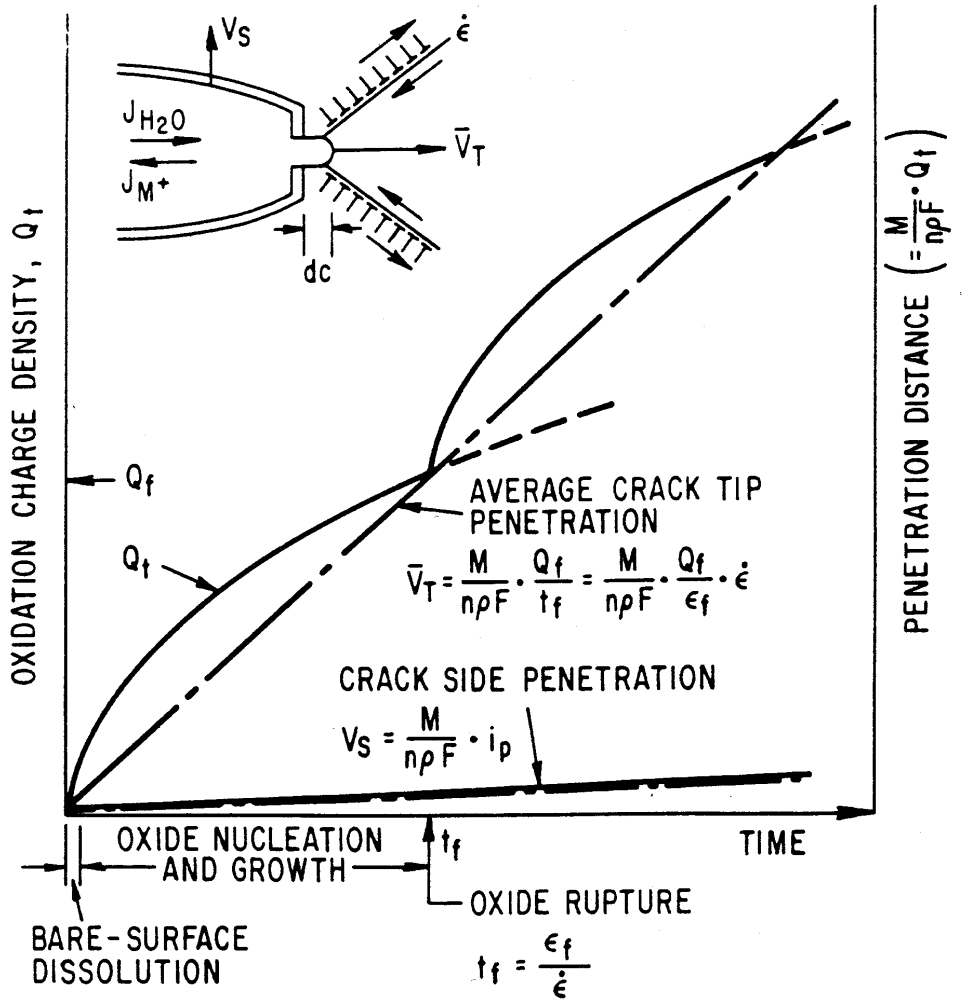

Source: Ford and Andresen 1988 [DIRS 118611], Figure 2; Andresen and Ford 1994 [DIRS 118581], Figure 1.

Figure 6-2. Schematic Oxidation Charge Density versus Time for a Strained Crack Tip and Unstrained Crack Sides in the Slip Dissolution Mechanism

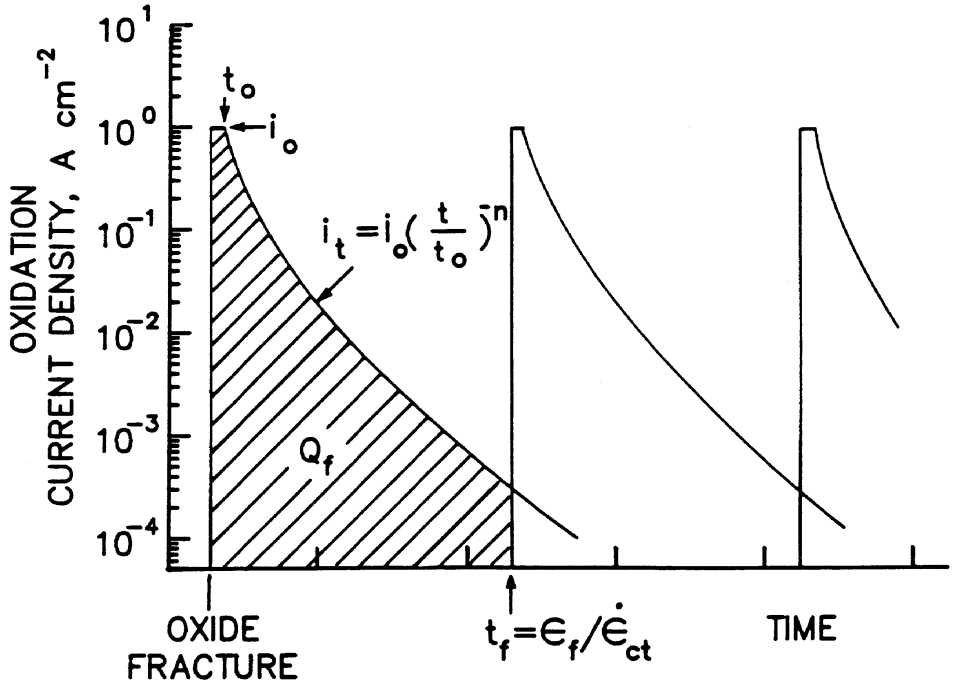

$$V = \frac{da}{dt} \; ; \; \bar{V}_{av} = \frac{M}{Z\zeta F} \cdot \frac{Q_f}{t_f}$$

FOR HIGH $\dot{\epsilon}_{ct}$ AND/OR LONG t_o :

$$\bar{V}_{av} = \frac{M}{Z\zeta F} \cdot i_o$$

FOR LOW $\dot{\epsilon}_{ct}$ AND/OR SHORT t_o :

$$\bar{V}_{av} = \frac{M}{Z\zeta F} \frac{i_o t_o^n}{(1-n)\epsilon_f^n} \dot{\epsilon}_{ct}^n = f(n)\, \dot{\epsilon}_{ct}^n$$

Source: Andresen and Ford 1994 [DIRS 118581].

Figure 6-3. Schematic of Oxidation Current Density versus Time Following Repeated Oxide Rupture Events

This expression for the maximum environmental crack growth rate is the quantitative basis for the early observations relating the maximum oxidation current density on a straining surface to the maximum crack growth rate. These early correlations were obtained primarily for alloys in concentrated environments (boiling $MgCl_2$, 9M NaOH solutions, etc.) under dynamic straining conditions. By comparison, in environments more relevant to conditions at Yucca Mountain, it is expected that (a) the passivation rate is high (e.g., in less aggressive chemistries or for lower-susceptibility materials) and, thus, 'n' (in Equation 4) will be high; (b) the onset of repassivation is rapid, and, thus, t_o is short; and (c) under constant load or displacement conditions, the

periodicity of oxide rupture, $\varepsilon_f/\dot{\varepsilon}_t$, is much greater than t_o. Consequently, the oxidation charge rate, Q, is given by the following equation:

$$Q_f = \int_0^{t_f} i_t dt = \frac{i_o t_o^n}{(1-n)\left(\varepsilon_f / \dot{\varepsilon}_{ct}\right)^{n-1}} \quad \text{(Eq. 8)}$$

Under these circumstances, a bare surface will not be maintained at the crack tip, and the crack propagation rate (Ford [167203], Equation 5) is given by the substitution of Equation 8 into Equation 2:

$$V_t = \frac{M}{z\rho F} \frac{i_o t_o^n}{(1-n)\varepsilon_f^n} (\dot{\varepsilon}_{ct})^n \quad \text{(Eq. 9)}$$

This is an expanded version of Equation 5 and relates the parameters 'A' and 'n' to the specific oxidation rates (Equation 4) and the fracture strain of the oxide at the crack tip:

$$A = \frac{M}{z\rho F} \frac{i_o t_o^n}{(1-n)\varepsilon_f^n} \quad \text{(Eq. 10)}$$

6.3.3 Model Quantification

As the repassivation current follows a power law response (Equation 4), the faradaic relationship between the oxidation rate following oxide rupture and crack advance increment per time (growth rate, V_t), coupled with the relationship between crack tip strain rate, $\dot{\varepsilon}_{ct}$, and periodicity of oxide rupture, distills to the expression shown in Equation 9.

Evaluation of the crack advance mechanism leads to the conclusion that the film rupture–slip oxidation mechanism represents a justifiable model that is capable of being quantitatively evaluated for hot water systems. The mechanism is justifiable because almost all engineering alloys depend on the presence of a stable oxide film to act as a kinetic barrier to rapid dissolution–oxidation, especially in hot water. It is quantifiable, because predictions result directly from measurements of repassivation kinetics, typically obtained by rapidly straining wires of base alloy or synthetic (e.g., representative of the grain boundary) composition (Figure 6-2).

According to Andresen and Ford (1994 [DIRS 118581], p. 62), the model can be quantified by evaluating the following processes: (1) the steady-state and transient compositions of the environment at the crack tip as a function of the conditions in the bulk (external) solution; (2) the oxidation rates for the material or environmental system expected at a strained crack tip; and (3) the oxide fracture strain and the crack tip strain rate, defined in terms of engineering parameters such as the stress intensity factor. For practical application, empirical approaches have been used for the model quantification processes.

The initial application of the slip dissolution–film rupture model was on the quantitative prediction of cracking in austenitic Stainless Steel Types 304 and 316 in 288°C high-purity BWR water (Ford and Andresen 1988 [DIRS 118611]). The quantification processes for the model are summarized as follows:

Step 1 Measurements of 'n' are obtained from repassivation tests as the repassivation current follows a power law response (Equation 4). Those tests typically involve rapidly straining wires to increase the anodic passive current density, and subsequently measuring the decay of the passive current density with time.

Step 2 Once 'n' is known, the value of 'A' is determined from Equation 10, which relates the parameters "A" and 'n' to the specific oxidation rates and the fracture strain of the oxide at the crack tip.

An alternative procedure, however, is used to quantify the model parameters. Based on this procedure, 'A' is directly determined from 'n' empirically. The empirical determination of A is based on stress corrosion cracking crack growth tests that measure the crack growth rate V_t at specific crack tip strain rate $\dot{\varepsilon}_{ct}$. The value of 'A' is calculated in accordance with Equation 5 for each set of n, V_t, and $\dot{\varepsilon}_{ct}$. Curve fitting is then used to develop the empirical relationship between 'A' and 'n'.

An empirical relationship between 'A' and 'n' (with 'A' in cm-$s^{(n-1)}$ and 'n' being dimensionless) of:

$$A = 7.8 \times 10^{-3}\, n^{3.6} \qquad \text{(Eq. 11)}$$

was provided by Ford and Andresen (1988 [DIRS 118611], p. 791) for Stainless Steel Type 304 in 288°C water. For Alloy 22 and Titanium Grade 7, independent experimental measurement of 'A' and 'n' is preferred but, due to lack of experimental data, the expression above is used for the slip dissolution mechanism of Alloy 22 for present purposes. The resulting model is validated experimentally as indicated in Section 7.

Substitution of Equation 11 into Equation 5 leads to:

$$V_t = 7.8 \times 10^{-3}\, n^{3.6}\, (\dot{\varepsilon}_{ct})^n \qquad \text{(Eq. 12)}$$

where V_t is in units of cm/s and $\dot{\varepsilon}_{ct}$ is in units of s^{-1}.

For sensitized Stainless Steel Type 304 in 288°C water, Figure 6-4 indicates that Equation 12 with n = 0.54 (i.e., $A = 8.5 \times 10^{-4}$) is a good prediction model for observed crack growth rate versus crack tip strain rate relationships. Further, this slip dissolution–film rupture model (using the Stainless Steel Type 304 'A' versus 'n' relationship in 288°C water) has been statistically validated for the chromium-containing, nickel-based Alloys 600 and 182 over a range of anionic impurity concentrations (Ford and Andresen 1988 [DIRS 118611], Figure 10).

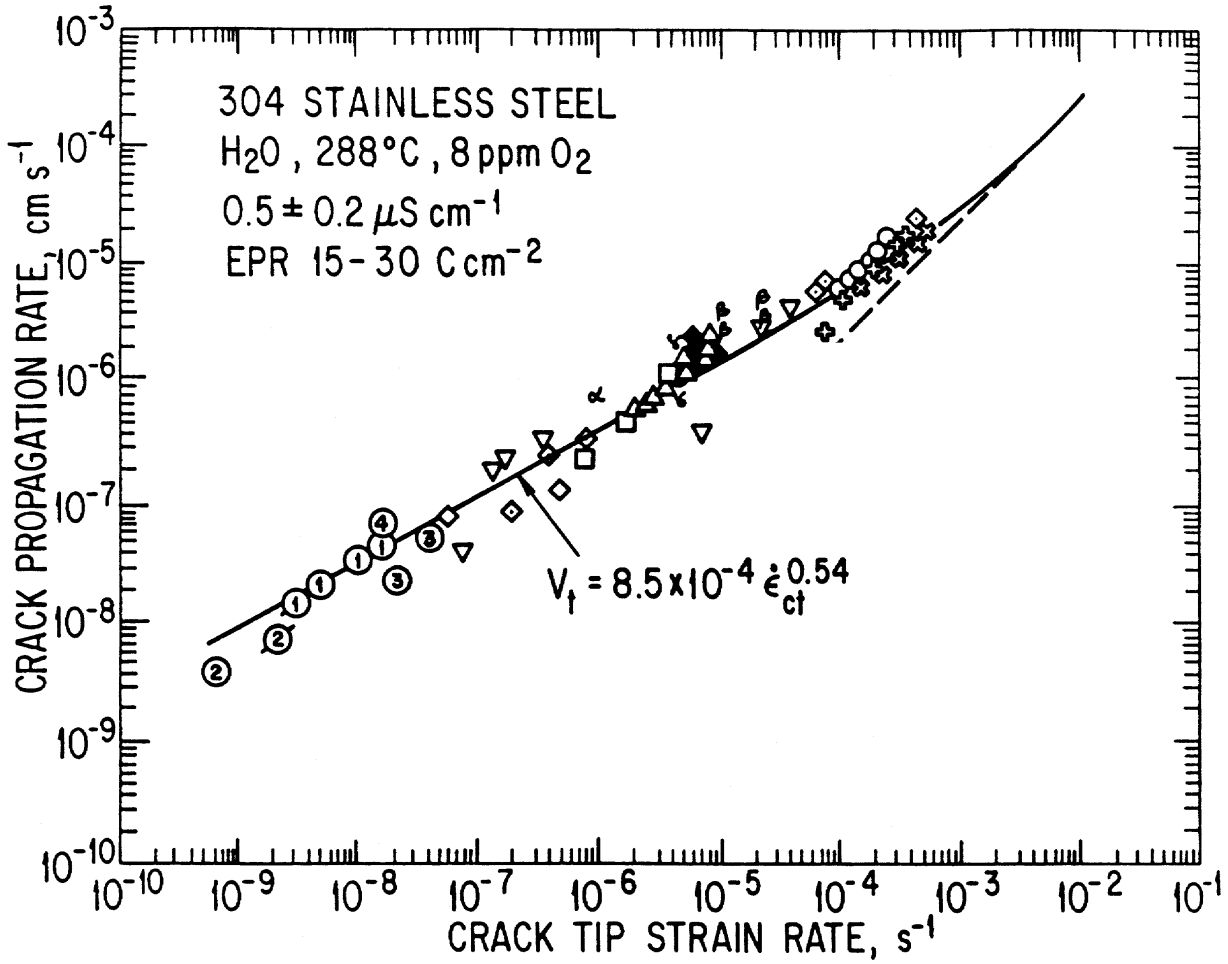

Source: Ford and Andresen 1988 [DIRS 118611], Figure 7, p. 791.

Figure 6-4. Crack Growth Rate (Presented by Observed Data Points and Predicted Curve) versus Crack Tip Strain Rate for Sensitized Stainless Steel Type 304 in Oxygenated 288°C Water

The crack tip strain rate, $\dot{\varepsilon}_{ct}$ in Equation 12, is related to the engineering stress parameters (such as the stress intensity factor) via formulations by Ford and Andresen (1988 [DIRS 118611], Table 1). According to Ford and Andresen (1988 [DIRS 118611], p. 791), the formulations provided are semiempirical relationships to normalize the effects of a wide range of stressing conditions on the environmentally assisted crack propagation rates. For constant load, the relationship is:

$$\dot{\varepsilon}_{ct} = 4.1 \times 10^{-14} K_I^4 \qquad \text{(Eq. 13)}$$

where the stress intensity factor K_I is in MPa $(m)^{1/2}$.

For constant load, substituting Equation 13 in Equation 5 leads to the following alternative crack growth rate equation:

$$V_t = \overline{A}(K_I)^{\overline{n}} \quad \text{(Eq. 14)}$$

where

$$\overline{A} = A\left(4.1x10^{-14}\right)^n \quad \text{(Eq. 15)}$$

$$\overline{n} = 4n \quad \text{(Eq. 16)}$$

6.3.4 Adaptation of Slip Dissolution Model To Alloy 22

Andresen and Ford (1994 [DIRS 118581], p. 62) indicated that the SDFR model has been applied to stainless steels, low-alloy and carbon steels, ductile nickel alloys, and irradiated stainless steels. Ford and Andresen (1988 [DIRS 118611], p. 789) also used the SDFR model for the Inconel 600 and 182 nickel-based alloys. Further, as indicated in Section 6.3.3, it was determined that the SDFR model (using the Stainless Steel Type 304 'A' versus 'n' relationship in 288°C water) was statistically valid for these chromium-containing, nickel-based Alloys 600 and 182 over a range of anionic impurity concentrations (Ford and Andresen 1988 [DIRS 118611], Figure 10).

Subsequently, Andresen (1991 [DIRS 166965], Figure 37) used the SDFR model for the higher chromium-content nickel-based alloy, Alloy 82 (UNS N06082), and determined that measured stress corrosion cracking growth rates agreed reasonably well with predicted rates. Alloy 82 (UNS N06082) (18% to 22% Cr, UNS NO6082) overlaps Alloy 22 (20% to 22.5% Cr) (DTN: MO0003RIB00071.000 [DIRS 148850], p.2) in chromium content. Analyses indicate that the inner, protective corrosion films that form in the passive potential range on such chromium-containing nickel-based alloys with greater than about 15% chromium contain a very thin passive film layer of primarily Cr_2O_3 (with some nickel content) at the oxide–alloy interface (Pensado et al. 2002 [DIRS 166944], p. 2-2). Such a thin, passive Cr_2O_3 film is likely to possess similar repassivation kinetics and mechanical properties (e.g., fracture strain) over the range of nickel–chromium-based alloys of interest. This is consistent with the model having been shown to apply or to give reasonable predictive results for a range of nickel base alloys with chromium contents spanning the Alloy 22 compositional range. Further, there is general correspondence (reasonable statistical agreement) between the observed stress corrosion cracking growth rate temperature dependencies for sensitized Stainless Steel Type 304 and nickel–chromium-based Alloy 600 over the temperature range of most interest (~50°C to 200°C) when compared under comparable stress intensity factor and environmental conditions (Andresen 1993 [DIRS 166966], Figures 15 and 16). For example, Figure 6-5 shows that crack growth rates for sensitized Stainless Steel Type 304 and Alloy 600 follow the same temperature dependency with reasonably similar crack growth rates over a temperature range from about 25°C to 275°C, which is broader than the temperature range of most interest (~50°C to 200°C) stated above.

As the SDFR was initially developed for stainless steels and nickel-based alloys Inconel 600 and 182 under higher temperature (~288°C) light water reactor coolant conditions, additional confidence in the applicability of this model to Alloy 22 can be gained from observation of the

response of Alloy 22 under similar light water reactor coolant conditions. Test results from DTN: MO0402GEA22SCC.000 [DIRS 167911] indicate the crack growth rate response of Alloy 22 exposed to 288°C relatively pure water (2 ppm O_2) is broadly consistent with the crack growth rate response of other materials, such as Alloys 600 and 182 (Andresen et al. 2002 [DIRS 166967]) and austenitic stainless steel (Andresen et al. 2002 [DIRS 167762]) under these same conditions. The measured crack growth rates show a similar dependency to parameters like corrosion potential and water purity (sulfate). For example, in all test cases, the change in corrosion potential from ~ +0.2 V_{SHE} to ~ –0.5 V_{SHE} (due to a change from 2 ppm O_2 to H_2-deaerated water) causes a drop of at least one order of magnitude in the crack growth rate, as indicated by Table 6-3. Also, as expected, Alloy 22 shows crack growth rates under repository-type oxidizing conditions (i.e., at $0.2V_{SHE}$) that are about one order of magnitude lower than those of the other materials under identical test conditions, demonstrating its superiority as a structural material under conditions where stress corrosion cracking is a concern.

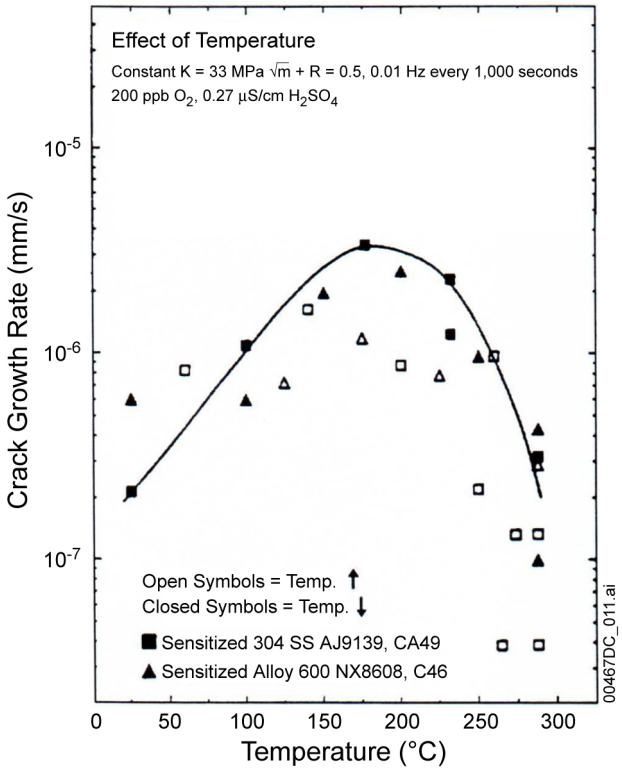

Source: Andresen 1993 [DIRS 166966], Figure 15.

Figure 6-5. Temperature-Dependence of Sensitized Stainless Steel Type 304 and Alloy 600

Table 6-3. Measured Crack Growth Rates (mm/s) in 288°C, Oxygenated Water Due to Drop in Corrosion Potential

Alloy	Stress Intensity Factor MPa√m	Corrosion Potential +0.2 V_{SHE}	Corrosion Potential -0.5 V_{SHE}	Reference
Alloy 22	27.5 [25 ksi (√in.)]	2.3×10^{-8}	4.0×10^{-9}	DTN: MO0402GEA22SCC.000 [DIRS 167911], Figure 3
Alloy 182	28.4	3.0×10^{-7}	6.0×10^{-9}	Andresen et al. 2002 [DIRS 166967], Figure 7
Alloy 600	30.0	3.3×10^{-7}	3.7×10^{-8}	Andresen et al. 2002 [DIRS 166967], Figure 8
Unsensitized Stainless Steel Type 316L	27.5 [25 ksi (√in.)]	4.1×10^{-7}	$>2.0 \times 10^{-8}$	Andresen et al. 2002 [DIRS 167762], Figure 5

In addition to the expected similarities in composition and mechanical properties, as indicated earlier in this section, for the passive films present on this class of alloys (i.e., austenitic Stainless Steel Types 304, 304L, 316, and 316L and nickel–chromium-based alloys (Alloys 600 and 22)), the expected microdeformation modes of the alloys per se should be comparable, based on examination of literature values for stacking fault energies (SFE) (Gordon 2004 [DIRS 167027]). A low value of SFE promotes coplanar dislocation arrays (promoting local stress buildups that can more easily rupture the passive surface film at slip offsets), whereas high SFE values promote dislocation tangles that tend to diffuse local stress buildups. These alloys all possess a face-centered cubic-crystallographic lattice structure and have similar relatively low values of estimated SFE ranging from about 20 to 30 ergs/cm^2 for Stainless Steel Types 304L and 316L to about 80 ergs/cm^2 for Alloy 600, with the estimated value for Alloy 22 being about 65 ergs/cm^2. This range is relatively low compared to published values of about 340 ergs/cm^2 for pure nickel or nickel alloys with much lower chromium contents (Gordon 2004 [DIRS 167027], Table 1). Although lower values of SFE can promote micro-stress and resulting micro-strain buildups at the surface region that may accelerate stress corrosion cracking initiation, the relatively high local deformation at a stressed crack or weld flaw tip is likely to lead to relatively high local strains regardless of SFE. Thus, this will tend to overwhelm any effect of SFE on stress corrosion cracking propagation.

Based on the above observations, there is ample reason to conclude that stress corrosion cracking of nickel-based Alloy 22 occurs by the same fundamental mechanism characterized by the slip dissolution stress corrosion cracking model:

$$V_t = A\,(\dot{\varepsilon}_{ct})^n \qquad \text{(Eq. 5)}$$

This model is experimentally benchmarked for Alloy 22 in a range of relevant repository brine environments for Yucca Mountain as described in the following equations.

The relationship between ‘A’ and ‘n’ described by Equation 11 (with ‘A’ in cm-s$^{(n-1)}$ and ‘n’ being dimensionless) becomes the following equation (with ‘A’ in mm-s$^{(n-1)}$ and ‘n’ being dimensionless):

$$A = 7.8 \times 10^{-2} n^{3.6} \qquad \text{(Eq. 17)}$$

For constant load condition, with V_t in mm/s and K_I in MPa $(m)^{1/2}$ in Equation 14, Equation 15 becomes:

$$\overline{A} = 7.8 \times 10^{-2} n^{3.6} (4.1 \times 10^{-14})^n \quad \text{(Eq. 18)}$$

Substitution of Equations 17 and 18 in Equation 5 leads to:

$$V_t = 7.8 \times 10^{-2} n^{3.6} (4.1 \times 10^{-14})^n (K_I)^{4n} \quad \text{(Eq. 19)}$$

For Alloy 22 under constant load condition, the parameter 'n' can be determined from Equation 19 based on crack growth rates measured at various levels of applied stress intensity factor, K_I. Stress corrosion cracking crack growth rate measurements from the General Electric Global Research Center (GEGRC) (DTN: LL021105312251.023 [DIRS 161253]) are used for the quantification of parameters for the SDFR stress corrosion cracking model to be used for Alloy 22. The test data were developed from three of the four Alloy 22 specimens (c144, c152, c153, and c200) tested at 110°C in a concentrated mixed-salt environment know as Basic Saturated Water (BSW) with a target composition and solution pH (pH = 13.4 at room temperature) listed in DTN: LL021105312251.023 ([DIRS 161253], p. 3 and 6). The compact tension specimens (loaded per ASTM E 399-90 [DIRS 117480]) used for the crack growth rate measurements were fabricated from Alloy 22 in a range of microstructural conditions. These included the solution-annealed condition (Specimens C144 and C152), the 20% cold-worked condition (Specimen C-153), and the thermally aged condition (700°C for 175 hours, Specimen C-200) as described in DTN: LL021105312251.023 [DIRS 161253].

The specimens were subjected to cyclic loading in order to initiate crack growth and followed by constant loading conditions with various hold times. The set of data from DTN: L021105312251.023 [DIRS 161253] used as input for establishing values of 'n' for Alloy 22 are summarized in Table 6-4 and are based on measured crack growth rates listed in Table 4-2. These data were selected based on the following criteria.

First, the minimum hold time is 24 hours (85,400 seconds) because Equation 19 is applicable only to constant loading condition. It is unrealistic to determine the parameters $\overline{A}$ and $\overline{n}$ (or 'A' and 'n') in this equation based on test data at relative short hold times. The only exception is the data point associated with specimen c144 for which the hold time is relatively short (3,000 seconds or approximately one hour), but crack growth appeared to cease (DTN: LL021105312251.023 ([DIRS 161253], p. 7), consistent with reaching the constant load state.

Secondly, data associated with specimen c200 were not included because this specimen was aged at 700°C for 175 hours. This aging condition is ultrasevere relative to the expected waste package closure weld thermal exposure. According to *Aging and Phase Stability of Waste Package Outer Barrier* (BSC 2004 [DIRS 171924], Section 8), material aging is not a concern for the waste package at temperatures less than 300°C for up to 500 years and less than 200°C for the next 9,500 years. It is noted in Table 6-4 that a crack growth rate of 10^{-11} mm/sec is used to represent the test results that indicated cracking appeared to cease propagating (i.e., the growth rate seemed to approach zero). The choice of 10^{-11} mm/sec is judged to be near the lower limit of practical growth rate measurement based on the observation that good statistical confidence in

growth rate exists when the crack growth increment is at least 10 times the limiting resolution of the technique (Andresen et al. 2002 [DIRS 166967], p. 4). The lower limit of crack growth increment cited by Andresen et al. (2002 [DIRS 166967], p. 4) is 1 micron. To gain statistical confidence using a 10-micron crack extension, a rate of 10^{-11} mm/sec would require a test time of about 30 years, which is relatively impractical.

As indicated by Pan et al. (2002 [DIRS 165536], Section 3.1) and described in more detail by Barkatt et al. (2000 [DIRS 154496]), stress corrosion cracking was observed in one of several Alloy 22 U-bend specimens exposed in 250°C concentrated groundwater purposely contaminated with 0.5% lead at pH 0.5. Therefore, to evaluate the potential effect of lead under more relevant conditions, crack growth rate measurements (DTN: LL021105312251.023 [DIRS 169321], pp. 10 to 11) were also obtained for Specimen c152 after the addition of 1,000 ppm of lead (added as $Pb(NO_3)_2$) to the autoclave BSW test solution. The lead addition was made following 8,670 hours of testing in 110°C BSW solution (DTN: LL021105312251.023 [DIRS 161253], composition p. 3; with solution pH = 13.4 at room temperature, p. 6). Because of the relatively high pH of this solution, most of the lead becomes insoluble in the test solution because of lead carbonate, lead sulfate, and possibly lead oxide precipitation. Based on a detailed comparison of crack growth rates made before and after the lead addition, in all cases the growth rate after the lead addition was the same or somewhat slower. The test conditions varied over a significant range in loading conditions and growth rates. In addition to these higher pH brine stress corrosion cracking crack growth rate results, there are also stress corrosion cracking-initiation test results obtained using Slow Strain Rate Tests (SSRT), at 76°C to 95°C in low pH, SAW brine solution (pH ~3) with and without 0.005% lead nitrate additions (Section 6.2.1, Table 6-2). These results also show no effect of lead on stress corrosion cracking susceptibility; thus, there appears to be no basis for concern that lead will affect stress corrosion cracking susceptibility in relevant concentrated brine environments over a broad range of pH values.

To characterize the uncertainty for ‘n,’ it can be determined from the ‘n’ values in the last column of Table 6-4 that the mean value of ‘n’, n_{MEAN}, is 1.304 and the standard deviation (SD), nSD, is 0.160, using “Excel” functions AVERAGE and STDEVP, respectively. Based on these mean and standard deviations, a normal distribution for ‘n’ can be constructed. The ‘n’ values at various percentiles, up to ±2(SD), are listed in Table 6-5, where the percentile value is obtained by the Excel function NORMDIST for each set of given values of ‘n’, n_{MEAN}, and n_{SD}. For TSPA-LA applications, ‘n’ should be sampled from a truncated normal distribution with a mean of 1.304, a standard deviation of 0.16, and an upper- and a lower-bound of 1.624 and 0.984, which is ±2(SD) of the normal distribution, respectively.

Table 6-4. Summary of Source Data for Alloy 22 SDFR Model Quantification

Specimen	Hold Time (hours)	Tested Stress Intensity Factor (MPa(m)^.5)	Measured Crack Growth Rate (mm/s)	Source	Calculated 'n' value[b]
c153	CL	30	2.50E-10	DTN: LL021105312251.023 [DIRS 161253], p. 11	1.168
c153	CL	30	5.00E-10	DTN: LL021105312251.023 [DIRS 161253], p. 11	1.119
c144	1	30	1.00E-11[a]	DTN: LL021105312251.023 [DIRS 161253], p. 7	1.391
c152	24	45	1.00E-11[a]	DTN: LL021105312251.023 [DIRS 161253], p. 10	1.563
c152	24	45	4.00E-10	DTN: LL021105312251.023 [DIRS 161253], p. 10	1.281

NOTES: CL = constant load.
[a]Crack growth rate of 1.0E-11 is used to represent test results where cracking appeared to cease propagating (i.e., the growth rate seemed to approach zero).
[b]Calculated from Equation 19.

Table 6-5. Distribution of the Parameter 'n'

'n' Value	Percentile
0.984 (-2 SD)	2.28
1.041	5.00
1.099	10.00
1.139	15.00
1.145 (-1 SD)	15.87
1.170	20.00
1.221	30.00
1.264	40.00
1.304 (Mean)	50.00
1.345	60.00
1.388	70.00
1.439	80.00
1.464 (+1 SD)	84.13
1.470	85.00
1.509	90.00
1.568	95.00
1.624 (+2 SD)	97.72

Source: Generated using Excel function NORMDIST; mean, upper-bound, lower-bound, standard deviation listed in Output DTN: LL030607012251.065.

The base-case slip dissolution–film rupture stress corrosion cracking model developed for Alloy 22, represented by Equation 19, is graphically illustrated in Figure 6-6 for 'n' values at 0.984 (the lower-bound), 1.304 (mean), and 1.624 (the upper-bound), as well as the graphical representation of Equation 19 for sensitized Stainless Steel Type 304 (with n=0.54, Section 6.3.3). Excellent resistance to stress corrosion cracking for Alloy 22 is illustrated in Figure 6-6, where even the higher crack growth rates exhibited by the top curve of Alloy 22 with

n=0.984 are about two orders of magnitude lower than the crack growth rates associated with stainless steel curve.

In summary, the five data points listed in Table 6-4 were used to obtain a mean value and a range for the 'n' parameter of the model. Then the model prediction was shown in Figure 6-6 over the range of stress intensity factor values (15 to 55 MPa√m) and the individual data points were also included in Figure 6-6 along with plus and minus 2-sigma limits for the 'n' parameter and not for the five data points.

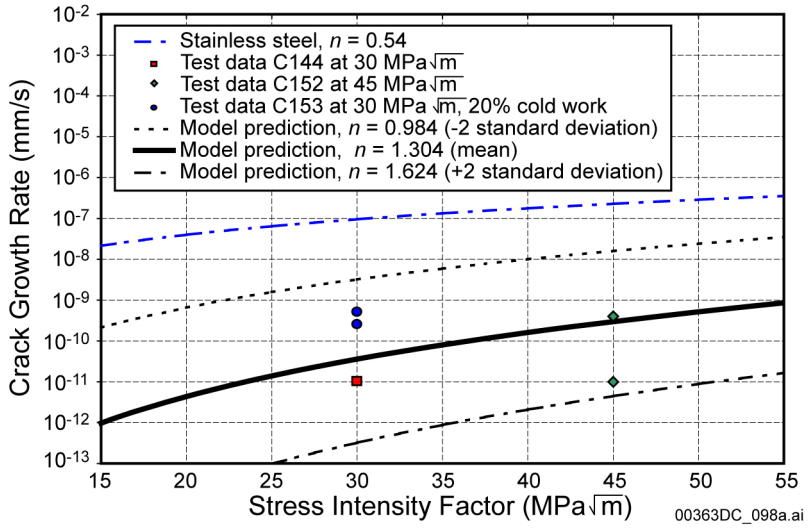

Source: Plot generated from Equation 19 using Alloy 22 n values from Table 6-5, and Stainless Steel n value from Section 6.3.3. Data points for specimens C144, C152, and C153 are from DTN: LL021105312251.023 [DIRS 161253] and are listed in Table 6-4.

Figure 6-6. Crack Growth Rate Versus Stress Intensity Factor for Alloy 22 Based on the SDFR Model

6.3.5 Threshold Stress Intensity Factor

The threshold stress intensity factor (K_{ISCC}) is a critical value of stress intensity factor (K_I) such that any preexisting crack will not grow or is in an arrest state if K_I corresponding to the crack size and the applied stress does not exceed K_{ISCC}. Preexisting cracks are usually caused by manufacturing processes (especially welding) or crack initiation (Section 6.2).

The concept of threshold stress intensity factor (K_{ISCC}) has been commonly used to assess the susceptibility of material to stress corrosion cracking. The description of this concept can be found in work by Jones and Ricker (1987 [DIRS 118672], pp. 145 to 163) and Sprowls (1987 [DIRS 118702], pp. 245 to 282). To apply the method, it is necessary to obtain values of (1) stress intensity factor K_I as a function of crack size correspondent to the stress state at and near the crack site, and (2) the threshold stress intensity factor K_{ISCC}. The calculations of stress intensity factor for the closure welds in the inner and outer lids of the waste package are described in Section 6.4. The threshold stress intensity factor is normally determined experimentally, but because of the extremely low growth rates observed for Alloy 22, very long test times are required. A more conservative approach has been selected. Roy et al. (1998 [DIRS 118696]) documented an attempt to obtain an experimentally measured K_{ISCC} for Alloy 22 at Lawrence Livermore National Laboratory using double cantilever beam-type fracture

mechanics specimens. However, review of these data revealed that the data were invalid as described in Dunn (1999 [DIRS 154481], Section 2.2.3, p. 2-5). There were discrepancies between the ASTM procedure and the Lawrence Livermore National Laboratory test results reported by Roy et al. (1998 [DIRS 118696]). The tests did not comply with the recommended test procedure for these double cantilever beam (DCB) specimens. The initial crack length used appears to be too short and the specimen crack length to thickness ratio, a/w of 0.31, was below the ASTM recommended range of 0.45 to 0.55. Thus, these results are not used as sources for threshold stress intensity factor.

Because of the extremely low stress corrosion cracking growth rates and the need for unacceptably long test times, an alternative approach, a more conservative crack-blunting criterion is used to define the threshold stress intensity factor. Based on the crack-blunting criterion (Andresen and Ford 1994 [DIRS 118581], p. 62), crack blunting occurs when the corrosion rate of the crack sides approaches the oxidation rate at the crack tip (i.e., the sharp crack will degenerate to a blunt pit). It follows that a stress corrosion cracking crack will not grow if the general corrosion rate at the crack sides exceeds the crack tip growth rate. If V_{gc} is the general corrosion rate, the threshold stress intensity factor K_{ISCC} can be calculated from the SDFR Model as represented by Equation 14, or the following rearrangement of this equation with $V_t = V_{gc}$:

$$K_{ISCC} = (V_{gc} / \overline{A})^{1/\overline{n}} \quad \text{(Eq. 20)}$$

The mean general corrosion rate, which can be calculated from Table 4-6, is used in Equation 20. Observation of Table 4-6 indicates that the general corrosion rate associated with sample DCA 177 is an outlier since it is about a factor of six higher than the mean value. If this outlier is removed from the data set, the mean general corrosion rate is 7.23 nm/yr. Values for $\overline{A}$ and $\overline{n}$ can be determined from Equations 16 and 18 for a given value of 'n.' The threshold stress intensity factor for Alloy 22, accordingly, can be expressed in Table 6-6, based on the 'n' values shown in Table 6-5.

The threshold stress intensity factor is applied to both incipient flaws (once the threshold stress for initiation is exceeded) and for weld flaws. At each time step, the stress intensity factor, K_I, at a growing crack tip or defect tip is compared with the K_{ISCC} value. At the point that the K_I value drops below K_{ISCC}, the crack will arrest.

For Alloy 22, it is recognized that at the lower stress intensity values (minus two sigma on the mean) in Table 6-6, the indicated K_{ISCC} may not be realistic. The implication is that the K_{ISCC} values at the lower limits are highly conservative, considering the high degree of stress corrosion cracking initiation and crack growth resistance of Alloy 22 and because the mean value (11.38 MPa$\sqrt{m}$) (obtained when the crack growth rate equals the general corrosion rate) is also conservatively obtained based on test data from much higher stress intensity values (30 and 45 MPa$\sqrt{m}$) at which maintaining crack growth under static loading conditions is difficult to accomplish.

Table 6-6. Distribution of the Threshold Stress Intensity Factor, K_{ISCC}, for Alloy 22

'n' Value	'K_{ISCC}' value (MPa√m)
0.984 (-2 SD)	2.65
1.041	3.65
1.099	4.90
1.139	5.90
1.145 (-1 SD)	6.06
1.170	6.76
1.221	8.35
1.264	9.85
1.304 (Mean)	11.38
1.345	13.10
1.388	15.04
1.439	17.56
1.464 (+1 SD)	18.87
1.470	19.19
1.509	21.36
1.568	24.89
1.624 (+2 SD)	28.50

Source: Generated using Equation 20; equation listed in Output DTN: LL030607012251.065.

6.3.6 Alternative Model: The Coupled Environment Fracture (CEF) Model

Alternative conceptual models (ACMs) are based on simplifications that are different from those employed, or not used, in the base model. An important reason for considering ACMs is to help build confidence that changes in modeling decisions or simplifications will not change conclusions regarding subsystem and total system performance. Conceptual model uncertainty results from sparse observational data and a lack of available information to corroborate or refute plausible alternative interpretations of the subsystem and the processes occurring within the subsystem.

In addition to the base-case slip dissolution–film rupture model, which provides formula for prediction of the crack growth rate, an alternative conceptual model, the coupled environmental fracture (CEF) model (Macdonald and Urquidi-Macdonald 1991 [DIRS 162702]; Macdonald et al. 1994 [DIRS 162701]), was developed based on the theory that the internal and external environments are coupled by the need to conserve charge in the system. Thus, as oxygen reduction on the external surface consumes the positive current emanating from the crack mouth, the solution of Laplace's equation for the external environment yields a boundary condition for solving Laplace's equation for the internal crack environment. The slip dissolution model describes metal dissolution at the crack tip, with the frequency of rupture of the passive film being a strong function of the stress intensity factor. The reduction of oxygen on the external surfaces is described in terms of a general Butler-Volmer equation that incorporates mass transport and charge transport phenomena. In this way, the model incorporates the effects of oxygen concentration, flow rate, and the conductivity of the external environment as well as accounting for effect of stress on crack growth. The CEF model represents an alternative

approach for the prediction of the crack growth rate. It is considered in this report only to corroborate the conservative predictions of the base-case model.

The CEF model is a physico-electrochemical model developed for intergranular stress corrosion cracking in sensitized Stainless Steel Type 304 in simulated light water reactor environments to explain and explore the effects of various environmental and mechanical variables on the kinetics of crack propagation. The goals are: (1) to derive a physically realistic model that unifies the electrochemical, chemical, and mechanical aspects of the propagation of cracks through sensitized Stainless Steel Type 304, and (2) to use this model to explore how the rate of crack propagation depends on various environmental variables, including oxygen concentration, conductivity, and mechanical (stress intensity) parameters. Macdonald and Urquidi-Macdonald (1991 [DIRS 162702]) and Macdonald et al. (1994 [DIRS 162701]) discuss the mathematical development of the model.

The slip dissolution–film rupture model and the CEF model are similar in several ways. Both were developed for intergranular stress corrosion cracking in sensitized Stainless Steel Type 304 simulated light water reactor environments. Both use Faraday's law to develop the equation for the crack growth rate. The departure point starts as the slip dissolution–film rupture model takes an empirical approach to develop a functional form to express the crack growth rate in terms of, explicitly, the crack tip strain rate and a couple of parameters (i.e., 'A' and 'n') while the CEF model stays with an implicit approach. The CEF model is more a theoretical model and the slip dissolution–film rupture model is a mixed theoretical and empirical model.

The slip dissolution–film rupture model and the CEF model predict the crack growth rate for stress corrosion cracking. However, it was discovered that the CEF model has the tendency of underestimating the crack growth rate, as compared to the slip dissolution–film rupture model when both models were applied to predict the crack growth rate for Stainless Steel Type 304 in a boiling water reactor (BWR) environment. Figure 6-7 illustrates this nonconservatism. Comparison with experimental data summarized by Ford and Andresen (1988 [DIRS 118611], Figure 22) for crack propagation rate versus stress intensity factor for sensitized Stainless Steel Type 304 in fully aerated, high purity water at elevated temperature indicated that the crack growth rate predicted by the CEF model (i.e., 3.2×10^{-9} cm/s at 20 MPa$\sqrt{m}$) (Macdonald and Urquidi-Macdonald 1991 [DIRS 162702], p. 78) tends to be at the lower end of the range cited by Ford and Andresen (1988 [DIRS 118611], Figure 22). For this reason, the CEF model was not included for further evaluation but used only to corroborate the conservative crack growth rate predictions of the base case slip dissolution–film rupture model.

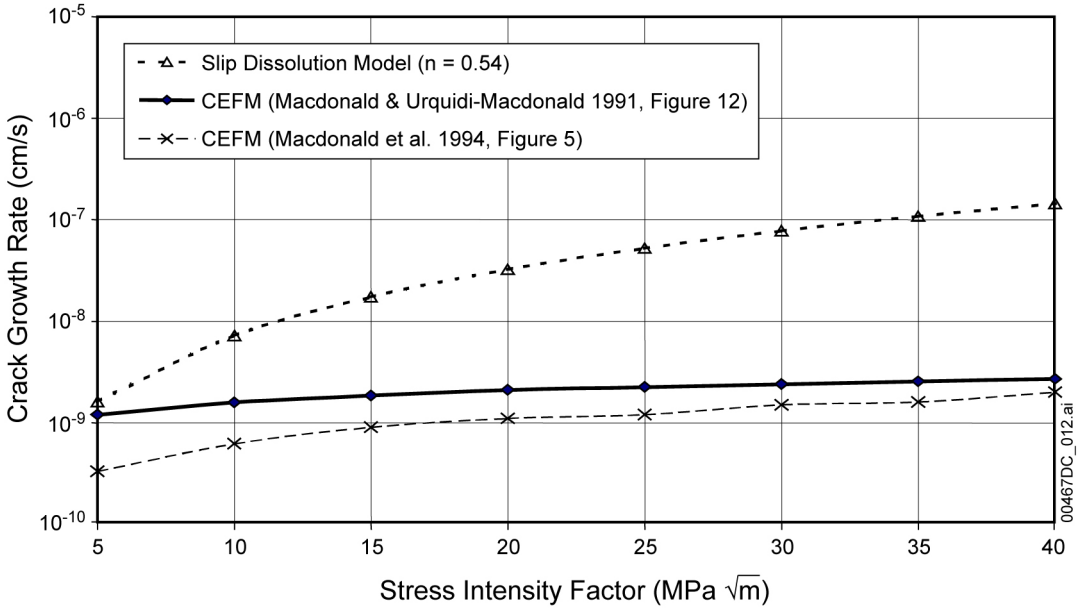

Source: Plot generated from data by Ford and Andresen (1988 [DIRS 118611], Figure 22), Macdonald and Urquidi-Macdonald (1991 [DIRS 162702], Figure 12), and Macdonald et al. (1994 [DIRS 162701], Figure 5).

Figure 6-7. Comparison of Predicted Crack Growth Rates for Stainless Steel Type 304

6.3.7 Stress Corrosion Cracking for the Drip Shield Titanium Grade 7 Material

The sources of stress that could result in stress corrosion cracking in the Titanium Grade 7 drip shield are: (1) weld-induced residual stress, (2) plasticity-induced residual stress caused by seismic events, and (3) residual stress produced by rockfalls. Annealing will mitigate weld-induced residual stresses. The threshold stress for crack initiation developed in Section 6.2.1 is used as the through-wall crack penetration (breach) criterion for both rockfall and seismic-induced stress. Seismic stress corrosion cracking is discussed further in Appendix B. An analysis of the consequence of residual stress produced by rockfalls is presented in this section.

Stress corrosion cracks in passive alloys such as Titanium Grade 7 tend to be very tight (small crack opening displacement) by nature because the slip dissolution–film rupture process results in a relatively high effective crack tip growth rate as compared to the general corrosion rate of the unstressed sides of the crack. As the crack grows through-wall, the tensile stresses normal to the crack walls are relieved. The resulting crack faces continue to corrode by general corrosion with a median rate of about 0.03 microns per year under the range of environmental conditions expected on the drip shield surfaces (BSC 2004 [DIRS 169845], Table 17).

According to Section 6.2.1, deformation induced residual stress resulting from rockfalls can cause stress corrosion cracking crack initiation in the drip shield if the stress exceeds the threshold stress for the drip shield material (Titanium Grade 7). Although initiation is assumed to occur immediately once the threshold stress is exceeded, it actually takes years to occur as indicated by the LTCTF Titanium Grade 16 and Titanium Grade 7 U-bend specimens described in Section 6.2.1, which did not experience stress corrosion cracking initiation after up to five years exposure at stresses at or somewhat above the yield strength. According to *Multiscale*

Thermohydrologic Model (BSC 2004 [DIRS 169565], Section 6.3.7), the drip shield can potentially reach temperatures over 250°C following a low-probability seismic collapsed drift and a low rubble thermal conductivity). However, aqueous surface brine films needed for stress corrosion cracking are unlikely to form above about 160°C and the drip shield is projected to spend most of its lifetime below 140°C. Therefore, the drip shield wall temperature at which the yield strength (YS) value is conservatively selected is 140°C. The YS for Titanium Grade 7 at 140°C, using a straight-line interpolation between the room temperature (20°C) and 204°C values from Table 4-5, is 220.7 MPa. Thus, the threshold stress for crack initiation is 0.5 (YS) (i.e., 110.4 MPa) (Section 6.2.1). The size (depth) of the initiated crack, based on Section 6.2.1, is 0.05 mm. Once initiated, it will take about 40 years for the crack to grow through the 15-mm drip shield wall (BSC 2001 [DIRS 156807], Table 5-13) based on an stress corrosion cracking crack growth rate of 1.25×10^{-8} mm/sec estimated by DTN: LL021105312251.023 ([DIRS 161253], Section 1.3, p. 14).

Once the stress corrosion cracking-initiated crack develops into a through-wall crack, the crack length "2c" and the crack gap (or width) "δ", according to *Plugging of Stress Corrosion Cracks by Precipitation* (BSC 2001 [DIRS 156807], Table 5-13) are 130 mm and 157 microns, respectively. Thus, the dense passive corrosion oxide film growing normal to each opposing crack face would need to grow until it fills the 157-micron gap. This is equivalent to ~103 microns of metal loss per crack side and results in a total per side oxide thickness of ~182 microns based on a TiO_2 oxide to metal volume ratio of 1.76 (Bradford 1987 [DIRS 151988], Table 2, p. 64). At a corrosion growth rate of 0.03 microns metal loss per year, it will take ~3,400 years for the crack to fill with corrosion product. In the interim, while the faces are corroding passively, but before the corrosion film grows to a thickness where it will completely fill the crack, there could be a small amount of water transport by surface diffusion (film flow) into the crack and through the drip shield. However, the small heat flux present across the drip shield wall will result in evaporation of the slowly flowing water and a resultant scale deposit (principally calcium carbonate [calcite]) will form over the crack where it intersects the upper drip shield surface, as well as within the crack. This formation of calciferous deposits is well documented (Cowan et al. 1976 [DIRS 105212], pp. 1 to 39 and 376 to 383) in seawater environments and in heat exchangers through which natural brines are forced to flow, such as in desalination plants (carrying ~6% NaCl solutions) and in potash plants (carrying >12% brine (NaCl/KCl mixtures). In both these cases, titanium surfaces are heat sources at operating temperatures of ~100°C. Such deposits form rapidly under flowing conditions, and have to be regularly removed to avoid loss of heat exchanger efficiency. Other minerals such as amorphous silica will also precipitate.

A detailed calculation of the expected rate of stress corrosion cracking plugging due to calcite precipitation resulting from evaporation of a pore water of typical composition dripping onto a drip shield at the crack location has been performed (BSC 2001 [DIRS 156807]). The calculation conservatively assumes that (BSC 2001 [DIRS 156807], Section 5.3) corrosion products generated on the crack faces as well as colloids, particulates, and any precipitated silica minerals do not help in plugging the crack opening and that there is a uniform water seepage flow in space and time. It was concluded that (BSC 2001 [DIRS 156807], Section 6.3) stress corrosion cracking cracks are sealed in a few hundred years at most when water is allowed to flow through the cracks at a low film flow rate. When the cracks are bridged by water, the sealing process may take thousands of years, but no flow occurs as the water is held by capillary

forces. In a more realistic case of a nonuniform flow onto the drip shield, more precipitation and faster plugging will occur.

Following plugging of such a drip shield crack, any solution flow through the crack would be dominated by an efficiency factor determined by the ratio of solution runoff on the drip shield surface compared to through crack flow that in turn is determined by scale porosity and permeability. Because of the expected high density of the calcite deposits (BSC 2001 [DIRS 156807]) and lack of a pressure gradient to drive water through the crack, the probability of solution flow through the plugged crack would approach zero. However, even if it were conservatively assumed that brine transport through any stress corrosion cracking breached areas occurs by advective flow, it is highly unlikely that the resultant under drip shield seepage flow would align with any through-wall stress corrosion cracking areas on the waste package. Thus, this discussion provides a sound technical basis for excluding further consideration of drip shield stress corrosion cracking in TSPA-LA.

Finally, multiple rockfalls on the same spot of the waste package are ruled out because of the small probability. Drip shield structural response to rockfalls induced by seismic events is addressed in *Drip Shield and Waste Package Emplacement Pallet Design Report* (BSC 2004 [DIRS 166879]), where the damaged area of the drip shield is calculated for each of the given rock masses. The damaged area is defined as a region of the drip shield where the calculated stress exceeds the threshold stress. Seismic stress corrosion cracking is discussed further in Appendix B.

6.4 EVALUATION OF STRESS INTENSITY FACTOR

6.4.1 Introduction

The stress intensity factor K_I is defined as a function of stress (σ) and crack depth size (a):

$$K_I(a, \sigma) = \beta \sigma (\pi a)^{1/2} \quad \text{(Eq. 21)}$$

where

β is a geometry factor dependent on the size and shape of the crack and the configuration of the structural component

σ is the tensile stress distribution through the wall thickness of the structural component.

Closed-form solutions are possible only in some simple cases of uniform tensile stress and simple geometry. For example, in considering the classical problem of a single-edge cracked plate with thickness "h," it has been shown that β can be expressed by the following formula (Ewalds and Wanhill 1984 [DIRS 118602], p. 49):

$$\beta = 1.12 - 0.231\left(\frac{a}{h}\right) + 10.55\left(\frac{a}{h}\right)^2 - 21.72\left(\frac{a}{h}\right)^3 + 30.95\left(\frac{a}{h}\right)^4$$

In most practical cases where stresses are nonuniformly distributed across the thickness, the stress intensity factor has to be calculated by some numerical algorithms, such as the finite

element method. Rice (1968 [DIRS 147983], p. 381) has shown that path-independent J-Integral taken over an arbitrary contour surrounding the crack tip is proportional to the square of the crack tip stress intensity factor K_I. According to Chan et al. (1970 [DIRS 147968], p. 8), by numerically evaluating the J-Integral for the finite element solution over a path surrounding the crack tip, an estimate of the crack tip stress intensity factor can be obtained.

Although finite element programs can be used to evaluate the stress intensity factor, the effort is usually quite time consuming because a series of elaborate finite element analyses must be completed for numerous crack sizes starting from 0 through the thickness of the containment wall. A simplified solution has been developed by using fracture mechanics to evaluate the parameter $(K_I)_{PCCRACK,}$ the stress intensity factor (Section 6.4.2.3). Then a geometry correction factor, G, which is usually a function of the crack size "a," is evaluated from the results of finite element analysis. Finally, the true stress intensity factor (K_I) is derived from $(K_I)_{PCCRACK}$ and G. This section summarizes the methodology, calculation procedures, and selected results, which are also discussed in detail in *Evaluation of the CRM-21 PWR and Viability Availability Waste Package* (SI 2003 [DIRS 162457]).

6.4.2 Calculations of Stress Intensity Factors for Waste Package Closure Welds

6.4.2.1 Introduction

Only weld-induced residual stress in the final closure welds of the waste package outer barrier are considered for performance assessment, based on the following reasons:

1. Stress corrosion cracking of the drip shield is excluded from the performance assessment. According to Section 6.3.7, the sources of stress corrosion cracking in the Titanium Grade 7 drip shield are (1) weld-induced residual stress; (2) plastic residual stress caused by seismic events; and (3) residual stress produced by rockfalls. The weld-induced residual stress is eliminated by annealing. The threshold stress for crack initiation developed in Section 6.2.1 is used as the through-wall crack propagation criterion for seismic-induced stress corrosion cracking. Seismic stress corrosion cracking is discussed further in Appendix B. An analysis of the consequence of residual stress produced by rockfalls presented in Section 6.3.7 indicated that stress corrosion cracking resulting from rockfall will result in very tight crack openings and will not degrade the water diversion function of the drip shield. The Stainless Steel Type 316 inner barrier of the waste package will also be excluded from the stress corrosion cracking evaluation because the TSPA-LA will not take credit for the inner barrier.

2. Sustained postclosure stresses in the waste package Alloy 22 outer cylinder including internal pressure stresses and waste package and pallet contact stresses are limited by design and are significantly below 0.9(YS) (BSC 2004 [DIRS 169766], Tables 2, 21, 22, and 23). Therefore, welds are potentially the regions most susceptible to stress corrosion cracking initiation and propagation because (1) welding can produce high-tensile residual stress in the weld area; (2) preexisting flaws due to fabrication and welding have much higher concentration in the weld than in the base metal; and (3) welding could result in segregation and nonequilibrium brittle phases, which could

enhance material susceptibility to stress corrosion cracking. All the welds, with the exception of the final closure welds, are subjected to solution heat treatment to relieve the residual stress when the entire waste package is heat treated before the loading of high level wastes. It is recognized that plastic deformation resulting from lower probability seismic events has the potential of leading to plastic upsets and resultant sustained residual stresses that may initiate cracks and drive them through the wall. Breach criteria (crack opening area) governing seismic initiated residual stress have been developed for the waste package material (i.e., Alloy 22) and are described in Appendix B. The breach criteria are based on a threshold stress, which was discussed in Section 6.2.1. Therefore, weld residual stress is the only type of stress of stress corrosion cracking concern for the waste package.

Since by definition, embedded flaws are not exposed to the external waste package aqueous surface environment, they will not be subjected to stress corrosion cracking and only outer surface-breaking flaws are of concern for performance.

Based on work by Bokhari (2003 [DIRS 162429], Attachment 1, Figure 1), the initially proposed waste package design final closure lid design for the license application (LA) includes the following:

- The inner, stainless steel lid weld is sealed using a spread ring and seal weld.
- The outer lid mitigation method is laser peening.
- The middle Alloy 22 lid weld configuration (indicated as inner lid in Attachment 1, Figure 1 (Bokhari 2003 [DIRS 162429])) is a fillet-type seal weld and will not be stress mitigated.
- A sketch of the initially recommended LA design of the final closure lid area of the waste package (abstracted from Bokhari (2003 [DIRS 162429], Attachment 1, Figure 1) is shown in Figure 6-8. The outer closure lid laser peening stress mitigation process could be replaced with an alternate controlled plasticity burnishing stress mitigation process after further evaluation. Beneficial residual stress profiles resulting from both processes are discussed in Sections 6.4.4 and 6.4.5.

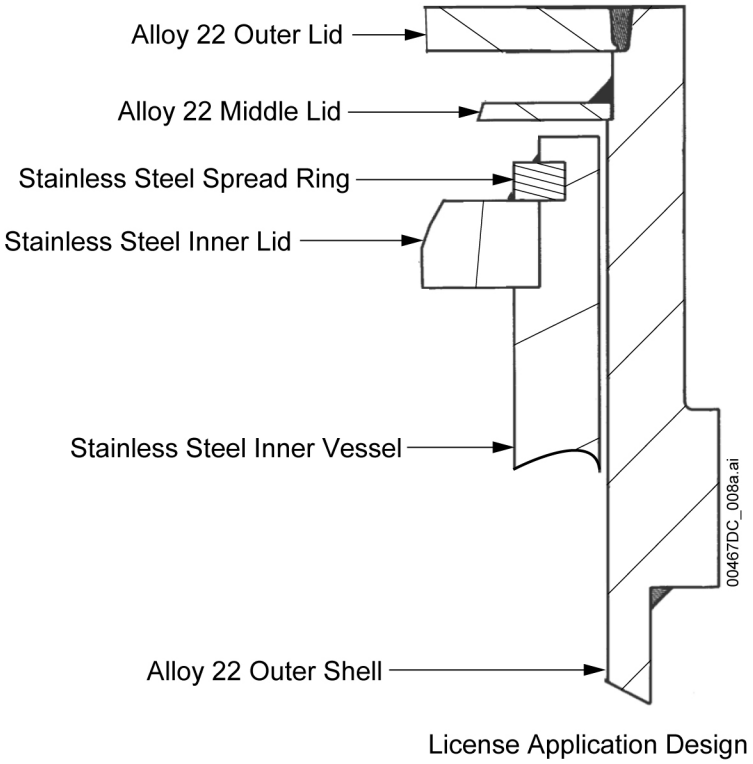

Source: Modified from Bokhari 2003 [DIRS 162429], Attachment 1, Figure 1.

NOTE: Lid thicknesses have been removed.

Figure 6-8. Sketch of Initially Recommended LA Design for Waste Package Final Closure Weld Region

For the TSPA-LA of the waste package subjected to stress corrosion cracking, stress and stress intensity factor profiles due to weld residual stress in the closure welds are needed for the 25-mm Alloy 22 (actually currently 1 in. or 25.4 mm) outer lid subjected to laser peening and the as-welded 10-mm Alloy 22 (actually currently 0.5 in. or 12.7 mm) middle lid (BSC 2004 [DIRS 170710]). These stress and stress intensity factor profiles were provided by a vendor and were saved in DTN: LL000316205924.142 [DIRS 148895]). They were calculated prior to the current LA design using two different waste package designs–one with an equivalent outer lid geometry and one with the middle lid weld geometry. These outer and middle lid equivalent designs are, respectively, 1) the CRM–21-PWR design (which has a single 25-mm Alloy 22 outer lid), as shown in Figure 6-9, and 2) the modified CRM–21-PWR design (which is similar to the CRM-21-PRW design but with the outer lid thickness reduced from 25 mm to 10 mm). It can be seen that the flat-head outer lid of the currently recommended waste package design is similar to the outer lid of the CRM–21-PWR design not only in their geometrical configurations but also in the welding processes. Section 6.2.2.1 indicates that the current welding process being considered for the waste package final closure lid weld is a gas tungsten arc welding process. Section 6.4.2.2 shows the heat generation rate used as the input for the thermal analysis of the CRM–21-PWR design is equivalent to that of a gas tungsten arc welding welding procedure. Therefore, calculated stress and stress intensity factor profiles for the 25-mm outer Alloy 22 lid of the CRM–21-PWR design are used for the as-welded and laser-peened Alloy 22 waste package outer lid (WPOL) of the current design and calculated stress and stress intensity factor profiles for the as-welded 10-mm Alloy 22 lid of the modified CRM–21-PWR design are

used for the proposed Alloy 22 waste package middle lid. As discussed earlier, subsequent to the proposed waste package closure lid design indicated by Figure 6-8, the middle lid thickness was changed to 0.5 in. (12.7 mm) (BSC 2004 [DIRS 170710]). However, as discussed in Section 6.4.2.4, this small increase in thickness (12.7 mm versus 10 mm) does not have a significant effect on calculated through-wall, as-welded residual stress and corresponding stress intensity distributions or on the estimated time for through-wall stress corrosion cracking growth. Further, the time required to remove the stress mitigated layer at the outer closure lid weld is greater than 10,000 years after permanent closure, as described in Section 6.4.5.

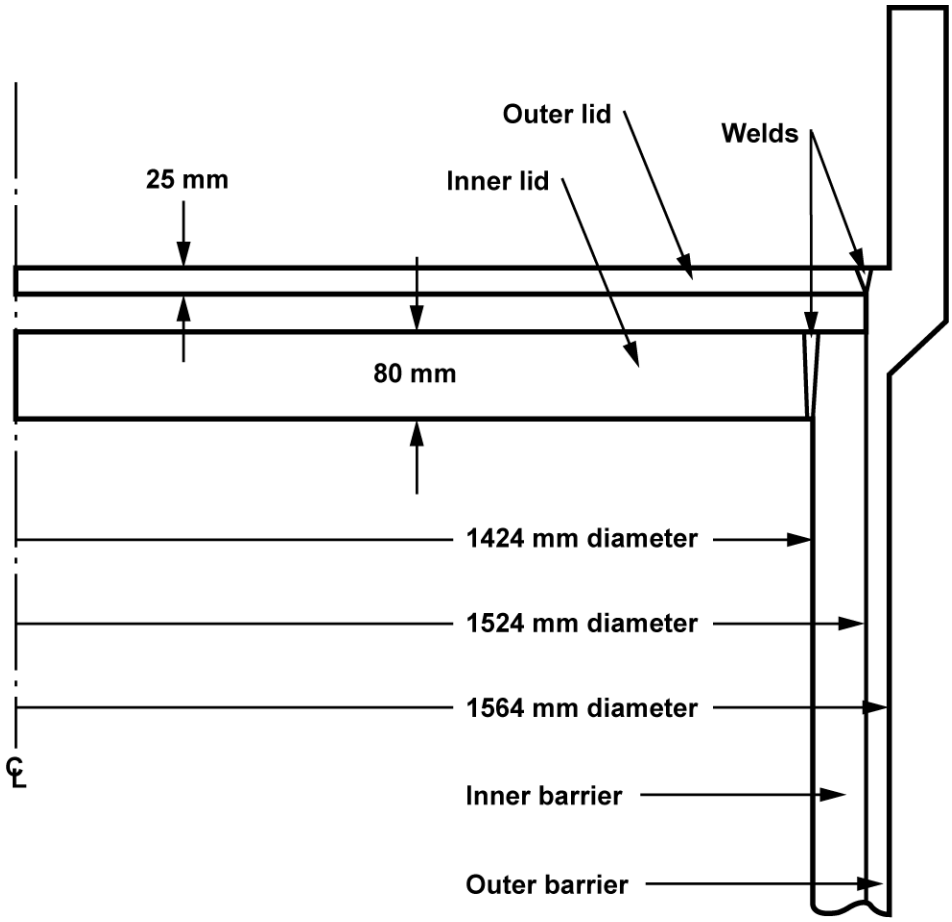

Source: SI 2003 [DIRS 162457], Figure 1-4.

Figure 6-9. Schematic and Dimensions for the CRM–21-PWR Waste Package Design

6.4.2.2 Stress Analysis

Finite Element Model–Determining the weld residual stress requires a thermal analysis to determine the temperature history caused by the welding process and a subsequent weld residual stress analysis. This problem has been solved using finite element analysis methods. Although the determination of weld residual stress for the waste package welds is a three-dimensional problem, it has been found that the use of two-dimensional axisymmetric modeling of the problem provides a reasonable estimate of the behavior (Chan et al. 1970 [DIRS 147968], p. 3).

Thus, the waste package closure weld models were treated as being two-dimensionally axisymmetric about the waste package axial centerline.

The finite element model for the CRM–21-PWR design of the waste package (Figure 6-9) is shown in Figure 6-10. The weld geometry and immediate neighboring material for the outer lid are modeled in detail with sufficiently small elements to capture the large thermal and strain gradients associated with the weld pass application. The element sizes become larger with distance from the weld since the field variable gradients are significantly lower. More on the finite element model is discussed in this section under "Thermal Analysis."

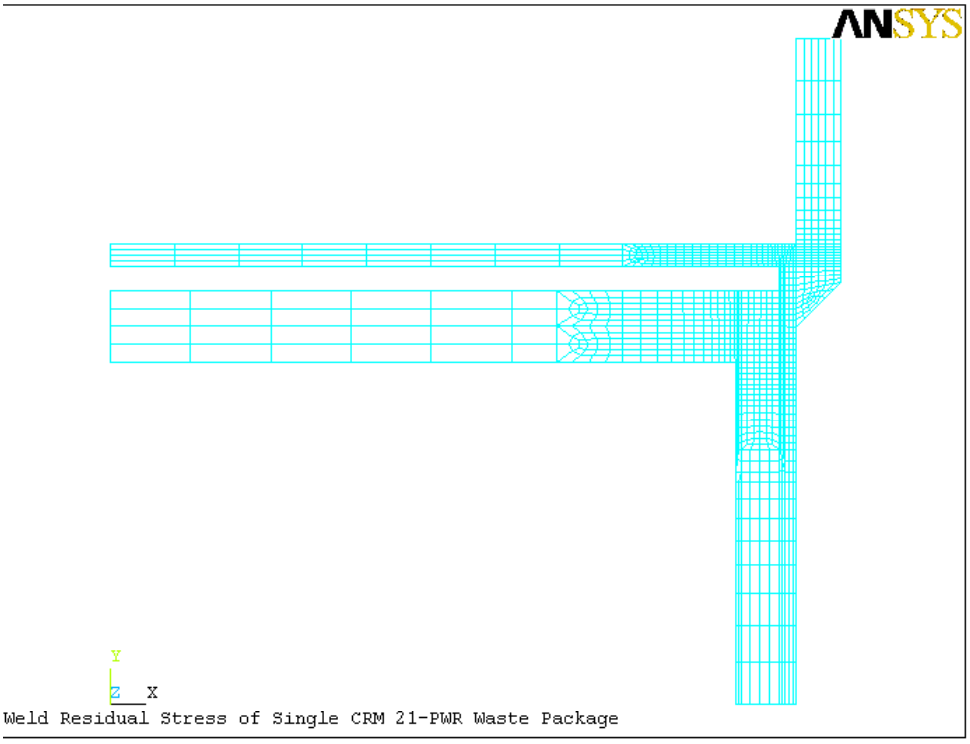

Source: SI 2003 [DIRS 162457], Figure 1-2.

Figure 6-10. Finite Element Model for the CRM–21-PWR Waste Package Design

Figure 6-10 shows the finite element model with all outer lid weld passes deposited. Material making up the individual weld passes is added to the model as each weld pass is simulated. This process continues until all weld beads (or groups of weld beads) are applied.

Figure 6-11 includes a close-up view of the outer-lid finite-element model (Figure 6-12) where axisymmetrical cross sections selected for stress output are identified. The radial stress in the x-direction (S_x) is normal to the section while the hoop stress in the z-direction (S_z) is tangential to the section. Similarly, Figure 6-12 is the close-up view of the modified CRM–21-PWR design that shows the cross sections for stress output. Section 1-1 is selected such that the stress normal to the section, S_n, is maximized. The stress component, S_n, is conservatively used as the radial stress, S_x, in the weld. Section 2-2, likewise, is selected such that the hoop stress, S_z, is maximized and this stress component is conservatively used as the hoop stress in the weld. The

distance (or crack depth) measured from the outer surface of the closure lid on Sections 1-1 or 2-2 is projected to a vertical cross section that is normal to the plane of the closure lid.

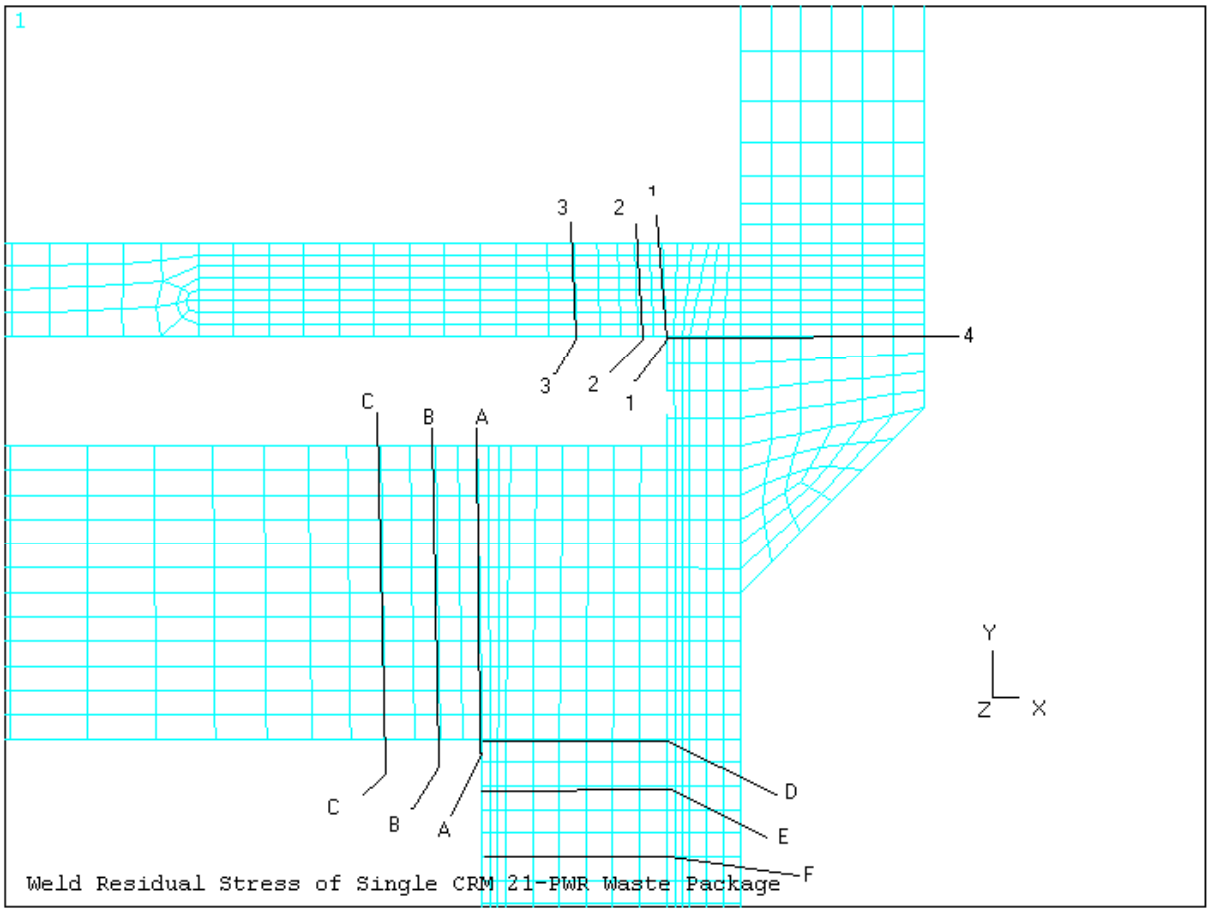

Source: SI 2003 [DIRS 162457], Figure 2-1.

Figure 6-11. Selected Cross-Sections for CRM–21-PWR Waste Package Design

Material Properties—The material properties are important to the determination of the final weld residual stress. The material properties used in this evaluation for Alloy 22 are discussed in detail in *Evaluation of the CRM-21 PWR and Viability Availability Waste Package* (SI 2003 [DIRS 162457]). For the thermal analysis, the material properties used are thermal conductivity, specific heat, and density. For the stress analysis, the material properties used are coefficient of thermal expansion, Young's modulus, Poisson ratio, density, and yield strength. Nonlinear properties, such as the elastic–plastic behavior and temperature dependency, are also used.

Thermal Analysis—A thermal analysis of the waste package closure was performed to simulate the temperature history caused by each weld pass. Each weld pass will result in a different temperature field because as passes are applied, more material is added, residual stress from previous passes are being incorporated, and the relative location of the weld heat input is changing with respect to the lid thickness.

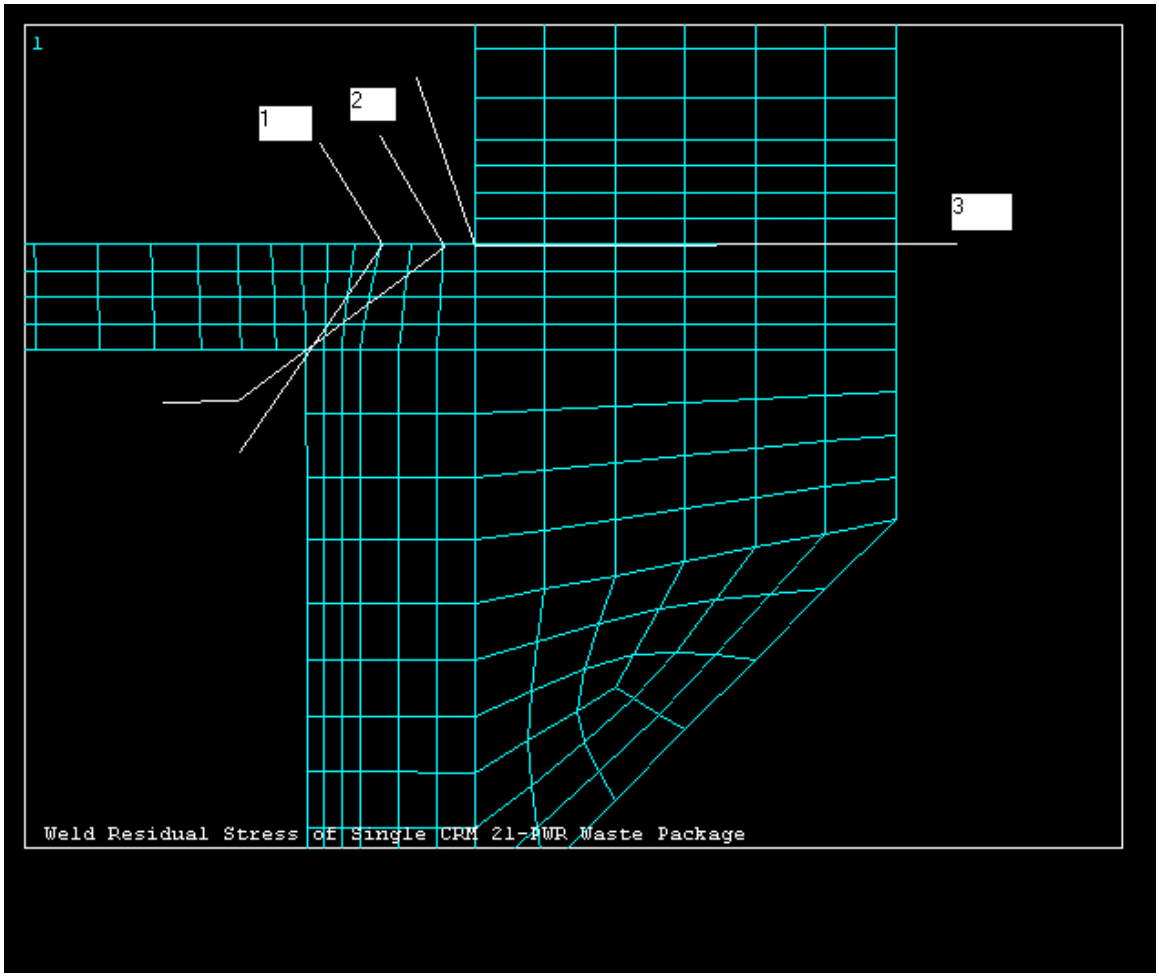

Source: Adapted from Figure 6-11 to show close-up view with cross sections used for stress outputs shown in Figure 6-14.

Figure 6-12. Selected Cross-Sections for the Modified CRM–21-PWR Waste Package Design

The finite element analysis was performed on the CRM–21-PWR closure lid design, as the detailed LA design configuration and dimensions were not then available. However, that design is consistent with the currently described LA design in terms of having a flat, outer final closure lid with a thickness of 1 inch. Thus, the analysis on 1-inch-thick welded Alloy 22 was representative and expected to yield residual stress results similar to those expected for the TSPA-LA waste package. Nominal welding parameters and not the extreme ranges of these parameters were used in the analysis and weld heat inputs were not bounded (maximum or minimum), although the analysis also added a factor of 15% to account for the heat input represented by the filler metal. To provide a basis for expected stress variability due to the range of process parameters, a literature search on the expected range of residual stress variability in similar thickness weldments provided the basis for the expected uncertainty limits to be used for the calculated residual stresses (Section 6.4.5). The heat input used in the finite element calculation can be compared with maximum and minimum expected heat inputs once the detailed welding process and control limits have been specified.

In the design approach, the closure weld is susceptible to stress corrosion cracking initiation and growth and this degradation mode is to be precluded by mitigating the tensile residual stresses by implementing a mechanical stress mitigation process, laser peening (with controlled plasticity burnishing as an alternative process). A series of design prototype waste packages will be fabricated to characterize the closure weld in great detail.

The effect of each weld pass was simulated through heat generated in the finite elements, which represent the weld pass, and then the heat is transferred to the adjoining parts of the waste package. The heat generated in the weld pass, represented by the net heat input (H_{net} in joules/in.) of the welding process can be calculated with $H_{net} = f_1 EI/v$ (Connor 1991 [148469], p. 33, Equation 2.3) for given welding parameters including voltage (E), amperage (I), travel velocity of the heat source (v in in./sec) and heat transfer efficiency (f_1). Based on a gas tungsten arc welding process, the amperage, voltage and average travel speed are, respectively, 330 to 335 A, 12.1 to 13.0 V and 8.0 in./min (0.133 in./sec) (CRWMS M&O 1998 [DIRS 107722], Table 7-1, p. 12). The heat transfer efficiency (f_1) for gas tungsten arc welding, according to Connor (1991 [148469], Figure 3.1A, p. 69) is 21% to 48%. Using the average values for E (12.55 V), I (332.5 A), v (0.133 in./sec), and f_1 (0.345) and adding 15% to the final result (to represent heat contributed by the filler material), the net heat input is found to be 12,400 joules/in., which is close to the heat generation rate (12,268 joules/in.) used in the finite element thermal analysis (SI 2003 [DIRS 162457], p. 1-8).

For the axisymmetric representation of the three-dimensional problem, it is desired to convert the nonaxisymmetric heat input into an equivalent axisymmetric heat input, which is representative of what a typical point on the circumference of the weld would experience. Since a typical point on the circumference would essentially experience an impulse heat input (i.e., a large amount of heat input over a short amount of time), the heat input is represented by a triangular-shaped pulse for two seconds (ramp up in one second and ramp down in one second) followed by a cooling period. The length of cooling period after the deposit of weld beads is determined by the time required for the weld torch to travel around the circumference of the closure weld.

Weld Residual Stress Analysis—The stress analysis is performed for all individually modeled weld passes. For example, if six weld passes are modeled, then six thermal stress analyses are performed. The analysis of Weld Pass 1 uses the temperature history for Weld Pass 1 thermal analysis. The analysis of Weld Pass 2 uses the Weld Pass 2 thermal analysis and the residual stress due to Weld Pass 1 as the initial condition. This process continues until all weld passes are analyzed. The final solution (at ambient conditions) is the room temperature weld residual stress.

6.4.2.3 Stress Intensity Factor Calculations

For the waste package closure welds, the flaw orientations most likely susceptible to crack propagation are those of a circumferential flaw (parallel to weld) and a radially oriented flaw (perpendicular to weld). Figure 6-13 shows the flaw orientations with respect to the weld. A radially oriented flaw would be potentially driven by hoop stress. A circumferentially oriented flaw would be driven by radial stress.

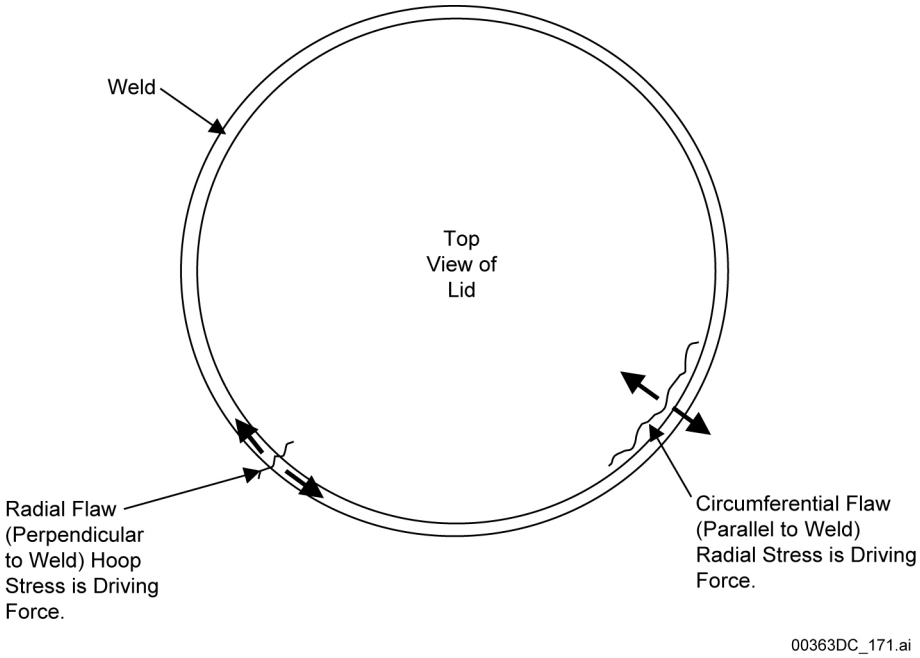

Figure 6-13. Flaw Orientation for Lid Welds

A general form of the stress intensity factor is expressed by Equation 21, i.e.:

$$K_I = \beta \sigma (\pi a)^{1/2} \quad \text{(Eq. 21)}$$

As indicated in Section 6.4.1, β is a geometry factor dependent on the size and shape of the crack and the configuration of the structural component, and σ is the stress distribution through the wall thickness of the structural component. Closed-form solutions of Equation 21 are possible only in some simple cases of uniform tensile stress and simple geometry.

Although finite element analyses can be used to evaluate the stress intensity factor (Section 6.4.1), the effort is usually quite time consuming because a series of elaborate finite element analyses must be completed for numerous crack sizes starting from 0 through the thickness of the containment wall.

A simplified solution procedure was developed by using fracture mechanics to evaluate the parameter $(K_I)_{PCCRACK}$ for a given stress distribution. Then a geometry correction factor, G, as a function of the crack size "a," was developed by curve fitting from comparing the simplified solutions with the results of finite element analysis for only a limited number of crack sizes. Given the geometry correction factor, the true stress intensity factor, K_I, for any crack size can be derived from $(K_I)_{PCCRACK}$ and G, without going through the finite element analysis using the following relationship:

$$K_I = G\,(K_I)_{PCCRACK} \quad \text{(Eq. 22)}$$

For a circumferential flaw, $(K_I)_{PCCRACK}$ was derived from an infinite single edge cracked plate (SECP) with an infinitely long flaw. For a radial flaw, $(K_I)_{PCCRACK}$ was derived from an elliptical surface crack in an infinite plate with a crack aspect ratio of 1 (a semicircular crack). In

either case, the stress distribution was calculated by using a third order polynomial of the type represented by the following equation:

$$\sigma = A_0 + A_1x + A_2x^2 + A_3x^3 \quad \text{(Eq. 23)}$$

where x is the distance from the outer surface of the closure lid and A_0, A_1, A_2, and A_3 are coefficients of the third-order polynomial fit of the through-wall stress distribution (or profile).

The model of a circular crack in an infinite plate is a better representation of a limited-length radial crack in the closure weld rather than an infinite edge crack in an infinite SECP. It is judged that a radial crack in the closure weld would not grow into a long semielliptical crack due to the rapid decay of hoop stress in the radial distance away from the weld and base metal interface, as indicated by examination of Figure 6-14, where "1-1", "2-2", and "3-3" are section identifications as indicated in Figure 6-11.

The stress intensity factor for an infinite SECP with an infinitely long flaw is (Buchalet and Bamford 1976 [DIRS 118597], Equation 2, p. 388):

$$(K_I)_{SECP} = \sqrt{(\pi a)}\left[A_0F_1 + \left(\frac{2a}{\pi}\right)A_1F_2 + \left(\frac{a^2}{2}\right)A_2F_3 + \frac{4a^3}{3\pi}A_3F_4\right] \quad \text{(Eq. 24)}$$

where F_0, F_1, F_2, and F_3 are magnification factors and A_0, A_1, A_2, and A_3 are coefficients of the third-order polynomial fit of the through-wall stress distribution (or profile) as indicated in Equation 23.

The magnification factors F_0, F_1, F_2, and F_3 are functions of the crack depth ("a") versus thickness ("h") ratio (a/h). They are graphically presented by Buchalet and Bamford (1976 [DIRS 118597], Figure 6), and used to calculate the stress intensity factor.

The SECP stress intensity factor is for the ideal geometry and must be modified by the geometry correction factor (G) to consider the actual geometry. Figure 6-15 shows, for a circumferential flaw, the G-factor distribution in the closure weld of the outer lid of the CRM–21-PWR waste package as a result of curve fit based on the exact G values calculated at four discrete points corresponding to crack-versus-thickness ratios of 0.2, 0.3, 0.4, and 0.6. Figure 6-15 indicates, for shallow flaws, the correction factor is near 1. For deeper flaws, the correction becomes significant, and using the SECP solution would be very conservative. For a radial flaw, the simplified solution obtained from a fracture mechanics crack model that contains a semicircular surface flaw in a flat plate and is judged to be close to the final solution. Therefore, the geometrical correction factor received a value of unity for the case of radial cracks.

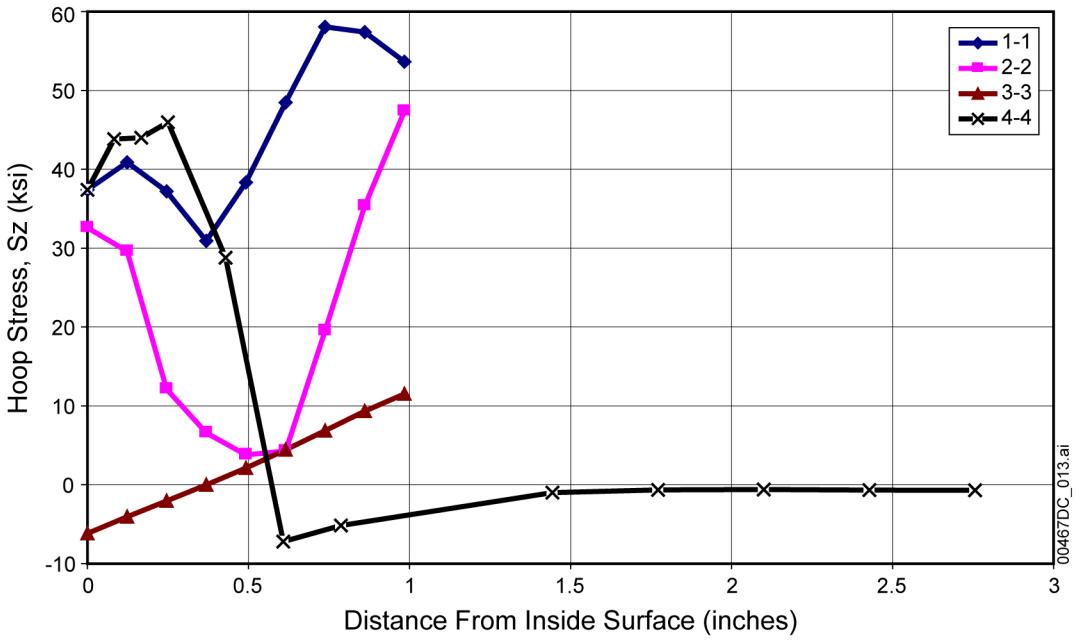

Source: SI 2003 [DIRS 162457], Figure 2-10.

Figure 6-14. Hoop Stresses in Outer Lid of CRM–21-PWR Design

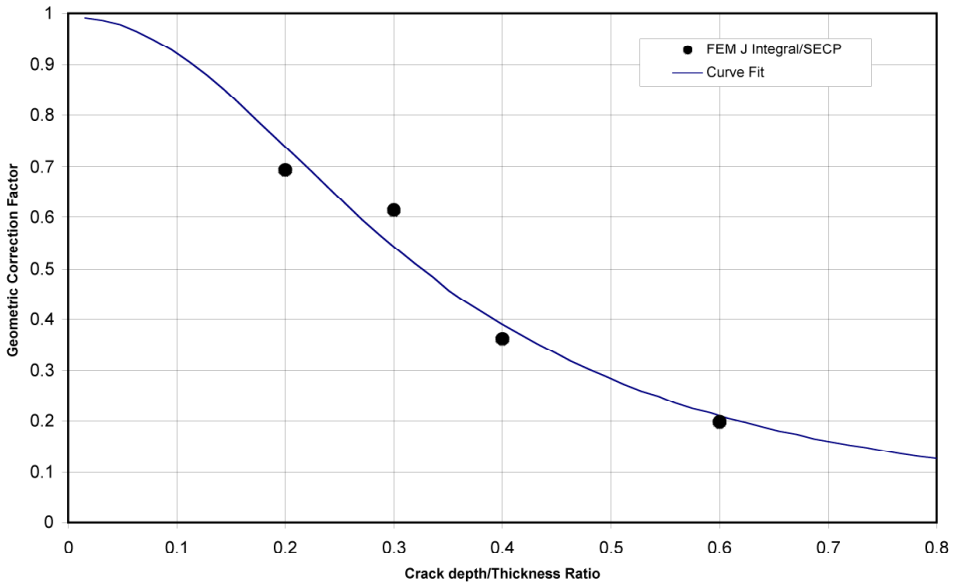

Source: SI 2003 [DIRS 162457], Figure 3-11.

Figure 6-15. Outer Lid Circumferential Flaw Geometric Correction Factor

6.4.2.4 Numerical Results

According to Section 6.4.2.1, calculated stress and stress intensity factor profiles for the 25-mm outer Alloy 22 lid of the CRM–21-PWR design are used for the as-welded and laser-peened outer Alloy 22 lid of the proposed design and calculated stress and stress intensity factor profiles

for the as-welded 10-mm Alloy 22 lid of the modified CRM–21-PWR design are used for the middle Alloy 22 lid of the current design.

The values of the coefficients in Equation 23 for the closure-lid welds of both waste package designs are documented in DTN: LL000316205924.142 [DIRS 148895]. For radial and hoop stresses in ksi in the 25-mm outer closure-lid weld of the CRM–21-PWR design, the coefficients, A_0, A_1, A_2, and A_3 with stress in ksi and distance, x, in inches are obtained from DTN: LL000316205924.142 [DIRS 148895], file name: Skvrbr1, sheet "UnAnneal, S_x", cells C9 to C12 for radial stress and sheet "UnAnneal, S_z", cells C9 to C12 for hoop stress. The coefficients are listed in the first and second rows of Table 4-3. Table 6-7 shows the converted stress coefficients, A_0, A_1, A_2, and A_3, in the metric unit system. The unit conversions used are: 1 in. = 25.4 mm; and 1 ksi = 6.8947568 MPa.

Table 6-7. Stress Coefficients for the As-Welded Waste Package Outer Lid

Stress Coefficient	Unit	Radial Stress	Hoop Stress
A_0	MPa	116.321	382.136
A_1	MPa/mm	9.107	8.096
A_2	MPa/mm^2	-3.146	-1.991
A_3	MPa/mm^3	0.111	0.060

Source: Table 4-3 (first and second rows) with stress coefficients converted to metric units.

Similarly, for radial and hoop stresses in ksi in the 10-mm lid of the modified CRM–21-PWR design, the stress coefficients with stress in ksi and distance, x, in inches are obtained from DTN: LL000316205924.142 [DIRS 148895], file name: Thinlid11, sheet "UnAnneal,1-1.Sn," cells C9 to C12 for radial stress and sheet "UnAnneal, 2-2, S_z", cells C9 to C12 for hoop stress. The coefficients are listed in the third and fourth rows of Table 4-3. Table 6-8 shows the converted stress coefficients, A_0, A_1, A_2, and A_3, in the metric unit system.

Table 6-8. Stress Coefficients for the As-Welded Waste Package Middle Lid

Stress Coefficient	Unit	Radial Stress	Hoop Stress
A_0	MPa	181.636	219.908
A_1	MPa/mm	-177.592	56.494
A_2	MPa/mm^2	23.385	-20.848
A_3	MPa/mm^3	-0.900	1.083

Source: Table 4-3 (third and fourth rows) with stress coefficients converted to metric units.

Tables 6-9 and 6-10 show calculated stress profiles (using Equation 23 and the stress coefficients in Tables 6-7 and 6-8) and stress intensity profiles (obtained directly from Table 4-4) for the outer and middle lids of the waste package design. The 'x' values to be used in Equation 23 to calculate the radial and hoop stress profiles are listed in the first column of Table 6-9 or 6-10. For the 10-mm middle lid, the projected distance should be used as the value of 'x' in Equation 23 to calculate the stress profiles (Section 6.4.2.2 and Figure 6-12).

Table 6-9. Stress Intensity Factor (SIF) Profiles for As-Welded Waste Package Outer Lid

Depth (mm)	Radial Stress (S_x) (Mpa)	SIF due to S_x (MPa$\sqrt{m}$)	Hoop Stress (S_z) (Mpa)	SIF due to S_z (MPa$\sqrt{m}$)
0.3988	119.4598	4.5146	385.0522	9.1593
0.8001	121.6510	6.5821	387.3707	12.9737
1.1989	122.9098	8.2395	389.0855	15.9139
1.6002	123.2952	9.6422	390.2419	18.4031
1.9990	122.8448	10.8381	390.8484	20.6048
2.4003	121.5958	11.8425	390.9359	22.6028
2.7991	119.6065	12.8589	390.5265	24.4741
3.2004	116.8946	13.7858	389.6383	26.2367
3.5992	113.5369	14.5688	388.3055	27.9039
3.9980	109.5607	15.2083	386.5472	29.4912
4.3993	104.9776	15.7061	384.3711	31.0103
4.7981	99.8883	16.0778	381.8281	32.4703
5.1994	94.2707	16.4072	378.9090	33.9004
5.5982	88.2385	16.7029	375.6738	35.3092
5.9995	81.7579	16.8783	372.1047	36.6797
6.3983	74.9532	16.9527	368.2700	38.0157
6.7970	67.8273	16.9314	364.1710	39.3202
7.1984	60.3743	16.8188	359.8023	40.5961
7.5971	52.7311	16.7108	355.2424	41.8581
7.9985	44.8434	16.7482	350.4565	43.1357
8.3972	36.8535	16.7231	345.5282	44.3927
8.7986	28.7025	16.6321	340.4181	45.6302
9.1973	20.5362	16.4938	335.2140	46.8495
9.5987	12.2935	16.3042	329.8729	48.0515
9.9974	4.1211	16.0808	324.4855	49.2372
10.3962	-3.9906	16.0751	319.0413	50.4839
10.7975	-12.0500	15.9957	313.5283	51.7195
11.1963	-19.9125	15.8601	308.0395	52.9442
11.5976	-27.6353	15.6646	302.5282	54.1589
11.9964	-35.0781	15.4259	297.0873	55.3639
12.3977	-42.2929	15.1398	291.6709	56.5598
12.7965	-49.1458	15.0982	286.3704	57.8007
13.1978	-55.6811	15.0836	281.1418	59.0538
13.5966	-61.7735	15.0159	276.0744	60.3022
13.9954	-67.4234	14.8966	271.1577	61.5462
14.3967	-72.6196	14.7274	266.3850	62.7862
14.7955	-77.2538	14.5229	261.8399	64.0228
15.1968	-81.3421	14.6570	257.4879	65.2900
15.5956	-84.7903	15.1057	253.4070	66.5871
15.9969	-87.5993	15.4787	249.5687	67.8801
16.3957	-89.6911	15.7929	246.0446	69.1690
16.7945	-91.0432	16.0516	242.8325	70.4537
17.1958	-91.6143	16.2578	239.9383	71.7343
17.5946	-91.3547	16.6700	237.4217	73.0349
17.9959	-90.2182	17.6878	235.2739	74.4062
18.3947	-88.1765	18.5558	233.5452	75.7773

Table 6-9. Stress Intensity Factor (SIF) Profiles for As-Welded Waste Package Outer Lid (Continued)

Depth (mm)	Radial Stress (S_x) (Mpa)	SIF due to S_x (MPa√m)	Hoop Stress (S_z) (Mpa)	SIF due to S_z (MPa√m)
18.7960	-85.1608	19.2803	232.2369	77.1483
19.1948	-81.1667	19.8861	231.3887	78.5193
19.5961	-76.1004	20.3775	231.0131	79.8904
19.9949	-69.9834	20.7777	231.1380	81.2616

Output DTN: LL030607012251.065.

Source: Table 4-4.

Table 6-10. Stresses and Stress Intensity Factors for the As-Welded Waste Package Middle Lid

Depth (mm)	Radial Stress (S_x) (MPa)	SIF due to S_x (MPa√m)	Hoop Stress (S_z) (MPa)	SIF due to S_z (MPa√m)
0.1593	153.9288	4.9033	228.3849	7.5754
0.3203	127.1172	6.2685	235.9015	10.9665
0.4797	101.7315	6.8580	242.3296	13.7144
0.6407	77.2206	6.9761	247.8300	16.1330
0.8000	54.0676	6.7631	252.3158	18.3358
0.9593	31.9924	6.3044	255.8750	20.3775
1.1203	10.7596	5.8250	258.5570	22.3816
1.2797	-9.2150	5.2651	260.3330	24.3197
1.4407	-28.3699	4.6000	261.2667	26.1726
1.6000	-46.3322	3.8615	261.3655	27.9459
1.7593	-63.3265	3.0726	260.6697	29.6433
1.9203	-79.5368	2.2534	259.1863	31.2668
2.0797	-94.6509	1.4282	256.9724	32.8922
2.2407	-109.0061	0.5951	254.0088	34.5292
2.4000	-122.3284	-0.2400	250.3830	36.1060
2.5593	-134.7922	-1.0656	246.0945	37.6220
2.7203	-146.5363	-1.8707	241.1150	39.0762
2.8797	-157.3405	-2.6491	235.5736	40.4676
3.0407	-167.4522	-3.4047	229.3818	41.8264
3.2000	-176.6850	-4.1787	222.6938	43.2168
3.3593	-185.1690	-4.9390	215.4749	44.5479
3.5203	-193.0032	-5.6775	207.6685	45.8181
3.6797	-200.0480	-6.3965	199.4620	47.0265
3.8407	-206.4725	-7.0865	190.7114	48.1718
4.0000	-212.1664	-7.7528	181.6234	49.2531
4.1593	-217.2211	-8.2576	172.1366	50.3451
4.3203	-221.7016	-8.7427	162.1726	51.3729
4.4797	-225.5376	-9.2143	151.9633	52.3351
4.6407	-228.8312	-9.6605	141.3230	53.2313
4.8000	-231.5367	-10.0894	130.4975	54.0602
4.9593	-233.7127	-10.4950	119.4050	54.8214
5.1203	-235.3959	-10.9446	107.9526	55.4811
5.2797	-236.5735	-11.4131	96.4029	56.0586
5.4407	-237.2926	-11.8636	84.5422	56.5637
5.6000	-237.5602	-12.3055	72.6415	56.9965

Table 6-10. Stresses and Stress Intensity Factors for the As-Welded Waste Package Middle Lid (Continued)

Depth (mm)	Radial Stress (S_x) (MPa)	SIF due to S_x (MPa√m)	Hoop Stress (S_z) (MPa)	SIF due to S_z (MPa√m)
5.7593	-237.4080	-12.7309	60.6057	57.3567
5.9203	-236.8501	-13.1320	48.3342	57.6444
6.0797	-235.9201	-13.7114	36.1065	57.7587
6.2407	-234.6208	-14.4707	23.6946	57.6946
6.4000	-233.0011	-15.2333	11.3811	57.5522
6.5593	-231.0713	-15.9891	-0.9356	57.3322
6.7203	-228.8287	-16.7277	-13.3570	57.0353
6.8797	-226.3414	-17.4611	-25.6005	56.6626
7.0407	-223.5802	-18.4707	-37.8942	56.1419
7.2000	-220.6238	-20.3589	-49.9583	55.3276
7.3593	-217.4669	-22.2128	-61.8935	54.4422
7.5203	-214.0957	-24.0173	-73.7955	53.4878
7.6797	-210.6019	-25.7872	-85.3924	54.6294
7.8407	-206.9348	-27.4989	-96.8987	56.2191
8.0000	-203.1923	-29.1709	-108.0509	57.7865

Output DTN: LL030607012251.065
Source: Table 4-4.

A comparison of the near-outer-surface as-welded hoop stresses for the 25-mm-thick outer lid (Table 6-9) and the 10-mm-thick middle lid (Table 6-10) indicates that for both cases, the tensile stresses in about the outer 1 mm of the lids exceeds the stress corrosion cracking stress initiation criteria of 0.9 YS (YS listed in Section 6.2.1 as 285 MPa) or 257 MPa although only slightly for the 10-mm middle lid.

6.4.3 Impact of Corrosion

The results presented in Section 6.4.2.3 were performed for the as-built condition. Thus, the full thickness for all the waste package components was used. In order to simulate the effect of wall thinning caused by general corrosion, a layer of elements from the outside surface of the outer lid was removed. The thickness of this layer is 0.125 inch (about 3.18 mm), which is equivalent to the removal of 12.7% of the wall of the outer lid. The general corrosion rates are very low for the Alloy 22 material. Based on the mean general corrosion rate of 7.23 nm/yr (Section 6.3.5), the 0.125-inch removal is the amount of material that will corrode in 439,140 years. Removal of these elements causes a redistribution of the stress pattern.

Figure 6-16 shows the row of elements removed to simulate the general corrosion of the outer lid surface. Figures 6-17 and 6-18 show, respectively, the through-wall radial stress profiles (with and without corrosion effects) and hoop-stress profiles at Section 1-1 in Figure 6-16. These results demonstrate the redistribution of the residual stress. In general, the stress distribution appears to be not very sensitive to the effects of corrosion.

Figures 6-19 and 6-20 show the stress intensity factor distribution for Section 1-1 in Figure 6-16 for circumferential and radial cracks. These figures show the stress intensity factor as a function of distance from the outside surface and normalized distance from the outside surface. These figures also demonstrate that the overall effect of general corrosion is small.

(a)

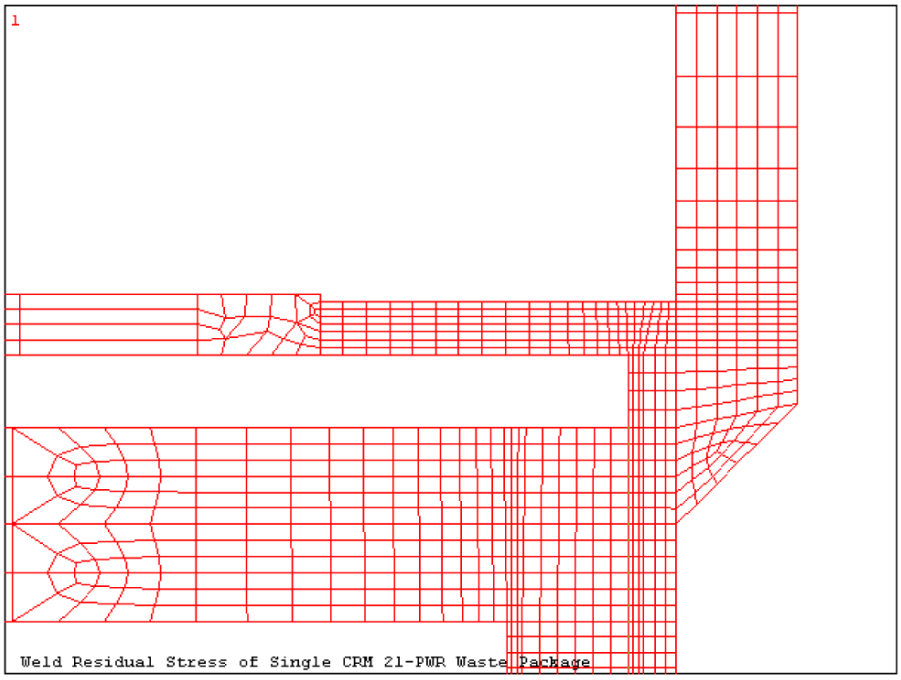

(b)

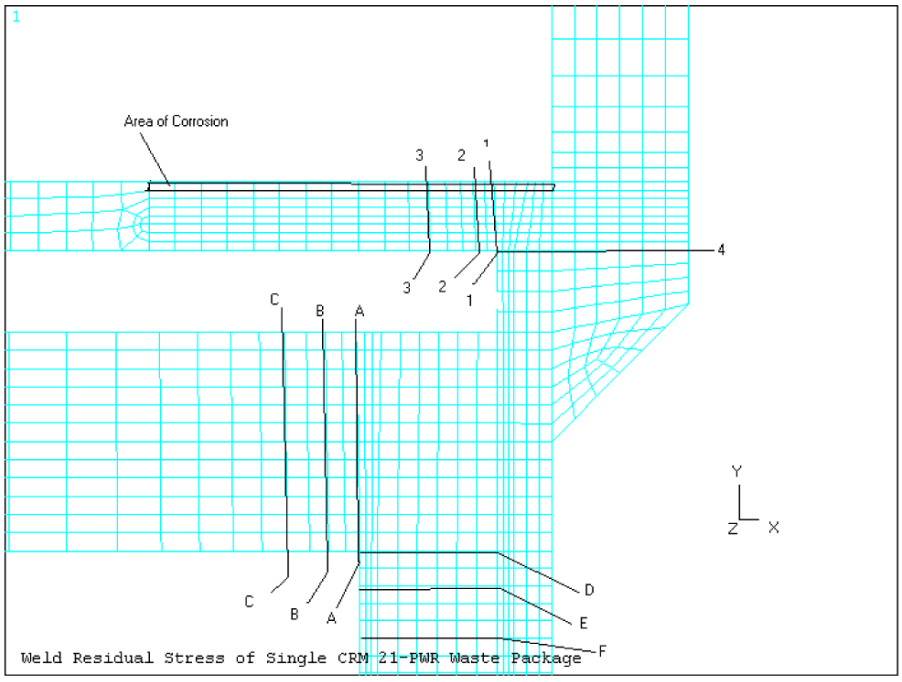

Source: SI 2003 [DIRS 162457], Figure 4-1.

NOTES: (a) Finite element model.
(b) Sections for stress profile.

Figure 6-16. Finite Element Model Used for Study of Corrosion

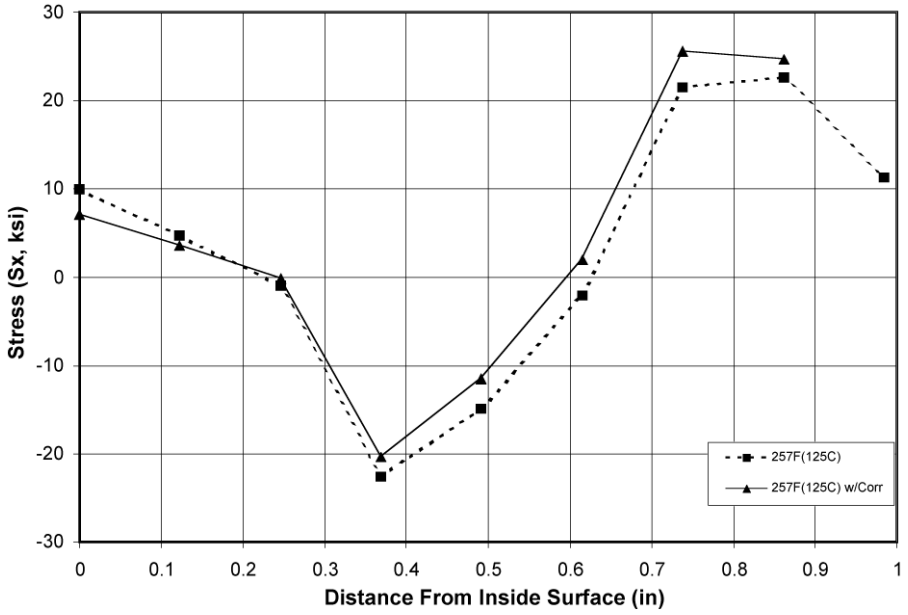

Source: SI 2003 [DIRS 162457], Figure 4-2.

Figure 6-17. Effect of Corrosion on Radial Stress in Outer Lid

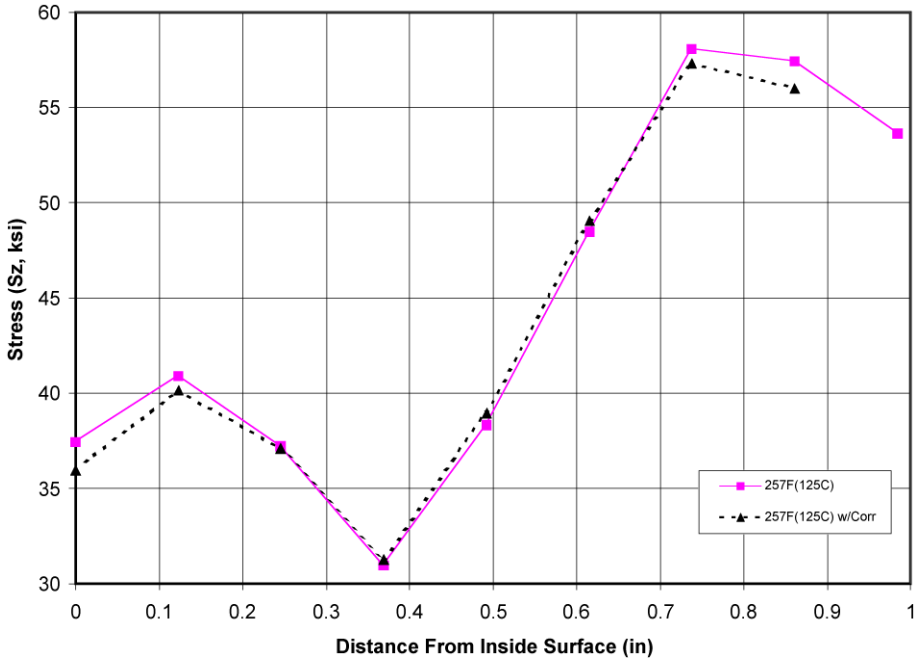

Source: SI 2003 [DIRS 162457], Figure 4-4.

Figure 6-18. Effect of Corrosion on Hoop Stress in Outer Lid

(a)

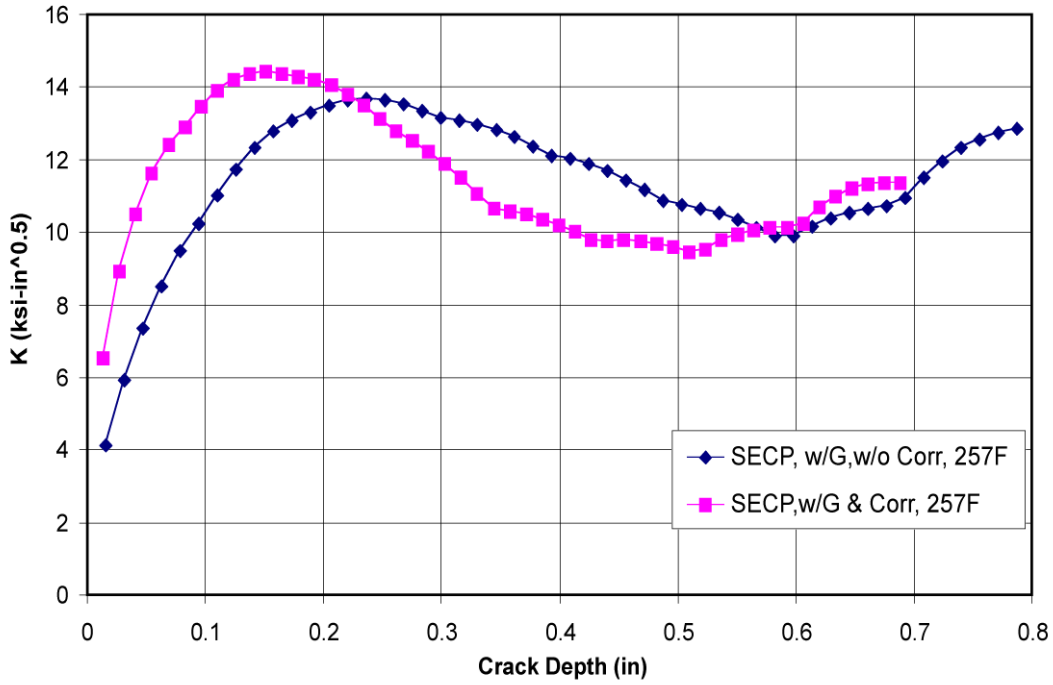

(b)

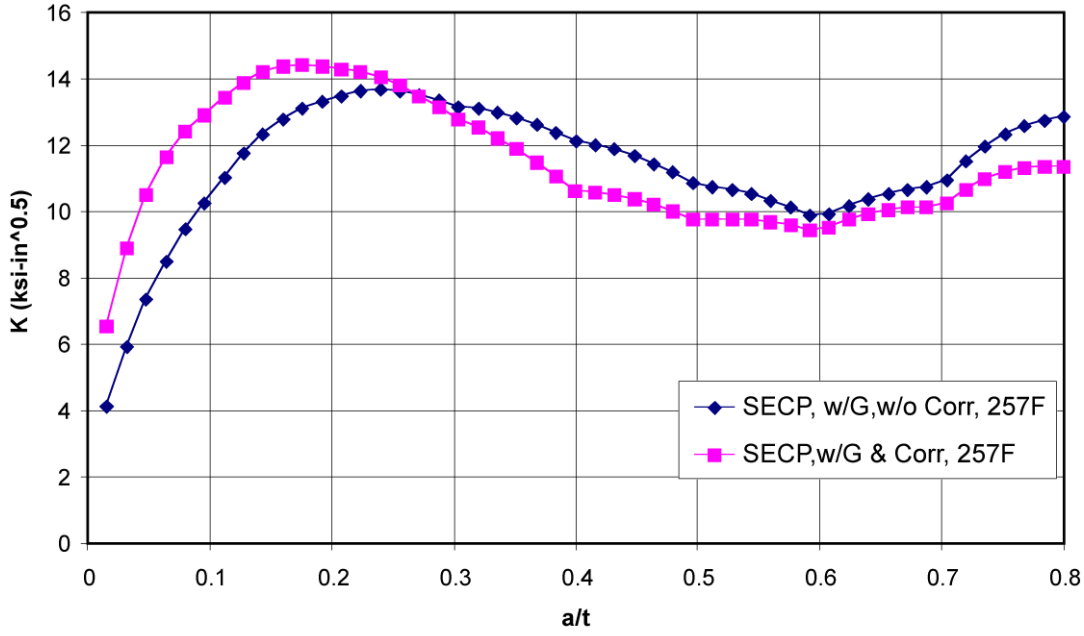

Source: SI 2003 [DIRS 162457], Figure 4-6.

NOTES (a) X-axis is crack depth in inches.
(b) X-axis is shown as the ratio of crack depth (a) versus thickness (t).

Figure 6-19. Stress Intensity Factor for Full-Circumference Flaw in Outer Lid

(a)

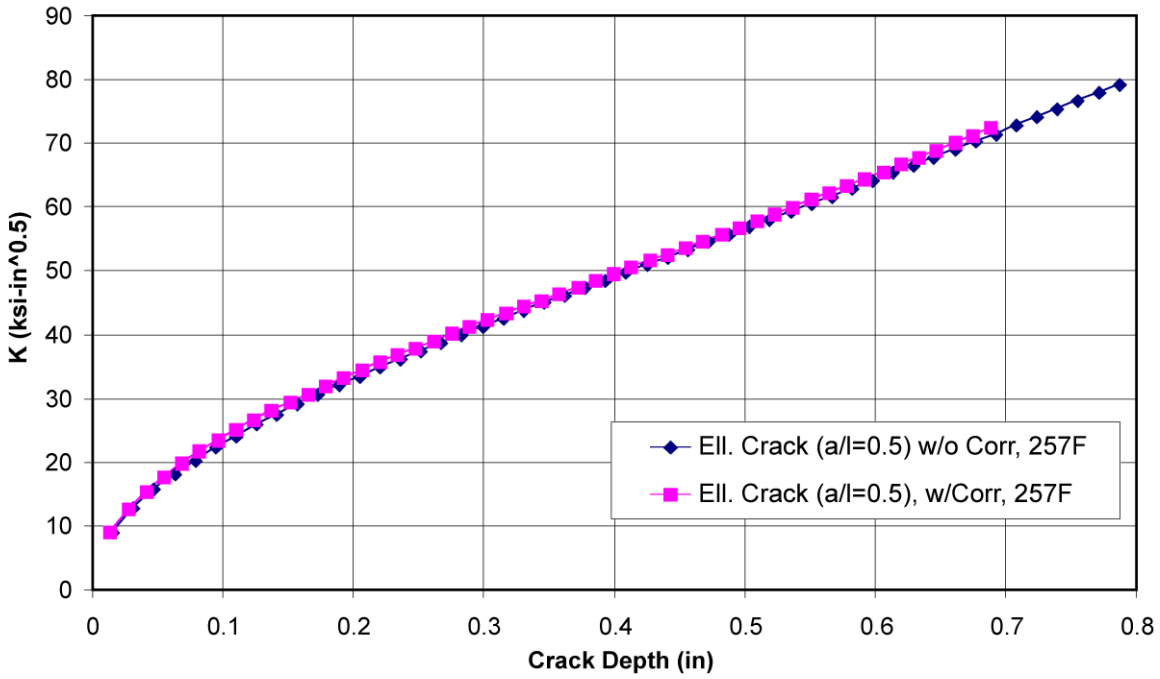

(b)

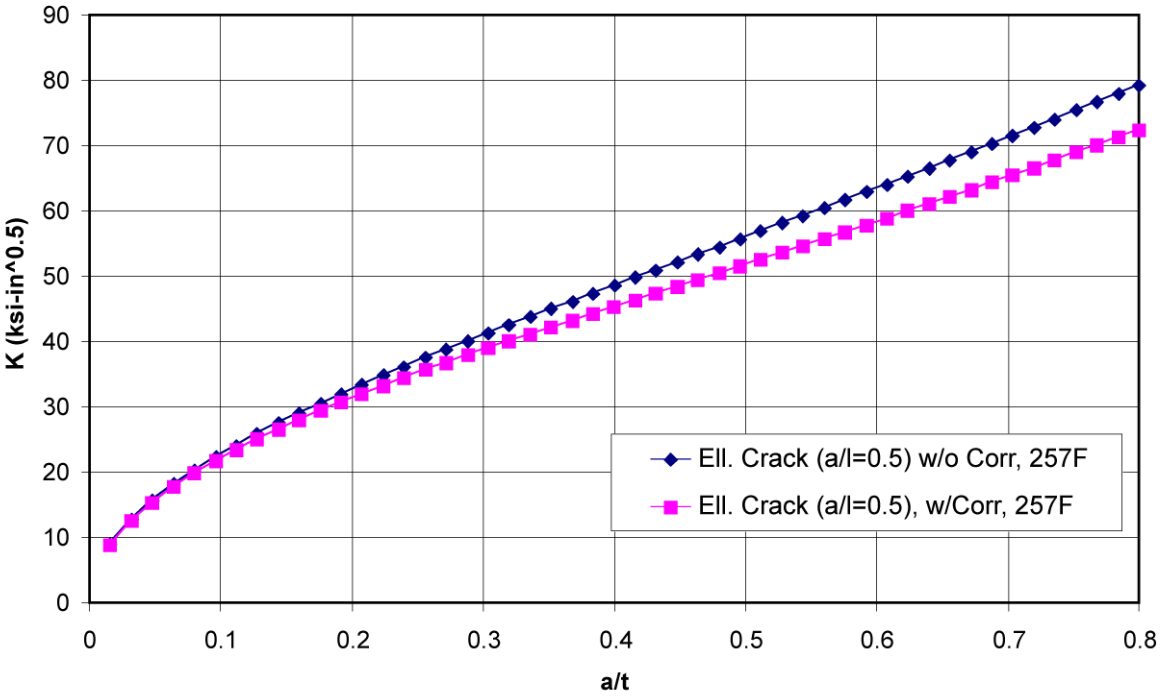

Source: SI 2003 [DIRS 162457], Figure 4-7.

NOTES: (a) X-axis is crack depth in inches.
(b) X-axis is shown as the ratio of crack depth (a) versus thickness (t).

Figure 6-20. Stress Intensity Factor for Radial Elliptical Crack in Outer Lid

6.4.4 Mitigation of Weld Residual Stress

Stress is one of the three basic factors that cause initiation and propagation of cracks in structural components due to stress corrosion cracking. The other two factors are metallurgical susceptibility and environment. Stress corrosion cracking can be reduced to a manageable state if the weld residual stress in the waste package can be effectively mitigated.

Weld residual stress can be mitigated by optimizing the waste package design geometrical configuration. Residual stress can also be mitigated through specially designed weld processes, such as "narrow-groove" and other low heat input welding processes, as well as spray cooling of final weld passes to produce compressive outer surface stress.

For the final closure welds of the waste package, according to Bokhari (2003 [DIRS 162429], Attachment 1), a nonthermal stress-mitigation process (laser peening or low-plasticity burnishing) was selected to replace the prior local induction-annealing residual stress-mitigation process, as this results in less possibility of harming Alloy 22 characteristics through heat treatment (local induction annealing), thus reducing performance uncertainty. For the purpose of license application (LA), Bokhari (2003 [DIRS 162429], Attachment 1, Figure 1) indicates that laser peening is the nonthermal mitigation method selected. The laser peening treatment, which is used for the 25-mm outer lid of the outer barrier to evaluate stress mitigation, involves use of the laser peening process, where a high-powered laser beam introduces shock pulses on the material surface. Laser peening is similar to the traditional shot-peening procedure, but is better adapted to waste package closure cell remote application. For laser peening, the intense stream of tiny metal or ceramic balls used in the traditional shot peening is replaced by high-energy lasers with pulse lengths in the tens of nanoseconds, short enough to generate a rapid, yet energetic shock. This process can produce a uniform layer of highly shocked and compressed material that is extremely resistant to cracks and corrosion.

According to measured data reported by Hornbach (1999 [DIRS 147757], Figures 18 to 21), laser peening is capable of producing a compressive surface layer of about 60 mils (1.5 mm) with compressive stress in the range of 20 to 60 ksi for a one-inch-thick welded Alloy 22 plate. A typical example for is shown in Figure 6-21 (DTN: LL000320005924.145) for measured stress profiles at the weld centerline for stress component 1 (S1, parallel to the weld center line) and stress component 3 (S3, perpendicular to the weld center line) before and after laser peening. It is evident from this figure that compressive stresses on the order of 40 ksi persist to a depth of at least 0.06 in. (1.5 mm).

Therefore, to demonstrate the effect of laser peening on the stress intensity factor, the weld-induced residual stress in the 25-mm outer lid of the CRM–21-PWR design was reduced from tensile stress to 40 ksi compressive stress for a depth of 0.06 in. (1.5 mm) at the outside surface (Figure 6-22). Using a depth of compressive stress of 0.06 in. (1.5 mm) is conservative, as measured results from more recently processed, multipass laser peened 1-inch welded Alloy 22 plate, (Figure 6-32), as well as an assessment based on measured laser-peened depth of compression versus plate thickness (Chen et al. 2002 [DIRS 165441], Figure 20) indicates a compressive stress depth significantly greater than 0.06 in. (1.5 mm) is readily obtainable for a 25-mm-thick Alloy 22 weldment. However, assuming a compressive depth of 0.06 in. (1.5 mm), the residual stress is then varied linearly from 0.06 in. (1.5 mm) to 0.12 in. (3.0 mm) below the

surface. From this point on, the stress remains undisturbed (i.e., uses the as-welded stress distribution). The stress intensity factor was calculated for the reduced stress profile and compared to the stress intensity factor previously calculated for the original stress profile as shown in Figure 6-23 (i.e., graphical presentations of (a) Column 3 and (b) Column 5 of Tables 6-9 and 6-12). It is evident that for the laser-peened outer lid, the radial through-wall stress intensity factor is less than zero indicating circumferential cracks will not propagate entirely through the wall thickness.

For radial and hoop stresses in ksi in the laser-peened 25-mm outer lid of the waste package design, the stress coefficients with stress in ksi and distance x in inches are obtained from DTN: LL000316205924.142 [DIRS 148895], file name: Skvrbr1, sheet "Peening, S_x," cells C9 to C12 for radial stress and sheet "Peening, S_z", cells C9 to C12 for hoop stress. The coefficients are listed in the fifth and sixth rows of Table 4-3. Table 6-11 shows the converted stress coefficients, A_0, A_1, A_2, and A_3, in the metric unit system. Table 6-12 shows the calculated stress and stress intensity profiles for the outer waste package lid subjected to laser peening.

Based on the hoop-stress profile and yield stress of 285 MPa for Alloy 22, examination of Table 6-12 indicates the depth to which the outer weld stress is in compression is about 1.92 mm, and the depth to which it is less than 90% of yield stress is about 4.6 mm.

Any thermally induced stress relaxation of the through-wall stress distribution is expected to be small at waste package temperatures below about 300°C. A small amount of stress relaxation was potentially observed based on measured leg springback in 5-year exposed U-bend specimens tested at 90°C and removed from the LLNL Long Term Corrosion Test Facility and disassembled (Fix et al. 2003 [DIRS 162700], p. 5). However, stress relaxation reduces subsurface tensile stresses, as well as the beneficial outer surface compressive stresses, and it is unlikely that relaxation of stresses in a surface stress mitigated layer would significantly change the depth to reach stresses below the threshold stress value for stress corrosion cracking initiation discussed in Section 6.2.1. Even the full removal (by corrosion) of the outer ~3mm of mitigated surface layer did not significantly change the through-wall stress distribution as described in Section 6.4.3.

Table 6-11. Stress Coefficients for the Laser-Peened Waste Package Outer Lid

Stress Coefficient	Unit	Radial Stress	Hoop Stress
A_0	MPa	-265.920	-292.607
A_1	MPa/mm	103.987	178.277
A_2	MPa/mm^2	-9.857	-14.135
A_3	MPa/mm^3	0.254	0.320

Source: Table 4-3, (fifth and sixth rows) with units converted to metric system; Output DTN: LL030607012251.065, Table 8-1.

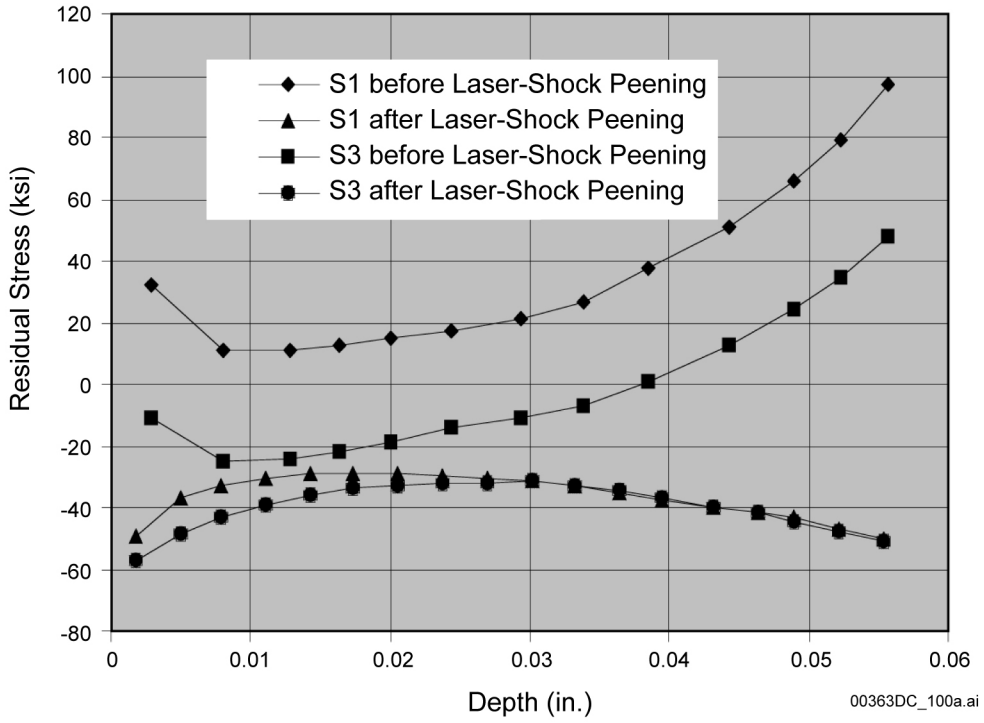

Source: DTN: LL000320005924.145 [DIRS 148482].

Figure 6-21. Mitigation of Weld Stress in Alloy 22 with Laser Peening

Table 6-12. Stresses and Stress Intensity Factors for Laser-Peened Waste Package Outer Lid

Depth (mm)	Radial Stress (S_x) (MPa)	SIF due to S_x (MPa$\sqrt{m}$)	Hoop Stress (S_z) (MPa)	SIF due to S_z (MPa$\sqrt{m}$)
0.3988	-226.0035	-9.1866	-223.7417	-5.6943
0.8001	-188.9005	-11.7979	-158.8532	-6.4965
1.1989	-154.9833	-13.0189	-98.6408	-6.1528
1.6002	-123.7220	-13.4298	-42.2143	-5.1372
1.9990	-95.4153	-13.2965	9.8344	-3.6697
2.4003	-69.6047	-12.7780	58.2916	-1.8824
2.7991	-46.5198	-12.2958	102.6663	0.1212
3.2004	-25.7687	-11.7214	143.6471	2.2821
3.5992	-7.5170	-11.0116	180.8374	4.5533
3.9980	8.4709	-10.2080	214.6297	6.8939
4.3993	22.3728	-9.3437	245.3299	9.2702
4.7981	34.1098	-8.4525	272.6715	11.6543
5.1994	43.9293	-7.6096	297.1262	14.0165
5.5982	51.8041	-6.8298	318.5068	16.3364
5.9995	57.9323	-6.0675	337.2088	18.6024
6.3983	62.3334	-5.3416	353.1178	20.8003
6.7970	65.1483	-4.6612	366.4827	22.9177
7.1984	66.4775	-4.0331	377.4871	24.9441
7.5971	66.4012	-3.4507	386.1141	26.9023
7.9985	65.0162	-2.8535	392.5969	28.8612

Table 6-12. Stresses and Stress Intensity Factors for Laser-Peened Waste Package Outer Lid (Continued)

Depth (mm)	Radial Stress (S_x) (MPa)	SIF due to S_x (MPa$\sqrt{m}$)	Hoop Stress (S_z) (MPa)	SIF due to S_z (MPa$\sqrt{m}$)
8.3972	62.4372	-2.2745	396.9757	30.7287
8.7986	58.7292	-1.7170	399.4297	32.5008
9.1973	54.0361	-1.1860	400.0499	34.1745
9.5987	48.3961	-0.6829	398.9677	35.7479
9.9974	41.9777	-0.2101	396.3190	37.2200
10.3962	34.8443	-0.3513	392.2239	38.4530
10.7975	27.0415	-0.5163	386.7654	39.5674
11.1963	18.7651	-0.7070	380.1350	40.5636
11.5976	10.0075	-0.9242	372.3715	41.4432
11.9964	0.9766	-1.1690	363.6954	42.2086
12.3977	-8.3447	-1.4403	354.1195	42.8627
12.7965	-17.7414	-1.7949	343.8874	43.4439
13.1978	-27.2353	-2.1728	332.9919	43.9342
13.5966	-36.6092	-2.5554	321.6934	44.3269
13.9954	-45.8267	-2.9438	310.0462	44.6272
14.3967	-54.8472	-3.3378	298.0958	44.8409
14.7955	-63.4595	-3.7396	286.1158	44.9743
15.1968	-71.6755	-4.0160	274.0769	45.0329
15.5956	-79.2941	-4.1354	262.2538	45.0208
15.9969	-86.3145	-4.2182	250.6192	44.9464
16.3957	-92.5507	-4.2696	239.4426	44.8182
16.7945	-97.9528	-4.2904	228.7710	44.6449
17.1958	-102.4495	-4.2805	218.6644	44.4361
17.5946	-105.8869	-4.3087	209.3730	44.2112
17.9959	-108.2109	-4.5204	200.9017	43.9968
18.3947	-109.2950	-4.7313	193.4801	43.7750
18.7960	-109.0551	-4.9400	187.1369	43.5578
19.1948	-107.3973	-5.1487	182.0747	43.3569
19.5961	-104.2024	-5.3536	178.3522	43.1853
19.9949	-99.4140	-5.5551	176.1390	43.0560

Source: Table 4-4.

Output DTN: LL030607012251.065.

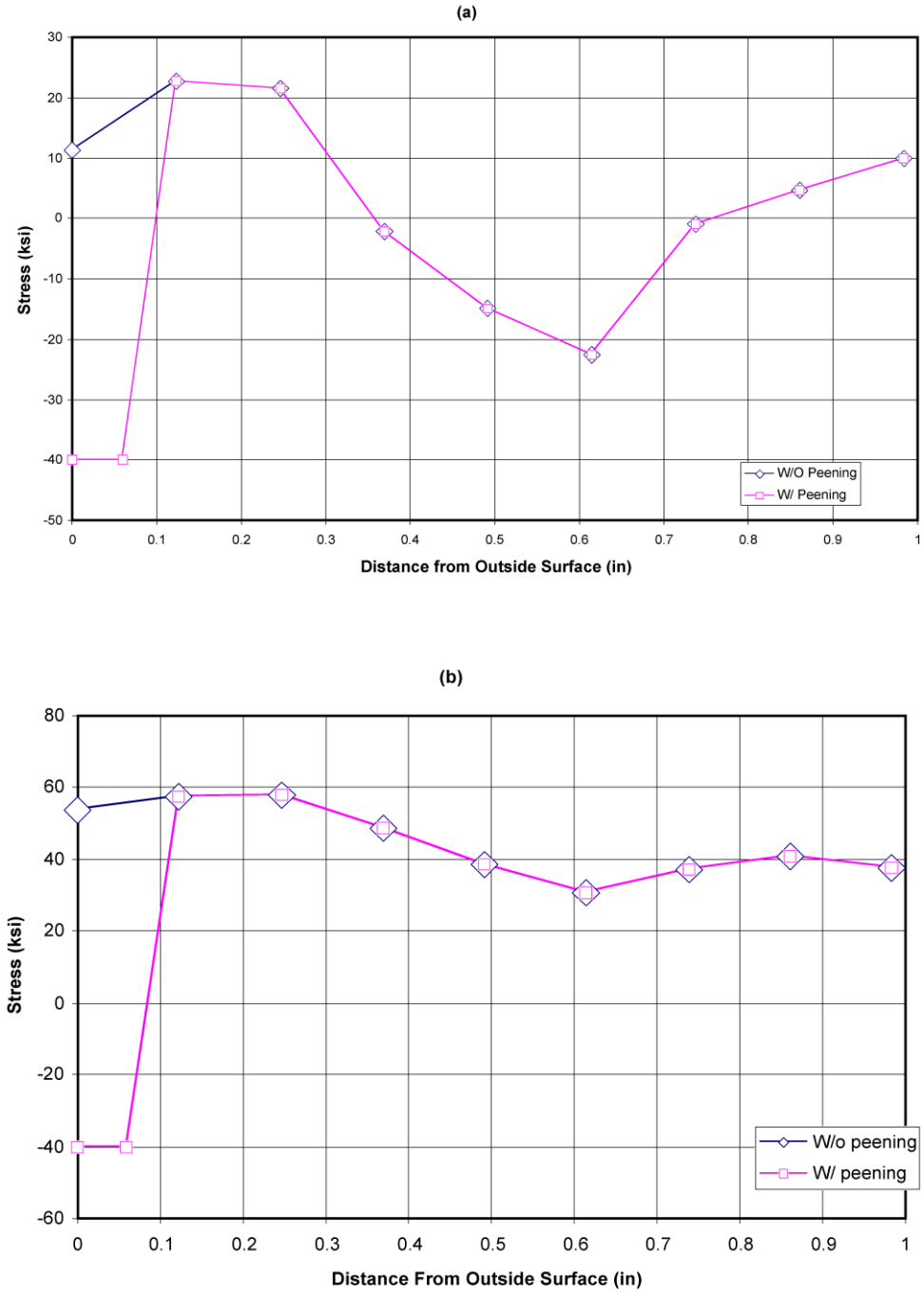

Source: DTN: LL000316205924.142 [DIRS 148895], File dgzRs1R11, Sheets 1-1 S_x and 1-1 S_z.

NOTE: (a) Radial Stress, S_x, and (b) Hoop Stress, S_z.

Figure 6-22. Stress in Outer Lid With and Without Laser Peening

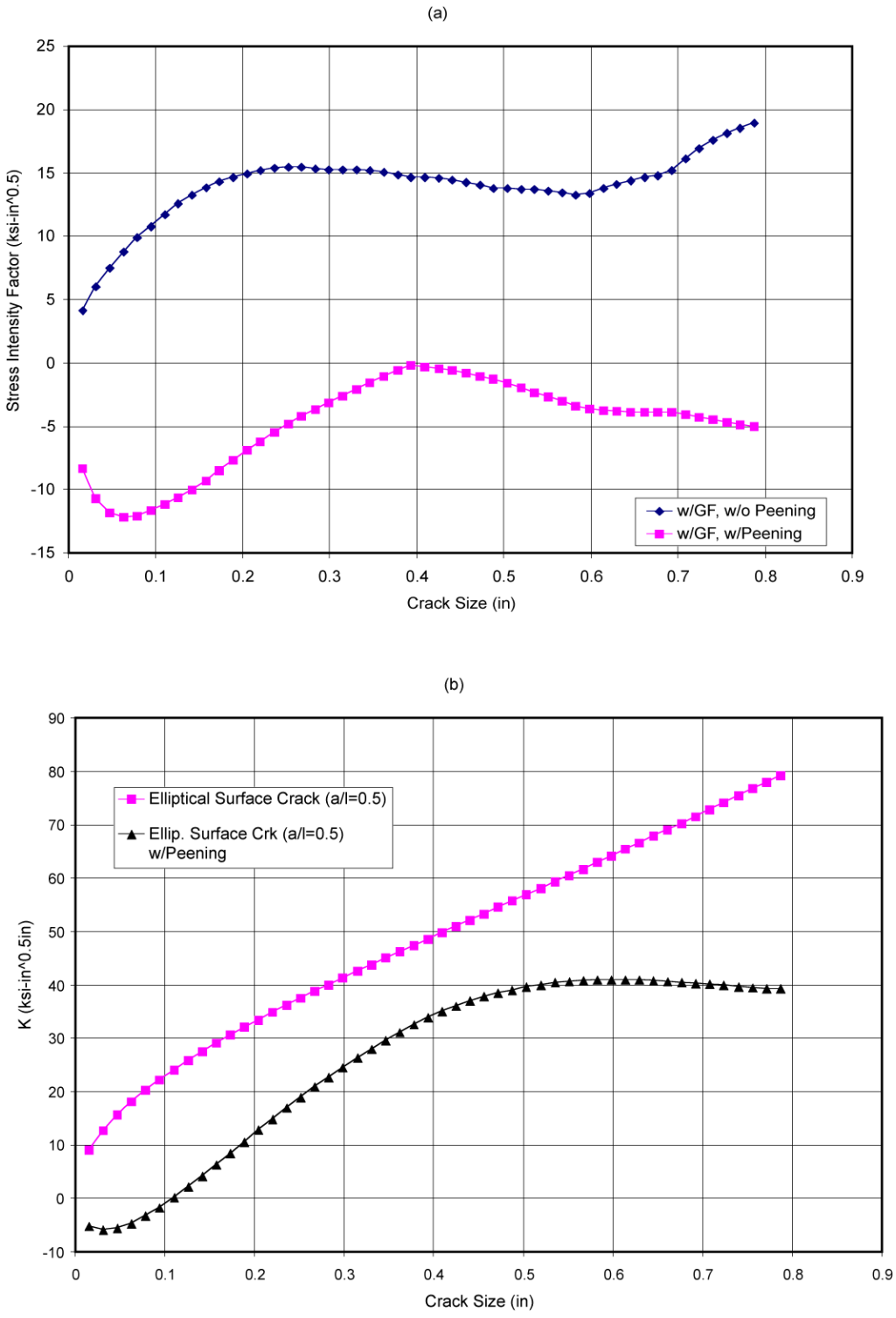

Source: Graphical presentations of (a) Column 3 and (b) Col. 5 of Tables 6-9 and 6-12.

Figure 6-23. Stress Intensity Factors due to (a) Radial Stress and (b) Hoop Stress With and Without Laser Peening

6.4.5 Uncertainty and Variability of Residual Stress and Stress Intensity Factor in Waste Package

Section 6.4.2.2 states that, although the determination of weld residual stress for the waste package welds is a three-dimensional problem, a two-dimensional axisymmetric modeling approach has been used for the finite element analyses of the weld residual stresses. The result is that the stress distribution is axisymmetrical about the waste package axial centerline (i.e., constant along the circumference). An assessment of circumferential residual stress variation in stainless steel piping welds (DTN: MO0409GGSIACAL.000 [DIRS 171792], Calculation TRW-06Q-304) indicated that the residual stress shows a sinusoidal distribution around the circumference with a range of about 5 ksi about the mean stress. Based on this conclusion, the variability of the mean stress along the circumference (∇S) is represented by the following equation:

$$S_\theta(x) = S_0(x) - \nabla S(1 - \cos(\theta)) \quad \text{(Eq. 25a)}$$

where

θ is the angle measured in degrees from a reference location ($\theta = 0°$) on the circumference
$S\theta(x)$ is the weld residual stress profiles at an angle θ
$S0(x)$ is calculated weld residual stress profile at $\theta = 0$
∇S is taken to be 2.5 ksi or 17.236893 MPa.

Variability in stress intensity factor is treated similarly to that for stress because stress intensity factor is a linear function of stress:

$$K_\theta(x) = K_0(x)\,(S_\theta(h) / S_0(h)) \quad \text{(Eq. 25b)}$$

where h is the thickness of the closure lid.

The uncertainty of the weld residual stress calculated by the simplified finite element analysis can be adequately represented by a normal distribution with the calculated residual stress as the mean ($S_\theta(x)$) and a 3-sigma bound to be defined.

Mohr (1996 [DIRS 147981], p. 39) indicated that the uncertainty range of the residual stress is a function of the yield strength of the material and varies about the mean by ±35% of the yield strength. The high degree of uncertainty (or variability) associated with Mohr's data was related to the large scatter in measured residual stress data resulting from use of a large number of different carbon steel welded pipes covering a range of thicknesses, welding processes, weld joint configurations, weld heat inputs, yield strengths, etc. In the case of the final closure welds of the dual-lid improved waste package design, the various parameters contributing to residual stress variation are closely controlled. This includes close, automated control on the welding process parameters, the use of a single alloy for the base material and for the weld wire, close control of the weld joint configuration and spacing, etc.

In contrast to the high degree of scatter noted by Mohr (1996 [DIRS 147981]), data available on shot-peened (analogous to laser-peened) nickel alloy Incoloy 908 (Pasupathi 2000

[DIRS 149968]) indicate a narrow residual stress scatter range for as-welded and as-welded plus shot-peened nickel alloy material with one-sigma value of ±3% of the measured stress value for shot-peened surfaces (Pasupathi 2000 [DIRS 149968], Tables II and VI) or an uncertainty range of about ±9% at the 3-sigma level. In comparison, the residual stresses measured on a peened surface by the X-ray diffraction technique (Lu 1996 [DIRS 149957], Table 5-4, p. 103) showed an average measurement uncertainty of about ±15 MPa, which is about ±5% of the Alloy 22 yield strength. Values of yield strength, YS, of Alloy 22 are listed in Table 4-5. For conservative purpose, the higher YS value at the room temperature may be used.

The data listed by Pasupathi (2000 [DIRS 149968]) are for both welded and nonwelded samples (peened and unpeened), many of which also contain some cold work due to tube-reduction drawing. Thus, they represent a range of metallurgical and process variables that the waste package closure-lid weld regions also contain (cold-work, as-annealed, and as-welded conditions for peened and unpeened material). Further, in the case of the final closure welds of the dual-lid waste package design, good process control plus periodic quality control measurements will be used in the site closure cell on the final, postprocessed Alloy 22 material. The quality control measurement process(es) to be used will depend on the finally selected stress mitigation process. For the laser peening process, the so-called Almen strips, which are commonly used to control shot-peening processing and laser-peening processing, may be used. Almen strips are thin rectangular strips that, when peened from one side, deflect with the deflection related to the depth of applied residual compressive stress resulting from the process. If stresses are found to deviate from the specified range, the weld can be reprocessed, repaired, or scrapped.

Thus, based on the above discussion, a 3-sigma stress uncertainty range of ±15% of the material mean yield strength appears to be a conservative representation of the realistic case that is achievable through appropriate levels of process controls.

The minimum and maximum stresses at the 3-sigma level, $S_\theta(x)\min$ and $S_\theta(x)\max$ in the weld can be obtained from the mean stress, $S_\theta(x)$, by the following equations:

$$S_\theta(x)\min = S_\theta(x)\left(\frac{S_\theta(h)-\Delta S}{S_\theta(h)}\right) \quad \text{(Eq. 26a)}$$

$$S_\theta(x)\max = S_\theta(x)\left(\frac{S_\theta(h)+\Delta S}{S_\theta(h)}\right) \quad \text{(Eq. 26b)}$$

where $S_\theta(h)$ is the mean residual stress on inside surface (x=h, where 'h' is the thickness of the closure lid) and ΔS is the amplitude of variation between the maximum and minimum stresses at the inner surface of the waste package lid. The stress intensity factor calculated from the mean stress as described in Section 6.4.2.2 is the mean stress intensity factor $K_\theta(x)$. The minimum and maximum stress intensity factors are calculated similarly to those for stress because stress intensity factor is a linear function of stress.

$$K_\theta(x)\min = K_\theta(x)\left(\frac{S_\theta(h)-\Delta S}{S_\theta(h)}\right) \quad \text{Eq. 26c)}$$

$$K_\theta(x)\max = K_\theta(x)\left(\frac{S_\theta(h)+\Delta S}{S_\theta(h)}\right) \quad \text{(Eq. 26d)}$$

where θ is the angle measured from a reference location (θ = 0°) on the circumference and ΔS = 0.15 YS (YS is the mean yield strength given in Table 4-5).

As described in Section 6.2.2, the hoop stress, which promotes radially oriented crack growth, is the dominant component of stress in the waste package outer barrier final closure lid weld regions and, thus, only the hoop stress profiles are considered in calculating the expected range of stress and stress intensity factor through-wall variation. The stress and stress intensity factor profiles in the waste package outer barrier closure weld regions are variable and uncertain. Variability (angular variation) in the hoop stress (σ in MPa) as a function of depth (x in mm) in the closure weld regions of the Alloy 22 waste package outer barrier is given by a third order polynomial equation (Equation 23), repeated here, where the values of the coefficients are given in Section 6.4.4, Table 6-11 and are listed in metric units in Section 8.3, Table 8-1.

$$\sigma(x,0) = A_0 + A_1 x + A_2 x^2 + A_3 x^3 \quad \text{(Eq. 23)}$$

The second argument in the stress function is used to represent angular variation (θ = 0, arbitrarily chosen) around the circumference of the Alloy 22 waste package outer and middle closure-lid welds. The angular variation is included using the following functional form, based on Equation 25a:

$$\sigma(x,\theta) = \sigma(x,0) - (17.236893)\times(1-\cos(\theta)) \quad \text{(Eq. 25a′)}$$

Defined in Equation 25a′, $\sigma(x, 0)$ uses the stress coefficients (Ai) defined in Equation 23 with x in units of mm and the stress variability term defined in Equation 25a and listed in Table 8-1. Using Equation 25a′, Figure 6-24 shows the median (not accounting for uncertainty, which is discussed below) stress variation with angle for the waste package outer barrier outer closure lid weld region and Figure 6-25 shows the median stress variation with angle for the waste package outer barrier middle closure lid weld region. Also included on the graphs is the stress threshold for nucleation of incipient flaws. The depth on these graphs does not start at zero thickness, nor extend to the full lid thickness. For consistency, stress values were calculated at the same depth values as for the corresponding stress intensity factor profiles that were calculated using Equation 25b and are shown plotted with angle for the outer and middle closure lid weld regions in Figures 6-26 and 6-27, respectively.

Uncertainty for the outer and middle closure lid weld regions (with relevant parameter values listed in Table 8-1) were calculated for the residual stress distributions based on Equations 26a and 26b and are shown plotted in Figures 6-28 and 6-29, respectively at θ = 0. Similarly, uncertainty for the outer and middle closure lid weld regions (with relevant parameter values

listed in Table 8-1) were calculated for the stress intensity factor distributions based on Equations 26c and 26d and are shown plotted in Figures 6-30 and 6-31, respectively.

As can be seen from Figure 6-28, the analysis results predict that the threshold stress (90% of yield strength) for the laser peened outer closure lid will be reached at a depth of about 4.6 mm, based on mean values. More conservatively, the analysis predicts the threshold stress will be reached at a depth of about 3.8 mm, based upon the upper bound of uncertainty. Corroborative measurements of the through-wall residual stress have been made on Alloy 22 gas tungsten arc weldments (1-inch thick) processed with a several pass laser-shock peening process and with an alternate controlled plasticity-burnishing stress mitigation process. These measurements shown in Figure 6-32 and Figure 6-33, respectively, show that the predicted values shown in Figure 6-24 are very conservative estimates of the depth of compression that can be achieved through stress mitigation. These experimental measurements were obtained using the 1-inch ring-core technique and are reported in DTN: MO0301SPAXRA52.001 [DIRS 165147]. Note the stresses parallel to the weld centerline are referred to as being in the "parallel direction."

The time-to-breach due to stress corrosion cracking at the stress-mitigated closure weld will be determined primarily by the time required to corrode through the material to a level where the stress exceeds 90% of the yield strength. Added to this is the time required for the initiated crack to propagate through the remaining lid thickness. Any relaxation of the residual-stress gradient tends to reduce the compressive surface-stress magnitude and the subsurface tensile-stress magnitude and thus, may increase the depth to reach 90% of the yield strength. Further, as the outer compressive surface layer is slowly removed by general corrosion, the neutral axis shifts inward.

The scenario for removal of the compressive layer by corrosion is relatively easy to assess. Because of very low general corrosion rates of the waste package outer barrier for the conditions expected in the repository, waste package performance is not limited by general corrosion during the regulatory time period. As a bounding and conservative analysis, for a constant waste package surface temperature of 150ºC, the median penetration depth by general corrosion over 10,000 years, using the median general corrosion rate of 51.8 nm/yr (BSC 2004 [DIRS 169984], Section 8.1) is about 518 μm, which is about 11% of the mean depth of the stress mitigated layer (about 4.6 mm, Figure 6-28). Using an upper-bound value of the general corrosion rate of 256 nm/yr (99.99th percentile rate at 150°C (BSC 2004 [DIRS 169984], Section 8.1)) the total penetration depth by general corrosion is about 2,560 μm, which is about 56% of the about 4.6-mm mean depth of the stress-mitigated layer and about 67% of the total maximum uncertainty (minimum depth) of the stress-mitigated layer (about 3.8 mm, Figure 6-28). This bounding analysis demonstrates that the final closure lid weld stress-mitigated layer is deep enough to extend the lifetime of the waste package well beyond 10,000 years after permanent closure using conservative values of mitigated layer depth.

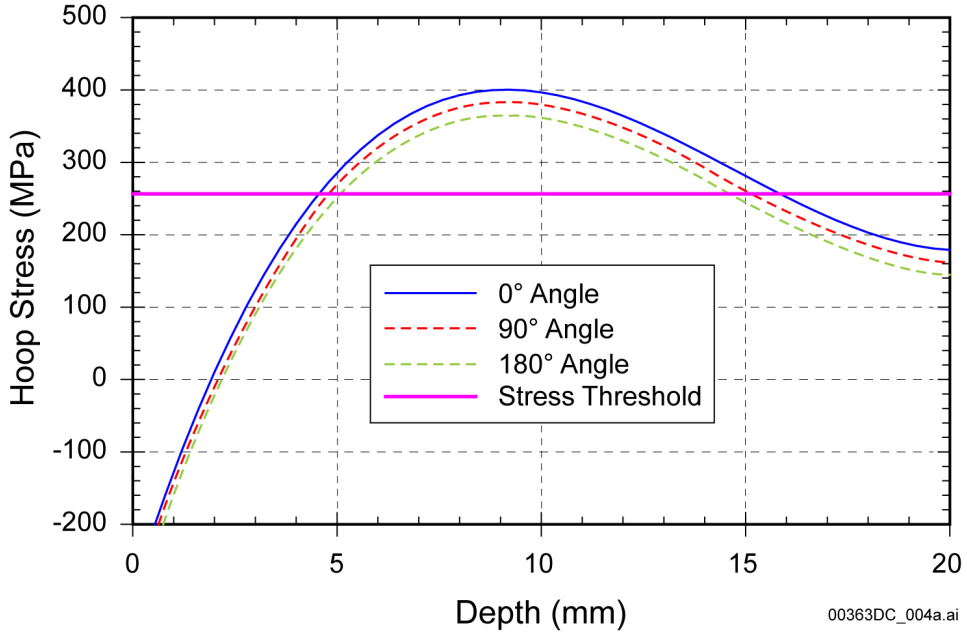

Source: Figure 6-24 generated for this report using Equation 25a and data reside in Output DTN: LL030607012251.065 and plotted graph in Output DTN: MO0310MWDWAPAN.002.

Figure 6-24. Variation of Hoop Stress Versus Depth for Waste Package Outer Closure Lid

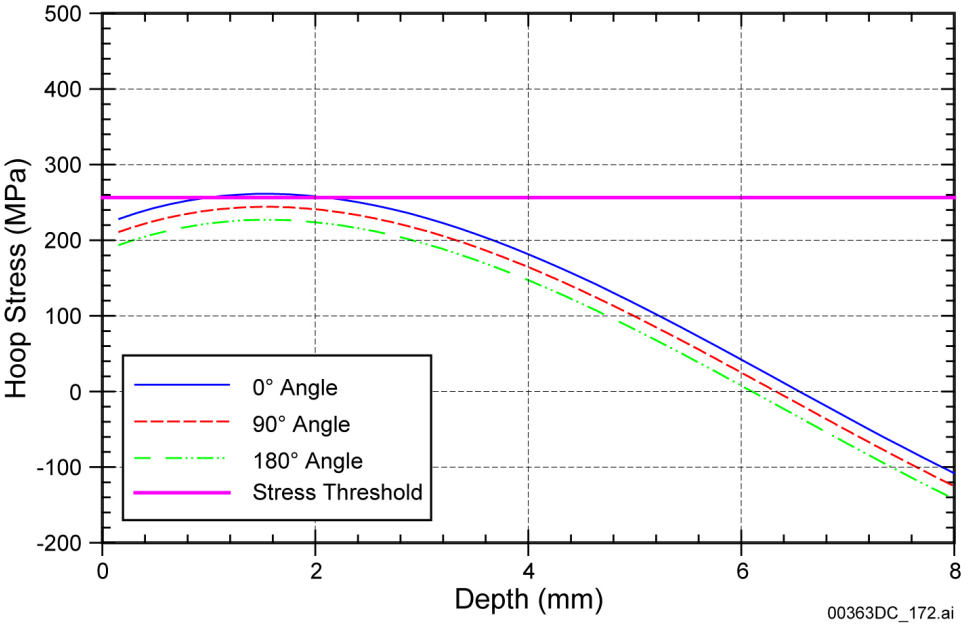

Source: Figure 6-24 generated for this report using Equation 25a and data reside in Output DTN: LL030607012251.065 and plotted graph in Output DTN: MO0310MWDWAPAN.002.

Figure 6-25. Variation of Hoop Stress Versus Depth for Waste Package Middle Closure Lid

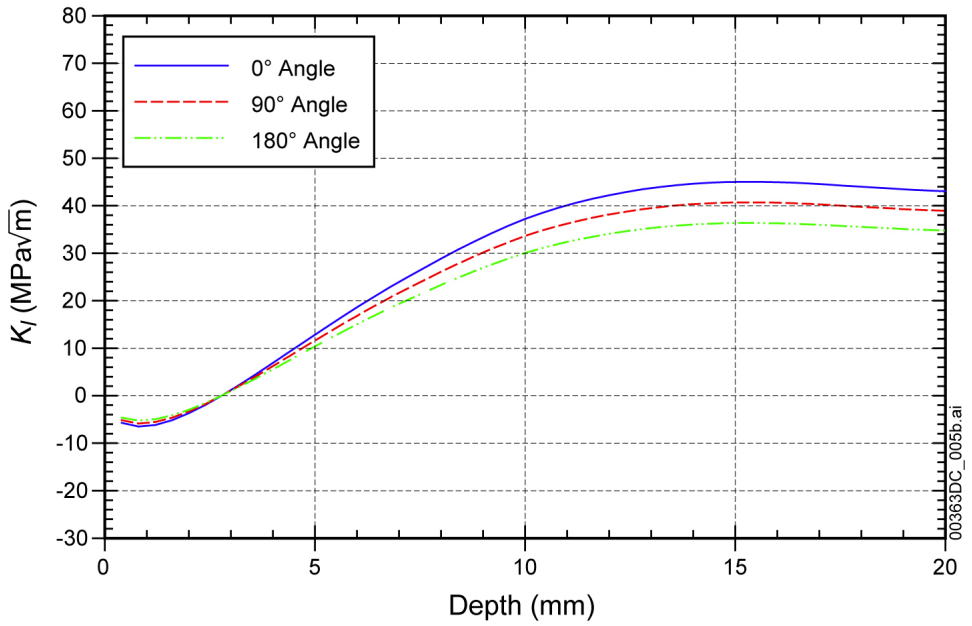

Source: Figure 6-26 generated for this report using Equation 25b and data reside in Output DTN: LL030607012251.065 and plotted graph in Output DTN: MO0310MWDWAPAN.002.

Figure 6-26. Variation of Stress Intensity Factor Versus Depth for Waste Package Outer Closure Lid.

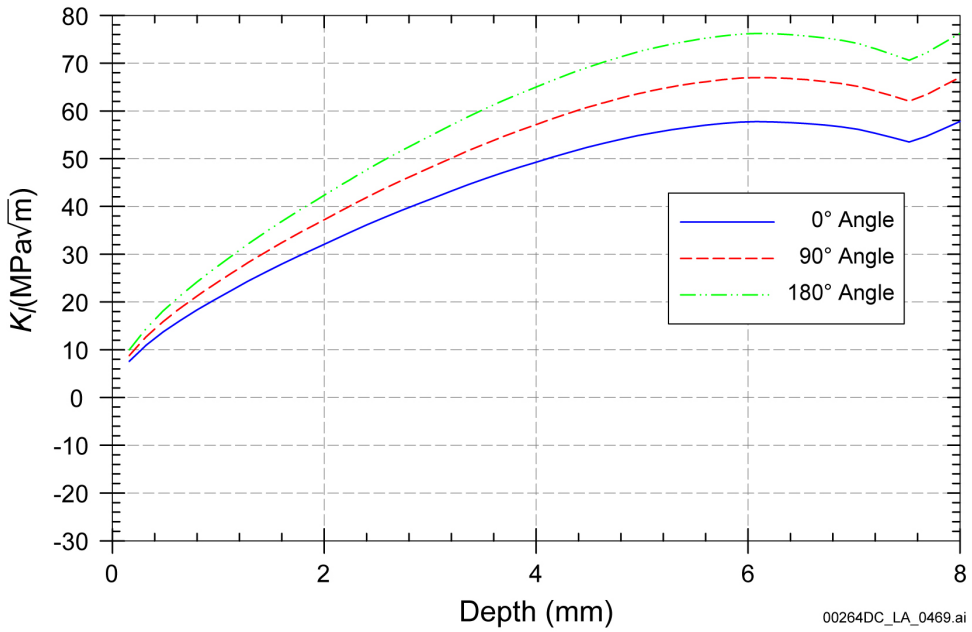

Source: Figure 6-27 generated for this report using Equation 25b and data reside in Output DTN: LL030607012251.065 and plotted graph in Output DTN: MO0310MWDWAPAN.002.

Figure 6-27. Variation of Stress Intensity Factor Versus Depth for Waste Package Middle Closure Lid

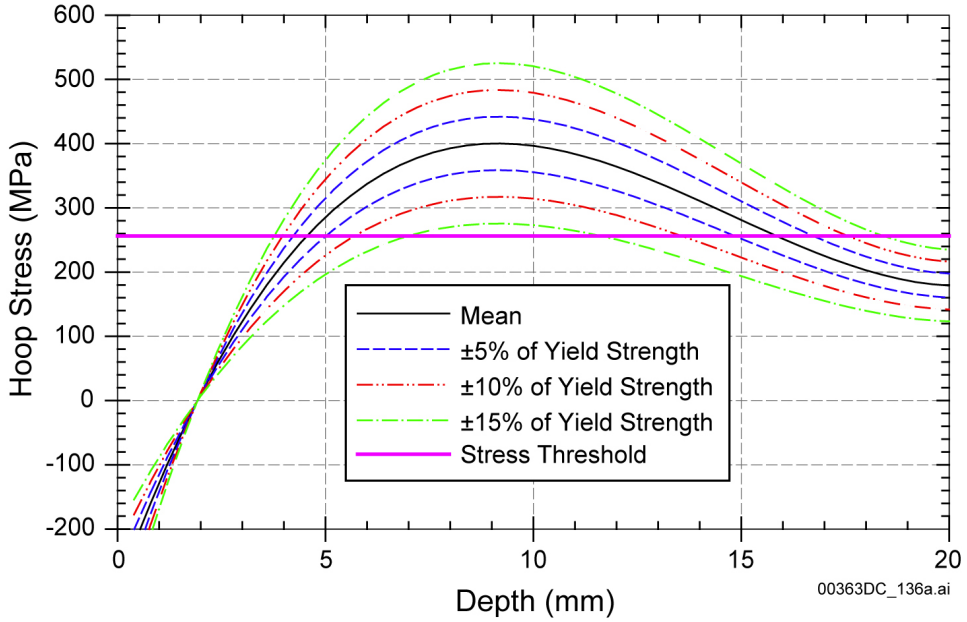

Source: Figure 6-28 generated for this report using Equation 26a and data reside in Output DTN: LL030607012251.065 and plotted graph in Output DTN: MO0310MWDWAPAN.002.

Figure 6-28. Variation of Hoop Stress (θ = 0) Versus Depth for Waste Package Outer Closure Lid

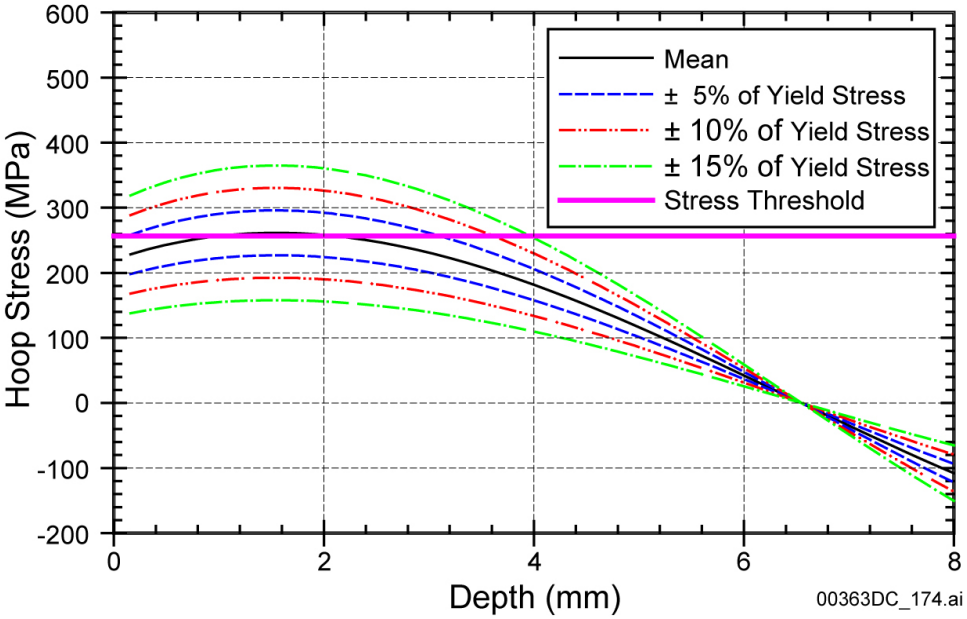

Source: Figure 6-29 generated for this report using Equation 26b and data reside in Output DTN: LL030607012251.065 and plotted graph in Output DTN: MO0310MWDWAPAN.002.

Figure 6-29. Variation of Hoop Stress (θ = 0) Versus Depth for Waste Package Middle Closure Lid

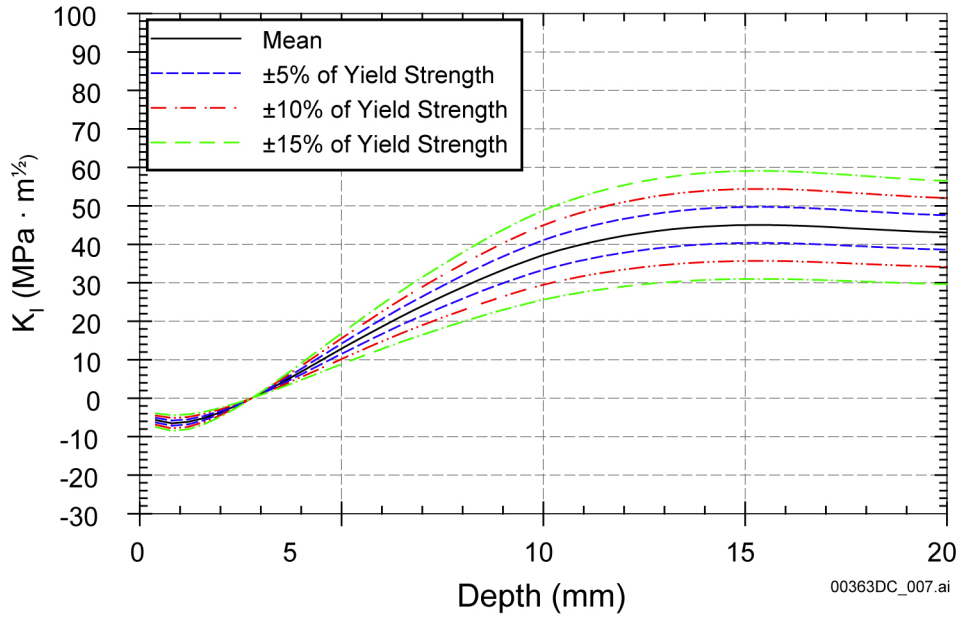

Source: Figure 6-30 generated for this report using Equation 26c and data reside in Output DTN: LL030607012251.065 and plotted graph in Output DTN: MO0310MWDWAPAN.002.

Figure 6-30. Variation of Stress Intensity Factor (θ = 0) Versus Depth for Waste Package Outer Closure Lid

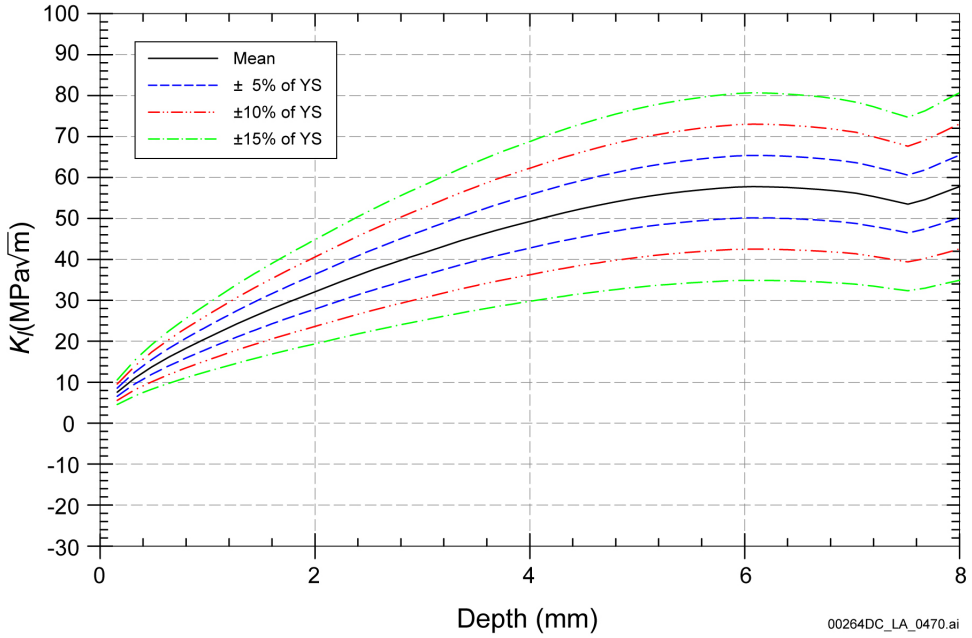

Source: Figure 6-31 generated for this report using Equation 26d and data reside in Output DTN: LL030607012251.065 and plotted graph in Output DTN: MO0310MWDWAPAN.002.

Figure 6-31. Variation of Stress Intensity Factor (θ = 0) Versus Depth for Waste Package Middle Closure Lid

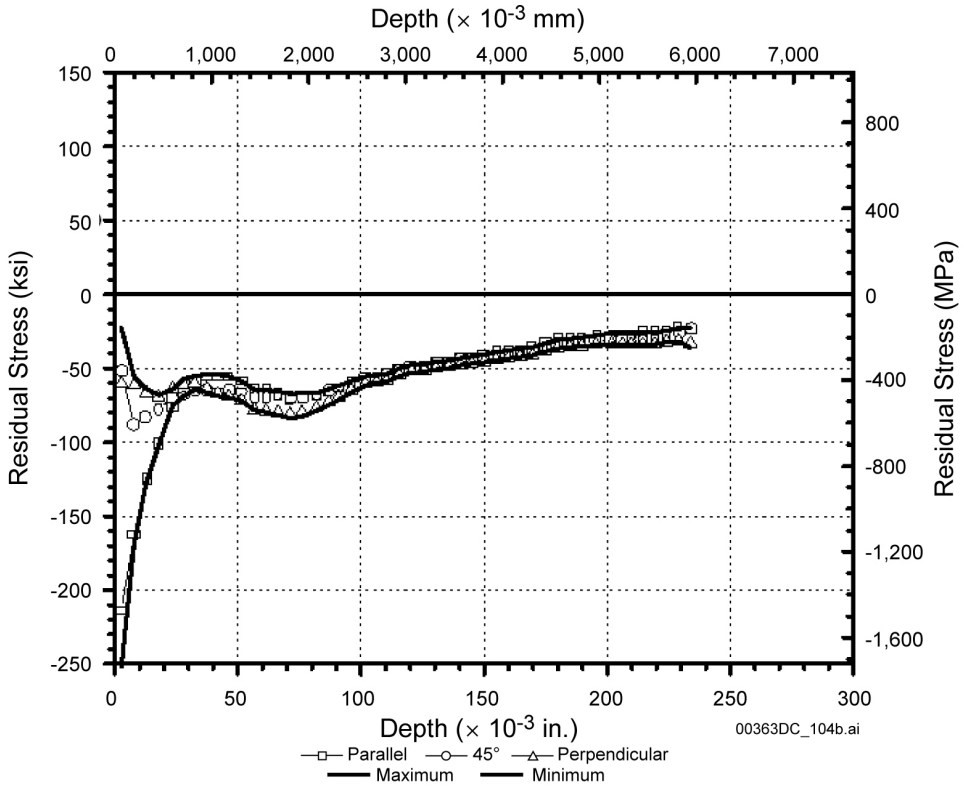

Source: DTN: MO0301SPAXRA52.001 [DIRS 165147], Figure 4.

Figure 6-32. Measured Stress (Using 1-Inch Ring Core Method) Versus Depth for Alloy 22 Laser-Peened 1-Inch-Thick Gas Tungsten Arc Welding Welded Plate

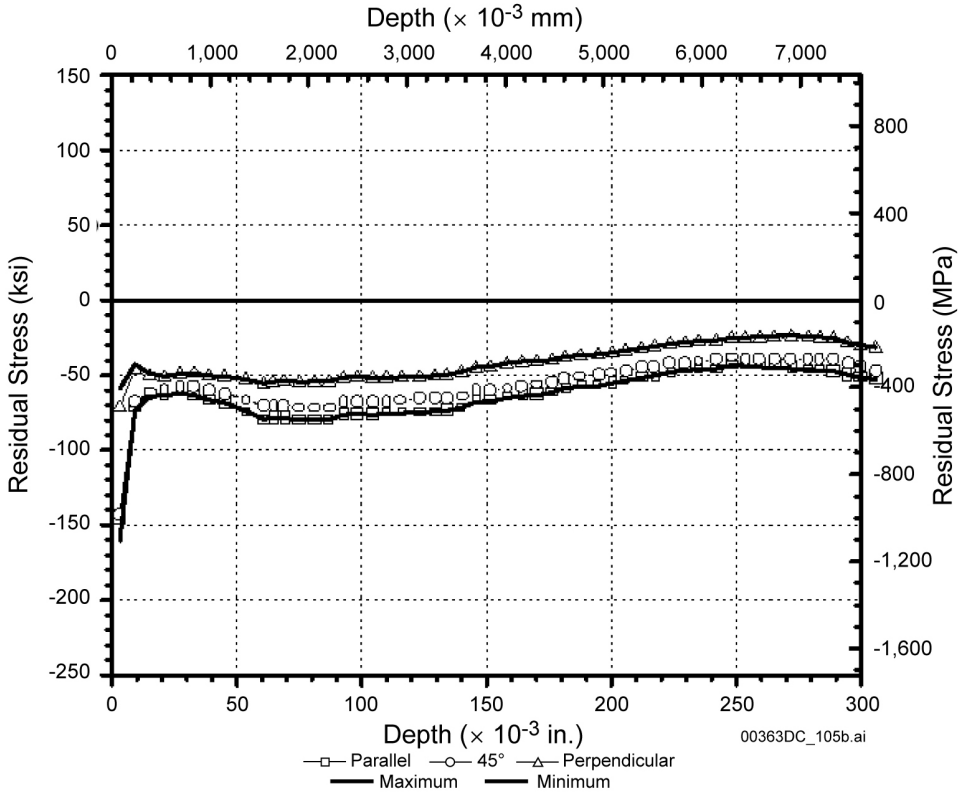

Source: DTN: MO0301SPAXRA52.001 [DIRS 165147], Figure 7.

Figure 6-33. Measured Stress (Using 1-Inch Ring-Core Method) Versus Depth for Alloy 22 Controlled Plasticity Burnished 1-Inch-Thick Welded Plate

6.5 ESTIMATE OF LENGTH AND INTERCRACK SPACING OF RADIAL THROUGH-WALL CRACKING AND CRACK OPENING

The information provided in Section 6.5 is not used directly in the SDFR model. Rather, it is provided as information that can be used for performance assessment in calculating radionuclide release rates through stress corrosion cracks.

6.5.1 Estimated Length and Intercrack Spacing of Radial Through-Wall Cracking

As discussed in Section 6.2.2.3, radially oriented flaws are important to stress corrosion cracking of waste packages since the hoop stress, which drives the radially oriented cracks, is usually the dominant stress component. The stress intensity factor resulting from the through-wall hoop stress gradient (or profile) can result in propagation of through-wall stress corrosion cracking for cracks in the radial direction. Based on stress distributions shown in Figure 6-14, rapid-weld residual stress decay is observed with increasing distance normal to the weld–metal interface (i.e., in the radial direction). As the tensile stress decays, the driving force for crack extension in the radial direction also decreases rapidly and appears to fully attenuate at distances from the weld center line on the order of the welded plate thickness. Thus, the expected maximum length of these radial cracks is approximately two times the plate thickness.

With respect to the expected minimum spacing between parallel through-wall radial cracks, detailed analysis (Structural Integrity Associates 2002 [DIRS 161933]) indicated, because of stress field interactions between closely spaced parallel cracks that for a one-inch-thick plate, the distance between two neighboring through-wall cracks would need to be greater than the plate thickness for the stress (and resultant stress intensity factor) to be sufficient to drive a flaw through-wall.

6.5.2 Estimate of Crack Opening

Leak through a crack can occur if the crack grows into a through-thickness crack. Leak rate depends on the size of crack opening, among other factors. A simplified crack opening calculation approach is described below.

1. A crack is either circumferential (perpendicular to the radial stress) or radial (perpendicular to the hoop stress) in the outer surface of the closure weld of the waste package.

2. A circumferential crack is treated as a semielliptical crack with depth, "a," and length, "2c." The aspect ratio "c/a" for a radial crack is "1" (i.e., a semicircular crack (c = a)).

3. The crack length "2c" of a circumferential crack remains unchanged but the final length of a through-wall crack is at least twice the wall thickness. Consequently, most cracks will grow in both directions of the minor (depth "a") and major (length "2c") axes and become semicircular (i.e., a = c) when they become through-wall cracks. According to fracture mechanics (Ewalds and Wanhill 1984 [DIRS 118602], Section 2.5, p. 43), "a" tends to grow faster than "c" because the stress intensity factor tends to have a maximum value at the end of the minor axis and a minimum value at the end of the major axis. Eventually, a semielliptical crack will become a semicircular crack. The crack length "2c" will remain unchanged only for very long cracks with initial crack length greater than twice the wall thickness. For such long cracks, the occurrence rate is usually very low. The length of a semicircular crack will always be equal to twice the crack depth.

4. The crack opening has an elliptical shape with length "2c" and a gap "δ."

Tada et al. (2000 [DIRS 167756], p. 125), showed that the opening of a crack, δ, with length, 2c, in an infinite sheet is given for plane stress condition as:

$$\delta = \frac{(4c)\sigma}{E} \qquad \text{(Eq. 28)}$$

where

σ = stress
E = Young's Modulus

The opening area, A_{cr}, for an elliptical crack, therefore, can be estimated by:

$$A_{cr} = \frac{\pi}{4}\delta(2c) = \frac{(2\pi c^2)\sigma}{E} \quad \text{(Eq. 29)}$$

When Equations 28 and 29 are used to estimate the crack opening and opening area, σ is the maximum stress across the thickness of either the radial stress (for a circumferential crack) or the hoop stress (for a radial crack).

6.6 FEATURES, EVENTS AND PROCESSES

The development of a comprehensive list of features, events, and processes (FEPs) potentially relevant to postclosure performance of the repository is an ongoing, iterative process based on site-specific information, design, and regulations. To support TSPA-LA, the FEP list was reevaluated in accordance with *The Enhanced Plan for Features, Events, and Processes (FEPs) at Yucca Mountain* (BSC 2002 [DIRS 158966], Section 3.2). Table 6-13 provides a list of FEPs included in this report and provides specific references to within this report where the FEPs are discussed. A description of these FEPs can be found in DTN: MO0407SEPFEPLA.000 [DIRS 170760], while a complete list of all FEPs related to waste package and drip shield degradation can be found in *FEPs Screening of Processes and Issues in Drip Shield and Waste Package Degradation* (BSC 2004 [DIRS 169997]).

Table 6-13. Included FEPs

FEP No.	FEP Name	Section Where Disposition is Described
2.1.03.02.0A	Stress corrosion cracking (SCC) of waste packages	Section 6.1

This report does not provide a direct basis for the inclusion of FEP 2.1.03.02.0A in the Total System Performance Assessment for License Application (TSPA-LA). Rather, its results are used by *WAPDEG Analysis of Waste Package and Drip Shield Degradation* to develop a basis for implementing or excluding these FEPs in the TSPA-LA.

7. MODEL VALIDATION

Model validation activities for the SDFR model are described below. Validation activities for the seismic crack density model are discussed in Appendix B in Section B7.

7.1. INTENDED PURPOSE OF THE MODEL

Stress corrosion cracking is a potential corrosion mode that can result in penetration of the drip shield, waste package outer barrier and the stainless steel structural materials. The purpose of this report is to provide the evaluation of the potential for stress corrosion cracking of the drip shield, the waste package outer barrier, and waste package stainless steel inner structural cylinder under exposure conditions consistent with the repository during the regulatory period of 10,000 years after permanent closure. As no lifetime credit is taken for the stainless steel structural material, it is not modeled. For the drip shield and waste package outer barrier, the critical environment is conservatively taken as any aqueous environment contacting the metal surfaces. The output models feed outputs to *FEPs Screening of Processes and Issues in Drip Shield and Waste Package Degradation* and is included in abstracted form in *WAPDEG Analysis of Waste Package and Drip Shield Degradation*.

This stress corrosion cracking model directly supports the following TSPA components:

- Drip Shield Stress Corrosion Cracking and Other Corrosion Modes
- Waste Package Stress Corrosion Cracking and Other Corrosion Modes.

Thus, this report supports TSPA-LA.

7.1.1 Confidence-Building During Model Development to Establish Scientific Basis and Accuracy for Intended Use

Section 2.2.1 of *Technical Work Plan for: Regulatory Integration Modeling and Analyses of the Waste Form and Waste Package* (BSC 2004 [DIRS 171583]) specifies the following steps for confidence building during model development:

- The model will contain documentation of decisions and activities implemented during the model development process to build confidence and verify a reasonable and credible technical approach using scientific and engineering principles.

- The development of the model should be documented in accordance with the requirements of Section 5.3.2(b) of AP-SIII.10Q.

The development of the SDFR SCC crack growth rate model was conducted according to the following criteria:

> *(1) Selection of input parameters and/or input data, and a discussion of how the selection process builds confidence in the model* (AP-SIII.10Q 5.3.2(b)(1); AP-2.27Q, Attachment 3, Level I (a)).

The bases for selecting the input data listed in Section 4.1 and used to determine and develop the SDFR model for application to the waste package are documented in Section 6.3.4. Detailed discussion about model concepts can be found in Section 6. Thus, this requirement can be considered satisfied.

> *(2) Description of calibration activities, and/or initial boundary condition runs, and/or run convergences, and a discussion of how the activity or activities build confidence in the model. Inclusion of a discussion of impacts of any non-convergence runs.* (AP-SIII.10Q 5.3.2(b)(2)).

Not applicable.

> *(3) Discussion of the impacts of uncertainties to the model results including how the model results represent the range of possible outcomes consistent with important uncertainties.* (AP-SIII.10Q 5.3.2(b)(3); AP-2.27Q, Attachment 3, Level 1 (d) and (f)).

Uncertainties associated with the model analysis are discussed in Section 6.3.4 for the 'n' model parameter and in Section 6.4.5 for the through-wall stress and stress intensity factor model parameter. Thus, this requirement can be considered satisfied.

> *(4) Formulation of defensible assumptions and simplifications.* (AP-2.27Q, Attachment 3, Level I (b)).

No assumptions were used for model development. A discussion of simplifications and their rationale are provided in Section 6. Thus, this requirement can be considered satisfied.

> *(5) Consistency with physical principles, such as conservation of mass, energy, and momentum.* (AP-2.27Q, Attachment 3, Level I (c)).

Discussion of relevant physical phenomena and processes are discussed in Section 6.3.2 for the waste package and in Section 6.3.7 for the drip shield.

> *(6) Description of simulation conditions set up to span the range of intended use and avoid inconsistent outputs. (AP-2.27Q, Attachment 3, Level I (e)).*

Stress corrosion crack growth rate data were obtained over a range of chemical conditions, and applied stress intensity factor levels Sections 6.3.4 and 7.4.2.3. Experimental tests were conducted in a range of concentrated J-13-type brines or other similar composition solutions, Sections 6.3.4 and 7.4.2.3, as well as accelerated test temperatures. Sets of test specimens were exposed over a range of pH values, test temperatures as well as the presence of potential deleterious impurity elements such as lead. Thus, this requirement can also be considered satisfied.

7.1.2 Confidence-Building After Model Development To Support The Scientific Basis Of The Model

Postmodel development validation is required by AP-2.27Q for Level I, Level II, and Level III models. For confidence building after model development, Table 2-1 of *Technical Work Plan for: Regulatory Integration Modeling and Analysis of the Waste Form and Waste Package* (BSC 2004 [DIRS 171583]) specifies this model as Level III with two validation activities for the SDFR model and an independent technical review for the seismic crack density model that also includes two additional validation activities. The validation criterion for the SDFR model is that corroborating data must match qualitatively. Validation is described in the following subsections. Corroborating or supporting data and information used to develop and validate the SDFR model parameters are listed in Table 7-1.

Table 7-1. Supporting (Corroborating) Information Used to Validate the SDFR Model

Criterion	Supporting (Corroborating) Information Source	Data/Information
1	Andresen and Ford (1994 [DIRS 118581])	Corroborative information regarding application of the SDFR Model to a range of alloy systems
1	Ford and Andresen (1988 [DIRS 118611], p. 789)	Corroborative data supporting use of the SDFR model for other Nickel Alloys, Inconel 600/182
1	Andresen (1991 [DIRS 166965], Figure 37)	Corroborative data supporting use of the SDFR model for a Nickel Alloy (Alloy 82 (UNS N06082)) with chromium content similar to Alloy 22
3	Ford and Andresen (1988 [DIRS 118611], p 791)	Model parameter ‘n’ and ‘A’ = f(n) for stainless steels
3	Ford and Andresen (1988 [DIRS 118611], Figure 10)	Model parameter ‘n’ and n = f(A) for stainless steels are applicable for nickel alloys 600/182
3	Mohr (1996 [DIRS 147981])	Weld residual stress uncertainty range of +/- 35%
3	Pasupathi (2000 [DIRS 149968]	Uncertainty in shot peened residual stress in nickel alloy
5	Ford and Andresen (1988 [DIRS 118611])	Faraday’s Law used to relate SCC crack advance to metal oxidation charge density per film rupture.
5	Bradford (1987 [DIRS 151988]	Titanium oxide to metal volume ratio used for crack plugging analysis
6	LLNL (DTN : LL030300612251.035 [DIRS 166971])	Alloy 22 experimental crack growth rates in a range of relevant test environments used to validate SDFR model

7.2. DETERMINATION OF THE LEVEL OF CONFIDENCE REQUIRED

Laboratory test results indicate that the waste package outer barrier material, Alloy 22, is highly resistant to stress corrosion cracking initiation and propagation on smooth surfaces and at defects such as those that might exist in the region of the closure welds. Thus, although stress corrosion cracking is unlikely to initiate or propagate, or both, under waste package highly static loading conditions where the only significant tensile stresses are final closure lid welding-related stresses, the stress corrosion cracking potential will be mitigated by a residual stress reversal process (laser peening or potentially controlled plasticity burnishing) that results in a compressive layer over the outer waste package closure lid weld region surfaces. Under compression, stress corrosion cracking does not initiate or grow. However, once the surface compressive layers are removed by general corrosion, current predictions indicate that stress

corrosion cracking will initiate and can grow in the through-thickness direction. The time required for corrosion to remove the compressive layers is calculated to be greater than the regulatory period. Further, if stress corrosion cracking were to initiate and grow through-wall, the cracks would be extremely tight and very limited in length (Section 6.3.7). Consequently, any water transport through the waste package or the drip shield (in the absence of oxide plugging) and any radionuclide egress through these tight waste package outer barrier cracks would be restricted to diffusive flow and, thus, would be very limited. In establishing the required level of confidence for the stress corrosion cracking model, the following criteria were considered:

Is the model extrapolated over large distances, spaces, or time frames?

Yes. The stress corrosion cracking model is extrapolated over the entire repository footprint and over the entire regulatory compliance period.

Does the model have large uncertainties?

No. While there is uncertainty in the parameters used in the stress corrosion cracking model, these uncertainties are not large.

Will the model be used to demonstrate compliance or licensing positions?

Yes. The stress corrosion cracking model is used as an input to WAPDEG, which provides realistic waste package and drip shield stress corrosion cracking degradation estimates as a function of time under the exposure conditions anticipated in the potential repository. The stress corrosion cracking model inputs to IWPD support several primary factors and TSPA-LA components.

Will the output of the model have impacts (positive or negative) on TSPA-LA dose calculation results?

Yes. Although the effect of stress corrosion cracking penetrations in the drip shield and waste package outer barrier are estimated to have relatively small impacts on TSPA-LA dose calculations, the stress corrosion cracking model is used as an input to WAPDEG that is used to provide realistic waste package and drip shield degradation estimates as a function of time under the exposure conditions anticipated in the repository. The WAPDEG model supports several primary factors and TSPA-LA components.

Consistent with the above and as per *Technical Work Plan for: Regulatory Integration Modeling and Analysis of the Waste Form and Waste Package* (BSC 2004 [DIRS 171583], Section 2.2), waste package models must obtain Level III validation, which requires that the model must meet at least two of the validation activities listed in Section 5.3.2c of AP-SIII.10Q, *Models*. This requirement is met for the Alloy 22 waste package outer barrier material.

However, as described in more detail in Section 6.3.7, for the drip shield, even if stress corrosion cracking propagates through-wall, the seepage diversion function of the drip shield will remain intact. On this basis, stress corrosion of the drip shield is categorized as an excluded

FEP (2.1.03.02.0B) and thus is not considered further with respect to the SDFR crack growth model validation activities (Section 7.4).

Furthermore, although the threshold stress intensity factor and the threshold stress for SCC initiation are not models per se, rather they are parameters or criteria that are coupled to the SDFR Model, it is important to demonstrate a defensible technical basis for each parameter. Consequently, a non-validation related activity (Activity Four) is included for each of these parameters for both Titanium Grade 7 and Alloy 22 materials.

7.3. VALIDATION ACTIVITIES AND ASSOCIATED CRITERION USED TO DETERMINE THAT THE REQUIRED LEVEL OF CONFIDENCE HAS BEEN OBTAINED

The stress corrosion cracking model involves the slip dissolution–film rupture (SDFR) crack growth model, the threshold stress intensity factor (K_{ISCC}) for crack growth, and the threshold stress for crack initiation, all of which are described in peer-reviewed scientific journals. As described in Section 7.2, the threshold stress intensity factor and the threshold stress for SCC initiation are not models per se, but rather are parameters or criteria that are coupled to the SDFR model. However, while validation of these parameters is not required per AP-SIII.10Q, it is important to demonstrate a defensible technical basis for each parameter.

With respect to the SDFR SCC crack growth rate model, validation is done through the use of the validation activities defined in AP-SIII.10Q, Section 5.3.2c. Two validation activities (VA) were selected, which are consistent with *Technical Work Plan for: Regulatory Integration Modeling and Analysis of the Waste Form and Waste Package* (BSC 2004 [DIRS 171583], Table 2-1). They are in summary, 1) quantitative comparisons of crack growth rate model predictions to observed rates available in the peer-reviewed published literature (AP-SIII.10Q, Section 5.3.2.c.3), and 2) demonstration of consistency of crack growth rate model predictions to "Q" data generated by the Project (AP-SIII.10Q, Section 5.3.2.c.1). In addition, a third SDFR validation activity, corroboration of results with an alternative mathematical model, (AP-SIII.10Q, Section 5.3.2.c.2) is implemented. This activity is in addition to the two identified in *Technical Work Plan for: Regulatory Integration Modeling and Analysis of the Waste Form and Waste Package* (BSC 2004 [DIRS 171583]). These three SDFR model-related validation activities are listed below and are consistent with those identified in AP-SIII.10Q, Section 5.3.2.c.

In addition, Activity Four demonstrates the appropriateness of the parameters for the threshold stress intensity factor and the threshold stress for SCC initiation.

These various activities, listed below, will be compared with the criterion listed in Table 2-1 of *Technical Work Plan for: Regulatory Integration Modeling and Analysis of the Waste Form and Waste Package* (BSC 2004 [DIRS 171583]) (i.e., the "Corroborating data must match qualitatively").

Activity One: Demonstrate that the crack growth rates, predicted by the film rupture–repassivation crack growth model, are consistent with observed rates published in the peer-reviewed literature (AP-SIII.10Q, Section 5.3.2.c.3).

Activity Two: Demonstrate that the crack growth rates, predicted for Alloy 22 and Titanium Grade 7 by the film rupture–repassivation crack growth model, are consistent with experimental rates obtained from data not used to develop the model (AP-SIII.10Q, Section 5.3.2.c.1).

Activity Three: Demonstrate that the crack growth rates, predicted by the film rupture–repassivation crack growth model, are consistent with growth rates predicted by an alternative mathematical model (AP-SIII.10Q, Section 5.3.2.c.2).

Activity Four: Demonstrate that the establishment of the threshold stress intensity factor (K_{ISCC}) and threshold stress represent an acceptable approach for Alloy 22 and Titanium Grade 7 under environmental conditions relevant to the waste package and drip shield, respectively.

This latter activity (Activity Four) is applicable to both the threshold stress intensity factor parameter (K_{ISCC}) and the threshold stress criterion for SCC initiation on a 'smooth' surface (i.e., in the absence of fabrication defects such as weld flaws). While the technical work plan states 'VA = NA', this report provides a defensible basis consistent with VA 1 (AP-SIII.10Q, Section 5.3.2.c.1, compare with laboratory results). Since there is no relevant theoretical basis in the literature to describe these parameters, they are each selected based on a conservative empirical approach. Therefore, they do not require validation and the technical work plan (Table 2-1) activity listed does not cite an AP.SIII.10Q, Section 5.3.2.c specific model validation activity. However, a description of the defensible and conservative basis for selection of the values for each of these parameters is described in Section 7.4 to provide additional confidence.

To meet the model validation acceptance criterion (corroborating data must match qualitatively) for the SDFR model, it is informative to consider what is the indicated range of scatter and, based on this, what is a reasonable match between experimentally generated crack growth rate results and model predictions. Examination of the literature dealing with measured versus predicted stress corrosion cracking growth rates, indicates that in general, crack growth rates within two or three orders of magnitude may be considered to be within reasonable agreement. For example, see work by Andresen (1991 [DIRS 166965], Figures 2, 37, and 38) and Andresen (2002 [DIRS 166967], Figure 1) for the nickel alloys (Alloys 600, 82, and 182), exposed to 288°C water environments where it is evident that scatter of this magnitude occurs. The issue of reasonable agreement is discussed further in Section 7.4.1. However, considering the spread in measured versus predicted rates observed in the literature, terms such as "consistent" and "reasonable" are used in the model validation section to define a "qualitative match."

7.4 COMPARISON OF ACTIVITIES PERFORMED TO GENERATE CONFIDENCE IN THE MODEL WITH MODEL VALIDATION CRITERION

According to *Technical Work Plan for: Regulatory Integration Modeling and Analysis of the Waste Form and Waste Package* (BSC 2004 [DIRS 171583], Section 2.2.5), the developed model is to be validated in accordance with the activities described in the previous section with specific activities to be performed to generate the desired confidence in the model or model parameter (i.e., to meet the criterion listed in the technical work plan). All activities are applicable to Alloy 22, whereas only Activity Two (comparison of experimental crack growth rates with model predictions) and Activity Four (related to an acceptable approach for establishment of a threshold stress and threshold stress intensity factor) are applicable to the drip

shield (Titanium Grade 7). However, as described in Section 6.3.7, the only stress corrosion cracking breach criterion for the Titanium Grade 7 drip shield is the threshold stress (for stress corrosion cracking initiation). Thus, whether from rockfall or from direct seismic-related residual stresses as described in Appendix B, if the resultant stresses exceed the threshold stress criteria, the crack growth rate is such that "breach" (i.e., through-wall stress corrosion cracking) occurs essentially instantaneously, consistent with a threshold stress intensity factor value of zero. Further, as described in more detail in Section 6.3.7, even if stress corrosion cracking propagates through-wall, the seepage diversion function of the drip shield will remain intact. On this basis, stress corrosion of the drip shield is categorized as an excluded FEP (2.1.03.02.0B and is not considered further in this SDFR model validation (Section 7.4), except with respect to establishment of a threshold stress as described in Activity Four (confidence building, not validation). This section shows that the required confidence level for the waste package related SDFR model (Level III) has been achieved because all activities specified in the technical work plan are fully (or very conservatively) complied with to generate confidence in the model and the validation criterion listed in Table 2-1 (Corroborating data must match qualitatively) has been successfully met.

7.4.1 Activities Performed for Validating the SDFR Model Using Peer-Reviewed Literature

The applicable Activity relating to validation of the SDFR model is Activity One listed in Section 7.3:

> Demonstrate that the crack growth rates, predicted by the film rupture–repassivation crack growth model, are consistent with observed rates published in the peer-reviewed literature.

The film rupture–repassivation crack growth model terminology is often used when referring to the slip dissolution–film rupture (SDFR) model and the two are equivalent. The input parameter (exponent 'n') of this crack growth rate prediction model (Equation 19), used to compare model predicted rates with corresponding literature values, is that obtained for stainless steel as documented in Section 6.3.3. The model predictions are compared to results, already published in peer-reviewed literature, that were calculated using the same input parameters. This ensures that the model details and calculation methods described in the earlier version or in Section 6 yield results fully consistent with the peer-reviewed journal-published values. The activities performed to satisfy Activity One and to achieve the desired confidence in the model are discussed.

As documented in Section 6.3.3, input parameter (exponent 'n') obtained for sensitized Stainless Steel Type 304 is 0.54. Figure 6-4 indicates that crack growth rates predicted by the slip dissolution–film rupture crack growth model are in reasonable agreement with observed rates published in the peer-reviewed literature for stainless steel. Figure 7-1 indicates that the range of the prediction error (i.e., the ratio of the difference of the predicted and the observed values divided by the observed value) for the majority of results is –3 to +3 and, if including the extreme results, is –5 to +7 with positive ratio indicating overprediction and negative ratio, underprediction. It is, therefore, concluded that the prediction error, as discussed in the previous statement, is well within 2 orders of magnitude and, thus, within the required accuracy

prescribed in Section 7.3. This has ensured that the model details and calculational methods yield results fully consistent with the peer-reviewed journal-published values and are, therefore, qualitatively corroborated.

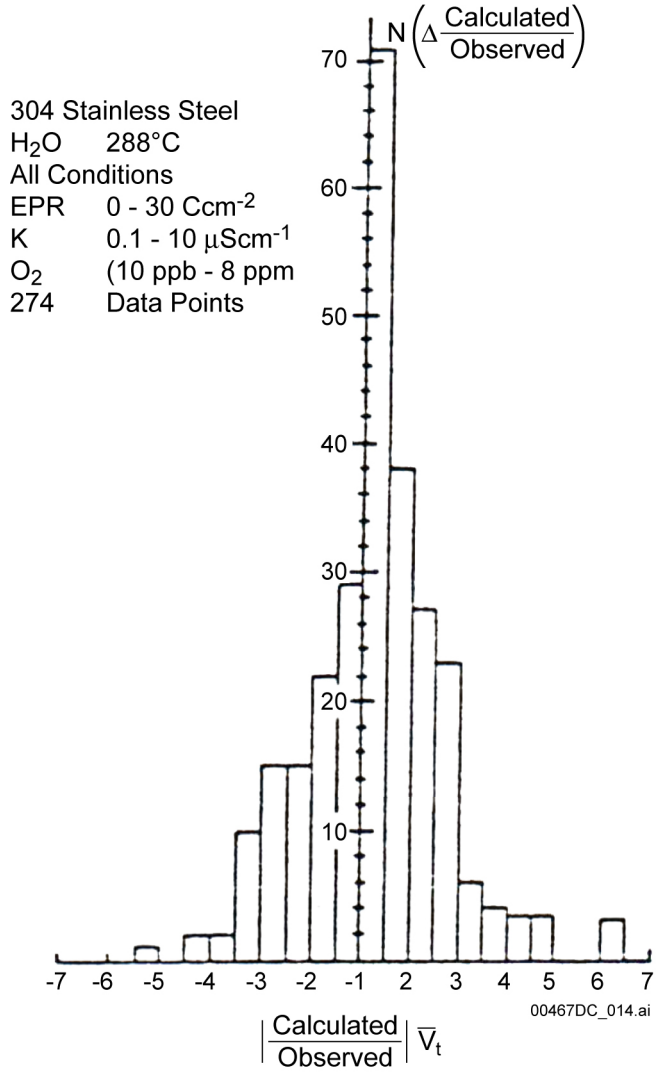

Source: Ford and Andresen 1988 [DIRS 118611], Figure 8.

Figure 7-1. Frequency Distributions of the Ratio of the Calculated to Observed Crack Growth Rates for Stainless Steel Type 304

7.4.2 Activity Performed for Validating the SDFR Model Applicable to Alloy 22 using Independently Obtained Experimental Data

The applicable activity is Activity Two, Section 7.3:

> Demonstrate that the crack growth rates, predicted for Alloy 22 and Titanium Grade 7 by the SDFR crack growth model, are consistent with experimental rates.

Having established the validity of the model predictions of crack growth rate versus stress intensity for stainless steel, the model is then utilized to predict selected crack growth rates as a function of stress intensity for Alloy 22 utilizing model input parameters developed specifically for Alloy 22 using qualified experimental data generated under an approved test program at the General Electric Global Research Center.

Validity and predictive capacity of the model developed for Alloy 22 is then established if crack growth rates predicted for this material by the SDFR crack growth model are in reasonable agreement (qualitatively consistent) with growth rates determined independently under an approved test program at Lawrence Livermore National Laboratory. The activities performed to satisfy Activity Two listed in Section 7.3 and to achieve the desired confidence in the model, in accordance with Section 2.2.2 of the technical work plan (BSC 2004 [DIRS 171583]), are discussed below.

7.4.2.1 Stress Corrosion Cracking Behavior of Nickel-Chromium Base Alloys at Temperatures Relevant to the Waste Package

In addition to stainless steels, the model has been shown to apply to several nickel-based alloys, including Alloy 600, a nickel-based alloy with lower chromium-content than Alloy 22. Table 7-2 lists nominal composition for Alloys 600, 182 and 82 and specified composition for Alloy 22.

Table 7-2. Nominal Chemical Composition of Several Ni-Cr Base Alloys (wt %)

Alloy Composition	Alloy 22 (ASTM B 575-94 [DIRS 100497])	Alloy 600 (UNS N06600)*	Alloy 182 (AWS ERNICRFE-3)*	Alloy 82 (AWS ERNICR-3)*
Element				
C	0.015 max.	0.07	0.04	0.02
Co	2.5 max.	-	-	-
Cr	20-22.5	16.1	14.0	19.6
Fe	2.0-6.0	9.4	6.9	1.2
Mn	0.50 max.	0.2	7.9	2.9
Mo	12.5-14.5	0.2	-	-
Ni	Balance	73.7	~68.5	73.1
P	0.02 max.	0.01	0.013	0.003
S	0.02 max	0.002	0.003	0.001
V	0.35 max	0.03	-	-
W	2.5-3.5	-	-	-

NOTE: *Heat compositions from (Andresen 1991 [DIRS 166965], Table I).

To apply this model to Alloy 22 under relevant conditions, the following discussion shows that (1) results demonstrating that the observation of similar stress corrosion cracking growth behavior of stainless steel and Alloy 600 also applies over the range of temperatures relevant to the waste package (~50°C to 200°C); and (2) results are consistent with the model for other nickel–chromium alloys with higher chromium content than Alloy 600 (similar to Alloy 22). Demonstration of the applicability of the model to these other nickel–chromium alloys supports the applicability of the SDFR model to Alloy 22 with respect to chromium, which is the alloy

addition responsible for formation of the protective Cr_2O_3-passive film for stainless steels and chromium-containing nickel-based corrosion-resistant passive alloys including Alloy 22 (DTN: LL021105312251.023 [DIRS 161253], Section 3.3). Specifically, in addition to stainless steel (i.e., activities performed to meet Activity One), the SDFR model has been validated for a range of alloys, including irradiated stainless steels; Inconel 600 and 182 nickel-chromium base alloys; and, subsequently, the higher chromium content nickel–chromium-base alloy, Alloy 82 (UNS N06082) (Section 6.3.4), where extensive observations are presented to indicate that there is ample reason to conclude that stress corrosion cracking of nickel-chromium-molybdenum base Alloy 22 occurs by the same fundamental mechanism characterized by the SDFR stress corrosion cracking model, but with alloy specific values for the 'A' and 'n' parameters.

Andresen and Ford (1994 [DIRS 118581], p. 62) indicated that the SDFR model has been applied to stainless steels, low alloy and carbon steels, ductile nickel alloys, and irradiated stainless steels. Ford and Andresen (1988 [DIRS 118611], p. 789) also used the SDFR model for the nickel-chromium based alloys Inconel 600/182. Further, as indicated in Section 6.3.3, it was determined that the SDFR model (using the Stainless Steel Type 304 'A' versus 'n' relationship in 288°C water) was statistically valid for the chromium-containing, nickel-based Alloys 600 and 182 over a range of anionic impurity concentrations (Ford and Andresen 1988 [DIRS 118611], Figure 10). Subsequently, Andresen (1991 [DIRS 166965], Figure 37), used the SDFR model for comparison of crack growth rate predicted versus measured values with reasonable agreement for the higher chromium content-nickel-based alloy, Alloy 82 (UNS N06082). Alloy 82 (18% to 22% Cr, UNS N06082) overlaps Alloy 22 (20% to 22.5% Cr) (DTN: MO0003RIB00071.000 [DIRS 148850], p. 2) in chromium content. Analyses indicate that the inner, protective corrosion films that form in the passive potential range on such nickel-based, chromium-containing alloys with greater than about 15% chromium contain a very thin passive film layer of primarily Cr_2O_3 (with some nickel content) at the oxide–alloy interface (Pensado et al. 2002 [DIRS 166944], p. 2-2). Such a thin, passive Cr_2O_3 film possesses similar repassivation kinetics (depending on actual chromium content) and mechanical properties (e.g., fracture strain) over the range of nickel–chromium-based alloys of interest. This is consistent with the model having been shown to apply or to give reasonable predictive results for a range of nickel-based alloys with chromium contents spanning the Alloy 22 compositional range.

Further, there is general correspondence (reasonable statistical agreement) between the observed stress corrosion cracking growth rate temperature dependencies for sensitized Stainless Steel Type 304 and Alloy 600 over the temperature range of most interest (~50°C to 200°C) when compared under comparable stress intensity factor and environmental conditions (Andresen 1993 [DIRS 166966], Figures 15 and 16). For example, from examination of Figure 6-5 in Section 6.3.4 (Andresen 1993 [DIRS 166966], Figure 15), it is seen that crack growth rates for sensitized Stainless Steel Type 304 and Alloy 600 follow the same temperature dependency with reasonably similar crack growth rates over a temperature range from about 25°C to 275°C, which is broader than the temperature range of most interest (~50°C to 200°C) stated above.

In addition to the similarities in composition and mechanical properties, as indicated earlier in this section, for the passive films present on this class of face-centered cubic crystal structure austenitic alloys, (i.e., austenitic stainless steels and nickel–chromium-based alloys such as Alloys 600, 82, and 22), the expected microdeformation modes of the alloys are also comparable,

based on examination of literature values for stacking fault energies (SFE) (Gordon 2004 [DIRS 167027]). A low value of SFE tends to promote coplanar dislocation arrays (promoting local stress buildups that can more easily rupture the passive surface film at slip offsets) whereas high SFE values promote dislocation tangles that tend to diffuse local stress buildups. These alloys possess a face-centered cubic-crystallographic lattice structure and have similar relatively low values of estimated SFE ranging from about 20 to 30 ergs/cm^2 for Stainless Steel Types 304L and 316L to about 80 ergs/cm^2 for Alloy 600 with the estimated value for Alloy 22 being about 65 ergs/cm^2. This range is relatively low compared to published values of about 340 ergs/cm^2 for pure nickel or nickel alloys with much lower chromium contents (Gordon 2004 [DIRS 167027], Table 1). Although lower values of SFE can promote microstress and strain buildups that may accelerate stress corrosion cracking initiation, the relatively high local deformation at a stressed crack or weld flaw tip is likely to lead to relatively high local strains and to overwhelm the effect of SFE on micro stress or strain buildups with respect to stress corrosion cracking propagation.

7.4.2.2 Stress Corrosion Cracking Behavior of Alloy 22 at Higher Temperatures (~288°C)

Other General Electric Global Research Center results are described for Alloy 22 tested at higher temperatures (~288°C) illustrating that Alloy 22 follows similar behavior to Stainless Steel Types 304 or 316 and Alloy 600 at similar temperatures (~288°C), further supporting the argument that the initial application of the model to BWR coolant temperatures of ~288°C is consistent with the application at lower waste package temperatures. The results were discussed in Section 6.3.4 and are summarized below.

As the SDFR was initially developed for stainless steels and nickel-based alloys Inconel 600 and 182 under higher temperature (~288°C) light water reactor coolant conditions, additional confidence in the applicability of this model to Alloy 22 can be gained from observation of the response of Alloy 22 under similar conditions. Test results from DTN: MO0402GEA22SCC.000 [DIRS 167911] indicate the crack growth rate response of Alloy 22 exposed to 288°C relatively pure water (2 ppm O_2) is broadly consistent with other materials, such as Alloys 600 and 182 (Andresen et al. 2002 [DIRS 166967]) and unsensitized austenitic stainless steel (Andresen et al. 2002 [DIRS 167762]) under these same conditions. The measured crack growth rates show a similar dependency to parameters like corrosion potential and water purity (sulfate). For example, in all test cases, the change in corrosion potential from ~ +0.2 V_{SHE} to ~ –0.5 V_{SHE} (due to a change from 2 ppm O_2 to H_2-deaerated water) causes a drop of at least one order of magnitude in the crack growth rate, as indicated by Table 6-3 in Section 6.3.4. Also, as expected, Alloy 22 shows crack growth rates under repository type oxidizing conditions (i.e., at $0.2V_{SHE}$), which are about one order of magnitude lower than those of the other materials under identical test conditions, consistent with the higher ‘n’ parameter values obtained for Alloy 22 using Project-sponsored testing, Section 6.3.4, and demonstrating its superiority as a structural material under conditions where stress corrosion cracking is a concern.

7.4.2.3 Stress Corrosion Cracking Behavior of Alloy 22 in Other Relevant Environments

Whereas the initial Alloy 22 crack growth rate data obtained at GE Global Research were generated in the pH ~13, BSW brine environment at 110°C, the discussion that follows demonstrates that stress corrosion cracking growth rate results obtained at LLNL in other relevant environments, SAW (pH ~ 2.8]) and SCW (pH ~ 9 to 10) at about 95°C as well as in BSW (pH ~13) at 100°C, fall within the model uncertainty bands predicted by the SDFR model, providing further qualitative corroboration of the model applicability to Alloy 22 over the range of repository-relevant environments consistent with the stress corrosion cracking model validation criterion (corroborating data must match qualitatively) cited in Section 7.3. Citing all of these results strongly supports the use of the SDFR model for Alloy 22.

The good crack growth rate predictive capability of Equation 19, benchmarked with the experimental results presented in Table 6-4, determined by direct measurements under an accepted Q test program at General Electric Global Research Center (GEGRC) (DTN: LL021105312251.023 [DIRS 161253]), has been validated with a separate set of measured crack growth rates (Table 7-3). These separate results are plotted in Figure 7-2 along with the initial GE crack growth rate measurements. This separate set of measured crack growth rates were collected using the reversing direct current crack growth measurement technique with compact tension type fracture mechanics specimens (loaded per ASTM E 399-90 [DIRS 117480]) tested at LLNL (DTN: LL030300612251.035 [DIRS 166971]). As can be seen from Figure 7-2, there is good agreement between the LLNL data and the predictive curves and statistical limits based on the GE crack growth rate results (i.e., five data points summarized in Table 6-4). Table 7-4 shows that the prediction error ratio is in the range of -0.93 to 54.87. While the prediction error ratio is generally within the expected two orders of magnitude, the prediction model has a tendency of overprediction (with positive error ratio) (i.e., on the conservative side), rather than underprediction (with negative error ratio). Also, for specimen DCT-22, the measured growth rate is below the crack growth detection limit and, thus, the comparison between measured and predicted rates is not directly relevant. Furthermore, it can be seen from Figure 7-2 that measured data fall nicely between the two bounds representing two standard deviations of the mean value. The agreement between the prediction and measured data shown in Figure 7-2 provides important input to the validation of the SDFR model for Alloy 22, corroborating the excellent qualitative match between model predictions and independently measured Alloy 22 crack growth rates over a range of environments and pH values.

Table 7-3. Summary of LLNL Crack Growth Rates in Compact Tension Specimens

Specimen ID	Test Solution	Nominal Test Temperature (°C)	Average Stress Intensity MPa√m	Crack Growth Rate (mm/sec)
DCT-13	BSW-13	100	45.13	2.12E-09
DCT-14	BSW-13	100	44.88	4.23E-09
DCT-16	BSW-13	100	46.38	1.41E-09
DCT-18	SAW	94	45.07	2.12E-10
DCT-19	SAW	94	45.08	1.41E-11
DCT-20	SCW	95	45.11	4.23E-10
DCT-21	SCW	95	44.68	2.82E-11
DCT-22	SCW	95	44.37	4.94E-12

Source: DTN: LL030300612251.035 [DIRS 166971], Figure 6.

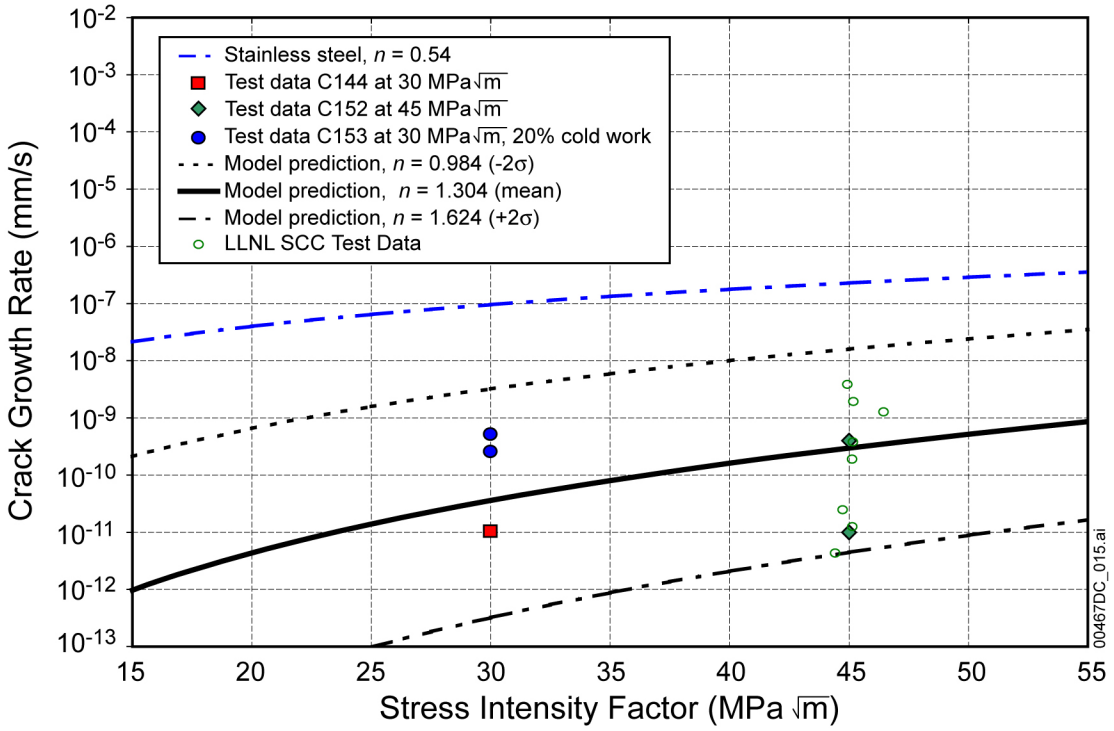

Source: Plot from Figure 6-6 with initial test data for C144, C152, and C153 from DTN: LL021105312251.023 [DIRS 161253] and LLNL test data from DTN: LL030300612251.035 [DIRS 166971].

Figure 7-2. Comparison of the SDFR Prediction Model and Measured Data for Alloy 22

Table 7-4. Comparison of Predicted and Measured Crack Growth Rates for Alloy 22

Specimen ID	Test Solution	Nominal Test Temperature (°C)	Average Stress Intensity MPa√m	Measured Crack Growth Rate (mm/s)	Predicted Crack Growth Rate (mm/s)	Prediction Error Ratio
DCT-13	BSW-13	100	45.13	2.12E-09	3.02E-10	-0.86
DCT-14	BSW-13	100	44.88	4.23E-09	2.93E-10	-0.93
DCT-16	BSW-13	100	46.38	1.41E-09	3.48E-10	-0.75
DCT-18	SAW	94	45.07	2.12E-10	3.00E-10	0.42
DCT-19	SAW	94	45.08	1.41E-11	3.00E-10	20.28
DCT-20	SCW	95	45.11	4.23E-10	3.01E-10	-0.29
DCT-21	SCW	95	44.68	2.82E-11	2.87E-10	9.18
DCT-22	SCW	95	44.37	4.94E-12	2.76E-10	54.87

NOTES: 1. Columns 1 through 5 are obtained from Table 7-3.
2. Values in Column 6 are obtained from Equation 19 (in Section 6.3.4) with n = 1.304.
3. Prediction error ratio (Col. 7) = (Col. 5 – Col. 6) / Col. 5

7.4.3 Corroboration of SDFR Model with Available Alternative Conceptual Models

Although not a required model validation activity per the technical work plan (BSC 2004 [DIRS 171583], Table 2-1), corroboration with available alternative conceptual models (ACMs) such as the coupled environment model, a mathematical model used to predict stress corrosion crack growth rates, can be used to validate the developed model. The alternative conceptual model is summarized, discussed, and contrasted with the base-case model. The developed base-case model should be comparable or more conservative than the alternative conceptual models. More details about alternative conceptual models are provided in Section 6.3.6.

Corroboration with available alternative conceptual models, such as the coupled environment fracture model for stress corrosion cracking, was considered for the validation of the base-case model. Section 6.3.6 concludes that the slip dissolution–film rupture and the CEF models are capable of predicting the crack growth rate for stress corrosion cracking. However, the CEF model has a tendency of underestimating the crack growth rate as compared to the slip dissolution–film rupture model when both models were applied to predict the crack growth rate for Stainless Steel Type 304 in the boiling water reactor (BWR) environment (Figure 6-7). Comparison with experimental data summarized by Ford and Andresen (1988 [DIRS 118611], Figure 22) for crack propagation rate versus stress intensity factor for sensitized Stainless Steel Type 304 in fully aerated, high-purity water at elevated temperature indicated that the crack growth rate predicted by the CEF model (i.e., 3.2×10^{-9} cm/sec at 20 MPa√m) is at the lower end of the range cited by Ford and Andresen (1988 [DIRS 118611]) and (Macdonald and Urquidi-Macdonald 1991 [DIRS 162702]). For this reason, the CEF model was not included for evaluation but only used to further validate the base case slip dissolution–film rupture model.

7.4.4 Activities Performed to Demonstrate the Technical Basis for the Selection of the Threshold Stress Intensity Factor and the Threshold Stress Parameter for SCC Initiation

As indicated in Table 2-1 of *Technical Work Plan For: Regulatory Integration Modeling and Analysis of the Waste Form and Waste Package* (BSC 2004 [DIRS 171583]), these activities (listed as Activity Four) are not for model validation but rather are for demonstration of the establishment of an acceptable approach for determining K_{ISCC} and the threshold stress for SCC initiation under environmental conditions relevant to the waste package and drip shield. Thus, to provide additional confidence, a defensible technical basis for selection of each of these parameters is described in the following subsections.

7.4.4.1 Activities Performed to Demonstrate the Technical Basis for the Threshold Stress Intensity Factor (K_{ISCC}) for Alloy 22

As described earlier in Section 7.4, consideration of K_{ISCC} in the Titanium Grade 7 drip shield is not relevant since the value is effectively zero (i.e., once SCC is initiated in the drip shield as a result of rockfall or seismic damage, it is conservatively assumed to propagate through-wall instantly regardless of the through-wall K_{ISCC} values).

In general, stress corrosion crack growth can occur at a rate, such as that predicted by the slip dissolution–film rupture (SDFR) model, only if the calculated stress intensity at any flaw of given dimensions of length and depth exceeds a threshold value known as K_{ISCC}. Since there is no accepted theoretical basis for deterministic calculation of K_{ISCC}, this parameter is conservatively determined by selecting a K_I value corresponding to a conservative lower limit value for the crack growth rate, V_t. To accomplish this, the general form of the previously validated SDFR model (see Activities One, Two, and Three) (i.e., Equation 14 is used to calculate the stress intensity factor value corresponding to a crack growth rate equal to the general corrosion rate, V_{gc}, in Section 6.3.5). This calculated value is defined as K_{ISCC}.

The theoretical basis for this approach is that if the crack growth rate equals the rate at which the surface recedes due to general corrosion, then it is not possible to maintain a sharp crack (the crack tip will blunt) and stress corrosion cracking will effectively arrest. Based on this 'crack blunting' theory (Andresen and Ford 1994 [DIRS 118581], p. 62), it follows that any existing stress corrosion crack will not continue to grow (i.e., will arrest, if the crack growth rate is equal to or less than the general corrosion rate). If V_{gc} is the mean general corrosion rate, the threshold stress intensity factor K_{ISCC} can be calculated from Equation 20 (a rearrangement of Equation 14) of Section 6.3.5, which represents the SDFR model for the case of constant (noncyclic) stress (i.e., for the waste package sustained loading conditions):

$$K_{ISCC} = (V_{gc} / \bar{A})^{1/\bar{n}} \qquad \text{(Eq. 20)}$$

The mean general corrosion rate, V_{gc}, based on Section 6.3.5, is 7.23 nm/yr. The threshold stress intensity factor for Alloy 22, accordingly, can be calculated and its distribution is listed in Table 6-6, based on the 'n' value distribution shown in Table 6-5. In conclusion, Activity Four is satisfied since an acceptable, conservative K_{ISCC} value was obtained by setting the crack

growth rate in the validated SDFR model to a value equal to the mean general corrosion rate at the alloy surface.

7.4.4.2 Activities Performed to Demonstrate the Technical Basis for the Threshold Stress for Alloy 22 and Titanium Grade 7

Similar to the previously described establishment of a K_{ISCC} value, the purpose of this activity is to demonstrate a defensible technical basis for selecting a threshold-stress parameter for SCC initiation. Thus, Activity Four specifies the demonstration of an acceptable approach for the establishment of a threshold stress for SCC initiation for Alloy 22 and Titanium Grade 7 under environmental conditions relevant to the waste package and drip shield, respectively.

Although the threshold stress concept is described in peer-reviewed journal papers, there is no firm accepted basis for calculating a threshold stress value for a given material or environment combination. The threshold stress is that value below which stress corrosion cracking will not initiate on a "smooth" metal surface. Therefore, as described in Section 6.2.1, a conservative, empirical approach is implemented to develop a defensible threshold-stress parameter. For the purpose of lifetime modeling, a 'smooth' surface is one that contains microscopic defects associated with incipient environmental crack formation, or metallurgical or mechanical defect sites. The initial defect depth is taken as 0.05 mm, a value qualified for use in Section 6.2.1 using AP-SIII.10Q, Section 5.2.1.k. Thus, when the metal surface stress exceeds the stress corrosion cracking threshold stress, SCC is initiated at these 'smooth' surface microdefects. Once initiated, the crack may either reach the arrest state or the "propagation" phase, once the crack tip stress intensity factor exceeds the threshold K_{ISCC} value described above. Since it is necessary to experimentally establish the threshold stress values, a conservative approach is taken based on qualified experimental data.

As addressed in Section 6.2.1, long-term SCC initiation stress measurement results have been obtained under constant active applied loading conditions using uniaxial tensile specimens covering a range of metallurgical conditions (Figure 4-1). These experimental measurements of crack initiation stress are presented in Figure 4-1 as the ratio of applied stress-to-yield strength (YS) versus time-on-test for specimens exposed in hot concentrated salt solution (pH = 10.3 at 105°C) designed to simulate the chemistry of concentrated Yucca Mountain ground water. Specimens have been on test for over 21,000 hours. It is indicated in Section 6.2.1 that Alloy 22 exhibits excellent stress corrosion cracking resistance since failure was not observed for any of the 120 Alloy 22 specimens under applied stress ratios of about 2.0 (YS) for annealed material and 2.1(YS) for welded material. These stress ratios correspond to about 89% to 96% of the ultimate tensile strength. Alloy 22 was also found to be highly resistant to stress corrosion cracking initiation in slow strain rate tests and U-bend tests covering a broad range of environments. Titanium Grade 7, although still fairly resistant to stress corrosion cracking, experienced stress corrosion cracking failures at applied stress ratios at and above 1.1 (YS) in the constant load tests. However, it (and its analog, Titanium Grade 16) did not exhibit stress corrosion cracking in two- to five-year exposed U-bend specimen tests covering a range of test environments. Thus, it is evident that the threshold stress for Alloy 22 in relevant environments is significantly above the yield stress level whereas the value for Titanium Grade 7 is likely at or slightly above the yield strength value.

As described in Section 6.2.1, these high SCC-initiation threshold stress values are independently corroborated for both Alloy 22 and Titanium Grade 7 based on examination of a series of U-bend SCC-initiation specimens stressed at or above yield strength levels. These specimens were exposed in the LLNL Long Term Corrosion Test Facility in a range of relevant brine environments for times out to five years. In all cases, high magnification examination of the highest stressed portions of these specimens indicated no SCC initiation consistent with the constant load test results and with a threshold stress above the yield strength.

In establishing a defensible 'safety factor,' it is appropriate to consider other accepted precedents based on threshold or runout stress measurements used in general engineering practice. For example, the ASME code (ASME 1969 [DIRS 162446], p. 20) utilizes a reduction factor of 2 on stress when dealing with high cycle fatigue (i.e., the code-allowable threshold value is set at half the experimentally measured runout threshold value known as the endurance limit, which is the maximum stress below which a material can presumably endure an infinite number of stress cycles). In dealing with stress corrosion cracking rather than fatigue, it is considered appropriate to also use a conservative 'safety factor' on the measured threshold values. Consequently, "threshold stress" values to be used are based on applying a conservative reduction factor of at least 2 on the measured threshold or runout stress ratio values obtained from the constant load tests described above. In addition, it is prudent to select a threshold stress value below the materials yield strength. Applying this philosophy and a reduction factor of 2.2, the threshold stress values selected are 0.9 (YS) for Alloy 22 and 0.5 (YS) for Titanium Grade 7. Based on the foregoing discussion, Activity Four, the demonstration of a defensible technical basis for the selection of the threshold stress for SCC initiation for Alloy 22 and Titanium Grade 7 has been satisfied.

INTENTIONALLY LEFT BLANK

8. CONCLUSIONS

In this section, output of the base-case stress corrosion cracking model is discussed. Output of the seismic crack density model is discussed in Appendix B, Section B8.

8.1 CONCLUSION

This document provides a detailed description of the process-level models and the associated outputs developed for use in the performance assessment of the Alloy 22 waste package outer barrier subjected to stress corrosion cracking due to weld-induced stress in the final closure lid welds. All the welds with the exception of the final closure lid welds are subjected to solution heat treatment to relieve the residual tensile stresses when the entire waste package is heat treated before the loading of spent fuel elements. It is recognized that dynamic loads resulting from unlikely seismic events have the potential of leading to plastic upsets and resultant sustained residual tensile stresses that may initiate cracks and drive them through the wall. Stress corrosion cracking through-wall propagation criteria governing seismic initiated stress corrosion cracking have been developed for the waste package material (i.e., Alloy 22). The breach criteria are based on a stress threshold as discussed in Section 6.2.1. Seismic stress corrosion cracking is discussed further in Appendix B.

The drip shield is excluded from the stress corrosion cracking evaluation because the drip shield is annealed to relieve the weld residual stress and stress corrosion cracking resulting from rockfall will result in very tight crack openings that will become plugged with oxide and thus will not degrade the water diversion function of the drip shield (Section 6.3.7). The only remaining issue of concern for stress corrosion cracking associated with the drip shield is the potential for crack initiation due to plastic deformation induced residual stress caused by unlikely seismic events. Through-wall crack penetration criteria governing seismic initiated residual stress for the drip shield material (i.e., Titanium Grade 7) are based on a stress threshold, which is discussed in Section 6.2.1. Once initiated, stress corrosion cracking is treated as being through-wall. The Stainless Steel Type 316 inner barrier of the waste package is excluded from the stress corrosion cracking evaluation because the TSPA-LA does not take credit for the inner barrier.

The base-case slip dissolution–film rupture model relates stress corrosion cracking initiation and subsequent crack advance to the metal oxidation that occurs when the protective film at the crack tip is ruptured. The slip dissolution–film rupture model can be applied to assess the breach (or the lack of it) of the waste package due to the stress corrosion cracking crack propagation for given manufacturing cracks (e.g., weld flaws) or cracks initiated by the combined effects of stress and environment, or both. The threshold stress intensity factor (SIF) is based on the theory that there exists a threshold value (K_{ISCC}) for the stress intensity factor such that there is no growth of a preexisting crack or flaw having a stress intensity factor less than the threshold value. The threshold SIF provides a criterion for determining if a stress corrosion cracking crack will reach an arrest state or enter a propagation phase.

The model validation is accomplished by comparing experimental measurements of key model parameters to data measurements and corroborative data available from the open scientific

literature and by comparing with another alternative conceptual model. Uncertainty and variability associated with model parameters are assessed.

The application of the stress corrosion cracking models to the waste package and drip shield also requires input of weld residual stress profiles and stress intensity factor profiles along with uncertainty and variability. These input data have been developed for the 25-mm outer lid (subjected to laser peening) and the as-welded 10-mm middle lid (which has a through-wall stress distribution similar to the currently proposed 12.7 mm (1/2 in.) middle lid thickness) and are reported in this section as output data. This report also provides other outputs needed as input for a complete TSPA-LA for the degradation of the waste package due to stress corrosion cracking effects in the following areas: threshold stress for crack initiation and an estimate of crack opening size. In addition, a summary of size, density, and orientation distributions for manufacturing flaws or defects, which are technical product output of the calculation *Analysis of Mechanisms for Early Waste Package/Drip Shield Failure* (BSC 2004 [DIRS 170024]), is provided in Section 6.2.2, but is not part of the technical product output.

8.2 COMPLIANCE WITH YMP ACCEPTANCE CRITERIA

Yucca Mountain Review Plan, Final Report (NRC 2003 [DIRS 163274]) contains Acceptance Criteria (AC) intended to establish the basis for the review of the material contained in the License Application. As this report serves, in part, as the basis for the License Application, it is important the information contained herein conforms to those same Acceptance Criteria.

This report addresses the degradation of two components of the engineered barriers, the waste package and drip shield. Based on the engineered barrier role of the waste package and the drip shield, the processes involved with their degradation, and the potential impact of their degradation, the YMRP Acceptance Criteria applicable to this report are identified in *Technical Work Plan for Regulatory Integration Modeling and Analysis of the Waste Form and Waste Package* (BSC 2004 [DIRS 171583], Table 3-1) and are delineated below in italics. A discussion of how this report addresses appropriate criteria follows each Acceptance Criterion, coupled with an indication of where within the report the appropriate information can be found.

8.2.1 System Description and Demonstration of Multiple Barriers

The waste package and the drip shield meet the definition of a barrier in 10 CFR 63.2 [DIRS 156605]. The following acceptance criteria can be found in Section 2.2.1.1.3 of *Yucca Mountain Review Plan, Final Report* (NRC 2003 [DIRS 163274]).

Acceptance Criterion 1 – Identification of Barriers is Adequate

> *Barriers relied upon to achieve compliance with 10 CFR 63.113(b), as demonstrated in the total system performance assessment, are adequately identified and clearly linked to their capability.*

This report addresses the system known as the engineered barrier system (EBS) and the barriers created by the waste package (WP) and the drip shield (DS). The engineered barrier system components are identified in Section 1.1. The drip shield barrier is to contribute to waste isolation by keeping seepage waters and dropping rocks away from the waste package for its

lifetime and, when breached by stress corrosion cracking, by reducing the contact of water with the waste package. The waste package barrier is to contribute to waste isolation by keeping water away from the waste for its lifetime and, when breached, by reducing the contact of water with the waste and radionuclide release rate from the waste.

Acceptance Criterion 2 – Description of Barrier Capability Is Acceptable

> *The capability of the identified barriers to prevent or substantially reduce the movement of water or radionuclides from the Yucca Mountain repository to the accessible environment or prevent the release or substantially reduce the release rate of radionuclides from the waste is adequately identified and described:*
>
> *(1) The information on the time period over which each barrier performs its intended function, including any changes during the compliance period, is provided;*
>
> *(2) The uncertainty associated with barrier capabilities is adequately described;*
>
> *(3) The described capabilities are consistent with the results from the total system performance assessment;*
>
> *(4) The described capabilities are consistent with the definition of a barrier at 10 CFR 63.2.*

The drip shield barrier contributes to waste isolation by keeping seepage waters and dropping rocks away from the waste package for its lifetime and, when breached by stress corrosion cracking, by reducing the contact of water with the waste package. The waste package barrier contributes to waste isolation by keeping water away from the waste for its lifetime and, when breached, by reducing the contact of water with the waste and radionuclide release rate from the waste. The drip shield barrier capability is addressed in this report principally in Section 6.3.7. The waste package barrier function of isolating the waste from water is addressed throughout this report and more specifically in Sections 6.4.2.1, 6.4.5, and 8.3. Although SCC can lead to waste package barrier breach at the outer closure lid weld, stress mitigation of this weld (Section 6.4.5) is calculated to extend the barrier lifetime beyond the regulatory period.

Acceptance Criterion 3 – Technical Basis for Barrier Capability is Adequately Presented.

> *The technical bases are consistent with the technical basis for the performance assessment. The technical basis for assertions of barrier capability is commensurate with the importance of each barrier's capability and the associated uncertainties.*

As the Acceptance Criteria delineated above address the overall description and capability of the engineered barriers as a unit, compliance with these criteria are addressed partially in this report and more fully in other reports. The technical basis for the drip shield barrier capability is documented in Sections 6.3.7, 7.3, and 7.4 and for the waste package barrier capability in Sections 7.3, 7.4, and Appendix B, Section B7.

8.2.2 Degradation of Engineered Barriers

The following acceptance criteria can be found in Section 2.2.1.3.1.3 of *Yucca Mountain Review Plan, Final Report* (NRC 2003 [DIRS 163274]).

Acceptance Criterion 1 – System Description and Model Integration are Adequate

> *(1) TSPA adequately incorporates important design features, physical phenomena and couplings and uses consistent assumptions throughout the degradation of engineered barriers abstraction process;*

The models and analyses addressed in this report accurately reflect the relevant waste package design features as discussed in Sections 6.3.4, 6.4.2, and 6.4.3 of the main body of the report and Appendix B in Sections B1, B6, B.6.1, B.6.2, and B.6.4, and the drip shield in Sections 1.1 and 6.3.7.

> *(2) Abstraction uses assumptions, technical bases, data and models that are appropriate and consistent with [those used] in other abstractions.*

Not applicable.

> *(3) The descriptions of the engineered barriers, design features, degradation processes, physical phenomena, and couplings that may affect the degradation of the engineered barriers are adequate.*

Throughout this report, detailed descriptions of the relevant design features (waste package in Section 6.4 and drip shield in Section 6.3.7), degradation processes (waste package and drip shield in Sections 1.1, 6.2, and 6.3), physical phenomena (Section 6.3.2 for the waste package and Section 6.3.7 for the drip shield), and couplings (Sections 1.1 and 6.3.7) that may affect the degradation of the engineered barriers are provided. These descriptions are consistent with the information delineated elsewhere in other reports and are adequate for their intended purposes (i.e., to enable the modelers to develop and implement appropriate models and to enable the reviewer to understand the bases for the analytical activities performed by the applicant and the results thereof.).

> *(4) Initial and boundary conditions are propagated consistently throughout the abstraction process.*

Throughout this report, relevant initial and boundary conditions for the performed analyses (i.e., waste package closure configuration, welding process, heat treatments, anticipated temperature, pressure) are used in a manner that is consistent with the data received from other abstractions and models. Examples can be found in Sections 6.3 and 6.4.

One FEP was identified related to the potential degradation of the waste package and drip shield. Section 6.6 indicates the waste package stress corrosion cracking FEP was included. Table 6-13 provides the location where an explanation related to these decisions is discussed.

(6) Guidance in NUREG 1297 and NUREG 1298 [re: Expert Elicitation] are followed.

Not applicable.

Acceptance Criterion 2 – Data Are Sufficient for Model Justification

(1) Parameters used to evaluate the SCC degradation of EBS are adequately justified;

The input data and parameters used for the performance of the waste package and drip shield stress corrosion cracking degradation models and model related parameters came, primarily, from four sources:

- Other analysis models performed for the Yucca Mountain Project
- Laboratory experiments and tests performed for the project
- Industry reviewed and accepted technical or scientific reports and papers
- Industry handbooks.

Justification for the use of specific parameters is typically provided in the section in which the parameter is initially discussed (Section 4.1), used (Sections 6.2 and 6.3) or in the source document for the specific parameter. As a result, the parameters used for the analysis have been adequately justified.

(2) Sufficient data have been collected to establish initial and boundary conditions;

Extensive scientific investigations and experiments have been performed to develop the data necessary to support the analyses provided in this report. In those instances where insufficient data was available for the specific materials used for the waste package or drip shield stress corrosion cracking degradation, data on alloys known to be analogous to those anticipated in the waste package were used with conservative assumptions to provide the basis for the performed analyses. Initial and boundary conditions have been adequately and appropriately established and justified.

(3) Data on the degradation of the engineered barriers (predominately stress corrosion cracking and to a lesser extent general corrosion and phase stability) are based on laboratory measurements, industrial and/or natural analogs and tests designed to replicate anticipated conditions. As appropriate, sensitivity or uncertainty analyses are provided and are shown to be adequate.

Data related to the various potential drip shield and waste package degradation modes (in particular for stress corrosion cracking and to a lesser extent for general corrosion and phase stability) are discussed in various subsections throughout this report. Specifically, the data associated with the drip shield is discussed in Sections 6.2.1 and 6.3.7 and with the waste package in Sections 6.2.1, 6.3.4, and Appendix B.

(4) Degradation models and related parameters for the applicable processes are adequate. For example, the SCC propagation model (SDFR Model), the threshold SCC initiation stress parameter and the threshold stress intensity factor parameter are described in significant detail. The SDFR Model is applied specifically to the waste package outer barrier material and the threshold SCC initiation stress criterion to both the waste package and the drip shield. Effects of general corrosion and phase stability on SCC are given appropriate consideration and treatment relative to their effect on SCC susceptibility.

The various stress corrosion cracking models (i.e., the SDFR model and the alternative CEF model) related to potential waste package stress corrosion cracking crack propagation are discussed in Section 6.3 and waste package and drip shield stress corrosion cracking crack initiation parameters are discussed in detail in various sections throughout this report. Specifically, the SCC approach associated with breaching of the drip shield is discussed in Sections 6.2.1 and 6.3.7, and the modeling of the waste package outer barrier stress corrosion cracking is discussed in Sections 6.2 and 6.3.

Acceptance Criterion 3 – Data Uncertainty is Characterized and Propagated Through The Model Abstraction

(1) Models use parameter values, assumed ranges, probability distributions and/or bounding assumptions that are technically defensible, reasonably account for uncertainties and variabilities, and do not result in under-representation of the risk estimate.

Each of the models and related SCC initiation and crack arrest criteria developed in this report uses parameter values, assumed ranges, probability distributions or bounding assumptions, or both, that are technically defensible, reasonably account for uncertainties and variabilities, and do not result in under-representation of the risk estimate. In each situation, discussion and consideration of the uncertainties associated with specific data are addressed in detail. Examples include the discussion of the range of expected residual stress variation, associated data and data uncertainty in Section 6.4.5, the development of the threshold stress intensity factor, associated data and data uncertainty is discussed in Section 6.3.5, and the modeling of the Alloy 22 stress corrosion cracking growth rate, associated data, and data uncertainty are addressed in Section 6.3.4.

(2) Appropriate parameters, based on techniques that may include laboratory experiments, field measurements, and industrial analogs are used.

The SDFR model, and related SCC initiation and crack arrest criteria addressed in this report use data and parameters that have been developed based on a variety of techniques including laboratory experiments, and industrial analogs. Examples of each category include:

- The use of iron and nickel–chromium-based industrial alloy crack growth rate data experimentally developed or compiled from the literature for the study of stress corrosion cracking propagation rates in water containing oxygen as a function of temperature in Section 6.3.4

- Review of the stress corrosion cracking crack patterns (morphology) in actual industrial equipment (i.e., light water reactors) (Appendix B, Section B.6.3)

- Experimental measurement of stress corrosion cracking initiation stress using constant load specimens, U-bend specimens and SSRT specimens in a range of brine environments (Section 6.2.1)

- Use of experimentally measured residual stress distributions resulting from laser peening stress mitigation process to benchmark calculated through-wall residual stress distribution conservatively expected in final closure lid weld region (Sections 6.4.4 and 6.4.5).

(3) Assumed range of values and probability distributions for parameters used in conceptual and process-level models are not likely to underestimate the actual degradation and failure of engineered barriers.

In those instances where uncertainties exist regarding the range of values and probability distributions, modelers were careful to choose values that were anticipated to either provide conservative results or to provide a distribution that bounds the expected range of values. Results of such calculated values were compared with values predicted by an alternative model or laboratory experiments, or both, to demonstrate the inherent conservatisms in the analyses. Examples include the comparison of the crack propagation SDFR model-predicted rates with experimentally independently measured rates (Section 7.4.2.3 and Table 7-4).

(4) Appropriate methods of NDE of fabricated-engineered barriers are used to assess the type, size and location of fabrication defects that may lead to premature failure of engineered barriers.

NDE performed to characterize welding flaws on waste package closure lid weld mockups were verified by destructive metallography and were used to assess the expected type, size and orientation of welding related fabrication defects that could lead to premature stress corrosion cracking related failure of the outer Alloy 22 waste package barrier (Section 6.2.2).

(5) Where sufficient data do not exist, the definition of parameter values and conceptual models is based on appropriate use of other sources, such as expert elicitation.

In most instances where sufficient data for the exact materials to be used in the repository and processes addressed in this section were not found to be available, data from analogous materials was either found to be or was made available. As a result, the use of expert elicitation in the development and implementation of the stress corrosion cracking related models was extremely limited as it was determined that the data and information that was available was adequate to support the required analyses. However, an independent technical review that involved expert elicitation was performed to verify the applicability and conservative nature of the seismic crack density model in Appendix B (Section B7.3).

Acceptance Criterion 4 – Model Uncertainty is Characterized and Propagated Through the Model Abstraction

(1) Alternative modeling approaches are considered and are consistent with available data and current scientific understanding.

An alternative modeling approach for the SDFR model that is consistent with available data and current scientific understanding was considered and evaluated.

The use of the Coupled Environmental Fracture (CEF) stress corrosion cracking propagation rate model was considered and model predictions were compared with available literature experimental data for stainless steel. The SDFR model selected was found to be conservative relative to CEF model (Sections 6.3.6 and 7.4.2.4).

A conservative threshold stress intensity factor parameter approach was developed for use since experimental measurement of this parameter was not feasible because of the high resistance of Alloy 22 to stress corrosion cracking propagation (Section 6.3.5).

An alternative seismic crack density model was evaluated for its prediction of stress corrosion cracking crack area density and found to be reasonably consistent with the base-case model in Appendix B (Sections B6.4.3 and B7.3).

(2) Consideration of conceptual model uncertainty is consistent with available site characterization data, laboratory experiments, and the treatment of uncertainty does not result in under-estimation of the risk estimate.

Consideration of uncertainties in the models used in this report is an integral part of the performed analyses. Conceptual model uncertainty is consistent with the information that has been developed from laboratory experiments. Care has been taken to ensure that the treatment of uncertainty does not result in under-estimation of the risk estimate. Examples of the treatment of such uncertainties are as follows:

- Treatment of residual stress and stress intensity factor uncertainty is described in Section 6.4.5.
- A conservative approach was used to determine the threshold stress for stress corrosion cracking initiation parameter for both Alloy 22 waste package outer barrier and the Titanium Grade 7 drip shield as described in Section 6.2.1.
- Treatment of uncertainty in the threshold stress intensity factor parameter is described in Section 6.3.5 and the range of values is listed in Table 6-6.

(3) Alternative modeling approaches, consistent with available data and current scientific understanding, are used and the modeling results are evaluated using tests that are sensitive to the processes modeled.

Wherever it was deemed appropriate (and accepted alternative models were known to exist), alternative modeling approaches, consistent with available data and current scientific

understanding, were considered. In all instances, it was determined that the base-case model provided a similar but more conservative result than would be achieved through the use of the alternative models. Thus, although due consideration was given to the use of alternative modeling approaches, no alternative models were used.

Acceptance Criterion 5 – Model Abstraction Output Is Supported By Objective Comparisons

(1) Models implemented in this report for input to total system performance assessment abstraction (provide results consistent with output from detailed process-level models and or empirical observations (laboratory and field testing, and/or natural analogs).

The results of model abstractions developed in this report are for use as input to WAPDEG and thus direct input for use in the total system performance assessment abstraction. Thus, AC 5-1 is not applicable.

(2) Numerical corrosion models used to calculate the lifetime of the engineered barriers are adequate representations, considering the associated uncertainties in long term behavior, range of conditions (including residual stresses) and the variability in fabrication processes.

The numerical stress corrosion models used to calculate the lifetime of the waste package are based on appropriate design considerations and are validated against laboratory results to ensure that they are adequate representations of the involved processes, considering the associated uncertainties in long term behavior, range of conditions (including residual stresses) and the variability in fabrication processes (Sections 6.2.2, 6.4.2.1, and 6.4.2.2).

(3) Evidence is sufficient to show that models will not underestimate the actual degradation and failure of engineered barriers.

In those instances where there was doubt about the appropriateness or accuracy of the models, related parameters or data, modelers were careful to select a conservative approach or conservative data that would result in an overestimation of risk rather than an underestimation (Sections 6.2.1, 6.3.5, 7.4.3, and 7.4.4). The results of analyses were compared against results obtained from laboratory tests or industrial experience to demonstrate the conservatism of the analytical methods. Examples of such instances are provided in Section 7.4.2.3.

(4) Mathematical degradation models are based on the same environmental parameters, material factors, assumptions and approximations shown to be appropriate for closely analogous applications.

Mathematical degradation models presented in this report are based on environmental parameters, material factors, assumptions and approximations that have been demonstrated to be appropriate for closely analogous applications. In those instances where it was determined that adequate data did not exist to support the modeling effort, data from testing of analogous materials was used. Examples of such instances can be found in Section 6.3.4.

(5) Accepted and well documented procedures are used to construct and test the numerical models that simulate the EB chemical environment and degradation of EBS;

The development and testing of the numerical models and related parameters used to simulate the repository environment and analyze the potential degradation of the engineered barrier components, including the drip shield and waste package, were performed in accordance with previously established well-documented Yucca Mountain project procedures that are based on industry established norms. These procedures also established the appropriate quality assurance requirements for such activities and appropriate checking, auditing and other activities were performed to ensure the adequacy and appropriateness of the models and data. Examples of such QA requirements and associated procedures can be found in Sections 2, 9.2, and Appendix B, Section B2, respectively.

(6) Sensitivity analyses or bounding analyses are provided to support the abstraction of the degradation of engineered barriers.

Bounding analyses associated with the abstraction of the stress and stress intensity factor through-wall gradients driving the stress corrosion cracking degradation of the waste package engineered barrier were performed and are documented herein. Examples of such activities can be found in Section 6.4.5.

In addition to the above, Acceptance Criterion 5 (Model Output is Supported by Objective Comparisons) is addressed in Tables 8-1, 8-2, and 8-3. Objective comparisons with experimental data and relevant literature are described for predicted-versus-measured Alloy 22 crack growth rates in Sections 6.3.5, 7.4.2.2, and 7.4.2.3.

The above Acceptance Criteria (3, 4, and 5) are also addressed by the waste package degradation analysis, which describes the abstracted stress corrosion cracking models and related parameters and the propagation of uncertainties in those models and parameters for the case of nonseismic related stress corrosion cracking. Acceptance Criteria 3 through 5 will also be addressed in the seismic consequence abstraction model report, which describes the abstracted stress corrosion cracking models and the propagation of uncertainties in those models for the case of seismic stress corrosion cracking.

8.3 SUMMARY OF OUTPUT

Output from Appendix B for the seismically induced crack area density distribution is provided in DTN: MO0403SPASCRKD.000.

Tables 8-1, 8-2, and 8-3 summarize stress corrosion cracking model report output data listed in DTN: LL030607012251.065 and associated output stress and stress intensity factor distribution plots are given in DTN: MO0310MWDWAPAN.002. These can be used as input for the WAPDEG with no restrictions if the waste package design, material, and environment are consistent with those considered in the reported modeling activities. The model uses 25-mm and 10-mm measurements (Section 6.4.2.1 and Table 8-1) for the outer and middle lids of the waste packages potentially subject to stress corrosion cracking. The current proposed increase in middle closure lid thickness to 12.7 mm has no significant effect on model predictions of the

time for stress corrosion cracking to initiate and propagate through the combination of both lids. The annealing process will eliminate weld-induced residual tensile stresses in the as-fabricated waste package Alloy 22 outer cylinder thus precluding stress corrosion cracking for this region of the waste package.

Stress profiles for radial stress and hoop stress versus depth are presented in look-up Table 8.2 and Table 8.3. For the laser-peened waste package outer lid, it is clear from Table 8-3 that the hoop stress and corresponding stress intensity factors (SIF) are the predominant stress and SIF components. As described in Section 6.4.4, the modeled depth of laser-peened compressive stress (-40 ksi) is conservatively taken as 1.5 mm. However, based on the hoop stress profile, Figure 6-28, the estimated depth to which the outer weld stress is below the threshold stress depth (depth to which it is less than 90% of yield strength (i.e., 257 MPa)) is about 4.6 mm for the mean value and about 3.8 mm for the upper uncertainy bound value. Thus over 10,000 years, using the conservative 150°C median general corrosion rate of 51.8 nm/yr (BSC 2004 [DIRS 169984], Section 8.1), the depth of metal removal is about 518 μm, which is about 11% of the mean depth of the stress mitigated layer. Using an upper-bound value of the general corrosion rate of 256 nm/yr (99.99th percentile rate at 150°C, (BSC 2004 [DIRS 169984], Section 8.1) the total penetration depth by general corrosion is about 2,560 μm, which is about 67% of the estimated maximum uncertainty-level depth of the stress mitigated layer. This bounding analysis demonstrates that the final closure lid weld stress mitigated layer is deep enough to extend the lifetime of the waste package well beyond 10,000 years.

Table 8-1. Summary of Output

Output Name	Output Value or Equation	Unit	Note
Yield strength (YS) for Alloy 22 from Table 4-5	372 at room temperature 338 at 366K 283 at 477 K	MPa	Linear between temperatures (Section 6.2.1)
Yield strength (YS) for Titanium Grade 7 from Table 4-5	275 to 450 at room temperature 138 to 152 at 477K	MPa	Same as above and use average at temperature
Threshold stress (Alloy 22)	0.9 (YS) (Section 6.2.1)	MPa	YS at 200°C (473K) for waste package
Threshold stress (Titanium Grade 7)	0.5 (YS) (Section 6.2.1)	MPa	YS at 140°C (413K) for drip shield
Initial size of incipient cracks	0.05 (Section 6.2.1)	mm	
Depth of plate to be included for embedded flaws	0.25 (Section 6.2.2.2)	Fraction of the plate thickness	
Oblique flaws to be added to radial flaws	0.005 [a)] (Section 6.2.2.3)	Fraction of the total flaws	
Mean of repassivation slope, Alloy 22 SDFR model	1.304 (Section 6.3.4)	Dimensionless	
Standard deviation of repassivation slope, Alloy 22 SDFR model	0.16 (Section 6.3.4)	Dimensionless	

Table 8-1. Summary of Output (Continued)

Output Name	Output Value or Equation	Unit	Note
Lower bound of repassivation slope, Alloy 22 SDFR model	0.984 (Section 6.3.4)	Dimensionless	
Upper bound of repassivation slope, Alloy 22 SDFR model	1.624 (Section 6.3.4)	Dimensionless	
Crack growth rate, V_t	$V_t = 7.8\times10^{-2} n^{3.6} \left(4.1\times10^{-14}\right)^n (K_I)^{4n}$ (Section 6.3.4, Equation 19), where KI is the SIF in MPa√m	mm/s	'n' is the repassivation slope
Mean general corrosion rate, V_{gc}, Alloy 22	7.23 (Section 6.3.5)	nm/y	
Threshold stress intensity factor, K_{ISCC}	$K_{ISCC} = (V_{gc} / \overline{A})^{1/\overline{n}}$ (Section 6.3.5, Equation 20), where $\overline{A} = 7.8\times10^{-2} n^{3.6} \left(4.1\times10^{-14}\right)^n$ (Section 6.3.4, Equation 18) and $\overline{n} = 4n$ (Section 6.3.3, Equation 16)	MPa√m	'n' is the repassivation slope Vgc in mm/s
Radial stress coefficient A_0, WPML, as-welded	181.636 (Section 6.4.2.4, Table 6-8)	MPa	
Radial stress coefficient A_1, WPML, as-welded	-177.592 (Section 6.4.2.4, Table 6-8)	MPa/mm	
Radial stress coefficient A_2, WPML, as-welded	23.385 (Section 6.4.2.4, Table 6-8)	MPa/mm^2	
Radial stress coefficient A_3, WPML, as-welded	-0.900 (Section 6.4.2.4, Table 6-8)	MPa/mm^3	
Hoop stress coefficient A_0, WPML, as-welded	219.908 (Section 6.4.2.4, Table 6-8)	MPa	
Hoop stress coefficient A_1, WPML, as-welded	56.494 (Section 6.4.2.4, Table 6-8)	MPa/mm	
Hoop stress coefficient A_2, WPML, as-welded	-20.848 (Section 6.4.2.4, Table 6-8)	MPa/mm^2	
Hoop stress coefficient A_3, WPML, as-welded	1.083 (Section 6.4.2.4, Table 6-8)	MPa/mm^3	
Radial stress coefficient A_0, WPOL, laser-peened	-265.920 (Section 6.4.4, Table 6-11)	MPa	
Radial stress coefficient A_1, WPOL, laser-peened	103.987 (Section 6.4.4, Table 6-11)	MPa/mm	
Radial stress coefficient A_2, WPOL, laser-peened	-9.857 (Section 6.4.4, Table 6-11)	MPa/m^2	
Radial stress coefficient A_3, WPOL, laser-peened	0.254 (Section 6.4.4, Table 6-11)	MPa/mm^3	
Hoop stress coefficient A_0, WPOL, laser-peened	-292.607 (Section 6.4.4, Table 6-11)	MPa	
Hoop stress coefficient A_1, WPOL, laser-peened	178.277 (Section 6.4.4, Table 6-11)	MPa/mm	

Table 8-1. Summary of Output (Continued)

Output Name	Output Value or Equation	Unit	Note
Hoop stress coefficient A_2, WPOL, laser-peened	-14.135 (Section 6.4.4, Table 6-11)	MPa/mm^2	
Hoop stress coefficient A_3, WPOL, laser-peened	0.320 (Section 6.4.4, Table 6-11)	MPa/mm^3	
Mean stress profile at θ=0, $S_0(x)$	$S0(x) = A_0 + A_1x + A_2x^2 + A_3x^3$ (Section 6.4.2.3, Equation 23)	MPa	x (in mm) is crack depth
$S_0(x)$, radial stress, WPML, as-welded	Table 8-2, 2nd column	MPa	Calculated from Equation 23
$S_0(x)$, hoop stress, WPML, as-welded	Table 8-2, 4th column	MPa	Calculated from Equation 23
SIF, $K_0(x)$, radial stress, WPML, as-welded	Table 8-2, 3rd column	MPa$\sqrt{m}$	
SIF, $K_0(x)$, hoop stress, WPML, as-welded	Table 8-2, 5th column	MPa$\sqrt{m}$	
$S_0(x)$, radial stress, WPOL, laser-peened	Table 8-3, 2nd column	MPa	Calculated from Equation 23
$S_0(x)$, hoop stress, WPOL, laser-peened	Table 8-3, 4th column	MPa	Calculated from Equation 23
SIF, $K_0(x)$, radial stress, WPOL, laser-peened	Table 8-3, 3rd column	MPa$\sqrt{m}$	
SIF, $K_0(x)$, hoop stress, WPOL, laser-peened	Table 8-3, 5th column	MPa$\sqrt{m}$	
WPOL thickness (h)	25 (Section 6.4.2.1, Figure 6-8)	mm	
WPML thickness (h)	10 (Section 6.4.2.1, Figure 6-8)	mm	
Stress variability, ∇S	17.236893 (Section 6.4.5)	MPa	
Stress profile, $S_\theta(x)$, at angle θ from $S_0(x)$	$S_\theta(x)= S_0(x) - \nabla S(1 - \cos(\theta))$ (Section 6.4.5, Equation 25a)	MPa	
SIF profile, $K_\theta(x)$, at angle θ from $K_0(x)$	$K_\theta(x)= K_0(x) (S_\theta(h) / S_0(h))$ (Section 6.4.5, Equation 25b)	MPa$\sqrt{m}$	
Variation amplitude of $S_0(x)$, ΔS	0.15 (YS) (Section 6.4.5; use YS value at the room temperature)	MPa	Uncertainty for ΔS is represented by a normal distribution truncated at ±3-sigma (±15% YS).
Lower bound of stress variation	$S_\theta(x)\min = S_\theta(x)\left(\frac{S_\theta(h)-\Delta S}{S_\theta(h)}\right)$ (Section 6.4.5, Equation 26a)	MPa	
Upper bound of stress variation	$S_\theta(x)\max = S_\theta(x)\left(\frac{S_\theta(h)+\Delta S}{S_\theta(h)}\right)$ (Section 6.4.5, Equation 26b)	MPa	

Table 8-1. Summary of Output (Continued)

Output Name	Output Value or Equation	Unit	Note
Lower bound of SIF variation	$K_\theta(x)\min = K_\theta(x)\left(\frac{S_\theta(h)-\Delta S}{S_\theta(h)}\right)$ (Section 6.4.5, Equation 26c)	MPa√m	
Upper bound of SIF variation	$K_\theta(x)\max = K_\theta(x)\left(\frac{S_\theta(h)+\Delta S}{S_\theta(h)}\right)$ (Section 6.4.5, Equation 26d)	MPa√m	

Output DTN: LL030607012251.065.

NOTE: [a] Note that a slightly more conservative value (0.8%) is recommended for this parameter in the *Analysis of Mechanisms for Early Waste Package/Drip Shield Failure* (BSC 2004 [DIRS 170024], Table 12).

Table 8-2. Stresses and Stress Intensity Factors for the As-Welded Waste Package Middle Lid

Depth (mm)	Radial stress (S_x) (MPa)	SIF due to S_x (MPa√m)	Hoop stress (S_z) (MPa)	SIF due to S_z (MPa√m)
0.1593	153.9288	4.9033	228.3849	7.5754
0.3203	127.1172	6.2685	235.9015	10.9665
0.4797	101.7315	6.8580	242.3296	13.7144
0.6407	77.2206	6.9761	247.8300	16.1330
0.8000	54.0676	6.7631	252.3158	18.3358
0.9593	31.9924	6.3044	255.8750	20.3775
1.1203	10.7596	5.8250	258.5570	22.3816
1.2797	-9.2150	5.2651	260.3330	24.3197
1.4407	-28.3699	4.6000	261.2667	26.1726
1.6000	-46.3322	3.8615	261.3655	27.9459
1.7593	-63.3265	3.0726	260.6697	29.6433
1.9203	-79.5368	2.2534	259.1863	31.2668
2.0797	-94.6509	1.4282	256.9724	32.8922
2.2407	-109.0061	0.5951	254.0088	34.5292
2.4000	-122.3284	-0.2400	250.3830	36.1060
2.5593	-134.7922	-1.0656	246.0945	37.6220
2.7203	-146.5363	-1.8707	241.1150	39.0762
2.8797	-157.3405	-2.6491	235.5736	40.4676
3.0407	-167.4522	-3.4047	229.3818	41.8264
3.2000	-176.6850	-4.1787	222.6938	43.2168
3.3593	-185.1690	-4.9390	215.4749	44.5479
3.5203	-193.0032	-5.6775	207.6685	45.8181
3.6797	-200.0480	-6.3965	199.4620	47.0265
3.8407	-206.4725	-7.0865	190.7114	48.1718
4.0000	-212.1664	-7.7528	181.6234	49.2531
4.1593	-217.2211	-8.2576	172.1366	50.3451
4.3203	-221.7016	-8.7427	162.1726	51.3729
4.4797	-225.5376	-9.2143	151.9633	52.3351

Table 8-2. Stresses and Stress Intensity Factors for the As-Welded Waste Package Middle Lid (Continued)

Depth (mm)	Radial stress (S_x) (MPa)	SIF due to S_x (MPa√m)	Hoop stress (S_z) (MPa)	SIF due to S_z (MPa√m)
4.6407	-228.8312	-9.6605	141.3230	53.2313
4.8000	-231.5367	-10.0894	130.4975	54.0602
4.9593	-233.7127	-10.4950	119.4050	54.8214
5.1203	-235.3959	-10.9446	107.9526	55.4811
5.2797	-236.5735	-11.4131	96.4029	56.0586
5.4407	-237.2926	-11.8636	84.5422	56.5637
5.6000	-237.5602	-12.3055	72.6415	56.9965
5.7593	-237.4080	-12.7309	60.6057	57.3567
5.9203	-236.8501	-13.1320	48.3342	57.6444
6.0797	-235.9201	-13.7114	36.1065	57.7587
6.2407	-234.6208	-14.4707	23.6946	57.6946
6.4000	-233.0011	-15.2333	11.3811	57.5522
6.5593	-231.0713	-15.9891	-0.9356	57.3322
6.7203	-228.8287	-16.7277	-13.3570	57.0353
6.8797	-226.3414	-17.4611	-25.6005	56.6626
7.0407	-223.5802	-18.4707	-37.8942	56.1419
7.2000	-220.6238	-20.3589	-49.9583	55.3276
7.3593	-217.4669	-22.2128	-61.8935	54.4422
7.5203	-214.0957	-24.0173	-73.7955	53.4878
7.6797	-210.6019	-25.7872	-85.3924	54.6294
7.8407	-206.9348	-27.4989	-96.8987	56.2191
8.0000	-203.1923	-29.1709	-108.0509	57.7865

Output DTN: LL030607012251.065; Section 6.4.2.4, Table 6-10.

Table 8-3. Stresses and Stress Intensity Factors for Laser-Peened Waste Package Outer Lid

Depth (mm)	Radial stress (S_x) (MPa)	SIF due to S_x (MPa√m)	Hoop stress (S_z) (MPa)	SIF due to S_z (MPa√m)
0.3988	-226.0035	-9.1866	-223.7417	-5.6943
0.8001	-188.9005	-11.7979	-158.8532	-6.4965
1.1989	-154.9833	-13.0189	-98.6408	-6.1528
1.6002	-123.7220	-13.4298	-42.2143	-5.1372
1.9990	-95.4153	-13.2965	9.8344	-3.6697
2.4003	-69.6047	-12.7780	58.2916	-1.8824
2.7991	-46.5198	-12.2958	102.6663	0.1212
3.2004	-25.7687	-11.7214	143.6471	2.2821
3.5992	-7.5170	-11.0116	180.8374	4.5533
3.9980	8.4709	-10.2080	214.6297	6.8939
4.3993	22.3728	-9.3437	245.3299	9.2702
4.7981	34.1098	-8.4525	272.6715	11.6543
5.1994	43.9293	-7.6096	297.1262	14.0165
5.5982	51.8041	-6.8298	318.5068	16.3364

Table 8-3. Stresses and Stress Intensity Factors for Laser-Peened Waste Package Outer Lid (Continued)

Depth (mm)	Radial stress (S_x) (MPa)	SIF due to S_x (MPa$\sqrt{m}$)	Hoop stress (S_z) (MPa)	SIF due to S_z (MPa$\sqrt{m}$)
5.9995	57.9323	-6.0675	337.2088	18.6024
6.3983	62.3334	-5.3416	353.1178	20.8003
6.7970	65.1483	-4.6612	366.4827	22.9177
7.1984	66.4775	-4.0331	377.4871	24.9441
7.5971	66.4012	-3.4507	386.1141	26.9023
7.9985	65.0162	-2.8535	392.5969	28.8612
8.3972	62.4372	-2.2745	396.9757	30.7287
8.7986	58.7292	-1.7170	399.4297	32.5008
9.1973	54.0361	-1.1860	400.0499	34.1745
9.5987	48.3961	-0.6829	398.9677	35.7479
9.9974	41.9777	-0.2101	396.3190	37.2200
10.3962	34.8443	-0.3513	392.2239	38.4530
10.7975	27.0415	-0.5163	386.7654	39.5674
11.1963	18.7651	-0.7070	380.1350	40.5636
11.5976	10.0075	-0.9242	372.3715	41.4432
11.9964	0.9766	-1.1690	363.6954	42.2086
12.3977	-8.3447	-1.4403	354.1195	42.8627
12.7965	-17.7414	-1.7949	343.8874	43.4439
13.1978	-27.2353	-2.1728	332.9919	43.9342
13.5966	-36.6092	-2.5554	321.6934	44.3269
13.9954	-45.8267	-2.9438	310.0462	44.6272
14.3967	-54.8472	-3.3378	298.0958	44.8409
14.7955	-63.4595	-3.7396	286.1158	44.9743
15.1968	-71.6755	-4.0160	274.0769	45.0329
15.5956	-79.2941	-4.1354	262.2538	45.0208
15.9969	-86.3145	-4.2182	250.6192	44.9464
16.3957	-92.5507	-4.2696	239.4426	44.8182
16.7945	-97.9528	-4.2904	228.7710	44.6449
17.1958	-102.4495	-4.2805	218.6644	44.4361
17.5946	-105.8869	-4.3087	209.3730	44.2112
17.9959	-108.2109	-4.5204	200.9017	43.9968
18.3947	-109.2950	-4.7313	193.4801	43.7750
18.7960	-109.0551	-4.9400	187.1369	43.5578
19.1948	-107.3973	-5.1487	182.0747	43.3569
19.5961	-104.2024	-5.3536	178.3522	43.1853
19.9949	-99.4140	-5.5551	176.1390	43.0560

Output DTN: LL030607012251.065; Section 6.4.4, Table 6-12.

9. INPUTS AND REFERENCES

9.1 DOCUMENTS CITED

166965 Andresen, P.L. 1991. "Fracture Mechanics Data and Modeling of Environmental Cracking of Nickel-Base Alloys in High Temperature Water." *Corrosion 91, The NACE Annual Conference and Corrosion Show, March 11-15, 1991, Cincinnati, Ohio. Paper No. 44,* Houston, Texas: National Association of Corrosion Engineers. TIC: 255507.

166966 Andresen, P.L. 1993. "Effects of Temperature on Crack Growth Rate in Sensitized Type 304 Stainless Steel and Alloy 600." *Corrosion, 49,* (9), 714-725. [Houston, Texas]: NACE International. TIC: 255500.

162528 Andresen, P.L. and Ford, F.P. 1985. "Modeling and Life Prediction of Stress Corrosion Cracking in Sensitized Stainless Steel in High-Temperature Water." *Predictive Capabilities in Environmentally Assisted Cracking, Presented at the Winter Annual Meeting of the American Society of Mechanical Engineers, Miami Beach, Florida, November 17-22, 1985.* Rungta, R., ed. PVP-Vol. 99. Pages 17-38. New York, New York: American Society of Mechanical Engineers. TIC: 254383.

118581 Andresen, P.L. and Ford, F.P. 1994. "Fundamental Modeling of Environment Cracking for Improved Design and Lifetime Evaluation in BWRs." *International Journal of Pressure Vessels and Piping, 59 (1-3),* 61-70. [New York, New York]: Elsevier Science. TIC: 247388.

167762 Andresen, P.L.; Angeliu, T.M.; Young, L.M.; Catlin, W.R.; and Horn, R.M. 2002. "Mechanisms and Kinetics of SCC in Stainless Steels." *Tenth International Conference on Environmental Degradation of Materials in Nuclear Power Systems–Water Reactors, August 5 to 9, 2001, Lake Tahoe, Nevada.* Houston, Texas: NACE International. TIC: 252999.

166967 Andresen, P.L., Young, L.M., Emigh, P.W., and Horn, R.M. 2002. "Stress Corrosion Crack Growth Rate Behavior of Ni alloys 182 and 600 in High Temperature Water." Paper No. 02510, Corrosion 2002, NACE, March 2002. TIC: 255502.

103753 ASM International. 1987. *Corrosion*. Volume 13 of Metals Handbook. 9th Edition. Metals Park, Ohio: ASM International. TIC: 209807.

162446 ASME (American Society of Mechanical Engineers) 1969. *Criteria of the ASME Boiler and Pressure Vessel Code for Design by Analysis in Section III and VIII, Division 2*. The American Society of Mechanical Engineers. 1969, Library of Congress Catalog Card Number 56-3934. TIC: 254727.

164859 Averbach, B.L. 1968. "Microcrack Formation." Section III of Chapter 7 of *Fracture, An Advanced Treatise*. Liebowitz, H., ed. Pages 449-455. New York, New York: Academic Press. TIC: 254807.

154496 Barkatt, A. and Gorman, J.A. 2000. *Tests to Explore Specific Aspects of the Corrosion Resistance of C-22*. Presentation to the Nuclear Waste Technical Review Board on August 1, 2000, Carson City, Nevada. [Washington, D.C.]: Catholic University of America. TIC: 249714.

164860 Bernstein, M.D. 1988. "Design Criteria for Boilers and Pressure Vessels in the U.S.A.." *Journal of Pressure Vessel Technology, 110,* 430-443. [New York, New York: American Society of Mechanical Engineers]. TIC: 254806.

162429 Bokhari, S.A. 2003. "Approved Baseline Change Proposal (BCP) YMP-2003-005, Design Changes to Site Recommendation (SR) Waste Package." Memorandum from S.A. Bokhari (DOE) to W.J. Arthur, III (OCRWM/CCB), R.A. Milner (OCRWM/CCB), and R.D. Brown (OCRWM/CCB), January 30, 2003, with attachments. ACC: MOL.20030508.0040.

151988 Bradford, S.A. 1987. "Fundamentals of Corrosion in Gases." In *Corrosion,* Volume 13, pp. 61-76 of *Metals Handbook.* 9th Edition. Metals Park, Ohio: ASM International. TIC: 209807.

156807 BSC 2001. *Plugging of Stress Corrosion Cracks by Precipitates*. CAL-EBS-MD-000017 REV 00. Las Vegas, Nevada: Bechtel SAIC Company. ACC: MOL.20011010.0168.

158966 BSC 2002. *The Enhanced Plan for Features, Events, and Processes (FEPs) at Yucca Mountain.* TDR-WIS-PA-000005 REV 00. Las Vegas, Nevada: Bechtel SAIC Company. ACC: MOL.20020417.0385.

170710 BSC 2004. *21-PWR Waste Package Configuration*. 000-MW0-DSU0-00403-000-00D. Las Vegas, Nevada: Bechtel SAIC Company. ACC: ENG.20040708.0005.

171924 BSC 2004. *Aging and Phase Stability of Waste Package Outer Barrier.* ANL-EBS-MD-000002 REV 02. Las Vegas, Nevada: Bechtel SAIC Company. ACC: DOC.20041005.0003.

170024 BSC 2004. *Analysis of Mechanisms for Early Waste Package/Drip Shield Failure.* CAL-EBS-MD-000030 REV 00C. Las Vegas, Nevada: Bechtel SAIC Company. ACC: DOC.20040913.0006.

169766 BSC 2004. *Commercial SNF Waste Package Design Report.* 000-00C-DSU0-02800-000-00B. Las Vegas, Nevada: Bechtel SAIC Company. ACC: ENG.20040709.0001

166879 BSC 2004. *Drip Shield and Waste Package Emplacement Pallet Design Report.* 000-00C-SSE0-00100-000-00A. Las Vegas, Nevada: Bechtel SAIC Company. ACC: ENG.20040225.0016.

169997 BSC (Bechtel SAIC Company) 2004. *FEPs Screening of Processes and Issues in Drip Shield and Waste Package Degradation.* ANL-EBS-PA-000002, Rev. 03. Las Vegas, Nevada: Bechtel SAIC Company. ACC: DOC.20041012.0004.

169845 BSC 2004. *General Corrosion and Localized Corrosion of the Drip Shield.* ANL-EBS-MD-000004 REV 02. Las Vegas, Nevada: Bechtel SAIC Company. ACC: DOC.20040921.0002.

169984 BSC 2004. *General Corrosion and Localized Corrosion of Waste Package Outer Barrier.* ANL-EBS-MD-000003 REV 02. Las Vegas, Nevada: Bechtel SAIC Company. ACC: DOC.20041004.0001.

169565 BSC 2004. *Multiscale Thermohydrologic Model.* ANL-EBS-MD-000049 Rev. 02. Las Vegas, NV: Bechtel SAIC Company.

168361 BSC 2004. *Q-List.* 000-30R-MGR0-00500-000-000 REV 00. Las Vegas, Nevada: Bechtel SAIC Company. ACC: ENG.20040721.0007

170992 BSC 2004. *Safety Classification of SSCs and Barriers.* 000-00C-MGR0-01000-000-00A. Las Vegas, Nevada: Bechtel SAIC Company. ACC: ENG.20040721.0005.

171583 BSC 2004. *Technical Work Plan For: Regulatory Integration Modeling and Analysis of the Waste Form and Waste Package*. TWP-WIS-MD-000009 REV 00 ICN 01. Las Vegas, Nevada: Bechtel SAIC Company. ACC: DOC.20040910.0001.

118597 Buchalet, C.B. and Bamford, W.H. 1976. "Stress Intensity Factor Solutions for Continuous Surface Flaws in Reactor Pressure Vessels." *Mechanics of Crack Growth, Proceedings of the Eighth National Symposium on Fracture Mechanics, Providence, Rhode Island, 26-28 August 1974.* ASTM Special Technical Publication 590. Pages 385-402. Philadelphia, Pennsylvania: American Society for Testing Materials. TIC: 247548.

147968 Chan, S.K.; Tuba, I.S.; and Wilson, W.K. 1970. "On Finite Element Method in Linear Fracture Mechanics." *Engineering Fracture Mechanics,* 1-17. Oxford, United Kingdom: Pergamon Press. TIC: 247507.

165441 Chen, H.-L.; Evans, K.J.; Hackel, L.A.; Rankin, J.E.; Yamamoto, R.M.; Demma, A.G.; Dewald, A.T.; Lee, M.J.; and Hill, M.R. 2002. *Mitigation of Tensile Weld Stresses in Alloy 22 Using Laser Peening.* UCRL-ID-151055. Livermore, California: Lawrence Livermore National Laboratory. ACC: MOL.20030911.0252.

148469 Connor, L.P., ed. 1991. *Welding Technology.* Volume 1 of *Welding Handbook.* 8th Edition. Pages 32-35 and 66-69. Miami, Florida: American Welding Society. TIC: 247231.

105212 Cowan, J.C. and Weintritt, D.J. 1976. *Water-Formed Scale Deposits.* Houston, Texas: Gulf Publishing Company. TIC: 245620.

124950 CRWMS M&O 1996. *Waste Package Closure Weld Development Report.* BBA000000-01717-2500-00006 REV 00. Las Vegas, Nevada: CRWMS M&O. ACC: MOL.19960909.0188.

107722 CRWMS M&O 1998. *Waste Package Phase II Closure Methods Report.* BBA000000-01717-5705-00016 REV 00. Las Vegas, Nevada: CRWMS M&O. ACC: MOL.19981208.0099.

171539 DOE (U.S. Department of Energy) 2004. *Quality Assurance Requirements and Description*. DOE/RW-0333P, Rev. 16. Washington, D.C.: U.S. Department of Energy, Office of Civilian Radioactive Waste Management. ACC: DOC.20040907.0002.

154481 Dunn, D.S.; Pan, Y-M.; and Cragnolino, G.A. 1999. *Effects of Environmental Factors on the Aqueous Corrosion of High-Level Radioactive Waste Containers—Experimental Results and Models.* CNWRA 99-004. San Antonio, Texas: Center for Nuclear Waste Regulatory Analyses. TIC: 246615.

167274 Estill, J.C.; King, K.J.; Fix, D.V.; Spurlock, D.G.; Hust, G.A.; Gordon, S.R.; McCright, R.D.; and Rebak, R.B. 2002. "Susceptibility of Alloy 22 to Environmentally Assisted Cracking in Yucca Mountain Relevant Environments." Corrosion/2002, [57th Annual Conference & Exposition, April 7-11, 2002, Denver, Colorado]. Paper No. 02535. Houston, Texas: NACE International. TIC: 252066.

118602 Ewalds, H.L. and Wanhill, R.J.H. 1984. *Fracture Mechanics.* New York, New York: Edward Arnold. TIC: 247389.

162700 Fix, D.V.; Estill, J.C.; Hust, G.A.; King, K.J.; Day, S.D.; and Rebak, R.B. 2003. "Influence of Environmental Variables on the Susceptibility of Alloy 22 to Environmentally Assisted Cracking." *Corrosion/2003, [58th Annual Conference & Exposition, March 16-20, 2003, San Diego, California]. Paper No. 03542,* [Houston, Texas]: NACE International. TIC: 254387.

169321 Fix, D.V.; Estill, J.C.; Wong, L.L.; and Rebak, R.B. 2004. "Susceptibility of Welded and Non-Welded Titanium Alloys to Environmentally Assisted Cracking in Simulated Concentrated Ground Waters." *Corrosion/2004, 59th Annual Conference & Exposition, March 28-April 1, 2004, New Orleans.* Paper No. 04551. Houston, Texas: NACE International. TIC: 255943.

167203 Ford, F.P. 1996. "Quantitative Prediction of Environmentally Assisted Cracking." *Corrosion Science, 52,* (5), 375-395. [Houston, Texas]: NACE International. TIC: 255526.

118611 Ford, F.P. and Andresen, P.L. 1988. "Development and Use of a Predictive Model of Crack Propagation in 304/316L, A533B/A508 and Inconel 600/182 Alloys in 288°C Water." *Environmental Degradation of Materials in Nuclear Power Systems—Water Reactors, [Proceedings of the Third International Symposium, Traverse City,*

Michigan, August 30-September 3, 1987]. Theus, G.J. and Weeks, J.R., eds. Pages 789 - 800. [Warrendale, Pennsylvania: Metallurgical Society]. TIC: 247505.

167027 Gordon, B. 2004. "Effect of Stacking Fault Energy on the Modeling of Stress Corrosion Cracking in Alloy 22, SIR-04-009, Rev. 0." Letter from B. Gordon (Structural Integrity Associates) to G.M. Gordon (BSC), January 26, 2004, with attachment. ACC: MOL.20040301.0287.

168053 Harris, D.O.; Dedhia, D.D.; and Lu, S.C. 1992. *Theoretical and User's Manual for pc–PRAISE, a Probabilistic Fracture Mechanics Computer Code for Piping Reliability Analysis.* NUREG/CR-5864. Washington, D.C.: U.S. Nuclear Regulatory Commission. ACC: MOL.20040310.0038

118624 Harris, D.O.; Lim, E.Y.; and Dedhia, D.D. 1981. *Probabilistic Fracture Mechanics Analysis.* Volume 5 of *Probability of Pipe Fracture in the Primary Coolant Loop of a PWR Plant.* NUREG/CR-2189. Washington, D.C.: U.S. Nuclear Regulatory Commission. TIC: 247333.

147757 Hornbach, D.J. 1999. *X-Ray Diffraction and Ring-Core Determination of the Residual Stress Distributions in One(1) Alloy C22 Welded Plate and One (1) Alloy C22 Test Bar.* 1034-8520. Cincinnati, Ohio: Lambda Research. TIC: 247252.

118672 Jones, R.H. and Ricker, R.E. 1987. "Stress-Corrosion Cracking." *Metals Handbook Ninth Edition.* Volume 13. Corrosion. 145-163. Metals Park, Ohio: ASM International. TIC: 209807.

170981 King, K.J.; Wong, L.L.; Estill, J.C.; and Rebak, R.B. 2004. "Slow Strain Rate Testing of Alloy 22 in Simulated Concentrated Ground Waters." *Corrosion/2004, 59th Annual Conference & Exposition, March 28-April 1, 2004, New Orleans*. Paper No. 04548. Houston, Texas: NACE International. TIC: 255943.

149957 Lu, J., ed. 1996. *Handbook of Measurement of Residual Stresses*. Lilburn, Georgia: Fairmont Press. TIC: 247903.

161780 Lundin, C.D. 2002. "Re: Welding Process Considerations for Waste Package Fabrication." Letter from C.D. Lundin to J.A. Cogar (BSC), September 11, 2002, with attachment. ACC: MOL.20021015.0209.

162702 Macdonald, D.D. and Urquidi-Macdonald, M. 1991. "A Coupled Environment Model for Stress Corrosion Cracking in Sensitized Type 304 Stainless Steel in LWR Environments." *Corrosion Science*, *32*, (1), 51-81. New York, New York: Pergamon Press. TIC: 254386.

162701 Macdonald, D.D.; Urquidi-Macdonald, M.; and Lu, Pai-Chuan 1994. "The Coupled Environmental Fractural Model - A Deterministic Method for Calculating Crack Growth Rates." *Corrosion 94*. Paper No. 246, Houston, Texas: NACE International. TIC: 254388.

147981 Mohr, W.C. 1996. "Internal Surface Residual Stresses in Girth Butt-Welded Steel Pipes." *Residual Stresses in Design, Fabrication, Assessment and Repair, PVP-Vol. 321,* 37-44. New York, New York: American Society of Mechanical Engineers. TIC: 247502.

163274 NRC (U.S. Nuclear Regulatory Commission) 2003. *Yucca Mountain Review Plan, Final Report.* NUREG-1804, Rev. 2. Washington, D.C.: U.S. Nuclear Regulatory Commission, Office of Nuclear Material Safety and Safeguards. TIC: 254568.

165536 Pan, Y.-M.; Brossia, C.S.; Cragnolino, G.A.; Dunn, D.S.; Gute, G.D.; and Yang, L. 2002. *Stress Corrosion Cracking and Hydrogen Embrittlement of Container and Drip Shield Materials.* CNWRA 2003-02. San Antonio, Texas: Center for Nuclear Waste Regulatory Analyses. TIC: 254055

149968 Pasupathi, V. 2000. "Documentation of Literature on Residual Stress Measurements." Interoffice correspondence from V. Pasupathi (CRWMS M&O) to G.M. Gordon, May 19, 2000, LV.WP.VP.05/00-070, with enclosures. ACC: MOL.20000522.0146.

166944 Pensado, O.; Dunn, D.S.; Cragnolino, G.A.; and Jain, V. 2002. *Passive Dissolution of Container Materials—Modeling and Experiments.* CNWRA 2003-01. San Antonio, Texas: Center for Nuclear Waste Regulatory Analyses. TIC: 254056.

147983 Rice, J.R. 1968. "A Path Independent Integral and the Approximate Analysis of Strain Concentration by Notches and Cracks." *Journal of Applied Mechanics, Transactions of the SME, 35,* 379-386. New York, New York: American Society of Mechanical Engineers. TIC: 247487.

118696 Roy, A.K.; Fleming, D.L.; Freeman, D.C.; and Lum, B.Y. 1998. *Stress Corrosion Cracking of Alloy C-22 and Ti GR-12 Using Double-Cantilever-Beam Technique.* UCRL-JC-132145. Livermore, California: Lawrence Livermore National Laboratory. ACC: MOL.19990420.0114.

149953 Shcherbinskii, V.G. and Myakishev, V.M. 1970. "Statistical Distribution of Welding Defects with Respect to Azimuth." *Central Scientific-Research Institute of Technical Engineering. Translated from Defektoskopiya, No. 4., UDC 620.179.16,*143-144. New York, New York: Plenum Publishing Corporation. TIC: 247890.

162457 SI (Structural Integrity Associates), Inc. 2003. *Evaluation of the CRM-21 PWR and Viability Availability Waste Package*. Report No. SIR-99-094. Revision 1. Prepared for Bechtel SAIC Company, Las Vegas, Nevada, by Structural Integrity Associates, Inc., San Jose, California. March 2003. ACC: MOL.20030327.0004.

163114 Smith, D. 2003. *Weld Flaw Evaluation and Nondestructive Examination Process Comparison Results for High-Level Radioactive Waste Disposal Container Manufacturing Program.* TDR-EBS-ND-000007 REV 01. Las Vegas, Nevada: Bechtel SAIC Company. ACC: ENG.20030515.0003.

118702 Sprowls, D.O. 1987. "Evaluation of Stress-Corrosion Cracking." *Metals Handbook Ninth Edition.* Volume 13. Corrosion. 245-282. Metals Park, Ohio: ASM International. TIC: 209807.

161933 Structural Integrity Associates. 2002. *Structural Integrity Associates Support of Waste Package Design for Year 2001*. SIR-02-073. San Jose, California: Structural Integrity associates. ACC: MOL.20020709.0389.

167756 Tada, H.; Paris, P.C.; and Irwin, G.R. 2000. *The Stress Analysis of Cracks Handbook*. 3rd. New York, New York: American Society of Mechanical Engineers. TIC: 255547.

122064 Timoshenko, S. and Goodier, J.N. 1951. *Theory of Elasticity.* 2nd Edition. New York, New York: McGraw-Hill. TIC: 224221.

9.2 CODES, STANDARDS, REGULATIONS, AND PROCEDURES

100497 ASTM B 575-94. 1994. *Standard Specification for Low-Carbon Nickel-Molybdenum-Chromium and Low-Carbon Nickel-Chromium-Molybdenum Steel Alloy Plate, Sheet, and Strip*. Philadelphia, Pennsylvania: American Society for Testing and Materials. TIC: 237683.

137688 ASTM G 30-94. 1994. *Standard Practice for Making and Using U-Bend Stress-Corrosion Test Specimens*. Philadelphia, Pennsylvania: American Society for Testing and Materials. TIC: 246890.

117480 ASTM E 399-90 (Reapproved 1997). 1991. *Standard Test Method for Plane-Strain Fracture Toughness of Metallic Materials*. West Conshohocken, Pennsylvania: American Society for Testing and Materials. TIC: 246299.

171563 ASTM G 129-00. 2000. *Standard Practice for Slow Strain Rate Testing to Evaluate the Susceptibility of Metallic Materials to Environmentally Assisted Cracking*. West Conshohocken, Pennsylvania: American Society for Testing and Materials. TIC: 256501.

171562 ASTM G 49-85 (Reapproved 2000). 2000. *Standard Practice for Preparation and Use of Direct Tension Stress-Corrosion Test Specimens*. West Conshohocken, Pennsylvania: American Society for Testing and Materials. TIC: 249897.

156605 10 CFR 63. Energy: Disposal of High-Level Radioactive Wastes in a Geologic Repository at Yucca Mountain, Nevada. Readily available.

AP-2.22Q, Rev. 1, ICN 1. *Classification Analyses and Maintenance of the Q-List.* Washington, D.C.: U.S. Department of Energy, Office of Civilian Radioactive Waste Management. ACC: DOC.20040714.0002.

AP-2.27Q, Rev. 1, ICN 4. *Planning for Science Activities.* Washington, D.C.: U.S. Department of Energy, Office of Civilian Radioactive Waste Management. ACC: DOC.20040610.0006.

AP-3.15Q, Rev. 4, ICN 5. *Managing Technical Product Inputs.* Washington, D.C.: U.S. Department of Energy, Office of Civilian Radioactive Waste Management. ACC: DOC.20040812.0004.

AP-SIII.10Q, Rev. 2, ICN 7. *Models.* Washington, D.C.: U.S. Department of Energy, Office of Civilian Radioactive Waste Management. ACC: DOC.20040920.0002.

AP-SV.1Q, Rev. 1, ICN 1. *Control of the Electronic Management of Information.* Washington, D.C.: U.S. Department of Energy, Office of Civilian Radioactive Waste Management. ACC: DOC.20040308.0001.

LP-SI.11Q-BSC, Rev. 0, ICN 1. *Software Management*. Washington, D.C.: U.S. Department of Energy, Office of Civilian Radioactive Waste Management. ACC: DOC.20041005.0008.

9.3 SOURCE DATA, LISTED BY DATA TRACKING NUMBER

148895 LL000316205924.142. Stress Corrosion Cracking of the Drip Shield, the Waste Package Outer Barrier and the Stainless Steel Structural Material. Submittal date: 03/22/2000.

148482 LL000320005924.145. Corrosion Cracking of the Drip Shield, the Waste Package Outer Barrier and the Stainless Steel Structural Material. Submittal date: 03/22/2000.

161253 LL021105312251.023. Stress Corrosion Crack Growth and Initiation Measurements for C-22 and Ti-7, General Electric Global Research Center (GEGRC) 121202. Submittal date: 01/08/2003.

166971 LL030300612251.035. Reversing DC Test Generated Fatigue Crack Growth Data. Submittal Date: 07/09/2003.

163712 LL030412512251.057. LTCTF Corrosion Rate Calculations for Five-Year Exposed Alloy C22 Specimens Cleaned Under TIP-CM-51. Submittal date: 05/28/2003.

148850 MO0003RIB00071.000. Physical and Chemical Characteristics of Alloy 22. Submittal date: 03/13/2000.

152926 MO0003RIB00073.000. Physical and Chemical Characteristics of Ti Grades 7 and 16. Submittal date: 03/13/2000.

165147 MO0301SPAXRA52.001. X-Ray Diffraction and Ring Core Determination of the Subsurface Residual Stress Distributions in Two Alloy 22 Welded Plates. Submittal date: 01/30/2003.

167911 MO0402GEA22SCC.000. Alloy 22 Stress Corrosion Crack Growth Rate Data in 288°C Water. Submittal Date: 02/25/2004.

170760 MO0407SEPFEPLA.000. LA FEP List. Submittal date: 07/20/2004

171564 MO0409GE835924.000. Stress Corrosion Crack Initiation & Growth Measurements for C-22 and Ti-7 in Environments Relevant to High Level Nuclear Waste Packages. Submittal date: 09/09/2004.

171792 MO0409GGSIACAL.000. Structural Integrity Associates Calculation Files 2004. Submittal date: 09/22/2004

9.4 OUTPUT DATA, LISTED BY DATA TRACKING NUMBER

LL030607012251.065. Output of Stress Corrosion Cracking AMR ANL-EBS-MD-000005 REV. 01 ICN 00. Submittal date: 06/20/2003.

MO0310MWDWAPAN.002. WAPDEG Analysis of Waste Package and Drip Shield Degradation. Submittal date: 10/16/2003.

MO0403SPASCRKD.000. Seismic Crack Density Model Outputs For LA. Submittal date: 03/09/2004.

INTENTIONALLY LEFT BLANK

A. DATA QUALIFICATION PLAN

BSC	DATA QUALIFICATION PLAN	QA: QA Page 1 of 1

Section I. Organizational Information

Qualification Title

Qualification of Incipient Crack Size

Requesting Organization

Waste package Modeling and Materials

Section II. Process Planning Requirements

1. List of Unqualified Data to be Evaluated

1. Incipient crack size for use with the stress corrosion cracking model

2. Type of Data Qualification Method(s) [Including rationale for selection of method(s) (Attachment 3) and qualification attributes (Attachment 4)]

Technical Assessment.

This method was chosen because determination that confidence in the data acquisition or devlopmental results is warranted and confirmation that the data have been used in similar applications.

3. Data Qualification Team and Additional Support Staff Required

Chairperson: Stephen Lu
Team member: Gerald Gordon

4. Data Evaluation Criteria

One or more of the following criteria will be used:

1. Prior use of the data
2. Qualification of personnel or organizations generating the data
3. Reliability of the data source
4. Extent to which data demonstrate properties of interest.
5. Availability of corroborating data

5. Identification of Procedures Used

Section III. Approval

Qualification Chairperson Printed Name	Qualification Chairperson Signature	Date
Stephen Lu	Stephen Lu	3/4/04
Responsible Manager Printed Name	Responsible Manager Signature	Date
Curtis Clower	for C C	3/9/04

AP-SIII.2Q PA_ASIII2-1 (Rev. 01/29/2004)

INTENTIONALLY LEFT BLANK

B. SEISMIC CRACK DENSITY MODEL

B1. PURPOSE

As directed by the technical work plan (BSC 2004 [DIRS 171583]), an abstraction model (the seismic crack density model (SCDM)) for the crack area density (crack area per unit seismically damaged area) of waste packages subjected to seismic activity has been developed. This activity was conducted by the Performance Assessment/Confirmation Project (PACP) Waste Package Modeling Department (WPMD). This activity provided the PACP with estimates of crack area density (crack area per unit seismically damaged area). This abstraction model provides information to address requirements of *Yucca Mountain Review Plan, Final Report* (NRC 2003 [DIRS 163274]).

Seismic activity can lead the waste packages to impact other components in the drift including the emplacment pallets, drip shields, and other waste packages. If the seismically induced impacts are of sufficient magnitude, the impacts could physically dent the waste package outer barrier and potentially the waste package inner vessel. These deformations could cause cold work of the waste package barrier and vessel materials, producing a cold-worked gradient typically highest on the outer surface and smallest on the inner surface. Impacts could also create complex through-wall residual stress profiles. These stress profiles and cold-work gradients may lead to stress corrosion cracking in the seismically affected area of the waste packages.

Similar damage can be expected for drip shields under seismic loadings. However, as in the treatment of stress corrosion cracking due to rockfalls discussed in the main body of this report (Section 6.3.7), stress corrosion cracks in the drip shields are expected to be tight and plugged with corrosion products or mineral deposits, or both, leading to negligible water flow through these openings. However, even if advective or diffusive flow-through stress corrosion cracking were to occur, any resulting under drip shield seepage would be unlikely to align with any through-wall stress corrosion cracking present in the waste package Alloy 22 barrier.

This Appendix B evaluation addresses the potential for stress corrosion cracking that could occur in the waste package as a result of stresses and cold work generated by an unlikely seismic event. After initiation of stress corrosion cracking, it may provide a path for subsequent radionuclide release from the waste package but, similar to the drip shield case, aqueous transport and radionuclide release through stress corrosion cracking induced crack areas in the waste package is likely to be negligible due to plugging by corrosion products or mineral deposits, or both. However, conservatively, no credit is taken in TSPA-LA for the crack-plugging phenomenon in the waste package case.

The crack area density (crack area per unit seismically damaged area) determined in this Appendix is used as a scaling factor applied to the total seismic damaged area (determined in *Seismic Consequence Abstraction* (BSC 2004 [DIRS 169183])) to obtain the total area of the crack network through which radionuclide transport could occur. It is expected that the crack area density will serve as input to *Seismic Consequence Abstraction* (BSC 2004 [DIRS 169183]). This model should be used only as input to *Seismic Consequence Abstraction* (BSC 2004

[DIRS 169183]), and not for generic analyses of stress corrosion crack densities or morphologies under other loadings or for other applications.

B2. QUALITY ASSURANCE

The quality assurance (QA) program applies to the development of this technical product. *Technical Work Plan for: Regulatory Integration Modeling and Analysis of the Waste Form and Waste Package* (BSC 2004 [DIRS 171583]) determined that this activity is subject to *Quality Assurance Requirements and Description* (DOE 2004 [DIRS 171539]) requirements. All waste package configurations have been determined to be important to waste isolation in accordance with AP-2.22Q, *Classification Analyses and Maintenance of the Q-List* and, therefore, are classified as safety category (SC) in *Q-List* (BSC 2004 [DIRS 168361], Appendix A; BSC 2004 [DIRS 170992], Section 6.4.2). The drip shields have been determined to be important to waste isolation in accordance with AP-2.22Q and, therefore, are classified as safety category (SC) in *Q-List* (BSC 2004 [DIRS 168361], Appendix A).

The inputs to this report are documented according to AP-3.15Q, *Managing Technical Product Inputs*. The methods used to control the electronic management of data as required by AP-SV.1Q, *Control of the Electronic Management of Information*, were accomplished in accordance with the technical work plan. The process for control of the electronic management of information on evaluation of work activities, processes, or process functions, outlined in Section 5.0 of AP-SV.1Q, is followed to ensure accuracy, completeness, and security of information and data used in preparation of this report. Examples of process controls mentioned in AP-SV.1Q are (a) access to the information contained on personal computer is password protected; (b) secured backup copies are appropriately labeled and stored before changes are made and kept until the changes are confirmed and correct; (c) physical electronic media (tape, diskette, CD-ROM, etc.) are appropriately labeled; and (d) for nonphysical electronic media, transport mechanisms can be e-mail, TCP/IP, NetBios, etc. and methods of receipt verification may include visual inspection, transmission verification settings, check sums, application information integrity check, etc.

This document is prepared in accordance with AP-SIII.10Q, *Models,* and reviewed in accordance with AP-2.14Q, *Document Review.*

B3. USE OF SOFTWARE

B3.1 EXCEL 97 SR-2

Excel 97 SR-2 is a commercial off-the-shelf software program used in this report. The computations performed in this report using Excel use only standard functions and are documented in sufficient detail to allow an independent technical reviewer to reproduce or verify the results by visual inspection or hand calculation without recourse to the originator. The formulas or algorithms used and a listing of inputs to and outputs from the formulas or algorithms are sufficiently documented to allow results to be reproduced. Therefore this software is exempt from LP-SI.11Q-BSC, *Software Management*, Section 2.1. Excel 97 SR-2 is appropriate for its intended use because it offers the mathematical functionality necessary to perform and document the numerical manipulations used in this report. Excel 97 SR-2 was

executed on a Optiplex GX260 Workstation (CRWMS M&O tag 152849, located in the Summerlin Offices, Las Vegas, Nevada) equipped with the Windows 2000 operating system.

B4. INPUTS

B4.1 DIRECT INPUT

Data used to develop the SCDM are not used subsequently to validate the model.

Table B-1. Summary of Seismic Crack Density Model Direct Inputs

Input Name	Input Source	DTN	Input Value or Equation
Alloy 22 Yield Strength	Waste package material properties: corrosion-resistant materials.	MO0003RIB00071.000 [DIRS 148850]	372 MPa at room temperature 338 MPa at 366 K 283 MPa at 477 K
Alloy 22 Young's Modulus	Waste package material properties: corrosion-resistant materials.	MO0003RIB00071.000 [DIRS 148850]	206 GPa at room temperature 203 GPa at 366 K 196 GPa at 477 K
Crack Mouth Opening, (δ) of a Single Crack for Plane Stress Conditions in an infinite plate	Tada et al. 2000 [DIRS 167756], p. 125		$\delta = \frac{(4c)\sigma}{E}$ where δ is crack mouth opening, 2c is the crack length, σ is the value of plane stress, and E is the modulus of elasticity. Section B6.4.2, Eq. B-2
Solution for Radial and Tangential Stress in a Hollow Cylinder Under Internal Pressure Under Plane Stress Conditions	Timoshenko and Goodier (1970 [DIRS 121096], pp. 68 to 71)		$\sigma_r = \frac{a^2b^2(p_o - p_i)}{b^2 - a^2}\frac{1}{r^2} + \frac{p_i a^2 - p_o b^2}{b^2 - a^2}$ $\sigma_\theta = -\frac{a^2b^2(p_o - p_i)}{b^2 - a^2}\frac{1}{r^2} + \frac{p_i a^2 - p_o b^2}{b^2 - a^2}$ where σ_r is radial stress component, σ_θ is tangential stress component, p_I is internal pressure, p_o is external pressure, r is radius, a is inner radius and b is external radius Section B6.4.3, Equation B-15

These inputs are appropriate for their intended use because they are qualified developed data, some of which have established fact as their source. They provide reasonable and appropriate measures of the mechanical properties of the Alloy 22 material used in construction of the waste package outer barrier.

B4.2 CRITERIA

The technical work plan (BSC 2004 [DIRS 171583], Table 3-1) identified the Acceptance Criteria applicable to the seismic crack density model as part of the Acceptance Criteria identified for this report.

B4.3 CODES AND STANDARDS

No codes and standards were used to develop the model for this report.

B5. ASSUMPTIONS

No assumptions were used, in the absence of direct confirming data or evidence, to perform this model activity.

B6. MODEL DISCUSSION

Seismic activity can lead waste packages to impact other components in the drift including the emplacment pallets, drip shields, and other waste packages. If the seismically induced impacts are severe enough, the impacts can physically deform the waste package outer barrier and potentially the waste package inner vessel. These deformations could cause cold work of the waste package barrier and vessel materials, producing a cold-worked gradient typically highest on the outer surface and smallest on the inner surface. Impacts could also create complex through-wall residual stress profiles. These residual stress profiles and cold-work gradients could lead to stress corrosion cracking in the seismically affected areas. The conservative modeling assumption is made that, regardless of the actual chemical environment on the waste package surface, the environment is sufficiently severe to support stress corrosion cracking processes. Thus the requisite concurrent conditions for stress corrosion cracking are present, namely residual tensile stress, an environment that supports corrosion, and a material that is susceptible (cold worked Alloy 22).

Similar seismic damage can be expected for drip shields under seismic loadings; however, as in the treatment of stress corrosion cracking due to rockfalls discussed in this Section 6.3.7, stress corrosion cracks in the drip shields are expected to be tight and plugged with corrosion products or mineral deposits, or both, leading to negligible water flow through these openings. Therefore, since the primary role of the drip shield is to keep water from contacting the waste package, stress corrosion cracking of the drip shield does not compromise its intended design purpose. On this basis, stress corrosion cracking of the drip shield due to seismic activity is not considered further and does not need to be modeled in TSPA-LA.

This evaluation addresses the potential for stress corrosion cracking that could occur as a result of stresses and cold work generated by seismic activity. The stress corrosion cracks could provide a path for subsequent radionuclide release from the waste package.

The crack area density (crack area per unit seismically damaged area) determined in this Appendix is used as a scaling factor applied to the total seismic damaged area (determined in *Seismic Consequence Abstraction* (BSC 2004 [DIRS 169183]) to obtain the total area of the crack network through which radionuclide transport could occur. It is expected that the crack area density will serve as input to *Seismic Consequence Abstraction* (BSC 2004 [DIRS 169183]). This model should only be used as input to *Seismic Consequence Abstraction* (BSC 2004 [DIRS 169183]) and not for generic analyses of stress corrosion crack densities or morphologies under other loadings or for other applications.

B6.1 STRESS CORROSION CRACKING MORPHOLOGY

The purpose of this section is to present observations of stress corrosion crack morphology relevant to Alloy 22 (the waste package outer barrier material). It is known that Alloy 22 is potentially susceptible to stress corrosion cracking under repository-relevant environmental conditions. The morphology of stress corrosion cracking is expected to be transgranular and not intergranular, which is commonly observed (e.g., in high-tensile, Light Water Reactor (LWR) environments) (Andresen et al. 2001 [DIRS 167840]; Herrera 2004 [DIRS 168133], Section 2.0). Figures B-1 and B-2 present typical examples of transgranular stress corrosion cracking and intergranular stress corrosion cracking, respectively.

Depending on the stress distribution, cracking may initiate and propagate through-wall. *If* several cracks were to initiate in the same general area *and* coalesce *and* propagate through-wall *and* remain straight (i.e., perpendicular to the surface) *and* maintain smooth crack faces, a sizeable section of material could "fall out" leading to a larger area for release than would an array of separated stress corrosion cracks (Herrera 2004 [DIRS 168133], Section 2.0). However, the occurrence of all of these events in conjunction is improbable; therefore, only tight and relatively separate through-wall cracks are expected (Herrera 2004 [DIRS 168133], Section 2.0). Stress corrosion cracks would greatly impede radionuclide transport because of their tightness, the tortuous nature of the crack path, and the possibility (similar to cracks in drip shields) of being plugged with corrosion products or mineral deposits, or both, leading to negligible water flow through these openings (Section 6.3.7). Unlike cracks in the drip shield, cracks in the waste package could lead to release of radionuclides to the environment. For this reason, cracks in the waste package must be considered in TSPA-LA.

Source: Herrera 2004 [DIRS 168133], Figure 2-1.

Figure B-1. Typical Example of Transgranular Stress Corrosion Cracking in Stainless Steel

Source: Herrera 2004 [DIRS 168133], Figure 2-2.

Figure B-2. Typical Example of Intergranular Stress Corrosion Cracking in Stainless Steel

B6.2 NATURE OF SEISMIC DEFORMATION AND CRACK GROWTH

The nature of most seismically induced deformations in cylindrical vessels is such that it is very unlikely that a residual stress profile would be created that would allow an initiated stress corrosion crack to propagate through-wall and circumscribing the deformed area (Herrera 2004 [DIRS 168133], Section 3.0). Any through-wall residual stress fields resulting from impact loads would be a secondary-type stress (displacement controlled). There is no significant stress from other sources (e.g., due to internal pressure) since sustained, postclosure primary stresses in the waste package Alloy 22 outer cylinder including internal pressure stresses and waste package–pallet contact stresses are limited by design and are significantly below 0.9 (YS) (BSC 2004 [DIRS 169766], Tables 2, 21, 22, and 23). Further, for such outer surface-induced residual stress gradients, stresses and strains are of higher magnitude at the outer surface and tend to decrease through the thickness (Herrera 2004 [DIRS 168133], Section 3.0). Thus any stress corrosion cracking that initiates and propagates under such a driving stress intensity factor

may arrest before penetrating the full thickness (Herrera 2004 [DIRS 168133], Section 3.0). Therefore, seismically induced deformation-generated stresses are highly unlikely to lead to a residual stress profile that results in a sufficiently positive stress intensity factor as the crack grows to result in cracking through-wall and around the entire deformed area. Similarly, the stress intensity factor (K_I) will tend to decrease as the crack propagates due to stress relaxation associated with crack growth that relieves stresses normal to the crack faces.

Herrera (2004 [DIRS 168133], Section 4.0) concluded that cracks that are in close proximity can reduce the overall driving force for crack growth because the stress intensity factor (K_I) for parallel cracks is actually less than that for a single flaw. Similarly, as discussed in Section 6.5.1, detailed analysis presented in *Structural Integrity Associates Support of Waste Package Design for 2001* (Structural Integrity Associates 2002 [DIRS 161933]), indicates that the distance between two neighboring through-wall cracks would need to be greater than the wall thickness for the stress (and resultant stress intensity) to be sufficient to drive a flaw through-wall. In addition, neighboring cracks will also reduce the crack driving force by decreasing the overall residual stress state. In the case of a single crack embedded in a secondary stress field (e.g., residual stress), as the crack grows, the through-wall residual stress field will redistribute and can significantly change from the original distribution. As experience in boiling water reactors (BWRs) has shown (Herrera 2004 [DIRS 168133], Section 5 and Appendix A), cracks can actually initiate, grow partly through-wall, and arrest before penetration. The crack arrest is due to the redistribution of the weld residual stress such that the stress intensity factor drops below the threshold value for crack growth.

If two cracks are in close proximity in a residual stress field, this relaxing effect is amplified to the point that one of the cracks may grow significantly deeper than the second crack as the growth of one of the cracks significantly reduces the driving force on the second crack (Herrera 2004 [DIRS 168133], Section 4.0). This has been the experience in many light water reactor (LWR) cases (field experience and mockup testing of austenitic stainless steels and nickel-based alloys (Alloy 22 is also a nickel-based alloy)) (Herrera 2004 [DIRS 168133], Section 4.0) (Section B6.3). Through-wall growth of neighboring cracks has not been observed and it is expected that the stress-relieving effect of neighboring cracks is the cause for this behavior.

Even if through-wall stress corrosion cracking occurs such that it circumscribes the deformed area, the nature of stress corrosion cracking (crack face roughness) on this scale will preclude the deformed area from falling out (Herrera 2004 [DIRS 168133], Section 3.0). Stress corrosion cracking in Alloy 22 is expected to be transgranular, but whether transgranular or intergranular, the crack path is complex, with some local areas of branching, and all areas exhibiting a roughness and tortuosity that make it essentially impossible for separation of the inner “plug” to disengage from the rest of the material in the absence of superimposed primary load (e.g., significant internal pressure) (Herrera 2004 [DIRS 168133], Section 3.0). Any small internal pressure that develops from heat up of the waste package or corrosion due to the small amount of internal water vapor, or both, would not be sufficient to force the deformed area from the wall.

B6.3 LIGHT WATER REACTOR CASE HISTORIES

The previous section concluded that multiple surface cracks will not grow to through-wall cracks when they are in close proximity to each other. Herrera (2004 [DIRS 168133], Appendix A) summarizes several case histories of stress corrosion cracking for light water reactors (LWRs) (i.e., boiling water reactor (BWR) and pressurized water reactor (PWR) components). Some of the most significant incidences of cracking discussed included the presence of crevices and did not always occur in areas subjected to the full primary system pressure (i.e., cracking in regions subjected to low differential pressures such as the BWR core shrouds) top guides and steam dryers and in PWR tube sheet and tube support plate creviced regions and at tube bend areas. Cracking often occurred in regions removed from welds and appeared to be driven by cold work related residual stresses. In describing the total extent of cracking (i.e., length and depth), it is important to distinguish between cracking driven by a combination of residual stress plus primary pressure stress-induced loads, and that due solely to residual stresses. The seismically loaded waste package is similar to cases when cracking is caused solely by residual stress (in the absence of differential pressure).

Herrera (2004 [DIRS 168133], Appendix A) also reviewed a number of incidents of stress corrosion cracking observed in LWRs, involving austenitic stainless steels and nickel-based alloys (Alloy 22 is also a nickel-based alloy). In many of these cases, the cracking has been extensive, sometimes becoming fully circumferential on the component as driven by weld residual tensile stress plus pressure induced primary stresses. Even under these severe stress conditions, there has never been a documented case where any section of material dropped out as a result of the observed cracking. Observations in the BWR and PWR industry are consistent with the behavior of cracks that are located in close proximity. For example, the very few SCC-related steam generator tube ruptures observed occurred only under full-system differential pressure. Certainly, no material representing a continuous, through-wall circle has occurred that would give rise to a through-thickness piece being removed.

Therefore, based on the analyses presented in Sections B6.1 to B6.3, seismic activity will not result in large areas separating from the waste package outer barrier. Instead, a network of stress corrosion cracks is expected to form in the waste package outer barrier due to residual stresses induced by seismic activity. The remainder of this document is devoted to modeling the characteristics of such a network of stress corrosion cracks.

B6.4 ESTIMATION OF CRACK AREA DENSITY DUE TO SEISMIC ACTIVITY

This section outlines the overall approach to obtain an estimate of the crack opening area on a waste package damaged by a seismic event. The cracks within the damaged area are assumed to be caused as a result of stresses induced by a seismic event. In order to assess the damage scenario that these individual cracks would not lead to significant radionuclide release due to a collectively large opening of these cracks, it is necessary to assess the possible number of cracks in the damaged area and the opening areas of these cracks. The total crack opening area within the seismic damaged area can be used in an assessment for the waste package subjected to various seismic events.

This section provides the basis for the selection of the effective crack opening area for use in the waste package performance assessment. The previous discussion presented the justification that deformation of areas during seismic events will not result in areas falling out from the waste package wall. The expected behavior of flaws that are in close proximity, consideration of the stress–strain fields due to the deformation, and LWR field experience provides the basis for the conclusion that areas will not fall out of the waste package wall. Previous analytical work, supported by field experience, has demonstrated that through-wall flaws will not grow when they are in close proximity. Results of prior analyses indicate that through-wall flaws would not be present if the spacing were less than the thickness of the component (Section 6.5.1). Using this information, the following section provides an estimate of the crack density and crack opening area for use in the performance assessment of the waste packages.

B6.4.1 Technical Approach

Based on the previous discussions, it is considered unrealistic that the deformed area would fall out of the waste package wall. The most likely limiting case is that the damaged areas on the waste package are penetrated by a network of tight cracks. This network of cracks will allow diffusive transport, but prevent advective flow and advective transport because of the small effective crack opening area of individual cracks.

The seismic scenario requires three inputs to represent the effective area of a network of cracks:

(1) the total damaged area on the waste package

(2) the crack density in the damaged area on the surface of the barrier

(3) the crack opening area of an individual crack.

The damage abstractions for the seismic scenario will define the total damaged area on the barrier. The total area of the crack network, $A_{SCC,\ NET}$, is then the product of the seismically damaged area, A_D; the crack density, ρ_{SCC} (# cracks per unit area); and the crack opening area of an individual crack, A_{SCC} (area/crack), expressed as (Herrera 2004 [DIRS 168133], Section 6.1):

$$A_{SCC,\ NET} = A_D\ (\rho_{SCC}\ A_{SCC}) \qquad \text{(Eq. B-1)}$$

The factor ($\rho_{SCC}\ A_{SCC}$) (the crack area density or crack area per unit seismically damaged area (i.e., the fraction of the seismically damaged area, A_D) through which radionuclides can be released) can be viewed as a scaling factor applied to the seismically damaged area to obtain the total area of the crack network, $A_{SCC,\ NET}$. Section B6.4.2 provides estimates of the crack area density through analysis of networks of cracks arranged in a hexagonal geometry. Section B6.4.3 provides an alternative model for the crack area density by analysis of a damaged area with a circular geometry circumscribed by a single through-wall crack. Because the hexagonal array represents a high effective density (close spacing) of individual cracks, this hexagonal case, with crack center spacings set at the plate thickness, t, (Section B6.4.2) is considered a conservative representation. Section B6.4.3 provides an alternative model for the crack area density by analysis of a damaged area with a circular geometry circumscribed by a single through-wall crack. This is considered a limiting ‘realistic’ case.

B6.4.2 Primary Conceptual Model for Crack Area Density: Hexagonal Geometry

This section estimates the crack area density for a network of cracks arranged in a hexagonal geometry. Two crack arrangements are considered (Herrera 2004 [DIRS 168133], Section 6.2):

Case 1–The centers of elliptical cracks form a hexagonal array with major axis of length, $\frac{2t}{\sqrt{3}}$, where t is the wall thickness, with crack centers separated by $\frac{2t}{\sqrt{3}}$ (Figure B-3). For this case, the hexagon side length is $\frac{2t}{\sqrt{3}}$, and the perpendicular bisector (the distance from the hexagon center to the midpoint of one of the hexagon sides) is the wall thickness, *t*.

Case 2–The centers of elliptical cracks form a hexagonal array with major axis of length *2t*, where *t* is the wall thickness, with crack centers separated by *t* (Figure B-5). For this case, the hexagon side length is *t* and the perpendicular bisector is $\frac{\sqrt{3}t}{2}$. In this case, significant crack overlap is allowed to occur.

As discussed in Section 6.5.1, detailed analysis presented in *Structural Integrity Associates Support of Waste Package Design for 2001* (Structural Integrity Associates 2002 [DIRS 161933]), indicates that the distance between two neighboring through-wall cracks would need to be greater than the wall thickness for the stress (and resultant stress intensity) to be sufficient to drive a flaw through-wall. This conclusion is based on stress field interactions between closely spaced parallel cracks. Case 1 uses the crack arrangement such that the perpendicular bisector is the wall thickness, *t*, while Case 2 uses the crack arrangement such that the distance between crack centers is equal to the wall thickness.

The results from either of these conceptual models of crack arrangement are considered to be conservative because the crack centers are arranged in a densely packed closely spaced array, which allows for neighboring in-plane stress fields to overlap.

Both conceptual models use the recommendations in Section 6.5 regarding the estimated length, intercrack spacing, and intercrack opening for the weld regions in the waste package lid. While the seismically induced damage to the waste package can occur at any location on the surface of these structures, the generic recommendations provide reasonable guidance for estimating the crack density and crack area in the seismic scenario.

It was shown in Sections 6.5.1 and 6.5.2 that:

1. The minimum distance between two neighboring parallel through-wall cracks is equal to the plate thickness

2. The crack opening area is elliptical

3. The crack width of a single crack, δ, for plane stress conditions in an infinite plate is given as (Tada et al. 2000 [DIRS 167756], p. 125):

$$\delta = \frac{(4c)\sigma}{E} \quad \text{(Eq. B-2)}$$

where *2c* is the crack length, σ is the value of plane stress, and *E* is the modulus of elasticity. The crack width corresponds to the minor axis of the elliptical cross-section of the crack. The crack opening area, A_{SCC}, is equal to the area of the elliptical cross section:

$$A_{SCC} = \pi\left(\frac{\delta}{2}\right)\left(\frac{2c}{2}\right) = \pi\left(\frac{(2c)\sigma}{E}\right)c = \frac{(2\pi c^2)\sigma}{E} \quad \text{(Eq. B-3)}$$

B.6.4.2.1 Case 1: Hexagonal Array with Side Length and Crack Length of 2t/√3

Consider a hexagonal array with side length $\frac{2t}{\sqrt{3}}$, where t is the plate thickness (Figure B-3). Each point of the hexagonal array is the center of a crack with length $\frac{2t}{\sqrt{3}}$. This length allows for cracks, if they lie in the same plane, to just touch without overlapping as shown in Figure B-3. This crack length is smaller than that used for the waste package closure weld region as discussed in Section 6.5.1 of the main body of this report, in which it was concluded that the crack length was equal to twice the thickness. However, that conclusion was based on stress interaction between parallel cracks and, in this case, overlap between neighboring cracks is avoided (this is not true of the next case shown in Figure B-5).

The crack density, ρ_{SCC} is the average number of cracks in a hexagon of the array divided by the area of the hexagon. The number of cracks in each hexagonal unit cell is 3 regardless of crack orientation. This is easy to see for Figure B-3 in which the cracks are aligned in parallel. The crack at the center of the array in Figure B-3 provides a full crack. The cracks at each of the six corners of the hexagon are shared by two other hexagons, effectively contributing an average of one-third of a crack per corner, regardless of actual crack orientation (in Figure B-3, the cracks directly adjacent to the center contribute almost one-half of a crack and the other four edge cracks closer to (but not exactly) one-fourth of a crack). One should consider that the same shape is placed on each of the six corners of the hexagon and each corner is shared by three hexagons. Figure B-4 shows the cracks in random orientation to aid in visualization. Thus, each hexagon contains three full cracks. The area of the unit hexagon is calculated as the area of six equilateral triangles with side, $\frac{2t}{\sqrt{3}}$, as:

$$6\left(\frac{1}{2}\right)\left(\frac{2t}{\sqrt{3}}\right)(t) = \frac{6t^2}{\sqrt{3}} \quad \text{(Eq. B-4)}$$

It follows that the crack density, ρ_{SCC}, is given by:

$$\rho_{SCC} = \frac{3}{\left(\frac{6t^2}{\sqrt{3}}\right)} = \frac{\sqrt{3}}{2t^2} \qquad \text{(Eq. B-5)}$$

Then, using Equations B-3 and B-5 with 2c = $\frac{2t}{\sqrt{3}}$ (the crack length), the crack area density (crack area per unit seismically damaged area) can be expressed as:

$$\rho_{SCC} A_{SCC} = \frac{\sqrt{3}}{2t^2}\frac{(2\pi t^2)\sigma}{3E} = \frac{\pi\sigma}{\sqrt{3}E} \cong 1.81\frac{\sigma}{E} \qquad \text{(Eq. B-6)}$$

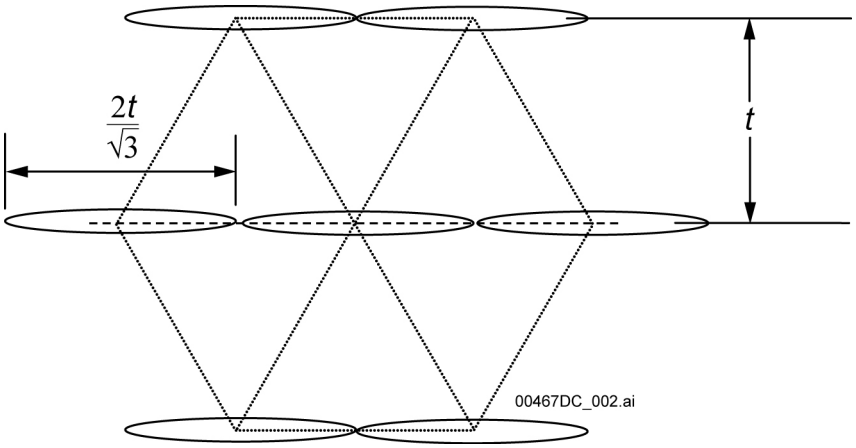

NOTE: Not to scale.

Figure B-3. Parallel Rows of Parallel Cracks Whose Centers are Arranged in a Hexagonal Array (with Row Spacing Equal to the Wall Thickness, *t*)

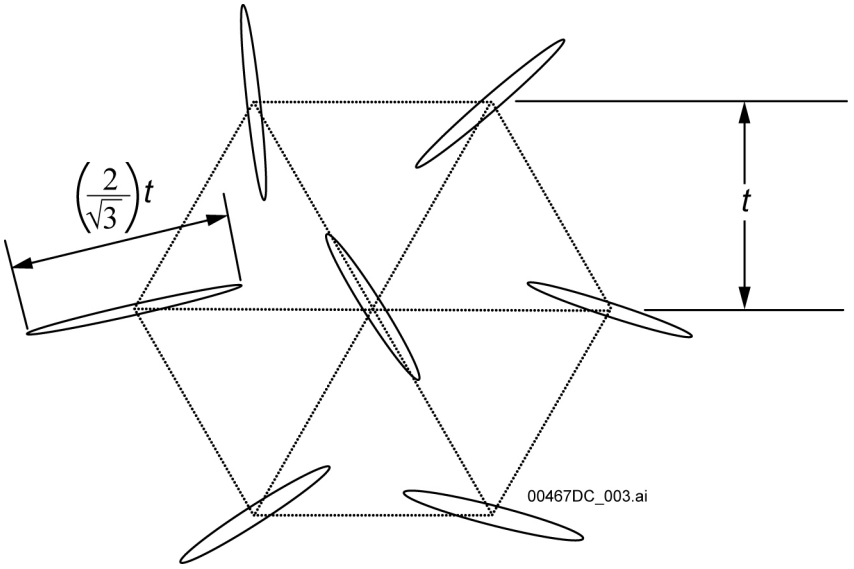

NOTE: Not to scale.

Figure B-4. Parallel Rows of Randomly Oriented Cracks Whose Centers are Arranged in a Hexagonal Array (with Row Spacing Equal to Wall Thickness, *t*)

B.6.4.2.2 Case 2: Hexagonal Array with Side Length, *t,* and Crack Length, *2t*

Consider a hexagonal array with side length *t*, where *t* is the plate thickness (Figure B-5). Each point of the hexagonal array is the center of a crack with length *2t*. This crack length is the same as used for the waste package closure weld region as discussed in Section 6.2.2, in which it was concluded that the crack length was equal to twice the thickness. This geometry allows for cracks, if they lie in the same plane, to overlap significantly (each crack overlaps about half of each of its neighboring cracks) as shown in Figure B-5. The maximum overlap occurs when the cracks are exactly in line. The overlap will decrease if the crack orientation has some offset from the in-line direction. Conservatively, in calculating the total crack opening area, crack overlap is not considered (i.e., overlapped areas are counted twice) in order to provide an upper bound on the crack area density.

The crack density, ρ_{SCC}, is the average number of cracks in a hexagon of the array divided by the area of the hexagon. As in the previous case, the number of cracks in each hexagonal unit cell is three regardless of crack orientation. The area of the unit hexagon is calculated as the area of six equilateral triangles with side *t* as:

$$6\left(\frac{\sqrt{3}}{4}\right)(t^2) = \frac{3\sqrt{3}t^2}{2} \qquad \text{(Eq. B-7)}$$

It follows that the crack density, ρ_{SCC}, is given by:

$$\rho_{SCC} = \frac{\#\,of\ cracks}{area\,of\ unit\ hexagon} = \frac{3}{\left(\frac{3\sqrt{3}t^2}{2}\right)} = \frac{2}{\sqrt{3}t^2} \qquad \text{(Eq. B-8)}$$

Then, using Equations B-3 and B-8 with *2c = 2t*, the total crack opening area per unit damage area can be expressed as:

$$\rho_{SCC} A_{SCC} = \frac{2}{\sqrt{3}t^2}\frac{(2\pi t^2)\sigma}{E} = \frac{4\pi\sigma}{\sqrt{3}E} \cong 7.26\frac{\sigma}{E} \qquad \text{(Eq. B-9)}$$

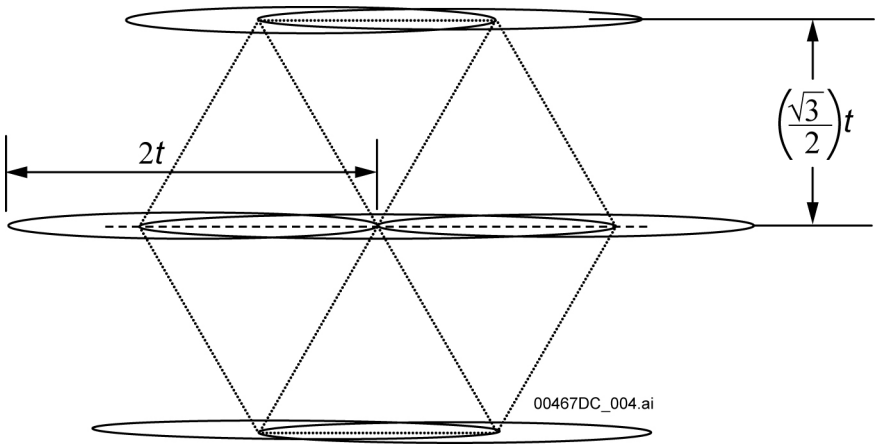

NOTE: Not to scale.

Figure B-5. Parallel Rows of Parallel Flaws (with Row Spacing Equal to (√3/2) Wall Thickness)

B6.4.2.3 Summary of Primary Conceptual Model for Crack Area Density

The crack area density for Case 1 (where cracks can barely touch) is $\frac{\pi\sigma}{\sqrt{3}E}$, and that for Case 2 (where significant crack overlap is allowed) is $\frac{4\pi\sigma}{\sqrt{3}E}$. The crack area density is shown to be proportional to the applied stress, essentially residual stress due to seismic activity, and inversely proportional to the Young's Modulus. It does not depend on the wall thickness. Therefore, the crack area density is recommended to be represented as a uniform distribution between $\frac{\pi\sigma}{\sqrt{3}E}$ and $\frac{4\pi\sigma}{\sqrt{3}E}$, i.e.:

$$\text{Crack Area Density} = C\frac{\pi\sigma}{\sqrt{3}E} \qquad \text{(Eq. B-10)}$$

where C = epistemic uncertainty factor given by a uniform distribution between 1 and 4.

The use of a uniform distribution is reasonable since it accurately reflects the lack of knowledge of the exact value of the crack area density. In general, a uniform distribution is appropriate for uncertain quantities where the range can be established by physical arguments or expert knowledge – but not much else is known about the relative likelihood of values within the range (Mishra 2002 [DIRS 163603], Section 2.3). The use of a distribution ranging up to the very

conservative upper bound allows for uncertainties, such as the potential for crack overlap and deviations from a regular array of identically shaped cracks, to be appropriately accounted for.

The yield strength of the material should be used as a very conservative estimate for the stress component in the crack area density calculation. The yield strength is considered conservative because the process of crack initiation and through-wall crack propagation will result in significant reduction in the residual stress. The use of material yield strength will give a conservative estimate of the crack area density appropriate for probabilistic evaluation. Values of the Alloy 22 yield strength and Young's Modulus at room temperature and at 150°C (the temperature at which the structural calculations of the waste package exposed to ground motion were conducted (BSC 2004 [DIRS 167083], Section 3)) are shown in the second and third columns of Table B-2. The value of the Alloy 22 yield strength at 150°C (~423 K) was determined by linear interpolation between the values for the Alloy 22 yield strength at 366 K and 477 K (Table B-1):

$$Yield\ Strength@423\,\mathrm{K} = 283\,\mathrm{MPa} - \left(\frac{477\,\mathrm{K} - 423\,\mathrm{K}}{477\,\mathrm{K} - 366\,\mathrm{K}}\right)\cdot(283\,\mathrm{MPa} - 338\,\mathrm{MPa}) \cong 310\,\mathrm{MPa} \quad \text{(Eq. B-11)}$$

The value of the Alloy 22 Young's Modulus at 150°C (~423 K) was determined by linear interpolation between the values for the Alloy 22 Young's Moduli at 366 K and 477 K (Table B-1):

$$Young's\ Modulus@423\,\mathrm{K} = 196\,\mathrm{GPa} - \left(\frac{477\,\mathrm{K} - 423\,\mathrm{K}}{477\,\mathrm{K} - 366\,\mathrm{K}}\right)\cdot(196\,\mathrm{GPa} - 203\,\mathrm{GPa}) \cong 199\,\mathrm{GPa} \quad \text{(Eq. B-12)}$$

In Table B-2, calculations of the crack length (hexagon side length), crack density, crack width, crack opening area, and crack area density are shown for various barrier thicknesses for both hexagonal cases are presented. Table B-2 shows that the range of the crack area density (crack area per unit seismically damaged area) ranges from 3.28×10^{-3} to 1.31×10^{-2} at room temperature, and 2.83×10^{-3} to 1.13×10^{-2} at 150°C. It is recommended that the room temperature range of crack area density be used for performance assessment as this choice yields higher (more conservative) crack area densities.

Table B-2. Crack Characteristics for Hexagonal Geometry

Temperature (°C)	Yield Stress (MPa)	Young's Modulus (GPa)	Case	Barrier Thickness[1] (mm)	Crack Length[2] (mm)	Crack Density[3] (/mm2)	Crack Width[4] (mm)	Crack Opening Area[5] (mm2)	Crack Area Density[6]
Room	372	206	1	18.0	20.8	2.67×10^{-3}	7.51×10^{-2}	1.23	3.28×10^{-3}
				20.0	23.1	2.17×10^{-3}	8.34×10^{-2}	1.51	3.28×10^{-3}
				23.0	26.6	1.64×10^{-3}	9.59×10^{-2}	2.00	3.28×10^{-3}
				25.0	28.9	1.39×10^{-3}	1.04×10^{-1}	2.36	3.28×10^{-3}
			2	18.0	36.0	3.56×10^{-3}	1.30×10^{-1}	3.68	1.31×10^{-2}
				20.0	40.0	2.89×10^{-3}	1.44×10^{-1}	4.54	1.31×10^{-2}
				23.0	46.0	2.18×10^{-3}	1.66×10^{-1}	6.00	1.31×10^{-2}
				25.0	50.0	1.85×10^{-3}	1.81×10^{-1}	7.09	1.31×10^{-2}
150°C	310	199	1	18.0	20.8	2.67×10^{-3}	6.48×10^{-2}	1.06	2.83×10^{-3}
				20.0	23.1	2.17×10^{-3}	7.20×10^{-2}	1.31	2.83×10^{-3}
				23.0	26.6	1.64×10^{-3}	8.27×10^{-2}	1.73	2.83×10^{-3}
				25.0	28.9	1.39×10^{-3}	8.99×10^{-2}	2.04	2.83×10^{-3}
			2	18.0	36.0	3.56×10^{-3}	1.12×10^{-1}	3.17	1.13×10^{-2}
				20.0	40.0	2.89×10^{-3}	1.25×10^{-1}	3.92	1.13×10^{-2}
				23.0	46.0	2.18×10^{-3}	1.43×10^{-1}	5.18	1.13×10^{-2}
				25.0	50.0	1.85×10^{-3}	1.56×10^{-1}	6.12	1.13×10^{-2}

Output DTN:MO0403SPASCRKD.000.

NOTES: 1. The values of the barrier thickness are for illustration purposes only.

2. The crack length equals $\frac{2t}{\sqrt{3}}$ for Case 1 and $2t$ for Case 2.

3. The crack density equals $\frac{\sqrt{3}}{2t^2}$ for Case 1 and $\frac{2}{\sqrt{3}t^2}$ for Case 2.

4. The crack width of a single crack is given by Equation B-2 for the given thickness for each case.
5. The crack opening is calculated from Equation B-3 for the two cases.
6. The crack area density is calculated from Equation B-6 for Case 1 and Equation B-9 for Case 2.

B6.4.3 Alternative Conceptual Model for Crack Area Density: Circular Geometry

This section considers a conceptual model of a through-wall crack circumscribing a circular damaged area. The main purpose of this model is to provide an alternative mathematical model for crack area density, which can be used in validation of the primary crack area density model. Even though this model leads to a fully circumscribed area, the inner area material would not fall out due to the roughness of crack surfaces. It should be emphasized that this calculation and associated postulated crack morphology are strictly for calculating an alternative crack opening area. It is not meant to imply that this of crack morphology is observed.

Timoshenko and Goodier (1970 [DIRS 121096], pp. 68 to 71) present the solution to a hollow cylinder under internal pressure (p_i) and external pressure (p_o) of inner radius (a) and external radius (b) (Figure B-6) under plane stress conditions. This solution can be easily adapted to determining the displacement about a hole in a two-dimensional infinite body subjected to a radial stress, S. The surface of the hole can be considered to be the crack surface for the

purposes of this analysis. For this radially symmetric problem (Timoshenko and Goodier 1970 [DIRS 121096], p. 70):

$$\varepsilon_\theta = \frac{u}{r} \quad \text{(Eq. B-13)}$$

Further, Hooke's Law can be written for an isotropic material for plane stress as:

$$E\varepsilon_\theta = \sigma_\theta - \nu\sigma_r \quad \text{(Eq. B-14)}$$

where

u = the radial displacement
r = distance from the origin in a polar coordinate system
E = Young's modulus and
ν = Poisson's ratio.

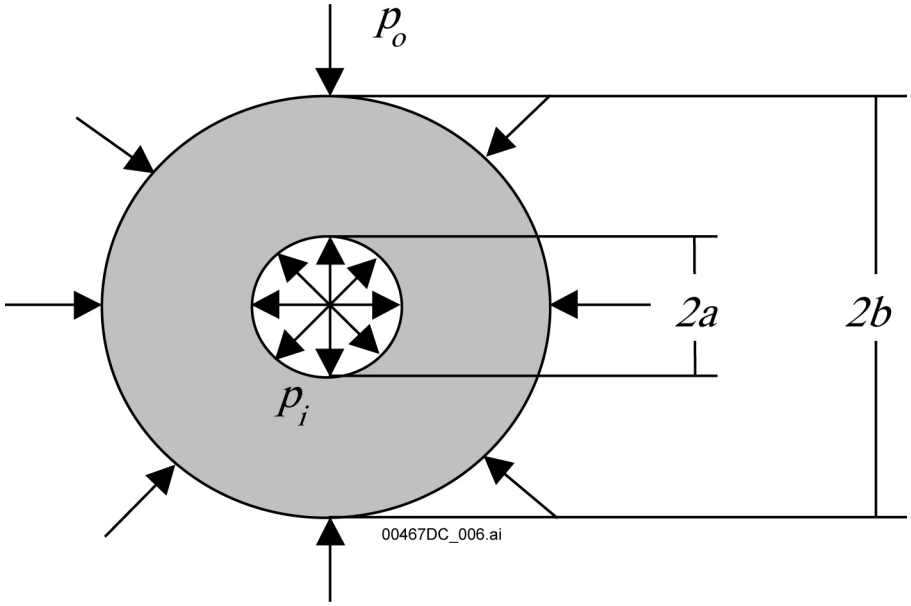

Figure B-6. Hollow Cylinder of Inner Radius *a* and Outer Radius *b* Subject to Internal Pressure p_i and External Pressure p_o

The following are expressions for the radial and tangential stress components (Timoshenko and Goodier 1970 [DIRS 121096], p. 70):

$$\sigma_r = \frac{a^2 b^2 (p_o - p_i)}{b^2 - a^2}\frac{1}{r^2} + \frac{p_i a^2 - p_o b^2}{b^2 - a^2}$$
$$\sigma_\theta = -\frac{a^2 b^2 (p_o - p_i)}{b^2 - a^2}\frac{1}{r^2} + \frac{p_i a^2 - p_o b^2}{b^2 - a^2} \quad \text{(Eq. B-15)}$$

For the purposes of this analysis, b approaches infinity (infinite plate), p_o = -S, and we are interested in the radial displacements at $r = a$ (the surface of the hole). With these conditions, at $r = a$, $\sigma_r = 0$ and $\sigma_\theta = 2S$. Using Equations B-13 and B-14, the radial displacement, u, at $r = a$ is:

$$u = \frac{2aS}{E} \qquad \text{(Eq. B-16)}$$

More generally, it has been shown by the above analysis that the radial displacement (u) at the surface of the hole of radius, r, under the action of a radial stress, σ, could be written as:

$$u = \frac{2r\sigma}{E} \qquad \text{(Eq. B-17)}$$

where r = radius of hole (i.e., radius of damaged area)
σ = applied stress.

The radial displacement (u) in Equation B-17 can be considered the crack opening for a crack circumscribing a damaged area with a radius of r. This is equivalent to the conservative case where the inner material is detached (i.e., cracked through-wall around the entire circumference) and not subjected to any stress (i.e., not decreasing the displacement particularly by "pulling" on the outer material). The crack opening area of this crack can be expressed as:

$$A_{SCC} = 2\pi ru = 2\pi r \frac{2r\sigma}{E} = \frac{4\pi r^2 \sigma}{E} \qquad \text{(Eq. B-18)}$$

The damaged area is $\pi r2$. Therefore the crack area density, realizing that there is one circular crack in each circular area of radius r, can be expressed as:

$$\rho_{SCC} A_{SCC} = \left(\frac{1}{\pi r^2}\right)\left(\frac{4\pi r^2 \sigma}{E}\right) = 4\frac{\sigma}{E} \qquad \text{(Eq. B-19)}$$

The crack area density ($\rho_{SCC}\ A_{SCC}$) depends only on the stress state and the Young's modulus. Values of the Alloy 22 yield strength and Young's modulus at room temperature and at 150°C are shown in the second and third columns of Table B-3. In Table B-3, calculations of the crack length, crack density, crack opening area, and crack area density are shown for various radii of the damaged area are presented. The crack area density calculated using values of the Alloy 22 yield strength and Young's Modulus at room temperature is about 7.22×10^{-3}, while the crack area density calculated at 150°C is about 6.23×10^{-3}.

Table B-3. Crack Characteristics for Circular Geometry

Temperature (°C)	Yield Stress (MPa)	Young's Modulus (GPa)	Radius[1] (mm)	Crack Length[2] (mm)	Crack Density[3] (/mm2)	Crack Width[4] (mm)	Crack Opening Area[5] (mm2)	Crack Area Density[6]
Room	372	206	18.0	113	9.82E-04	6.50E-02	7.35	7.22E-03
			20.0	126	7.96E-04	7.22E-02	9.08	7.22E-03
			23.0	145	6.02E-04	8.31E-02	12.0	7.22E-03
			25.0	157	5.09E-04	9.03E-02	14.2	7.22E-03
150°C	310	199	18.0	113	9.82E-04	5.61E-02	6.34	6.23E-03
			20.0	126	7.96E-04	6.23E-02	7.83	6.23E-03
			23.0	145	6.02E-04	7.17E-02	10.4	6.23E-03
			25.0	157	5.09E-04	7.79E-02	12.2	6.23E-03

Output DTN: MO0403SPASCRKD.000.

NOTES: [1]Values of the barrier thickness are for illustration purposes only.
[2]Crack length equals $2\pi r$.
[3]Crack density equals $1/\pi r^2$ from Equation B-13.
[4]Crack width is given by Equation B-17.
[5]Crack opening is calculated from $2\pi ru$ from Equation B-18.
[6]Crack area density is calculated from Equation B-19.

B7. VALIDATION

The seismic crack density model is an abstraction model whose primary purpose is to provide input to *Seismic Consequence Abstraction* (BSC 2004 [DIRS 169183]). The developed crack area density is used as a scaling factor applied to the total seismic damaged area to obtain the total area of the crack network through which radionuclide transport could occur.

This model was validated using the approach described in the technical work plan governing this activity (BSC 2004 [DIRS 171583]) and is consistent with AP-SIII.10Q, *Models*. This procedure calls for the determination of the level of confidence required for the model and identifies criteria that can be utilized to show that the level of confidence has been achieved. These criteria include performing an independent technical review. In addition, confidence building has been incorporated into this section.

B.7.1 DETERMINATION OF LEVEL OF CONFIDENCE REQUIRED

The current technical work plan for this report (BSC 2004 [DIRS 171583], Section 2.2.2) states that the seismic crack density model (SCDM) warrants a high level of confidence (Level III). This conclusion was based on the answers to several questions related to the characteristics of the SCDM. These questions and answers are repeated below:

Is the model extrapolated over large distances, spaces, or time frames?

Yes. The Seismic Crack Density Model is extrapolated over the entire repository footprint and over the entire regulatory compliance period.

Does the model have large uncertainties?

Yes. There is uncertainty in the parameters used in the Seismic Crack Density Model, these uncertainties can be large.

Will the model be used to demonstrate compliance or licensing positions?

Yes. The SCDM is used as an input to the seismic consequence report, which provides the estimates of the crack opening area for ingress of water into the waste package.

Will the output of the model have impacts (positive or negative) on TSPA dose calculation results?

Yes. Although the effect of nonseismic stress corrosion cracking penetrations in the drip shield and waste package outer barrier are estimated to have relatively small impacts on TSPA dose calculations, the SCDM is used as an input to *Seismic Consequence Abstraction* (BSC 2004 [DIRS 169183]) and the impacts of the model on dose calculations are expected to be large.

Based on the above, it is reasonable to assign the level of confidence needed for the SCDM to be high (Level III). This is consistent with the technical work plan (BSC 2004 [DIRS 171583], Table 2-1) that lists several postdevelopment model validation methods described in Section 5.3.2.c of AP-SIII.10Q, *Models*.

B7.2 IDENTIFICATION AND DOCUMENTATION OF VALIDATION ACTIVITIES AND ASSOCIATED CRITERION TO BE USED TO DETERMINE THAT THE REQUIRED LEVEL OF CONFIDENCE HAS BEEN OBTAINED

The technical work plan (BSC 2004 [DIRS 171583], Table 2-1) for this report identified the following criteria and associated activities to be used to determine that the required level of confidence has been obtained for the seismic crack density model (SCDM).

Criterion One: Corroborating data must match qualitatively

Activity One: Demonstrate corroborating data match qualitatively

Activity Two: Demonstrate the model results for crack patterns in the damaged areas are consistent with the results of an alternative conceptual model

Criterion Two: Independent technical review to demonstrate:

Corroborating data or alternative models selected by the technical reviewer must match qualitatively (corroboration will be considered successful if deemed defendable by the reviewer).

Activity One: Conduct an independent technical review for the crack density model (only), and the review will answer the following questions:

- Subactivity One: Are the representations of the damaged area in the form of a crack network instead of a hole consistent with observation in literature? This activity deals with the validity of the crack density representations in the seismically damaged areas.

- Subactivity Two: Are the model results for crack patterns in the damaged areas consistent with the results of an alternative conceptual model?

The activities and associated criteria are primarily related to confidence building during model development although they do provide additional confidence in the SCDM results. In particular, the criteria and related activity cited in Table 2-1 of the technical work plan (BSC 2004 [DIRS 171583]) are consistent with Section 5.3.2.c of AP-SIII.10Q, *Models*.

B7.3 DOCUMENTATION OF ACTIVITIES TO BE PERFORMED TO GENERATE CONFIDENCE IN THE MODEL DURING MODEL DEVELOPMENT

The criteria and related activities to be used to determine that the required level of confidence has been obtained for the seismic crack density model (SCDM) were listed in Section B7.2.

Criterion One, Activity One is satisfied by the discussions throughout this appendix but particularly those of Sections B6.2 and B6.3 in which the nature of stress corrosion cracking and analysis of BWR and LWR stress corrosion cracking case histories are discussed.

Among the observations made in Section B6.2:

- It is unlikely that the residual stress profile, which would be created by seismic loading, would allow an initiated stress corrosion crack to propagate both through-wall and circumscribing the deformed area

- The through-wall residual stress fields resulting from impact loads would be a secondary type stress (displacement controlled) and there is no source of significant internal pressure

- Stress fields would be expected to be maximum at the outer surface and decrease with depth

- The magnitude of the stress state will decrease as the crack propagates

- Stress field interactions between adjacent cracks would tend to decrease the driving force for crack growth

- The nature of stress corrosion cracks (crack face roughness, branching, and tortuosity) is such that large sections of material will not “fall out” of the cracked structure.

The primary observation made in Section B6.3 was, even under the severe stress conditions experienced in LWRs, there are no documented cases where any section of material dropped out as a result of cracking.

On the basis of these observations, a reasonable level of confidence has been obtained that representations of the damaged area in the form of crack network instead of a hole is consistent with observations in the literature and is the expected morphology of waste package through-wall stress corrosion cracking due to seismic loading.

Criterion One, Activity Two is satisfied by Section B6.4.3, in which an alternative mathematical model for stress corrosion crack morphology and damaged area shape is presented. The primary model for crack area density was summarized in Section B6.4.2. The crack area density based on hexagonal crack arrays was found to be given by a uniform distribution between $\frac{\pi\sigma}{\sqrt{3}E}$ and $\frac{4\pi\sigma}{\sqrt{3}E}$ (~$1.81\frac{\sigma}{E}$ and ~$7.26\frac{\sigma}{E}$). For the alternative model (Section B6.4.3), the crack area density based on a circular seismically damaged area with a single circumferential crack was found to be $4\frac{\sigma}{E}$. The crack area density from the alternative mathematical model lies between the bounds of the crack area density resulting from the primary mathematical model. Therefore, the results of the alternative mathematical model corroborate the results of the primary mathematical model. This model validation methodology is consistent with Section 5.3.2.c.2 of AP-SIII.10Q, *Models*.

To satisfy validation criterion two, a technical review, planned in the technical work plan for this activity (BSC 2004 [DIRS 171583], Section 2.2.3.2), was conducted by reviewers independent of the development, checking, and interdisciplinary review of the model documentation. The results of this technical review also serve to satisfy the model validation requirements of AP-SIII.10Q, *Models*, Section 5.3.2.c.5.

Technical reviewers were asked to address the following criteria (Pasupathi 2004 [DIRS 168350]):

1. Is the representation of the failure in the form of cracks in the damaged area technically appropriate?

2. Does the model consider a variety of crack patterns and distributions?

3. Are the crack networks considered in the model appropriate and reasonable?

4. Does the crack network representations considered in the model represent optimum crack density (i.e., number, size, shape and distribution of cracks) such that the largest possible crack opening area is included?

5. Do alternative models exist for crack geometry morphology?

6. Has uncertainty in the parameters used to describe the model been adequately characterized? If not, what additional uncertainties should be added?

7. Are there alternate crack patterns that are more defensible from a technical standpoint?

The responses to each of these independent technical review criteria are considered throughout the remainder of this section.

(1) Is the representation of the failure in the form of cracks in the damaged area technically appropriate?

Generally, the technical reviewers felt that the analysis has done a good job of looking at various crack geometries in the damaged area (Jones 2004 [DIRS 168353]). The representation of the failure in the form of cracks in the damaged area was found to be technically appropriate (Payer 2004 [DIRS 168352]). One technical reviewer (Beavers 2004 [DIRS 168354]) agreed that the damaged area likely failed by "SCC clusters" (arrays of cracks) rather than by the formation of large holes; however, the technical reviewer felt that the report sent for his review did not effectively prove this was the case. This technical reviewer (Beavers 2004 [DIRS 168354]) recommended that additional analysis and discussion be provided. The report in question was revised (Herrera 2004 [DIRS 168133]) in response to these comments and the revision forms the basis for the model documented in this appendix.

Conclusion/Response: On this basis, it is concluded that the technical reviewers agreed that the representation of the failure in the form of cracks in the damaged area is technically appropriate.

(2) Does the model consider a variety of crack patterns and distributions?

(3) Are the crack networks considered in the model appropriate and reasonable?

The technical reviewers generally provided their answers to both of these review criteria together. Therefore, their responses are treated together in this summary.

A variety of crack patterns and distributions are considered (Payer 2004 [DIRS 168352]). The technical reviewers felt that the crack networks considered in the model were appropriate and reasonable (Payer 2004 [DIRS 168352]; Jones 2004 [DIRS 168353]). The technical reviewers expressed concerns that a more relevant geometry might be cracks constrained to an annulus around the deformed area and not cracks distributed throughout the deformed area (Jones 2004 [DIRS 168353]; Beavers 2004 [DIRS 168354]). Additional analysis was recommended for this damaged area geometry (Jones 2004 [DIRS 168353]; Beavers 2004 [DIRS 168354]). One reviewer (Beavers 2004 [DIRS 168354]) suggested that a circular crack circumscribing the damaged area was also a reasonable geometry to consider.

Conclusion/Response: The area damaged by seismic activity is not assigned a specific shape, only an area, A_D. The hexagonal crack density is applied to whatever area is seismically damaged regardless of its specific shape. A circular crack circumscribing the damaged area was considered as an alternative conceptual model in this report. Given the preceding observations, it is concluded, overall, the report considers a variety of crack patterns and distributions and the crack networks considered in the model are appropriate and reasonable.

(4) Does the crack network representations considered in the model represent optimum crack density i.e. number, size, shape and distribution of cracks, such that the largest possible crack opening area is included?

In the context of this review, the wording "the largest possible crack opening area" should be restated as "an appropriate representation of crack area." The technical reviewers generally agreed that the hexagonal array of cracks was the optimum crack density or geometry for analysis, however, additional justification should be provided for the intercrack spacing (*t*, the wall thickness) (Beavers 2004 [DIRS 168354]; Jones 2004 [DIRS 168353]).

Conclusion/Response: The technical reviewers did not evaluate the documented basis for the intercrack spacing used, *Structural Integrity Associates Support of Waste Package Design for 2001* (Structural Integrity Associates 2002 [DIRS 161933]; Section 6.5.1). If the technical reviewers reviewed this detailed minimum crack spacing analysis, they would be more confident in the choice made for intercrack spacing.

On this basis, the crack network representations considered in the model represent the optimum crack density (i.e., the number, size, shape and distribution of cracks), such that an appropriate representation of crack area is included.

(5) Do alternative models exist for crack geometry morphology?

Two of the reviewers (Jones and Payer) were aware of alternative models for crack geometry, although only one (Jones) could specify what he thought was the most relevant geometry. The third reviewer (Beavers) was unaware of any alternative models for crack geometry (Payer 2004 [DIRS 168352]; Jones 2004 [DIRS 168353]; Beavers 2004 [DIRS 168354]).

Conclusion/Response: The area damaged by seismic activity is not assigned a specific shape, only an area, A_D. The hexagonal crack density is applied to whatever area is seismically damaged regardless of its specific shape. A circular crack circumscribing the damaged area was considered as an alternative conceptual model in this report. Given the preceding observations, overall, the technical reviewers were satisfied that alternative models for crack geometry or morphology were considered.

(6) Has uncertainty in the parameters used to describe the model been adequately characterized? If not, what additional uncertainties should be added.

One technical reviewer (Payer 2004 [DIRS 168352]) had no response. One reviewer (Beavers 2004 [DIRS 168354]) did not think the report, as supplied for review, adequately addressed uncertainty. Another reviewer (Jones 2004 [DIRS 168353]) pointed out several conservatisms in the analysis:

a) The analysis did not consider the decrease in residual stress as the crack propagates. There is a possibility of crack arrest, although no credit is taken for this process. Also decreased stress states would lead to narrower crack openings.

b) The analysis uses the crack mouth opening to represent the crack opening. The crack tip opening is less than the crack mouth opening. The reviewer supplied a crack mouth opening equation, which is less conservative than the one used in the analysis.

c) The use of the yield stress as the stress load on the cracks is conservative (the residual stress at penetration should be lower).

and pointed out some possible nonconservatisms:

d) The Tada analysis used to determine the crack opening is based on an infinite plate, how much difference would there be for a finite cylinder?

e) Deformation beyond the yield strength could result in work hardening and a higher value of yield strength.

Conclusion/Response: The crack opening results presented in this Appendix are based upon plane stress conditions in an infinite plate. The actual structure for the Alloy 22 waste package outer barrier consists of a cylindrical shell of finite length. It would be expected that crack openings in an infinite plate under plane stress would be different than in a finite cylindrical shell in that the membrane stresses and flexural stresses for given loadings in combination with other loads would be different. The analysis is used to determine a crack area density (crack area per unit seismically damaged area) given a seismically damaged area determined elsewhere (BSC 2004 [DIRS 167083]). That is, the spatial stress state is determined elsewhere and determined based upon consideration of a cylindrical shell of finite length. *Structural Calculations of Waste Package Exposed to Vibratory Ground Motion* (BSC 2004 [DIRS 167083], Section 3) uses a residual stress threshold, which is uniformly distributed between 80% and 90% of the yield strength of Alloy 22 at 150°C. This calculation uses a stress state that is equal to the yield strength at room temperature (i.e., the temperature and stress state used are conservative). Detailed comparisons between crack openings in infinite plates and finite cylinders were not undertaken in this analysis, however, the results of analyses such as those in *Structural Integrity Associates Support of Waste Package Design for 2001* (Structural Integrity Associates 2002 [DIRS 161933]) indicate that the presence of multiple cracks will tend to decrease the residual stress state to values well below the yield strength. This would result in crack openings that are smaller than those calculated. Coupling this result to the listed conservatisms outlined in this section (decreasing stress states as the crack propagates, conservative crack opening equations, the use of the yield strength at room temperature), it can be concluded that the current model will provide a reasonably conservative representation of the total crack opening area. On the basis of the discussion in this ection, it is concluded that uncertainty in the parameters used to describe the model been adequately characterized at least to the extent that the total crack opening area will not be underestimated using the current model.

(7) Are there alternate crack patterns that are more defensible from a technical standpoint?

This criterion is similar to criteria 2 through 5. As stated in the discussion of criterion 2, the technical reviewers did express concerns that a more relevant geometry might be cracks constrained to an annulus around the deformed area and not cracks distributed throughout the

deformed area (Jones 2004 [DIRS 168353]; Beavers 2004 [DIRS 168354]). One reviewer (Beavers 2004 [DIRS 168354]) indicated that while the "hexagon pattern is a reasonable, defensible crack pattern for the deformed area of the waste package" . . . "a combination of this pattern with the circumferential pattern to produce a series of circular cracks around the dents is the most reasonable pattern." Further conversation with this technical reviewer (Pasupathi 2004 [DIRS 168351]) led to the conclusion that what was meant by "circumferential pattern of cracks to produce a series of circular cracks" was actually cracks constrained to an annulus around the deformed area and not cracks distributed throughout the deformed area.

Conclusion/Response: The area damaged by seismic activity is not assigned a specific shape, only an area, A_D. The hexagonal crack density is applied to whatever area is seismically damaged regardless of its specific shape. A circular crack circumscribing the damaged area was considered as an alternative conceptual model in this report. Given the preceding observations, it is concluded that, overall, the technical reviewers were satisfied that alternative models for crack geometry or morphology were considered and the crack patterns analyzed were sufficient from a technical standpoint.

On this basis, the validation criteria from AP-SIII.10Q, *Models*, related to corroboration and those listed in the technical work plan governing this report (BSC 2004 [DIRS 171583], Section 2.2.5) have been satisfied and the SCDM is valid for use in TSPA-LA.

B8. CONCLUSIONS

Seismic activity can lead the waste packages to impact other components in the drift including the emplacement pallets, drip shields, and other waste packages. If the seismically induced impacts are of sufficient magnitude, the impacts may physically deform the waste package outer barrier and potentially the waste package inner vessel. These deformations could cause cold work of the waste package barrier and vessel materials, producing a cold-worked gradient typically highest on the outer surface and smallest on the inner surface. Impacts could also create complex through-wall residual stress profiles. These stress profiles and cold-work gradients could lead to stress corrosion cracking in the seismically affected area of the waste packages.

Similar damage can be expected for drip shields under seismic loadings, however, as in the treatment of stress corrosion cracking due to rockfalls discussed in Section 6.3.7, stress corrosion cracks in the drip shields are expected to be tight and plugged with corrosion products or mineral deposits, or both, leading to negligible water flow through these openings. Therefore, since the primary role of the drip shield is to keep water from contacting the waste package, stress corrosion cracking of the drip shield does not compromise its intended design purpose.

A number of incidents of stress corrosion cracking have been observed in LWRs involving both austenitic stainless steels and nickel-based alloys. In many of these cases, the cracking has been extensive, sometimes becoming fully circumferential on the component as driven by weld residual tensile stress plus pressure induced primary stresses. Even under these severe stress conditions, there has never been a documented case where has any section of material dropped out as a result of the observed cracking. Observations in the BWR and PWR industry are consistent with the expected behavior of flaws that are located in close proximity. For example,

the very few stress corrosion cracking related steam generator tube ruptures observed occurred only under full system differential pressure. Certainly, no material representing a continuous, through-wall circle has occurred that would give rise to a through thickness piece being removed.

On the basis of these results, it is concluded that seismic activity will not result in large areas separating from the waste package outer barrier. Instead a network of stress corrosion cracks is expected to form in the waste package outer barrier due to residual stresses induced by seismic activity. An uncertain distribution for the crack area density (crack area per unit seismically damaged area) was developed and is discussed in the next section.

B8.1 DEVELOPED OUTPUTS

For the Alloy 22 waste package outer barrier, the crack area density is given by (Section B6.4.2):

$$\text{Crack Area Density} = C\frac{\pi\sigma}{\sqrt{3}E} \qquad \text{(Eq. B-20)}$$

where C = epistemic uncertainty factor given by a uniform distribution between 1 and 4.

It is recommended that the room temperature Alloy 22 yield strength (372 MPa) and Young's modulus (206 GPa) be used (Table B-1). These values lead to the crack area density being uniformly distributed between 3.28×10^{-3} and 1.31×10^{-2} (Table B-2). These results are summarized below in Table B-4.

Table B-4. Crack Area Density Parameters and Their Sources

Parameter Name	Parameter Source (for TSPA)	Parameter Value	Units
Crack Area Density	DTN: MO0403SPASCRKD.000	Uniform distribution between 3.28×10^{-3} and 1.31×10^{-2}	N/A

B8.2 TREATMENT OF ACCEPTANCE CRITERIA

The acceptance criteria identified in Section B4.2 are discussed in Section 8.2.

B.9 INPUTS AND REFERENCES

This document may be affected by technical product input information that requires confirmation. Any changes to the document that may occur, as a result of completing the confirmation activities, are reflected in subsequent revisions. The status of the input information quality may be confirmed by review of the Document Input Reference System database.

B9.1 DOCUMENTS CITED

167840 Andresen, P.L.; Emigh, P.W.; Young, L.M.; and Gordon, G.M. 2001. "Stress Corrosion Cracking of Annealed and Cold Worked Titanium Grade 7 and Alloy 22 in 110°C Concentrated Salt Environments." *Corrosion/2001, [56th Annual Conference*

& Exposition, March 11-16, 2001, Houston, Texas, USA]. Paper No. 01130, Houston, Texas: NACE International. TIC: 255671.

168354 Beavers, J. 2004. Report Review. E-mail to P. Pasupathi. 02/24/2004. ACC: MOL2004.0311.0147.

169766 BSC (Bechtel SAIC Company) 2004. *Commercial SNF Waste Package Design Report.* 000-00C-DSU0-02800-000-00B. Las Vegas, Nevada: Bechtel SAIC Company. ACC: ENG.20040709.0001

170992 BSC 2004. *Safety Classification of SSCs and Barriers.* 000-00C-MGR0-01000-000-00A. Las Vegas, Nevada: Bechtel SAIC Company. ACC: ENG.20040721.0005.

168361 BSC 2004. *Q-List.* 000-30R-MGR0-00500-000-000 REV 00. Las Vegas, Nevada: Bechtel SAIC Company. ACC: ENG.20040721.0007.

169183 BSC 2004. *Seismic Consequence Abstraction.* MDL-WIS-PA-000003, Rev. 01. Las Vegas, Nevada: Bechtel SAIC Company.

167083 BSC 2004. *Structural Calculations of Waste Package Exposed to Vibratory Ground Motion.* 000-00C-WIS0-01400-000-00A. Las Vegas, Nevada: Bechtel SAIC Company. ACC: ENG.20040217.0008.

171583 BSC 2004. *Technical Work Plan For: Regulatory Integration Modeling and Analysis of the Waste Form and Waste Package*. TWP-WIS-MD-000009 REV 00 ICN 01. Las Vegas, Nevada: Bechtel SAIC Company. ACC: DOC.20040910.0001.

168133 Herrera, M.L. 2004. *Evaluation of the Potential Impact of Seismic Induced Deformation on the Stress Corrosion Cracking of the YMP Waste Packages*. SIR-04-015 Revision No. 1. San Jose, California: Structural Integrity Associates, Inc. ACC: MOL.20040311.0149.

168353 Jones, R.H. 2004. "RE: Independent Technical Review of the Seismic Crack Density Model." E-mail from R.H. Jones to J. Payer, J. Beavers, and P. Pasupathi, February 20, 2004, with attachment. ACC: MOL.20040311.0145.

163603 Mishra, S. 2002. *Assigning Probability Distributions to Input Parameters of Performance Assessment Models.* SKB TR-02-11. Stockholm, Sweden: Svensk Kärnbränsleförsörjning A.B. TIC: 252794.

163274 NRC (U.S. Nuclear Regulatory Commission) 2003. *Yucca Mountain Review Plan, Final Report.* NUREG-1804, Rev. 2. Washington, D.C.: U.S. Nuclear Regulatory Commission, Office of Nuclear Material Safety and Safeguards. TIC: 254568.

168350 Pasupathi, P. 2004. *Independent Technical Review of the Seismic Crack Density Mode.* Las Vegas, Nevada: Bechtel SAIC Company. ACC: MOL.20040311.0141.

168351 Pasupathi, P. 2004. *Additional Clarification Provided by the Independent Technical Reviewer on the Seismic Crack Density.* Las Vegas, Nevada: Bechtel SAIC Company. ACC: MOL.20040311.0148.

168352 Payer, J.H. 2004. "Independent Technical Reviews." E-mail from J.H. Payer to P. Pasupathi, February 29, 2004, with attachment. ACC: MOL.20040311.0143.

161933 Structural Integrity Associates. 2002. *Structural Integrity Associates Support of Waste Package Design for Year 2001.* SIR-02-073. San Jose, California: Structural Integrity Associates. ACC: MOL.20020709.0389.

167756 Tada, H.; Paris, P.C.; and Irwin, G.R. 2000. *The Stress Analysis of Cracks Handbook*. 3rd. New York, New York: American Society of Mechanical Engineers. TIC: 255547.

121096 Timoshenko, S.P. and Goodier, J.N. 1970. *Theory of Elasticity.* 3rd Edition. New York, New York: McGraw-Hill. TIC: 245469.

B9.2 CODES, STANDARDS, REGULATIONS, AND PROCEDURES

AP-2.22Q, Rev. 1, ICN 1. *Classification Analyses and Maintenance of the Q-List.* Washington, D.C.: U.S. Department of Energy, Office of Civilian Radioactive Waste Management. ACC: DOC.20040714.0002.

AP-2.27Q, Rev. 1, ICN 4. *Planning for Science Activities.* Washington, D.C.: U.S. Department of Energy, Office of Civilian Radioactive Waste Management. ACC: DOC.20040610.0006.

AP-3.15Q, Rev. 4, ICN 5. *Managing Technical Product Inputs.* Washington, D.C.: U.S. Department of Energy, Office of Civilian Radioactive Waste Management. ACC: DOC.20040812.0004.

AP-SIII.10Q, Rev. 2, ICN 7. *Models.* Washington, D.C.: U.S. Department of Energy, Office of Civilian Radioactive Waste Management. ACC: DOC.20040920.0002.

AP-SV.1Q, Rev. 1, ICN 1. *Control of the Electronic Management of Information.* Washington, D.C.: U.S. Department of Energy, Office of Civilian Radioactive Waste Management. ACC: DOC.20040308.0001.

LP-SI.11Q-BSC, Rev. 0, ICN 1. *Software Management.* Washington, D.C.: U.S. Department of Energy, Office of Civilian Radioactive Waste Management. ACC: DOC.20041005.0008.

B9.3 SOURCE DATA LISTED BY DATA TRACKING NUMBER

148850 MO0003RIB00071.000. Physical and Chemical Characteristics of Alloy 22. Submittal date: 03/13/2000.